IMPACTS OF CLIMATE CHANGE ON METAL CONTAMINATION IN WELL WATER THROUGH SALTWATER INTRUSION, FLOODING AND DROUGHT

by

Anita Taylor

Submitted in partial fulfillment of the requirements

for the degree of Master of Applied Science

at

Dalhousie University

Halifax, Nova Scotia

April 2024

Table of Contents

List of Tables

List of Figures

Abstract

Climate change can exacerbate groundwater contamination via secondary effects like droughts, floods, and saltwater intrusion. This thesis analyzed the influence of climate change factors on metal contamination in groundwater using well water quality data from British Columbia, Canada. An exploratory data analysis characterized trends between metal contamination (arsenic, cadmium, lead, manganese, uranium), climate factors (temperature, precipitation), and aquifer types based on the B.C. aquifer classification system. Correlation analysis revealed relationships between metals weakened or remained consistent in floods but decoupled in droughts, indicating distinct geochemical shifts. Saltwater intrusion altered correlations between metals, suggesting changed redox conditions and ion competition. Factor analysis identified key influencing variables, including groundwater geochemistry/saltwater intrusion, redox reactions, climate, aquifer confinement, and anthropogenic sources. Drought intensified geochemical interactions while floods overwhelmed natural processes. Arsenic contamination related strongly to saltwater intrusion. Overall, this research provides an initial knowledge foundation to build predictive models assessing climate change risks on groundwater quality. Further spatial analysis is needed to differentiate anthropogenic from natural sources. Incorporating additional hydrogeological data would strengthen understanding of climate influences on metal mobilization. This work highlights the need to consider climate change in protecting groundwater resources and human health.

List of Abbreviations and Symbols Used

IPCC	Intergovernmental Panel on Climate Change
US EPA	United States Environmental Protection Agency
B.C.	British Columbia
USGS	United States Geological Survey department
DRASTIC	Dimensionless index to assess groundwater vulnerability includes: Depth to water table, Recharge, Aquifer media, Soil media, Topography, Impact of vadose zone, Conductivity (Patel et al., 2022)
RASTERs	Matrix of pixels containing values that represent information. Often the raw form of data from satellites.
SWI	Saltwater Intrusion/Sea Water Intrusion
PCIC	Pacific Climate Impact Consortium
OBS	British Columbia Provincial Groundwater Observation Well Network
BCDC	British Columbia Data Catalogue
EMS ID	Environmental monitoring station ID
EC	Environmental Canada
BCH	British Columbia Hydro
CDWG	Canadian Drinking Water Guidelines/ Guidelines for Canadian Drinking Water Quality
U, U--T	Total Uranium of sample [mg/L]
As, As-T	Total Arsenic of sample [mg/L]
Mn, Mn-T	Total Manganese of sample [mg/L]
Pb, Pb-T	Total Lead of sample [mg/L]
Cd, Cd-T	Total Cadmium of sample [mg/L]
Fe, Fe-T	Total Iron of sample [mg/L]
K, K—T	Total Potassium of sample [mg/L]
Mg, Mg-T	Total Magnesium of sample [mg/L]
Cl, Chloride, Chlrid:D	Dissolved Chloride of sample [mg/L]

Ca, Ca-T	Total Calcium of sample [mg/L]
Sulfate, Sulfat:D,	Dissolved Sulfate of sample [mg/L]
P, P--T	Total phosphorous of sample [mg/L]
Total Kjeldahl Nitrogen, N.Kjel:T, Nitrogen	Nitrogen measured via Kjeldahl method. This method is a good general measure of organically used nitrogen because it accounts for biological incorporated nitrogen [mg/L]
total alkalinity at pH 4.5, Alkalinity Total 4.5, Alkalinity	Buffering capacity or the amount of acid needed to bring the pH to a 4.2, which carbonate, and bicarbonate are assumed to be converted to carbonic acid [mg/L $CaCO_3$]
Hardness	Amount of dissolved minerals (Calcium and Magnesium) in water [mg/L $CaCO_3$]
Specific Conductance, SC	Measure of the water's ability to conduce an electric current [µS/cm]
Residue Filterable 1.0u	Turbidity [mg/L]
Minimum temperature, MIN_TEMP	Mean monthly minimum temperature [°C]
Maximum temperature, MAX_TEMP	Mean monthly maximum temperature [°C]
Flood Drought, FD	Total monthly precipitation subtracted by simulated monthly precipitation/ climatology data simulation for the same location [cm]
Heatwave, HW, GettingHotter	Mean monthly maximum temperature subtracted by simulated monthly maximum temperature/ climatology data simulation for the same location [°C]
MinTemp, MT	Mean monthly minimum temperature subtracted by simulated monthly minimum temperature/ climatology data simulation for the same location [°C]
Aquifer Group 1, AG1, Aquifer_1	Unconfined aquifers with Aquifer subtype 1a, 1b, 1c, 2, 3 and 4a according by B.C. Aquifer subtype classification system
Aquifer Group 2, AG2, Aquifer_2	Confined aquifers with Aquifer subtype 4b and 4c according by B.C. Aquifer subtype classification system

Aquifer Group 3, AG3, Aquifer_3	Bedrock/fractured aquifers with Aquifer subtype 5a, 6a and 6b according by B.C. Aquifer subtype classification system
KDE	Kernal Density Estimator
One-hot encoding	Method of converting categorical values to numerical representations via 1s and 0s
KMO	The Kaiser-Meyer-Olkin test/values. Measures sampling adequacy for factor analyses.
X	Equivalent distance calculated by the haversine formula to account for latitude [m]
Y	Equivalent distance calculated by the haversine formula to account for longitude [m]
Months_Since_First_Sample	Numerical conversion to account for time in a factor analysis [Months]
F1, F2, F3, F4, F5	Factor 1, Factor 2, Factor 3, Factor 4, and Factor 5 of the main factor analysis
$F1_{As}$, $F2_{As}$, $F3_{As}$, $F4_{A}$, $F5_{As}$, $F6_{As}$	Factor 1, Factor 2, Factor 3, Factor 4, Factor 5 and Factor 6 with focus on Arsenic
$F1_{Mn}$, $F2_{Mn}$, $F3_{Mn}$, $F4_{Mn}$, $F5_{Mn}$, $F6_{Mn}$	Factor 1, Factor 2, Factor 3, Factor 4, Factor 5, and Factor 6 with focus on Manganese
$F1_{Pb}$, $F2_{Pb}$, $F3_{Pb}$, $F4_{Pb}$, $F5_{Pb}$, $F6_{Pb}$	Factor 1, Factor 2, Factor 3, Factor 4, Factor 5 and Factor 6 with focus on lead.
$F1_{U}$, $F2_{U}$, $F3_{U}$, $F4_{U}$, $F5_{U}$, $F6_{U}$	Factor 1, Factor 2, Factor 3, Factor 4, Factor 5 and Factor 6 with focus on Uranium.
$F1_{D}$, $F2_{D,}$ $F3_{D}$, $F4_{D}$, $F5_{D}$, $F6_{D}$	Factor 1, Factor 2, Factor 3, Factor 4, Factor 5 and Factor 6 of the drought factor analysis
$F1_{F}$, $F2_{F}$, $F3_{F}$, $F4_{F}$, $F5_{F}$, $F6_{F}$, $F7_{F}$	Factor 1, Factor 2, Factor 3, Factor 4, Factor 5, Factor 6, and Factor 7 of the flood factor analysis

Acknowledgements

I'd like to thank all those who supported me:

- To my mother Anne and sister Avea, who spent countless hours per week helping me edit and type, so I didn't have to "drop out".
- To Leili who helped me navigate campus and lab work while I had tumors in my shoulders, knees, arms, and spine; and took charge of communication when I went mute.
- To my friend Matthew who stood by me throughout burnout, lack of accommodations, helped me overcome neurodiverse barriers and connect with people who got me back on track.
- To Dale and the Neil Squire Society, who bought workplace accommodation technology and assisted me with disability technical support.
- To Brishna who helped bring me food when I was bedridden due to tumors and was refused for more disability support.
- To Chris and everyone who helped proofread my drafts
- To Dr McBean at University of Guelph who helped me edit and refine ideas.
- To my supervisor, Dr Gagnon at Dalhousie University.

Chapter 1: Introduction

1.1 Study Background

Climate change is one of the most pressing global challenges of the generation with severe primary and secondary consequences for both natural and human systems. Anthropogenic activities, especially fossil fuel burning and deforestation, have increased greenhouse gas emissions in the atmosphere resulting in changes to the earth's climate system. Said changes have profound implications on various aspects of human lives including ecosystems, agricultural, public health and water resources.

Numerous scientific studies since the Intergovernmental Panel on Climate Change (IPCC) have established knowledge on climate change, research priorities, policy discussions, and funding initiatives concerning the essential relationship with water resources. Most highlighted the need to address the impact of climate change; including impacts on water resources and water quality (Sýs et al., 2021). These studies and panels have provided evidence of rising sea levels, increased temperatures, altered precipitation patterns and more extreme intense weather events. Said studies linked these changes to human activities and further demonstrated the relationship between human activities and the destruction of the delicate balance of the planet's ecosystem.

With the development of general circulation models for climate change and the inclusion of new knowledge on metal transportation, scientists can predict future climate scenarios along with the identification of emerging contaminants. Recently, organisations are acknowledging the value of granting public access to their database thus allowing for more widespread analysis of models (Klein et al., 2017). Environmental monitoring databases specifically focused on climate change are also starting to utilise groundwater data and groundwater quality data (Amanambu et al., 2020; Water Protection & Sustainability Branch, 2024). Previously, most climate change water models were focused on hydrological/overland flow with groundwater studies being a secondary priority. Groundwater impact was analysed via localised studies for aquifer vulnerability like DRASTIC (Maqsoom et al., 2020). Currently, hydrodynamical climate risk models are now attempting to incorporate soil and ecological tools and Modflow-style models to account for hydraulic connectivity and solute transport (Amanambu et al., 2020).

Artificial intelligence and machine learning has led to the tracking of secondary effects of climate change such as water contamination. These additions are now starting to be used to investigate the impact of climate change on water resources. With increasing droughts caused by climate change, aquifer vulnerability has started to include not just water quantity but the effect on water quality (Barbieri et al., 2023). The effect of flooding on well water quality is starting to expand beyond biological contamination. Saltwater intrusion assessments have become a focus due to overpumping from droughts and rising sea levels. In addition, development of risk assessment frameworks such as US EPA risk assessment guidance have provided a structured approach to evaluating risks posed by metal contaminations in well water; inclusive of pathways, toxicity, and the potential impacts of climate change (Sýs et al., 2021).

1.2 Rationale for the Study

Well water is an essential source of drinking water, in both developed and developing countries throughout the world. Approximately two thirds of the population of Nova Scotia currently rely on private well water (G. W. Kennedy & Drage, 2020). Though the primary effects of climate change on the groundwater level have been studied, critical analysis on the secondary effects of climate change such as metal contamination is relatively scarce. This lack of data is important for assessing human health impacts as well as impacts on ecosystems and water resource management.

This thesis contributes to the understanding of the impact of climate change on metal contamination of Arsenic, Lead, Manganese and Uranium in groundwater/well water in British Columbia. Three critical trajectories were examined: saltwater intrusion, flooding, and drought.

These three events can exaggerate natural or existing sources of metal contamination or introduce new passages for anthropogenic sources (Kumar, 2012). Overpumping during drought seasons, rising sea levels and changing hydraulic patterns can lead to the intrusion of saltwater into aquifers and the alteration of the metal composition in well water. More frequent flooding events can immediately transfer and disperse metal contaminants from various sources, such as agriculture or heavy industry; and can alter soil composition and allow for the mobility of metals into the well water source over time (Ciszewski & Grygar, 2016). Rising temperatures can influence the mobility and release of metals from geological structures into well water (Hemmerle & Bayer, 2020).

Utilizing data from the Environmental Monitoring Stations from British Columbia, Canada, the resulting thesis research aims to discover relationships between metals such as uranium, arsenic, manganese and lead over a 40-year timeframe and climate change conditions. This framework can be used to highlight the necessity of metal contamination testing in well water. This analysis will help create of a base of knowledge that can be used to build future predictive models for groundwater contamination with climate change effects. In addition, this thesis could further contribute towards ecosystem models and human health models to improve informed decision making and policy development. Ultimately, the aim is to help build an understanding of how climate change will influence what is in groundwater.

1.3 Research Objectives

This study aims to gain an understanding on how climate change will influence what is in well water/groundwater. Biological contamination will not be a focus in this scope. The three main objectives are:

1) To assess the variations in metal contamination levels in well water under different climate change-induced factors, including saltwater intrusion, flooding and drought events.
2) To contribute to the existing knowledge based on the interactions between climate change and metal contamination in well water, providing insights for future predictive modelling that could influence policymaking, water resource management, and environmental planning.
3) To assess the potential impact of climate change on the vulnerability and resilience of well water as a source of drinking water, considering the specific metal contamination risks.

1.4 Hypotheses

1) Increased saltwater intrusion due to climate change may lead to elevated levels of metal contamination in well water.
2) Drought events resulting from climate change may result in higher concentrations of metals in well water via oxidation.
3) Flooding may lead to a dilution effect on metals in well water.

Chapter 2: Literature Review

2.1 Overview of Metal Contamination in Well Water

2.1.1 Sources of Metal Contamination in Well Water

2.1.1.1 Naturally Occurring/Geogenic Metals in Geological Formations

Geological formations naturally contain minerals with heavy metals that can leach into groundwater depending on the mineral composition of the surrounding rocks and soil, the local hydrogeology, and the dual chemical aquifer characteristics (Earle, 2019a). Said groundwater contamination is caused by processes such as volcanic eruptions, rock weathering and leaching into groundwater by the actions of water. Leaching occurs through geochemical interactions that dissolve present metals into groundwater.

One of the examples of this is in sedimentary formations such as limestone, dolomite or shale in which the associated arsenic release via weathering is influenced by redox conditions, pH and other minerals present (Bradl, 2005). Iron and manganese are also commonly found in these rock formations and their release is promoted in conditions with high oxygen levels (Earle, 2019a). Manganese in Nova Scotia is associated with the Windsor Group limestone formation (G W Kennedy, 2021). International examples of metal contamination include arsenic contamination in the Bengal delta in Bangladesh, in which sediments release levels of arsenic (Mukherjee & Bhattacharya, 2001). The High Plains Ogallala aquifer in the United States contains sedimentary rock formations associated with uranium and in reducing conditions, is leached into groundwater (Plumlee et al., 2004). For a larger conceptual example, arsenic from sedimentary formations would be formed during diagenesis and related arsenic rock cycles in Figure 2.1.1.

Igneous rock, formed from volcanic rock; and metamorphic rock, formed from rocks changed by heat and pressure underground can contain various trace metals, including uranium and radium either as composing or accessory minerals (Ulmer-Scholle et al., 2015). Examples of these are granite, syenite, basalt, gabbro, nepheline and andesite (Bradl, 2005). Here, metal leaching depends on various groundwater chemical factors such as mineral solubility, rock-water interactions, and water infiltration from fractures or fissures. Volcanic ash and lava flow contain heavy metals like lead, mercury and arsenic. These are released by volcanic activity and are transported into nearby soils and sediments. Afterwards, groundwater interacts with metal deposits resulting in metal leaching (Earle, 2019a). More international examples include arsenic

contamination in groundwater in the Andean region of Argentina and Chile; and manganese contamination from Basaltic formations in aquifers in India (Sujith et al., 2014; Tapia et al., 2019). Conceptually, these rock cycle processes for arsenic contamination are related to the metamorphism, volcanic emissions and hydrothermal activities in Figure 2.1.1.

Further in-depth lithology is out of scope.

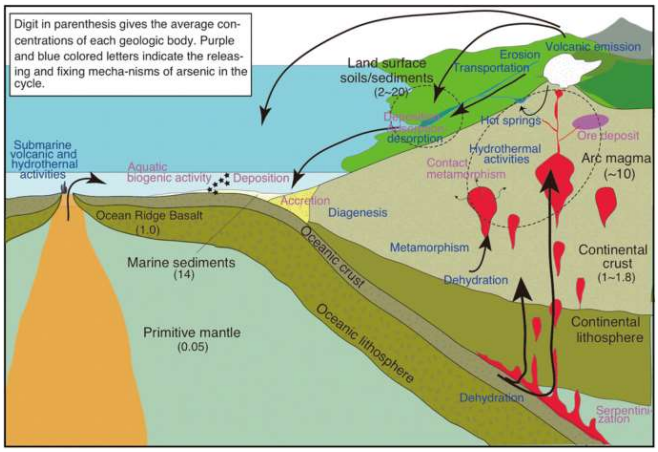

Figure 2.1.1: Arsenic geologic cycle. Digit in parenthesis gives the average concentrations of each geologic body. Purple and blue colored letters indicate the releasing and fixing mechanism of arsenic in the cycle. (Masuda, 2018).

2.1.1.2 Anthropogenic sources of Metal Contamination

Anthropogenic activities increase metal contamination in water sources, particularly groundwater, and subsequently well water. Emissions, effluence and waste disposal from mining smelting, manufacturing and other industrial activities can release various metals into the environment which enter groundwater systems via surface runoff, infiltration or direct contamination (A. Singh et al., 2022). In the Canadian context, mining activities are a significant source of contamination. For example, the mining operations from the Sudbury region in Ontario incur groundwater contamination from copper, nickel and cobalt (Vogels, 2014; Voutchkova et al., 2021). It is similar in the United States, where the Silver Valley region through Ohio and Idaho has groundwater affected by lead, zinc and other metal contamination due to mining operations (Snow, 2012). Additionally, groundwater can be contaminated by agricultural practices with the use of fertilizers, pesticides and animal waste via leaching and through groundwater recharge processes (P. Li et al., 2021). Climate change exaggerates the impact of these contamination sources by extreme weather events, erosion, and contaminant transportation.

Future research is required to fully understand how anthropogenic sources influence metal contamination.

2.1.1.3 Corrosion of plumbing materials and well infrastructure as a source of metal contamination

Another source of metal contamination in groundwater is due to the corrosion of piping materials and degradation of well infrastructure (Pieper et al., 2018). Critical components of a well such as pipes, fittings and pumps made of lead, copper and zinc; corrode over time and release metals into the water flow. Climate change influences corrosion by altering water chemistry parameters such as pH and dissolved oxygen levels. With increasing temperature fluctuations, this typically increases corrosion rates and leads to enhanced metal leaching (Staben et al., 2015).

In addition, rusted iron oxides may reduce/remove some water contaminates like arsenic similar to soil processes (van Genuchten et al., 2020).

The above considerations are beyond the scope of this thesis.

2.1.2 Common Metals Found in Well Water

The type of metal contamination found in well water/groundwater is dependent on geography, geology and water chemistry. In Nova Scotia, common contaminates are manganese, arsenic, magnesium, lead, uranium and fluoride due to the surrounding geography (G. Kennedy & Drage, 2018). Internationally, arsenic, cadmium, selenium, and copper are common (Khan et al., 2023).

Lead contamination in ground and well water is a concern due to the health effects particularly in pregnant women and children (Brender et al., 2006). The contaminate source tends to be lead leaching from plumbing materials such as pipes and fittings in the plumbing system, aggravated by low pH and prolonged contact time (Subramanian et al., 1995).

Galena, a lead sulfite material, is currently found in hydrothermal veins and mineral deposits (A. Singh et al., 2022). Groundwater interactions will cause lead-iron dissolution and subsequently cerussite, a lead carbonate mineral in oxidized lead deposits may contaminate groundwater flow (Jurgens et al., 2019). Current lead contamination research is often focused on piping and drinking water systems and not geological formations.

Zinc contamination is recognized in well water and drinking water systems, often leaching from corroded galvanized iron or zinc coated plumbing in low pH or acidic conditions (Oyem et al.,

2015). Zinc rich soils lead to groundwater contamination via erosion and deposition of zinc containing sediments with water infiltration into groundwater. Last, an additional source of zinc contamination can be via volcanic eruptions in volcanic regions (Oyem et al., 2015).

Groundwater contamination in copper is again typically due to the corrosion of copper plumbing materials such as pipes, fittings and fixtures, releasing copper ions into the waterflow through the distribution system. This is aggravated by acidic water, high chlorine levels and prolonged contact time with piping surfaces (Staben et al., 2015). In specific geochemical conditions, copper contamination can be caused by groundwater percolation through natural occurring geological formations including chalcopyrite, a copper bearing mineral from hydrothermal veins, porphyry rock, malachite, azurite and other natural sources with depositions of copper (Voutchkova et al., 2021). Cyprus and the Western United States (i.e. Arizona) have high natural copper contamination of groundwater due to these naturally occurring causes.

Iron contamination is formed by both natural sources and corroded iron plumbing (Health Canada, 2022). It is more of an aesthetic concern than a health concern.

Other contaminants are primarily caused by anthropogenic activities. For example, mercury contamination in groundwater arises from coal combustion, industrial discharges and mining via runoff and infiltration; or indirectly via deposition of atmospheric mercury onto land surfaces (Barringer et al., 2013). Natural geological sources of mercury can include certain mercury bearing minerals such as cinnabar, via volcanic eruptions which release elemental mercury vapor, and mercury sulfides (Herdianita & Priadi, 2008). Mercury contamination is particularly common around the Pacific Ring of Fire countries (Herdianita & Priadi, 2008). Areas that have concerns around natural mercury contamination also include regions in Guizhou Province, China (Beckers & Rinklebe, 2017).

Groundwater contamination with cadmium primarily arises from anthropogenic sources including mining, phosphate fertilizer production, improper waste disposal and industrial discharges (Butterman & Reston, 2004). Cadmium is relatively mobile in water and can leach into groundwater in areas that have high cadmium soil concentrations. Though it is a trace mineral and not commonly associated with specific formations, the leaching process can be enhanced by the weathering and erosion of sphalerite and volcanic activity. The Jinzu River

Basin and Toyama Bay, Japan contain cadmium rich sediments and have experienced natural contamination (Butterman & Reston, 2004).

2.1.2.1 Uranium

As stated previously, uranium can occur from anthropogenic pollution. In addition, uranium is naturally associated with igneous and metamorphic geological formations (Earle, 2019a). Uranium sources can come from groundwater interactions of uranium bearing minerals such as uraninite (pitchblende, a primary mineral ore of uranium) or coffinite (Nolan & Weber, 2015). This occurs in the High Plains and Central Valley aquifers in the U.S. (Figure 2.1.2) and may be also added by biotic nitrate reduction. Weathering of sedimentary deposits such as sandstones can also contain elevated levels of uranium. In Nova Scotia uranium is a significant risk in well water and is dominantly controlled by bedrock geology (G. Kennedy & Drage, 2018)(Figure 2.1.3).

Uranium is often released into groundwater through natural weathering and dissolution processes, dependent on pH redox factors (Alam & Cheng, 2014). Mineral release is often the controlling factor for groundwater contamination. De-adsorption from mineral surfaces along with respective reaction kinetics, oxidation conditions and thermodynamics also plays a role in uranium water contamination. Iron and magnesium oxide such as goethite, hermatite and ferrihydrite are known to absorb uranium ions and reduce their mobility and groundwater (Sato et al., 1997). Reductive precipitation often immobilizes uranium (Alam & Cheng, 2014). Other substances enhance uranium transport such as organic matter such as humic and fulvic acids via uranium complexes and thus facilitate U movement throughout the subsurface (Smedley & Kinniburgh, 2023). Carbonate minerals such as calcite or domate enhance the transportation of uranium by forming complexes with uranium ions and allowing them to be more mobile in water.

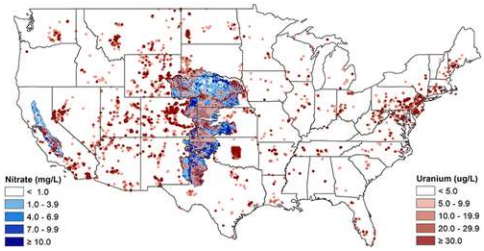

Figure 2.1.2: A map of uranium (red) and nitrate (blue) concentrations for groundwater aquifers in the US (Nolan & Weber, 2015).

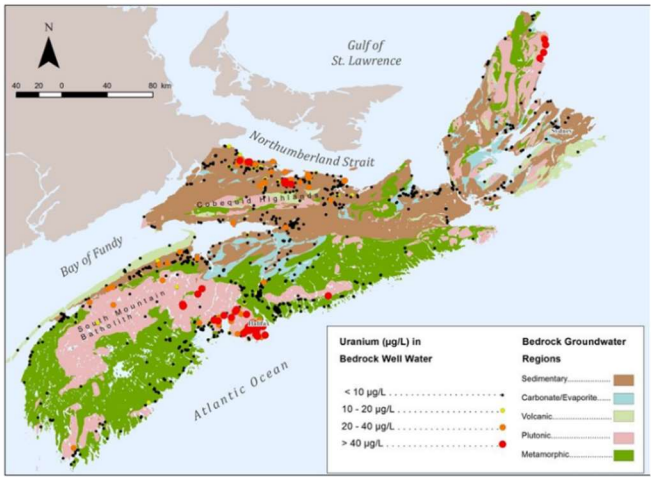

Figure 2.1.3: Uranium in well water/groundwater for Nova Scotia (G. Kennedy & Drage, 2018).

2.1.2.2 Arsenic

Arsenic contamination can be caused by anthropogenic sources. Often it is linked to geological formations rich with arsenic-bearing minerals released into the surrounding soil and water via natural weathering processes; and groundwater interactions leading to leaching and subsequent groundwater contamination (Bradl, 2005). Some recognized examples are arsenopyrite, an iron arsenic sulfide mineral found in hydrothermal mineral deposits, and Pyrite (Earle, 2019b). Arsenic is also naturally present in volcanic deposits and sedimentary deposits such as alluvial aquifers or deltaic environments (Mukherjee & Bhattacharya, 2001).

In Nova Scotia, arsenic contamination is naturally occurring, and influenced by bedrock geology (G. Kennedy & Drage, 2017) (Figure 2.1.5). Arsenic levels were more associated with drilled wells rather than dug or surface levels. Similarly, USGS found that 7% of sampled wells exceeded 10 µg/L for arsenic particularly in the Southwest U.S. and in the Glacial aquifer system in the Northern U.S. (DeSimone et al., 2014). The Pinemont Blue Ridge and Valley area in the Eastern Appalachian region, the Texas coastal upland aquifer system and the Mississippi River alluvial valley aquifer in the Southeastern U.S. are principal concerns for arsenic contamination (Figure 2.1.4). In the Southwest U.S. basin-filled aquifers, arsenic is sourced from volcanic and granitic bedrock (DeSimone et al., 2014). Groundwater residence time, high pH, arid climate and rock type contribute to the elevated concentrations. Internationally, Bengal Delta, Bangladesh, and West Bengal, India are severely contaminated with arsenic derived from Himalayan sediments that has caused an arsenic contamination crisis affecting the lives of millions of people (Mukherjee & Bhattacharya, 2001).

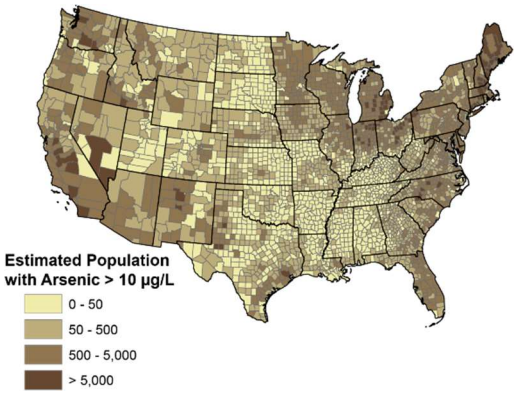

Figure 2.1.4: Estimations of private well users in U.S. counties that are contaminated with arsenic (DeSimone et al., 2014).

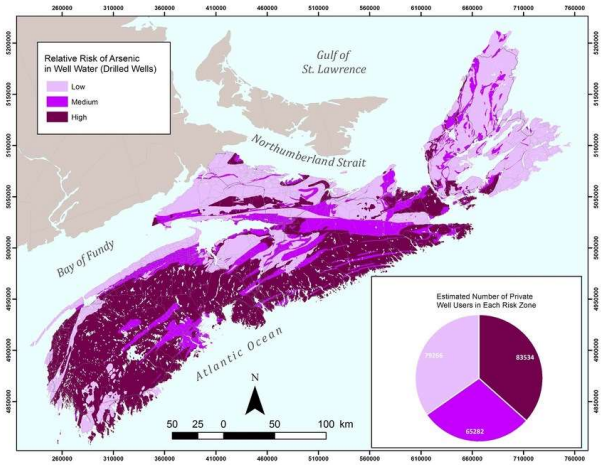

Figure 2.1.5: Arsenic risks in groundwater for Nova Scotia. (G. Kennedy & Drage, 2017)

2.1.2.3 Manganese

Manganese is naturally present in rocks and soils as it comprises 0.085% to 0.095% of the earth's crust and often enters groundwater through the dissolution of manganese bearing minerals and natural weathering processes (Daughney, 2003).

Manganese has multiple optimization states in the natural environment but is commonly found as the reduced water-soluble Mn(II) and the oxidized insoluble Mn(IV) (Z. Zhang et al., 2020). Common manganese oxides include pyrolusite (MnO_2), manganite (Mn_2O_3-H_2O), hausmannite (Mn_3O_4) and psilomelane. Other minerals include manganese carbonates (e.g., rhodochrosite, $MnCO_3$), manganese silicates (e.g., rhodonite, MnCa SiO_4) and ferromagnesian silicates (hornblende, olivine)(Earle, 2019b). In Nova Scotia, manganese contamination is related to sedimentary processes, replacement processes and vein processes (G W Kennedy, 2021).

Said contamination can be more pronounced in areas with low oxygen levels or reducing conditions which favor the release of manganese from minerals (Ahmad, 2012). The oxidized

form of manganese has low solubility in near neutral conditions and thus was found to be invertedly related to pH, which suggested that manganese precipitants form at higher pH levels in the presence of oxygen or carbonate. Elevated manganese concentrations in groundwater are assumed to be associated with less complex or evolved groundwater chemistry, with higher manganese concentrations near shallow water tables (Rusydi et al., 2021). Other studies show an increase in manganese dissolution with increased contact via higher aquifer residence time and increasing with total dissolved solids in a floodplain (Matsunaga et al., 1993). Pyrolusite, manganese oxide and rhodochrosite, a manganese carbonate mineral, are examples where these factors occur.

In Nova Scotia, 22.5% of well water samples exceeded Health Canada's maximum allowance for manganese (G. W. Kennedy & Drage, 2020) (Figure 2.1.7). Unlike other contaminates such as uranium, manganese contamination is also a concern in both bedrock and superficial aquifers in the sedimentary bases due to the geochemistry (G. W. Kennedy & Drage, 2020). The manganese deposits are associated with sedimentary processes hypogene originated, replacement and vein type processes. The carboniferous strata, notably Windsor group limestone or infilling fissures of crystalline rock is associated with manganese ores. Northeastern United States has a similar problem with manganese contamination in groundwater and thus has similar concerns with 46% of well water samples exceeding maximum standards in New England, U.S. (McMahon et al., 2019) (Figure 2.1.6). The province of Quebec, Canada, West Bengal State, India and Bangka Island, Indonesia also report a lot of manganese contamination (Federal-Provincial-Territorial Committee on Drinking Water, 2016; Sujith et al., 2014).

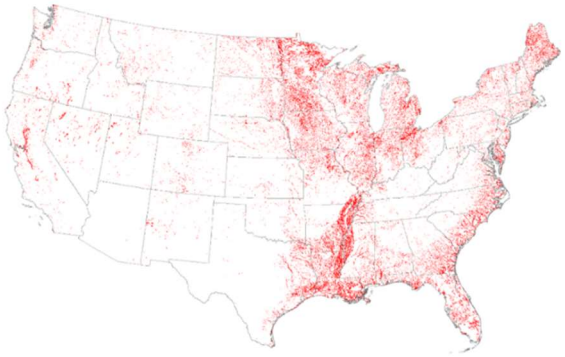

Figure 2.1.6: Red areas are representative of highest population densities that may be consuming water from domestic wells with elevated manganese concentrations (McMahon et al., 2019).

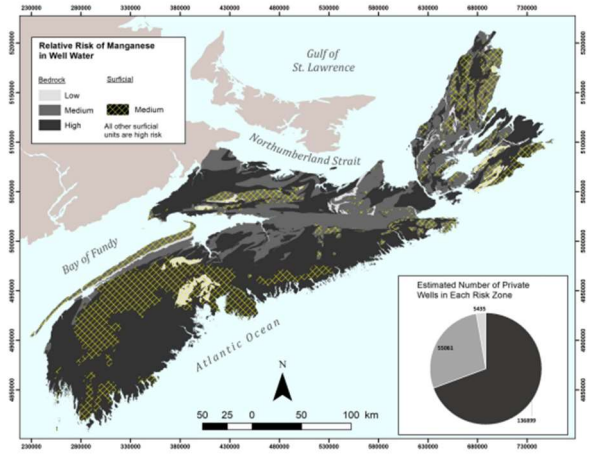

Figure 2.1.7: Mn contamination risk for Nova Scotia, Canada (G W Kennedy, 2021).

2.2 Health Effects of Well Water/Groundwater Metal Contamination

2.2.1 Adverse health effects of specific metals

One major concern related to groundwater metal contamination is the detrimental health effects on drinking water consumers. This section focuses the health effects of well water metal contamination with specific emphasis on the metals mentioned above, and their long-term and short-term effects for vulnerable populations.

Lead contamination in well water is a serious health concern. When consumed, lead accumulates in the body over time and has a detrimental effect on the developing nervous systems of young infants, children and pregnant women (Levallois et al., 2018). Higher levels of lead exposure can lead to neurotoxic effects such as cognitive function impairment, developmental delays, learning disabilities, decreased IQ and behavioral problems in children and adults.

One of the more publicized examples of lead contamination is the Flint, Michigan Water Crisis from 2014 (Hanna-Attisha et al., 2016). Due to lead contamination in the drinking water distribution system, the effect of widespread lead poisoning was studied with noticeable effects amongst young children. In the U.S., lead contamination in drinking water is classified as a prioritized public health issue with the Environmental Protection Agency proposing regulations to replace lead water pipes in U.S. cities within 10 years (US EPA, 2020). The total cost of lead contamination is substantial, as it includes healthcare expenses, structural changes, environmental regulatory changes, and the unmeasurable effects of the individuals affected by

developmental issues and loss of productivity in adulthood (Levallois et al., 2018). Consumption of high amounts of copper from copper contaminated water can lead to gastrointestinal symptoms such as nausea, vomiting and diarrhea (Bost et al., 2016). Prolonged exposure to elevated copper levels in water can result in long term health effects such as liver and kidney damage; the highest risk group being people with pre-existing liver and kidney conditions or genetic disorders that impair copper metabolism (Wilson's disease) (Gerhardsson, 2022). Infants and small children are considered to be high susceptibility to copper toxicity when they drink more water.

Iron contamination of well water gives rise to an aesthetic effect where elevated levels of iron cause unpleasant tastes, a metallic odor and discoloration (Abbaspour et al., 2014; Health Canada, 2022). Excessive intake of iron from contaminated water can cause gastrointestinal discomfort such as cramps, abdominal pain and diarrhea.

Excessive zinc intake through contamination of drinking water results again in gastrointestinal disturbances including nausea, vomiting, and abdominal cramps (Rehman et al., 2018). Over prolonged periods, higher levels of zinc in drinking water interferes with the absorption of other nutrients in the human body, leading to nutritional deficiencies in copper or iron.

Cadmium contamination in drinking water causes kidney damage, including tubular dysfunction and renal failure on a short time scale (Bae et al., 2001). Long-term, cadmium is a classified carcinogen and prolonged exposures to high levels is associated with an increase of lung and prostate cancer. Cadmium can accumulate in bones and lead to osteoporosis and weakening of skeletal systems of the human body (Agency for Toxic Substances and Disease Registry, 2004).

2.2.1.1 Uranium

The primary exposure route of uranium is estimated to be the direct ingestion of well water (Bjørklund et al., 2020). According to the Environmental Protection Agency (EPA), uranium makes up 99% of the toxicological and radiological dose to human consumers (Corlin et al., 2016). The EPA is concerned about potential toxicological and radiological risks to human drinking water consumers. Safe uranium content in water ranges is still being debated with 2.5 - 38 × higher than the current uranium EPA limit of 30 µg/L as the conservative and protective restriction by the EPA regarding to kidney hazards under long-term continuous exposures (Corlin et al., 2016).

Uranium is primarily eliminated by the human body through the kidneys thus elevated and prolonged contamination of it in drinking water results in kidney damage (M. Ma et al., 2020). The damage is related to the nephrotoxicity of uranium directly damaging renal tubular cells and leading to impaired kidney function with decreased filtration and excretion of waste products electrolyte imbalances and chronic kidney disease. This damage to the renal system occurs with accumulation of uranium in the kidneys resulting in inflammation oxidation stretch stress and alterations in cellular metabolism (M. Ma et al., 2020). The buildup leads to impaired kidney function and potential renal toxicity manifesting as Panera tubular dysfunction and acute kidney injuries. This is seen in Northern Sri Lanka where the hydro geochemistry has elevated uranium and cadmium levels and there is a higher prevalence of chronic kidney disease that consists of two to three percent of the population over eighteen years of age (Corlin et al., 2016).

As uranium is a radioactive element, its decay emits ionizing radiation and damages DNA (M. Ma et al., 2020). Uranium exposure is associated with an increase of certain cancers, due to DNA mutations promoting the development cancerous cells of leukemia, kidney and lung cancer. The exact mechanism is complex and often involves both direct DNA damage and indirect oxidation, stress and inflammation (Bjørklund et al., 2020).

Evidence suggests that uranium has adverse effects on reproductive health (Wang et al., 2020). In men, uranium exposure has been associated with decreased sperm quality and altered hormone levels. In women uranium exposure during pregnancy may pose risks to fetuses, potentially lower fetal growth, developmental abnormalities and a risk of premature birth (Wang et al., 2020). Uranium exposure has also been linked to an increase in birth rates of identical twins.

Uranium accumulates in human bone tissue after prolonged exposure and about 90% of the contamination accumulated will remain long term in human bone tissue for about 1.5 years (Kurttio et al., 2005). The effect of uranium accumulation in bone tissue is relatively unknown and requires further research.

The cost of uranium contamination in vulnerable populations is significant, as it includes healthcare expenses related to the diagnosis, and the management of long-term conditions such as kidney disease and cancer. Societal costs of uranium contamination include productivity losses due to illnesses, long term care for those with chronic conditions, and environmental remediation to mitigate and prevent further damage.

2.2.1.2 Arsenic

Arsenic is a known carcinogen. The genotoxic property of arsenic disrupts DNA repair mechanisms, leading to genetic alterations and the development of cancerous cells (Kapaj et al., 2006). Arsenic contamination leads to an increased risk of several types of cancer including skin, bladder, lung and kidney cancer. Dermatology manifestations of high levels of arsenic exposure in drinking water are hyperpigmentation and skin lesions, known as arsenic induced dermatosis which presents as hyperkeratosis to more severe skin cancer (Hopenhayn, 2006). Arsenic can cross the blood-brain barrier to accumulate in the central nervous system leading to neurotoxic effects. Research suggests chronic arsenic exposure is related to an increased risk of cardiovascular disease, inclusive of the development of atherosclerosis, hypertension, heart attacks and strokes (Bae et al., 2001).

Chronic arsenic exposure is also related to an increased risk of cardiovascular diseases (Kapaj et al., 2006). Arsenic induces oxidative stress inflammation, endothelial dysfunction and contributes to the development of atherosclerosis hypertension. This increases risks of heart attacks and strokes. Arsenic related respiratory health effects have been observed via inhalation of arsenic containing particles/dust that leads to respiratory tract irritation and chronic respiratory conditions (Martinez et al., 2011).

Arsenic is also associated with neurological and development impairments. It can cross the blood-brain barrier and accumulated in central nervous system leading to neurotoxic effects (Argos et al., 2012). Prenatal exposure is linked to developmental issues such as impaired cognitive function and increased infant mortality (Rodrigues et al., 2015). Further evidence suggests arsenic disrupts normal endocrine functioning as it interferes with hormone synthesis release and signaling pathways. This leads to the destruction of various hormonal systems including thyroid and reproductive systems.

Even low levels of exposure over prolonged period causes significant health risks (KAPAJ et al., 2006). Inorganic compounds are more toxic than organo arsenical compounds and trivalent arsenide is more toxic than pentavalent arsenate.

Meanwhile the cost of health damage related to diagnosis, treatment and management of arsenic related health conditions such as cancer and severe skin disorders, cardiovascular diseases and neurological impairment is quite substantial. The societal costs may encompass productivity

losses, long-term care for individuals with chronic conditions and public health interventions to address arsenic contamination and provide safe drinking water access.

2.2.1.3 Manganese

In lower doses, manganese is commonly associated with bad tastes, odor, and laundry clothing staining. In fact, Manganese is essential to human health as it acts as a cofactor in the active centers of various enzymes for development maintenance of nerve and immune functions and regulation (Federal-Provincial-Territorial Committee on Drinking Water, 2016).

However, prolonged exposure to elevated manganese levels leads to neurological effects, particularly in infants and children (Rodrigues et al., 2015). Some potential effects include neuro behavioral changes, such as mood swings and irritability. Other effects are more detrimental, including motor dysfunction, with movement and coordination difficulties; or with muscle rigidity, tremors, memory deficits and cognitive impairment resembling Parkinson's disease (Lucchini et al., 2014). Inhalation of manganese containing droplets during everyday activities such as showering or irrigation can lead to respiratory problems, including respiratory tract irritation resulting in coughing, wheezing, and shortness of breath (Federal-Provincial-Territorial Committee on Drinking Water, 2016). Studies show that chronic manganese exposure is associated with a hepatoxicity effect as manganese accumulates in the liver resulting in liver dysfunction and damage. Other studies show an impact on pancreatic function resulting in diabetes like symptoms.

Human and animal studies support the view that high levels of manganese taken internally significantly alters cardio functions by increasing heart rates (O'Neal & Zheng, 2015). Manganese exposure is assumed to inhibit myocardial contractions, dilate blood vessels and induce hypertension which also has a direct effect on mitochondrial functions.

Young infants and children are susceptible to the developmental effects of manganese exposure (Rodrigues et al., 2015). Manganese contamination can cross the placenta and accumulate in developing brains and lead to decreased cognitive abilities motor deficits and behavioral issues in children. The elderly are another population of concern due to the large number of people who develop idiopathic Parkinson's symptoms due to Manganese exposure and may have subclinical pathology (Parmalee & Aschner, 2016). Increased doses of manganese could push them past the point of no return. Gender and ethnicity and genetics and pre-existing conditions like chronic

liver disease also play a factor in manganese toxicity (O'Neal & Zheng, 2015). Manganese blood levels in a 2011 National Health and Nutrition Examination Survey (NHANES) of U.S. residents reported higher Mn blood concentration levels in women than men (Oulhote et al., 2014). It was suggested that sex related metabolic differences may underlie the concentration discrepancy. This was supported by studies among Chinese, Korean, Italian and Canadian populations (Oulhote et al., 2014).

Due to more understanding of the toxicity and biochemistry of manganese accumulation, manganese has started to become more of a governmental concern (Federal-Provincial-Territorial Committee on Drinking Water, 2016; O'Neal & Zheng, 2015). This is a concern in Nova Scotia and U.S., Korea, Italy and China. The cost of health damage associated with manganese varies on factors such as the concentration, duration of exposure, and individual susceptibility. This includes Healthcare expenses related to diagnostic treatment and management in conditions, detoxification and care for those who are critically ill due to health effects. Societal costs also include productivity losses and public health interventions.

2.2.2 Vulnerable Populations and Differential Health Impact

As previously mentioned above, children are particularly vulnerable to the health implications of metal contamination in well water (Mohod & Dhote, 2013). Their developing bodies, neurological systems and organs make them more susceptible to adverse effects when exposed to heavy metal contamination such as lead, arsenic or manganese.

Children may experience developmental effects as previously detailed, including neurological impairments. Lead and manganese adversely impact developing nervous systems and cause cognitive impairments, learning disabilities and behavioral problems that persist into adulthood affecting quality of life (Bae et al., 2001). Manganese exposure disrupts regular brain development and affects attention, memory and intellectual functioning (Rodrigues et al., 2015). Meanwhile, arsenic exposure during critical brain stage development leads to permanent neurological impairments such as decreased IQ, learning difficulties and behavioral issues.

Metal contamination causes growth deformities and developmental delays in children (Rodrigues et al., 2015). Exposure during the critical stages of growth results in delays in motor skills, and overall growth parameters; along with malformed limbs and deformities.

Children are most vulnerable during infancy and early childhood (Hanna-Attisha et al., 2016). Young children between the ages six months to six years or more vulnerable to lead exposure due to the higher rate of hand to mouth behavior, and thus increasing the likelihood of ingesting lead. Developing brains are more susceptible to manganese exposure particularly in infancy and early childhood, in which contamination has long-lasting impact on cognitive function and behavior (Rodrigues et al., 2015).

Pregnant women with developing fetuses are vulnerable to metal contamination in well water due to placental transfer, where metal contamination such as lead, arsenic and manganese can cross the placenta and reach the developing fetus (Rodrigues et al., 2015). This leads to implications such as birth defects for lead, arsenic, and mercury exposure that affects various organ system development and results in long-term health consequences for the unborn child. Arsenic interferes with the embryonic development and disrupts formation of essential organs and structures in developing fetuses (Brender et al., 2006). Arsenic is also associated with birth defects such as neural tube defects, limb abnormalities, and other health defects. Fetal exposure to manganese through the placenta is associated with adverse birth outcomes, including lower birth weight, smaller head circumference and developmental delays (Rodrigues et al., 2015).

During pregnancy, expectant mothers have physiological changes that increase absorption and distribution of metals throughout the body (Brender et al., 2006). This includes an increase in blood volume and hormone level changes thus impacting the way metals are metabolized and transported throughout the body (Oulhote et al., 2014). Arsenic in particular causes an increased risk of pregnancy complications such as preterm birth and preeclampsia (Brender et al., 2006). Lead and arsenic destruct metabolic and hormone processes in maternal bodies leading to disturbances in glucose metabolism, thyroid, and other physiological processes. Prolonged exposure to said metals during pregnancies also carry an increased risk of certain chronic diseases for the mother (Brender et al., 2006).

The elderly and those with compromised immune systems and pre-existing health conditions are also more susceptible to metal contamination in well water (Mohod & Dhote, 2013). Vulnerability of the elderly seems to be widened by advanced age particularly for those above sixty-five years, due to age-related changes in bodily systems and decreased physiological resilience (Gavino-Lopez et al., 2022). Those from lower socioeconomic backgrounds also face

vulnerabilities due to lack of access to proper healthcare, inadequate housing and lack of alternative water remediation. Lead exposure can also further impact cognitive function in individuals with age-related cognitive decline (N. Singh et al., 2017). Manganese exposure exasperates said age-related cognitive decline and leads to further impairment, touching deficits and motor dysfunction (Parmalee & Aschner, 2016). Arsenic exasperates cardiovascular disease is such as hypertension arthrosis and an increased heart attack and stroke risk (Argos et al., 2012).

Heavy metal exposure also exacerbates existing health conditions. People with pre-existing cardiovascular conditions such as hypertension coronary art disease or congestive heart failure are more vulnerable to cardiovascular effects of metal contamination and thus said conditions are exaggerated by arsenic and lead and result in increased risk of heart attacks and strokes (Bae et al., 2001). Those with pre-existing respiratory conditions like asthma, chronic obstructive pulmonary disease or bronchitis may also experience exaggerated symptoms when exposed to metal contaminants, such manganese and arsenic that irritate the respiratory tract (Agency for Toxic Substances and Disease Registry, 2004). Those with pre-existing kidney diseases or impaired kidney functions are vulnerable to the effects of cadmium and arsenic contamination that further compromise kidney functions and worsen existing kidney damage, potentially leading to renal dysfunction and failure (Mohod & Dhote, 2013). People with liver disease like cirrhosis or hepatitis are more susceptible to the hepatoxic effects of metal contamination like arsenic and manganese that contribute to liberal inflammation oxidative stress. Last, patients with compromised immune systems or undergoing immunosuppressive therapies are more vulnerable to the health effects of metal contamination as they have a reduced ability to mount an effective immune response thus have an increased susceptibility to infections and difficulties combating metal toxic effects (A. Singh et al., 2022).

2.2.3 Health Effects of Metal Contamination in Well Water

The toxicity effects of metal contamination in groundwater can be acute, chronic or cumulative. Acute toxicity refers to the immediate short-term health consequences that occur after a single high dose of a contamination (Rehman et al., 2018). Exposure typically occurs over a relatively brief period ranging from minutes to hours and acute effects/symptoms, manifest quickly and have an immediate onset. Examples include gastrointestinal issues from sink water contaminated with its copper leading to nausea, vomiting, diarrhea and destructing normal digestive processes

or high levels of zinc which cause abdominal pain, nausea and diarrhea (Koller, 1980). Another acute effect is respiratory problems from metal contaminated water vapors when showering. Aluminum, for example, leads to wheezing coughing and respiratory distress (Wallace & Buha Djordjevic, 2020).

Chronic toxicity is the long-term effects that develop over an extended period of continuous or repeated exposure to metal contamination (Mohod & Dhote, 2013). The time frame ranges from months to years depending on the substance and exposure duration. Said effects develop gradually and may become apparent after a significant duration of exposure. A common symptom of this is organ damage. Cadmium exposure leads to cadmium accumulations in kidneys and thus causes progressively renal damage (Alvarez et al., 2021). Hexavalent chromium damages the respiratory, liver and kidneys over time.

Cumulative toxicity refers to the gradual accumulation of metal contamination in the body because of repeated and continuous prolonged exposure (Wallace & Buha Djordjevic, 2020). The body may not be able to eliminate or excrete certain metals thus they build up over time and lead to an increasing risk of chronic health conditions. The primary root of exposure is often through ingestion (Mohod & Dhote, 2013). Metals are consumed, absorbed in the bloodstream through the gastrointestinal tract and distributed throughout the body. This buildup leads to increased health risks and potential development of chronic diseases. Some metals have affinities for certain organs and thus buildup of toxin levels occurs in specific tissues (Rehman et al., 2018). This buildup is known to cause carcinogenic effects, especially with arsenic, cadmium and chromium; and systematic effects over various body systems.

2.2.4 Long-term Implications and Potential for Synergistic Effects

Synergistic effects can occur with exposure to multiple metal contamination in well water. In this, the combined toxicity is greater than the sum of individual metal exposures (N. Singh et al., 2017). The interaction of different metals interacting within the body can have potential additive toxic effects as the presence of one metal may enhance the toxicity of another, leading to more severe health consequences.

Synergistic effects occur through various mechanisms including increased absorptions, metabolism and enhanced cellular damage (Cedergreen, 2014). For example, lead and cadmium exposure have a synergistic effect on kidneys (Bae et al., 2001). Both metals do cause kidney

damage but together their toxic effects are amplified and lead to a higher risk of renal dysfunction and severe kidney damage. Arsenic and chromium exhibit synergistic effects on lungs as with exposure to both contaminants, the combined effect on lung tissue is greater than the additive effect of each metal alone and thus increases the likelihood of cancer (Bae et al., 2001).

There are multiple mechanisms to explain how synergistic metals effects increase health issues. One mechanism is via increased absorption and bioavailability enhancement of one metal via another metal contaminate (Cedergreen, 2014). An example of this is if one metal disrupts bodily protective barriers and enabling easier entry for another metal into tissues. Another mechanism is by enhanced cellular damages as the presence of one metal can intensify damage caused by another's via mechanisms such as oxidative stress, DNA damage, destruction of cellular signaling pathways, or interference with enzyme functioning. Last, synergistic effects can be explained by certain metals affecting the metabolism and elimination of other metals and thus leading to accumulation in tissues and prolonged exposure which increases the toxic effects of the involved metals (N. Singh et al., 2017). Synergistic effects often are very common in industrialized, mining or agriculture areas with multiple heavy metal pollutants and emissions occurring at once.

Metal contamination can have both cumulative effects and synergistic effects in the body. Exposure to multiple metals may exhibit both the synergistic effects with combined toxicity greater than the sum of their individual effects and accumulative effects where the metals also accumulate in the body over time (Wallace & Buha Djordjevic, 2020). Thus, the presence of multiple metal contaminates both enhances individual toxic effects and contribute to a higher risk of long-term health problems due to cumulative buildup. An example is the lead and cadmium as previously mentioned (Bae et al., 2001). Not only is there a synergistic effect, both metals accumulate in the body over time leading to cumulative effects on overall health. The combined presence increases the severity of kidney damage and long-term metal accumulation in tissues. Other examples are arsenic and lead which exhibits synergistic effects on neurodevelopment in children and leads to more severe impairment (Bae et al., 2001).

2.3 Climate Change Impacts on Water Resources

Climate change is a global phenomenon that is increasingly becoming a more pressing issue and is caused mainly by the release of anthropogenic greenhouse gases such as methane, water vapor, carbon dioxide and nitric acid oxide (Kumar, 2012). Climate change manifests in various ways such as rising temperature, altered precipitation patterns, rising sea level, and more frequent and extreme weather events. These changes have significant implications for water resources with both surface and groundwater systems being affected. Consideration of these risks and effects is critical for understanding potential risks to water availability and quality thus especially the subsequent contamination of well water.

Global climate change disrupts the hydrological cycle that governs circulation and water distribution (Sýs et al., 2021). This includes increased evaporation from surface water bodies, soil and vegetation via higher temperatures accelerating water kinetic energy (Amanambu et al., 2020). Evaporation increases reduces the water available for groundwater recharge, river flows and water sources that contribute to well water. These effects then influence aquifer contaminate mobility (Peel et al., 2022). Figure 2.3.1 gives an overview of the watershed effects on a groundwater system including that of vegetation/stream (Riparian zones).

Hydraulic cycle changes also impact water storage systems such as reservoirs and lakes, exaggerating water scarcity and forcing populations to rely on groundwater as an alternative source (Sýs et al., 2021). Rising temperatures also diminish snowpacks and glaciers which are a critical recharge source for many regions (Schilling et al., 2020). This reduces the availability of meltwater during the dry season.

Another climate change disruption is the effect on precipitation patterns with timing, duration, and special distribution changes of rainfall (Sýs et al., 2021). This results in more frequent rainfall events in some regions and prolonged drought in others. Altered participation patterns lead to changes in runoff dynamics (Ciszewski & Grygar, 2016). With increased rainfall intensity comes rapid runoffs which cause erosion and sediment transport thus potential for contaminated sediments to enter into river and underground water sources (Basahi et al., 2018). Prolonged dry, reduced runoff results in a reduced recharge rate of water source (Fallahati et al., 2019). This reduction diminishes dilution effects and increases the likelihood of metal contaminations concentrated in well water.

Climate change also affects soil moisture content, a factor that plays a vital role in groundwater recharge (Wossenyeleh et al., 2020). Dry, increased soil moisture deficits reduce results in changing aquifer properties especially vadose effects leading to a higher concentration of contaminants in remaining water sources.

Sea level rise from meltwater can exacerbate the vulnerability of coastal regions, leading to saltwater intrusion into freshwater aquifers and jeopardize potable water sources (Basack et al., 2022a). This also is increased by coastal erosion and storm surges, which further degrade water quality, as salinized wall water infiltrates coastal aquifers.

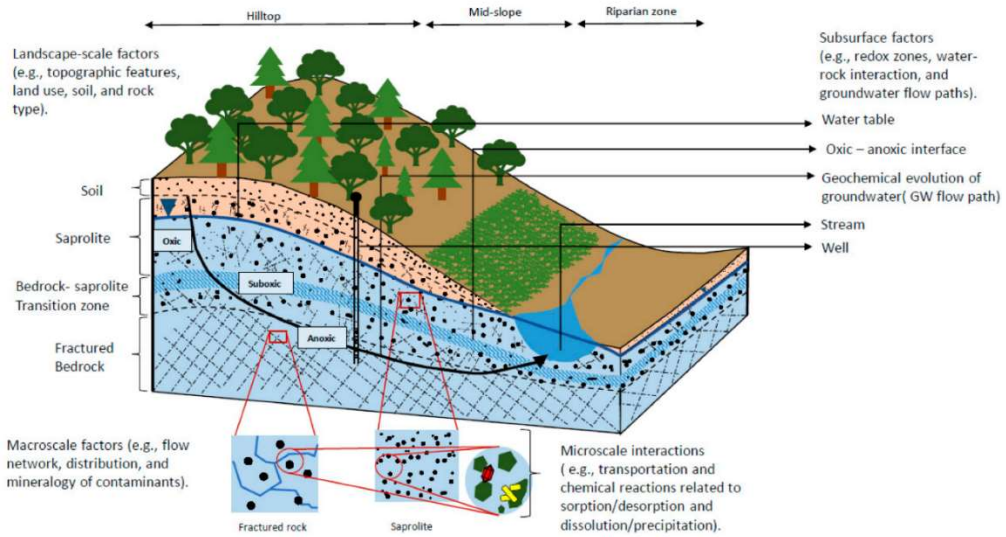

Figure 2.3.1: Conceptual model of groundwater geochemical evolution in saturated and unsaturated zones (Peel et al., 2022). This includes hydrogeochemical factors influencing contamination chemistry. Lithologic boundaries are represented by dashed lines.

2.3.1 Changes in Precipitation Patterns

2.3.1.1 Increased frequency and intensity of extreme weather events

Numerous studies have documented the increasing intensity and frequency of extreme weather events (Amanambu et al., 2020). This includes heavy rainfall, storms, hurricanes, and other intense precipitation events. These have profound implications for water resources and hydrological systems due to disaster events and infiltration (Saeed & Attaullah, 2014). In some areas, warmer temperatures increase atmospheric moisture content and the potential of more intense rainfalls. Excessive rainfall can overwhelm water treatment systems and lead to contamination infiltration into groundwater (Geris et al., 2022). This is demonstrated by Figure

2.3.2. Intense rainfall results in rapid runoff, soil erosion and flooding that pose risks to groundwater contamination of groundwater.

Excessive rainfall contributes to increased erosion and sediment transport especially in areas with steep slopes and inadequate vegetation covers (Geris et al., 2022). The sediments enter water sources introducing sediment-bound metals into groundwater. The generalized increased sediment load also impacts water quality and creates more water treatment processes challenges (Santos et al., 2011a).

More frequent and intense storms/hurricanes are also due to climate change. Warmer sea temperature provides more energy to fuel the weather systems resulting in more intense and destructive storms (Blake et al., 2003). Storms and hurricanes bring heavy rainfall, strong winds, storm surges and increased sediment transfer all which impact water quality in the hydrological systems and increase contaminations of well water with sediments from surrounding areas.

Urbanized areas with inadequate drainage and decreased potential for infiltration are more prone to be affected by flooding (Ciszewski & Grygar, 2016). Urban flooding leads to more runoff during heavy rainfall events and elevate the contamination risk via increases pollution/contaminates from urban areas into well sources. This type of flooding can compromise the integrity of well casing and allow contaminants to directly enter well water systems.

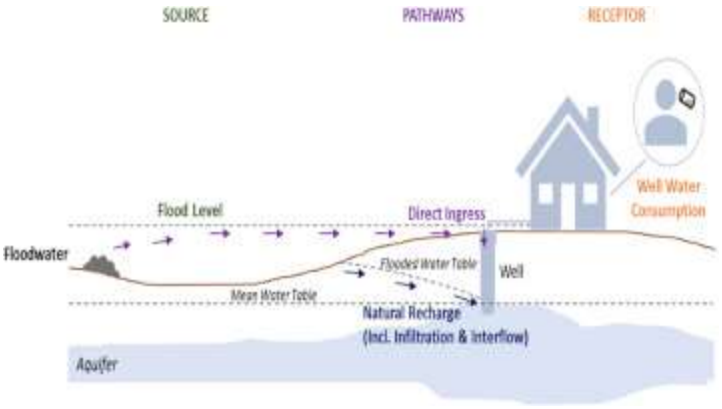

Figure 2.3.2: Schematic to demonstrate the connection between source contamination in groundwater carried by flood events(Andrade et al., 2018)

2.3.1.2 Shifts in regional rainfall patterns

Shifts with the distribution, timing, and quantity of rainfall in different areas another outcome of climate change. These shifts significantly impact water resources including groundwater and influence contamination.

Climate change can cause uneven distribution of rainfall as some regions experience increased rainfall while others experience drought (Barbieri et al., 2023). This results in water scarcity in areas with reduced with rainfall. Reduced precipitation impacts groundwater recharge which lowers water levels in aquifers and increases metal concentration. As the water table drops, previous untouched contamination zones may be exposed and released into groundwater (Appleyard et al., 2006). This also leads to special variations in groundwater distribution as set areas experience localized water scarcity.

Altered poor precipitation patterns can lead to changes in aquifer storage capacity, permeability and porosity (Wossenyeleh et al., 2020). These changes affect the movement of water within the aquifer and the transport of metals to well water sources. In addition, based on said geological characteristics, reduced rainfall and lower aquifer water levels might affect aquifer storage capacity (Wossenyeleh et al., 2020).

2.3.1.3 Implications for water availability and distribution

Precipitation pattern changes have widespread implications for water availability and distribution. Small changes in rainfall patterns lead to the direct impacts of the distribution quality and timing of water sources in both surface and groundwater. Water scarcity caused by reduced rainfall and prolonged dry, reduces the water availability for domestic agricultural and industrial needs (Fallahati et al., 2019). This might increase competition for limited surface water resources and require extensive alternatives such as groundwater. The reliance on groundwater and increased groundwater withdrawal heightens contamination risk due to changes in groundwater dynamics and untouched contamination zones (Fallahati et al., 2019). This results in the need for authorities to increase adaptive measures, water conservation efforts and monitor water quality.

2.3.2 Changes in Groundwater Resources

2.3.2.1 Influence of climate change on groundwater recharge

Groundwater recharge is the process which water infiltrates soil and replenishes aquifers. This is significantly influenced by climate change due to precipitation patterns, temperature and land surface conditions.

Changes in regional precipitation patterns was discussed above. Evapotranspiration is increased with warmer temperature and depletes soil moisture, thus reducing the amount of water for infiltration and decreased groundwater recharge (Figure 2.3.3) (Liu et al., 2020). Soil moisture content is reduced by prolonged dry thus further limiting water availability for infiltration and recharge.

Land use practices such as urbanization, agricultural practices and deforestation alter the capacity of the soil and the natural flow of water into soil and aquifers (Geris et al., 2022). Infiltration capacity, combined with the effects of climate change leads to a decreased groundwater charge and lower groundwater levels. Regions dependent on seasonal snow melt have reduced recharge rates due to the diminished snow accumulation and accelerated glacier melting from climate change temperature rise (JR Williams, 1970). This also affects the timing and volume of water at least during melt season as snowpacks act as a natural reservoir that slowly releases water to recharge in the surface.

Climate change into sea level rise also increases the risk of saltwater intrusion into coastal aquifers (Kumar, 2012) . With seawater infiltrating freshwater, the groundwater is contaminated, and usability is reduced. This leads to an increase in hydraulic pressure altering natural groundwater flow patterns and impeding freshwater infiltration (Nayak & Nandimandalam, 2023). Freshwater and saltwater interfaces shifting in land also reduces the availability of space for recharge and limits freshwater replenishment. These hamper the natural processes that maintain the balance of fresh water in the aquifer.

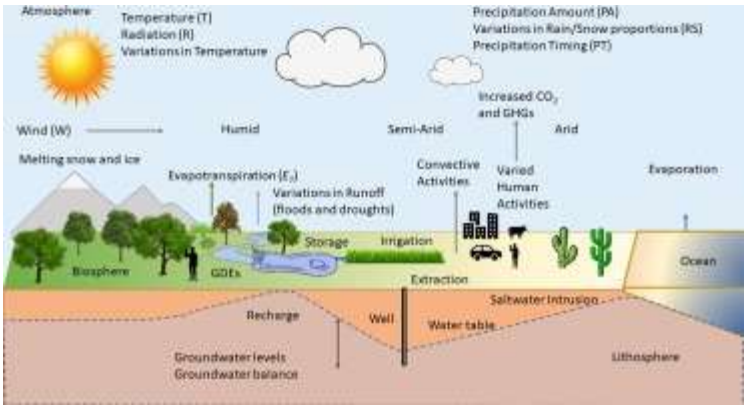

Figure 2.3.3: Schematic of the interaction of groundwater systems with climate change(Amanambu et al., 2020). Direct changes involve precipitation (form and timing), transpiration and evaporation. Indirect changes involve water extraction.

2.3.2.2 Effects of altered precipitation on aquifer levels

As an expansion of previous paragraphs, the recharge and discharge dynamic of aquifers is directly influenced by changes in intensity, distribution and timing of precipitation. Water use in times of drought can also drop groundwater levels.

Recharge reduction is caused by prolonged dry periods and/or decreased rainfall. This limits the water available for infiltration and subsequent recharge due to multiple aquifer and soil interactions (Mosley et al., 2014). Soil moisture content decreases and becomes less permeable, which reduces infiltration rates. Intense rainfall events also limit subsequently infiltration and recharge as via an increase in runoff and surface flow, if the soil is too impermeable or compacted to absorb the excess water. Vegetation dynamics caused by the impact of precipitation on vegetation growth and evaporative transportation also decreases recharge (T. Ma et al., 2020). Decreased plant growth and transpiration reduces the amount of water that is absorbed by the plants and subsequently released into the soil.

Less frequent rainfalls or concentrated intense rainfalls in shorter time periods prolongs times between recharge events (Kumar, 2012). This delayed recharge leads to situations with extraction rates overcoming recharge rates and results in overdraft from groundwater over abstraction (Staben et al., 2015). Aquifer depletion, uncertainties in water availabilities caused by climate change, also encourages well water users abstracting groundwater excessively as a precautionary during reduced rainfall. This overextraction further depletes aquifers. This overextraction can cause an upwelling and a shift in age depth distribution where water is drawn from more contaminated aquifers (Levy et al., 2021) (Figure 2.3.4).

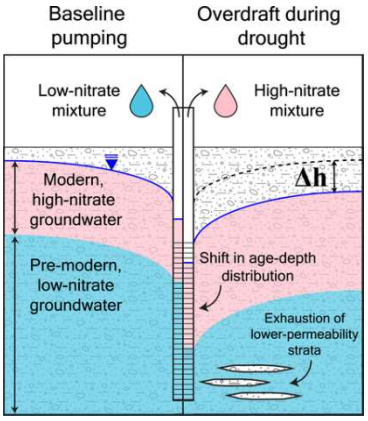

Figure 2.3.4: Model of overdraft effects on hydraulic head Δh and water quality for a well during drought (Levy et al., 2021)

Altered precipitation patterns also affect the seasonal variations in aquifer levels (Riches et al., 2007). Regions that rely on rainfall for recharge find that precipitation patterns changes impact the seasonality of aquifer levels. In dry seasons, less rainfall reduces the infiltration and recharge water amount, demand increases evaporation is increased due to higher temperatures and reduced soil moisture, and thus limits the water from reaching the aquifer (Levy et al., 2021). These interactions lead to lower aquifer levels.

Increased rainfalls can result in higher aquifer levels. Seasons or monsoons give opportunities for infiltration and recharge (Sahu et al., 2020). This along with reduced evapotranspiration rates reduced enhanced water aquifer recharge. Thus, aquifer levels may be higher during wet seasons (Riches et al., 2007). A leg effect between participation precipitation and aquifer response will be seen due to the time required for water to infiltrate soil and reach groundwater (Wossenyeleh et al., 2020). Thus, aquifer levels may continue to rise even after the end of the wet season with this water movement. The inverse will happen during dry seasons - aquifer levels may continue to decline after dry season as water is continuously extracted from the aquifer (Wossenyeleh et al., 2020).

Last, precipitation pattern changes affect the interactions between groundwater and surface water bodies. This can diminish the discharge of groundwater into streams lakes and rivers resulting in decreased base flow (Wei et al., 2016). Base flow is a sustained flow of water from groundwater into surface water bodies such as rivers lakes and streams and helps maintain surface water levels during dry periods. This provides a reliable water source for ecosystems and meeting water demands. In addition, surface water and groundwater are connected interconnected through exchanges that occur along the ground water-surface water interface (Lewandowski et

al., 2020). These may include movement of water from surface water into aquifers or upward movement of groundwater to surface water bodies. Participation pattern changes influence these exchanges through altering recharge/discharge dynamics.

All the above processes have significant implications for the aquifer storage capacity and aquifer understanding aquifer levels. Understanding of these interactions with climate change is critical and necessary for new sustainable water resource management (Amanambu et al., 2020). This includes monitoring aquifer levels assessing new recharge rates and implementing recharge enhancement strategies such as artificial recharge techniques and land management practices. Managing groundwater extraction rates along with promoting water conservation are critical for ensuring long-term sustainability and aquifer availability of groundwater with climate change.

2.3.2.3 Increased risk of groundwater depletion and saltwater intrusion

Increased water demand, rising temperatures, precipitation pattern changes and groundwater deletion depletion also can contribute to saltwater intrusion (Basack et al., 2022a). Saltwater intrusion occurs when saltwater infiltrates its freshwater aquifers and compromises its groundwater quality and usability.

Salt water is held back from inland freshwater systems via hydraulic pressure. The transition zone is where the hydraulic pressure of both freshwater and salt water is equivalent. Said saltwater-freshwater interface is a dynamic mixing zone influenced by tides, pumping rates, aquifer characteristics, head gradients (Basack et al., 2022b). Its behavior is related to the density and salinity to the two water types. Homogenous aquifers will have a uniform transition zone that is a consistent distance from the coastline with a smooth transition of water salinity and well-defined mixing gradient. Heterogeneous aquifers have variations in permeability, porosity and geological structures that influence the transition zone to be more complex and irregular (Hussain et al., 2019). Confined heterogenous aquifers may also exhibit different hydraulic head distributions.

In addition, there are multiple "modes" of saltwater intrusion (Figure 2.3.5). In some, denser saltwater found in coastal aquifers sinks to the bottom forming a saltwater wedge which infiltrates weaker inland freshwater (Basack et al., 2022b). Others such as upconing occur when saltwater rises below and intrudes into a freshwater aquifer, displacing it (Werner et al., 2013). This is observed with excessive pumping near the coastline – the withdrawal of freshwater

lessens the freshwater hydraulic head and creates a cone of depression, drawing saltwater towards the well.

Storm surges, increased sea levels and lower freshwater recharges elevated hydraulic saltwater pressure and press seawater further inland, displacing freshwater (Werner et al., 2013). In addition, storm surges from extreme weather events can cause drive seawater further inland into areas that are not typically prone to intrusion and alter the natural groundwater flow.

Saltwater intrusion makes potable water undrinkable and unsuitable for agricultural purposes due to the salinity level alone. However, it also causes increased corrosion and pitting of well structures that may result in introduced metal contamination (Tansel & Zhang, 2022). Similarly, the groundwater chemistry – pH, conductivity, and redox conditions changes. This in turn impacts the speciation and solubility of metals and can lead to the dissolution of metal contaminates already existing in soils and rock formations (Zhu et al., 2022a)

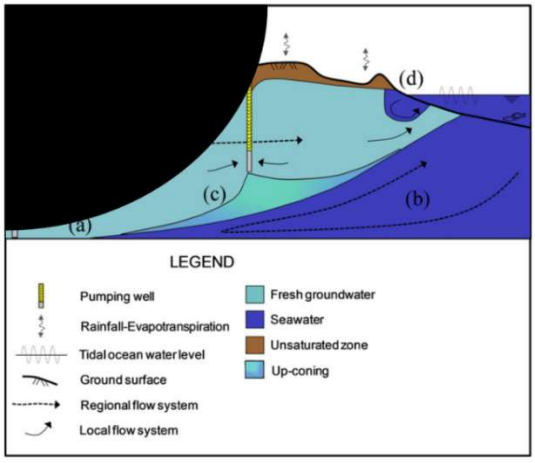

Figure 2.3.5: Diagram of saltwater intrusion in an unconfined aquifer. A) saltwater wedge toe, b) circulation in the seawater zone driven by densities, (c) seawater upconing and cone of depression. (Werner et al., 2013)

Chapter 3: Further Description of British Columbia

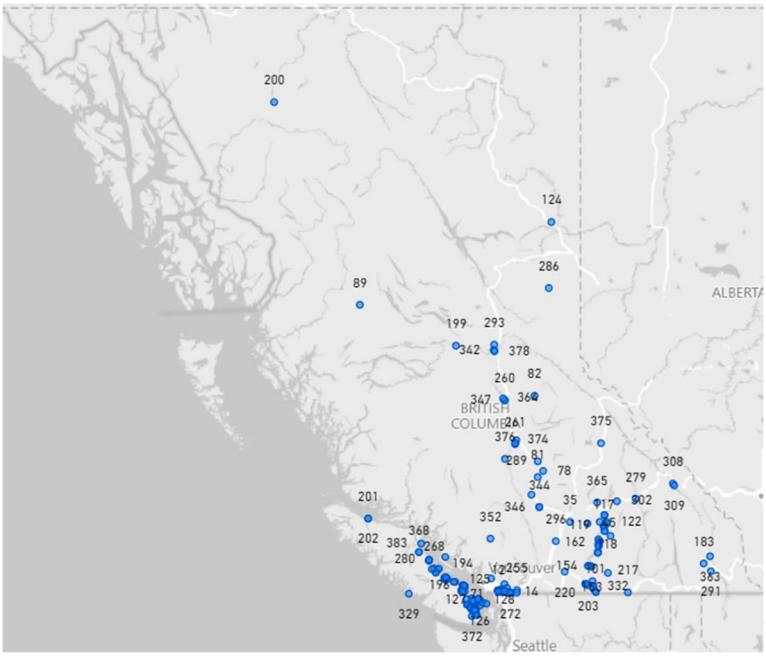

Figure 2.3.1: Power BI Map of observation well stations in British Columbia.

Figure 3.1 shows the observational wells (OBS wells) throughout British Columbia. The corresponding weather stations and maximized map of OBS well locations are seen in Appendix 8.1. The well and weather stations have differing locations that will introduce some inaccuracy. Future research should evaluate this level of inaccuracy on QGIS or ArcGIS via kriging.

Appendix 8.1 shows the map of aquifer regions along with the observed wells and aquifer characteristics. Said mapping only extends to highly industrialized or highly populated areas. This indicates a lack of data that future modeling needs to consider with as it will influence of both groundwater hydraulic and water contamination.

Time constraints meant that well data could not be spatially autocorrected. This is important as it differentiates between spatial influences (such as metals concentration due to a nearby mine) and general underlying patterns in bedrock and geology (Griffith, 1992). Future studies should utilize both Queens and Morran autocorrection as well as relevant kriging for more accurate numerical input. Likewise, spatial clustering algorithms such as DBScan could help further recognize any underlying patterns spatially (Hasana & Fitrianah, 2023). Spatial-temporal clustering such as such a time space cube would enable pattern mining and thus detect heavy metal hotspots throughout time and space (D. Xu et al., 2021). British Columbia is one of the most complex and

unique geological and hydrological provinces in Canada so utilizing satellite imaging research (especially using weather data) and geological RASTERs – especially that of lithology would add data to distinguish between better underlying patterns (Chouaib & Caissie, 2021; Fulton et al., 2004).The 100- and 10-year peak flows are shown in Appendix 8.1. The maximum monthly precipitation for each well given in Appendix 8.1. Though not all the monthly precipitation will go into runoff, it does give an indicator that in a lot of cases the 10- and 100-Year Peak flows would have been exceeded at times. Despite different duration of peak flow charts and monthly precipitations, further indication of floods can be supported by comparing the time of the monthly maximum precipitation to the low flows timing in Appendix 8.1 (D. Allen & Gleeson, 2023). High monthly maximum precipitation values in low flow months especially in colder climates are more likely to be runoff.

Peak flow lines indicate the severity of flooding. 100 Year Peak flow lines are higher magnitudes and may overwhelm flood protection barriers such as levees; and berms for wastewater lagoons and landfills, allowing more contamination to enter aquifers (Weiss et al., 2008). Larger peak flows enable contamination to be transported further laterally during overland flooding, exposing a broader area of subsurface to potential contamination (Hartmann et al., 2021). Recurrence intervals of the 10-year peak flow means that flooding is more frequent, so aquifers are exposed to contamination flooding more often, leading to a cumulative impact over time from less concentrated sources (Santos et al., 2011a). Future research areas could be to relate peak flows, hydraulic connectivity to groundwater metal pollution during flooding for a better understanding of these dynamics.

Maps of low flow zones and annual runoffs are in Appendix 8.1. British Columbia are divided into eight different low flow hydrology zones that are representative of the lowest flow rate during the corresponding driest seasons (Coulson & Obedkoff, 1998). These are broadly representative of water flow regimes, focused during drought, and based on average daily flow. These can coincide with decreased water table pressures, lower hydraulic pressure, and impacts the connected groundwater via reduced recharge (Mohan et al., 2023). Lower flow can affect shallow aquifers connected to intermittent streams or surface water via contamination infiltration during drought periods (Leyden et al., 2016). Reduced over bank flooding diminishes the flushing out of normal contaminates under regular flow conditions.

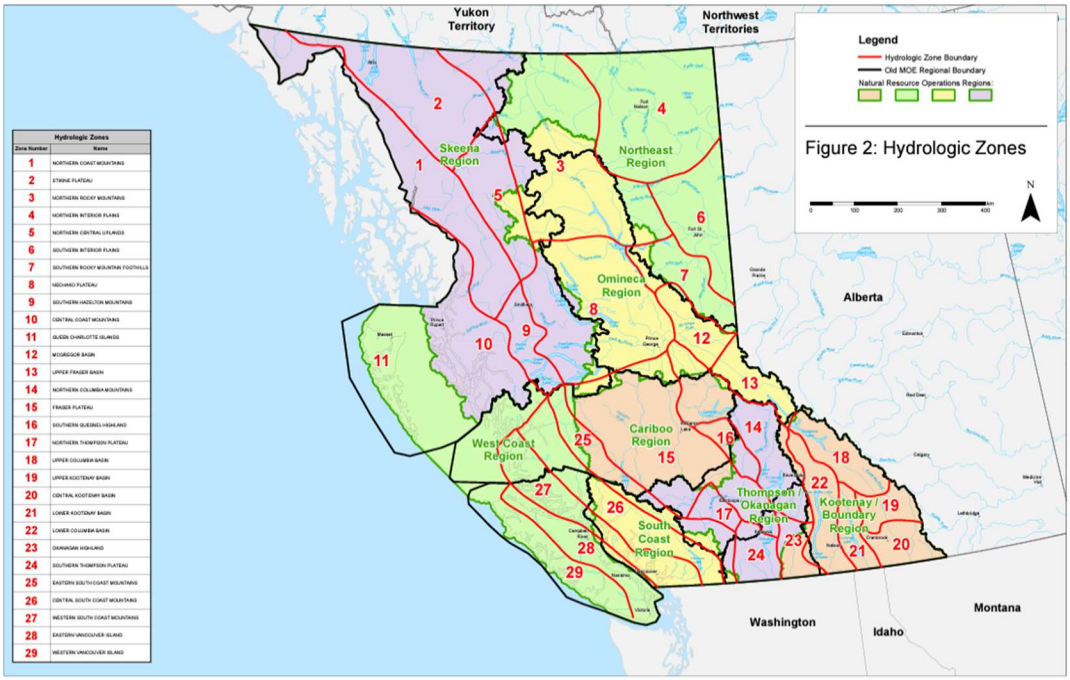

Figure 2.3.2: Map of B.C. hydrologic zones from (B.C. Ministry of Environment and Climate Change Strategy, 2023)

Figure 3.2 shows the previous British Columbia hydrologic zones while updated zones are shown in Appendix 8.1. Hydrologic zones are smaller defined zones have homogenous geomorphological and hydrologic characteristics that allow baseline assumptions to be made for hydrology within the same area (B.C. Ministry of Environment and Climate Change Strategy, 2023). Likewise, said zones indicate if the aquifer is dependent on pluvial (rainfall), nival (snow) or mixed recharge (D. M. Allen et al., 2014). Most of the well stations are located in ten hydrologic zones in the south. The Fraser Plateau had braided outwash channels that transport sediments with contamination from mining over large distances (Larry D. Jones, 1990). Meanwhile, fractured basal causes in the Thompson region transport uranium and arsenic from mineral spread. Appendix 8.1 shows an example of utilizing hydrogeologic boundaries along with B.C.'s stream maps to map and track the effect of mountain pine beetle on the watershed (Schnorbus et al., 2010). It is necessary to spatially link flow streams and watershed basins to aquifer contamination for future studies.

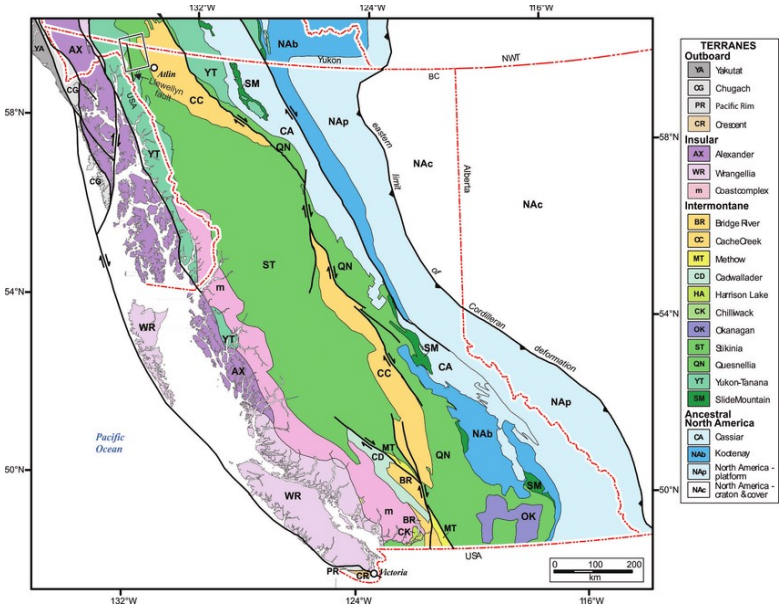

Figure 2.3.3: Map of geological terranes of British Columbia (Ootes et al., 2017) .

A geological map, geologic era of rock map and quaternity geology map of rock in British Columbia are in the Appendix 8.1.

The geology map (Appendix 8.1) explains where sedimentary, volcanic, metaphoric and intrusive rocks are located and what their dominant underlying structure is along with the corresponding timeline. This can indicate where some places might have groundwater contamination. Due to the complexity of this map, the figures of the geologic ear of rock and quaternary geology (Appendix 8.1) and Figure 3.3 provide a better explanation.

The geologic era (Appendix 8.1) represents the outward retreat of the coastline and plate tectonic processes during those time periods. The geology of British Columbia is dependent on that, especially isostatic rebound (land elevation rising after glaciers), connection/formation of different terrains and orogeny (tectonic collision of two plates) (Earle, 2019b). A very generalized overview of the Proterozoic era involved crust thinning and rifts suppressed by glaciers (Mossop & Shetsen, 1994). The Precambrian era involved multiple rifts with a supercontinent breakup. The Mesozoic to Cenozoic involved subduction and continental collisions (Earle, 2019b). The Mesozoic was characterized by terrain accretion and connecting of different continents. Thus, the geological eras represent the different terrains (Figure 3.3) and often are similar to major mineral belts (Ministry of Natural Gas Development, 2016; Ootes et al., 2017). Said terrains influences aquifers as it indicates dominant metals, trapped seawater

intrusion from previous eras, and formations of different aquifer heterogeneity (Ootes et al., 2017). Figure 3.3 also illustrates the major fault lines which indicate slips and different geological processes influences influencing infiltration.

Quaternary geology is the geology that happened from 2.58 million years ago to today (Fulton, 1989). Quaternary geology is primarily influenced during the Quaternary, a period consisting of numerous interglacial cycles. A lot of this geology is dominated by the retreat of the Cordilleran ice sheet and Winstonian glaciation (Fulton et al., 2004). This again will affect groundwater due to mineral deposits left behind by the formation, movement and dynamics of different ice sheets. Appendix 8.1 reveals locations where dominant quaternary geology factors exist.

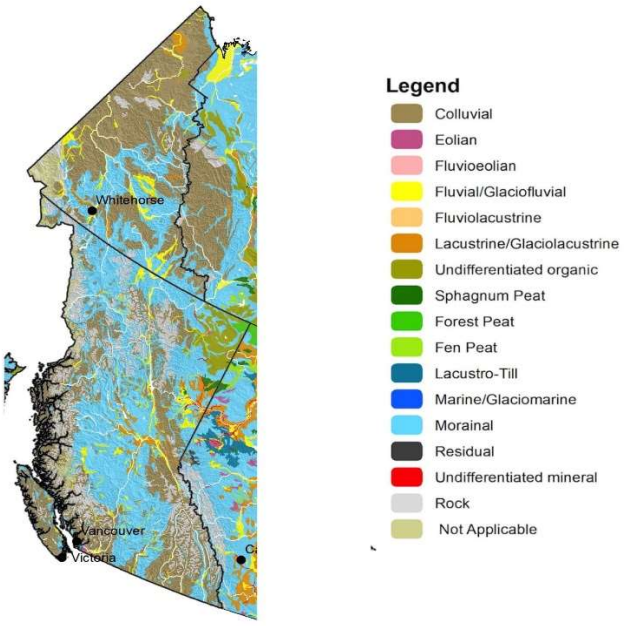

Figure 2.3.4: Soil parent materials in British Columbia (Lavkulich, 2021).

Appendix 8.1 represents the soil groups as specified by the Canadian soil classification that are dominant in B.C. (Lavkulich, 2021; Soil Classification Working Group, 1998). These are often influence the transportation and mobilization of contamination into aquifers.

The permeability of some soils, such as brunisolic soils and Orthic Humo-Ferric Podzols transport pollutants into bedrock aquifers while the acidic conditions of punzelic soil mobilize metals (Lavkulich, 2021). Gleysolic soils may act as aquatards but may as well transport contaminations within saturated lowland conditions (i.e. Saltspring Island Aquifier) (Santos et

al., 2011b). Brunisolic soils have variable oxidative conditions to mobilize Mn naturally and podzolic soils have low pH that enhances metal migration (Weiss et al., 2008). Likewise in the Quesnel highland, uriniferous zones leach uranium into shallow dug wells that are partially controlled by the redox conditions in the brunisolic regolith (Larry D. Jones, 1990).

The parent materials of the resulting soil groups in British Columbia are shown in Figure 3.4. These again influence aquifer contamination as pollutant sources, and via transportation/mobilization.

Alluvium/colluvium are highly permeable materials that rapidly transport contaminants if near/over contaminated sites and transport metals like Mn from mineralized outcrops into aquifers (Y. Yang et al., 2023). Organic compounds such as bogs release dissolved organic compounds and leech metals like manganese under anaerobic conditions (Ciszewski & Grygar, 2016). Meanwhile morainal (glacial drift) deposits containing heterogeneous mixtures of material that can provide multiple flow paths with coarse sediments, transport contaminants and fine sediment trapping plumes (Jia, 2015). With glacial fluvial outwash, for example sands and gravels can spread plumes over long distance especially in the Nelson region (Edwards et al., 2022). Residual soils can mean that weathering will mobilize arsenic in Central B.C. from mineralized bedrock (Lavkulich, 2021). Morainal parental materials are heterogeneous and thus delays flow, which controls contaminant mobility, traps contaminants through absorption, or facilitate plumes through preferential flow paths via course sediments such as kames or eskers (Ganoulis, 2009). Saturation zones within moraines can also mobilize contamination and change redox conditions (Mosley et al., 2014).

Chapter 4: Exploratory Data Analysis

4.1 Methodology for Data Sources, Storage and Management

4.1.1 Water Quality Data

Water quality sampling data was taken from the British Columbia Provincial Groundwater Observation Well Network (OBS) and Environmental Monitoring System (EMS) data repository via British Columbia Data Catalogue (BCDC) by contracting the related data curators(*Data Catalogue*, n.d.). Data was downloaded to a certain degree that the timeframe of samples collected were obtained from 02/01/1982 to 28/08/2022.

The samples utilized were assembled using discrete grab sampling and the corresponding methods of analysis along with full descriptions of corresponding lab codes, and collection methods that can be found in the EMS Electronic Data Transfer support tables (Ministry of Environment and Climate Change Strategy, 2023). Furthermore, sampling was done in accordance with the Manual of British Columbia Hydrometric Standards and Field Sampling Manual.

The assembly of data included a list of EMS ID, location name including OBS well number, longitude, latitude, start date including sampling time, state description, class description, method description, upper depth, lower depth, parameter code, result letter, and results. Following data standards, storage, organization and management are assembled in BCDC Catalogue Standards and Guidelines, according to B.C.'s Open Information and Open Data Policy (bcgov, 2024). Maps of the relevant aquifers and well stations are shown in Appendix 8.1. Moreover B.C. was chosen for analysis as it has an open data policy with more centralized access to water quality data, has a long-standing groundwater monitoring station system in place that frequently measures groundwater quality parameters and has other programs that assess multiple environmental parameters. B.C. also borders the coast allowing for potential saltwater intrusion analysis.

The original dataset of concentration was transformed via python in Jupyter, to transpose it for viewing all contaminants measured at each observation well (OBS) number along with 'start date', EMS ID, latitude and longitude. The upper depth and lower depths were discarded as those

were found to have inconsistent recording in the source data. Furthermore, result letters were discarded to simplify the code and used henceforth. However, time constraints meant that both water temperature and water depth were removed as most values were not linked to the directly EMS dataset.

The resulting dataset was then utilized to assess contents:

(i) Specifically, pesticides, silica, complex organic compounds, and complex toxins which were removed as they are considered unnecessary for the subsequent research analyses.

(ii) Observation Well Stations (OBS) wells, that had no associated concentration data, were as well removed.

(iii) Nitrogen measurement data except for Total Kjeldahl Nitrogen were removed due to lack of consistent data for nitrate/nitrate and to streamline the process as this method is a good general measure of organically used nitrogen because it accounts for biological incorporated nitrogen (Jones Jr., 1987).

(iv) Dissolved oxygen, carbon oxygen demand, total organic carbon and other organic carbon parameters were also removed due to lack of data in the source information.

(v) Total phosphorus has been used to account for phosphorus, including phosphate.

(vi) Dissolved sulfate was used as the measure for sulfur as it was the most complete dataset, acts as quality control for sensing, has the potential for future groundwater source identification, adds insight to anthropogenic activities and helps understand redox conditions (Miao et al., 2012; Porowski et al., 2019)

(vii) In addition, total alkalinity at pH 4.5 (Alkalinity Total 4.5) was used as a measure for alkalinity-based factors.

(viii) Fluoride was excluded due to lack of consistent data.

(ix) Total hardness was kept in the data assembly, along with Potassium and Calcium to facilitate future research potential.

(x) Sodium was removed from the dataset to avoid redundancy as seawater intrusion was measured by other factors.

(xi) Magnesium and calcium were also kept to potentially assist in filling in missing values.

(xii) Furthermore, the following were retained, namely, lead, manganese, uranium and cadmium were chosen as metals. Mn, and U are known to be naturally occurring and were investigated due to their use in future sensor research. Pb was retained despite having potential anthropogenic sources as Pb is required for future research. Furthermore, Cadmium was chosen due to potential future research for mining (although then later dropped after the exploratory data phase) (Butterman & Reston, 2004).

(xiii) Iron was chosen to help indicate any co-interactions between heavy metals and water contamination (Oyem et al., 2015). Other metals were dropped due to lack of data and/or the potential that other metals were caused mostly by anthropogenic means.

Additional data inclusion considerations consisted of:

(i) Saltwater intrusion is measured by specific conductance, chloride, and occasionally turbidity.

(ii) Residue Filterable 1.0u was used as a representation of color measure, residue measures and turbidity, as these constituents had the most complete datasets, which are often used as a turbidity indicator following (British Columbia Ministry of Forest, 2016).

(iii) pH as measured for grab samples was chosen over field values to maintain consistency with the other samples (Ministry of Environment and Climate Change Strategy, 2023).

(iv) Laboratory specific conductance was utilized over field specific conductance,

(v) “Cation Sum”, “Cation - Anion Balance percentage”, “Anion Sum” were deleted due to lack of data consistency.

(vi) Dissolved chloride (“Chlorid:D") was kept as another seawater indicator.

Missing values were filled by:

i. The dissolved values of U, As, Cd, Fe, Mn, Pb, Ca, K, Mg, Hardness, N.Kjel:T, and P, were used to fill in any corresponding missing values of total concentration.

ii. Alkalinity pH 4.5/4.2 values were used to fill Alkalinity Total 4.5 values due to similarity within methods (Ministry of Environment and Climate Change Strategy, 2023).

iii. Missing hardness data values were calculated via the following equation:

$$\text{Hardness} = 2.497\,(\text{Ca}) + 4.118\,(\text{Mg})$$ (U.S. EPA Office of Water, 2021)

iv. Further missing data was then filled by one-half of the lowest minimum detection limit for each element (Appendix 8.2).

Additionally, any missing values of pH were replaced by the pH mean using the closest monitoring system.

4.1.2 Characterization of Aquifer Types

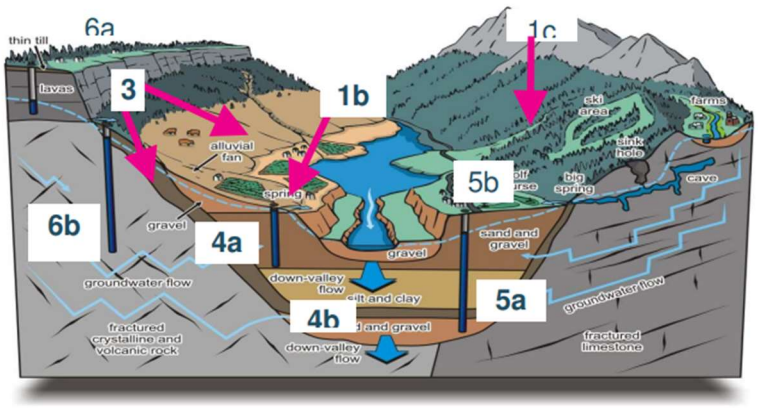

Figure 4.1.1: Diagram of B.C. Aquifer Subtype Classification in the Fraser Valley (Carmichael et al., 2008).

The B.C. Aquifer subtype classification system was utilized to account for differences between unconfined with hydrologic connection, confined, karst and bedrock aquifers (Figure 4.1.1 and Appendix 8.2) by assigning each a different subtype (Mike Wei et al., 2009). Following the aquifer subtypes were further grouped into "aquifer groups" – Aquifer Group 1 (AG1: unconfined with Aquifer subtype 1a, 1b, 1c, 2, 3 and 4a), Aquifer Group 2 (AG2: confined with Aquifer subtype 4b and 4c), Aquifer Group 3 (AG3: bedrock/fractured aquifers with Aquifer subtype 5a, 6a and 6b) and Aquifer Group 4 (AG4: karst based on Aquifer subtype 5b). This grouping is based on general aquifer similarity and similarities of hydraulic connection (Table 3.1.1)(Mike Wei et al., 2009) .

Table 4.1.1: B.C. preliminary framework for determining a hydraulic connection (Wei et al., 2016).

Aquifer Type	Rationale for Likelihood of Connection	Likelihood of Hydraulic Connection
Types 1a, 1b, 1c - Unconfined fluvial/glaciofluvial sand and gravel aquifers (along large, medium and small streams, respectively). Type 2 - deltaic sand and gravel aquifers. Type 3 - alluvial or colluvial sand and gravel aquifers. Type 4a - unconfined glaciofluvial sand and gravel aquifers.	Unconfined aquifers have a high likelihood to be hydraulically connected to a nearby stream(s) because there is no confining layer present to hydraulically isolate the aquifer from an overlying or bordering stream. The stream(s) that pumping of the well is likely to deplete should be specified so demand can be accounted for (see Section 3 for determining impact to specific streams).	Likely connected to an overlying or bordering stream.
Type 4b or 4c - Confined sand and gravel aquifers.	Aquifers that are separated from an overlying or bordering stream by a confining layer that is continuous are likely not considered hydraulically connected to that overlying or bordering stream. However, many aquifers that have been classified as confined aquifers in BC are variably or partially confined and do exhibit hydraulic connectivity to streams. Evidence that may indicate a confined aquifer is hydraulically connected to a stream include: • Lithological information from nearby wells indicating the lithology, thickness and degree of continuity of the confining layer (i.e., evidence of a semi- confined aquifer or windows in the confining layer) or geological evidence that the stream channel has incised into the aquifer, • Observed reduction in streamflow or water levels linked to pumping from the confined aquifer, • Stabilization of the drawdown during pumping.	Not likely connected or does not currently meet the test of reasonably likely to be connected unless there is evidence directly linking the aquifer to specific streams. Site specific evidence or local knowledge is generally needed before presence of hydraulic connection to specific streams can be confirmed.
Type 5a - Fractured sedimentary bedrock aquifers. Type 6a – Volcanic flow aquifers Type 6b - Crystalline bedrock aquifers.	For main valley bottom areas dominated by unconsolidated aquifers, the transmissivity of underlying or adjacent bedrock aquifers are commonly much smaller than unconsolidated aquifers; therefore the contribution to baseflow is generally smaller. For bedrock regions of higher relief, unstratified fractured crystalline bedrock aquifers (type 6b) can be considered hydraulically connected to headwater or tributary streams within their catchment. Additional evidence from pumping may help confirm connection, such as: • Observed reduction in streamflow linked to pumping from the bedrock aquifer, • Stabilization of the drawdown during pumping.	In general, not likely connected or does not currently meet the test of reasonably likely to be connected unless there is evidence directly linking the aquifer to specific streams. In areas of higher relief likely connected to lower order streams within the same catchment. Site specific evidence or local knowledge is generally needed before presence of hydraulic connection to specific streams can be confirmed.
Type 5b -Karstic limestone aquifers.	Although Karst formations are not well studied in BC, these systems can be highly heterogeneous and unpredictable. They can be hydraulically connected to surface water bodies, and potentially can have large conductivity, which can support base flows.	Likely connected.

Further in-depth lithology information was inaccessible due to database issues and therefore not incorporated. Furthermore, most well characteristics, including depth, water level, etc. were sparse and individually linked often on separate pdfs; therefore, other well characteristics were kept only to facilitate later research. Then well data were downloaded via "Well Search" from "The B.C. Groundwater Wells and Aquifers" portal with OBS well numbers, environmental monitoring station ID (EMS ID), corresponding aquifer ID number and well license number (Province of British Columbia, 2023). Aquifer data, including aquifer ID number, and corresponding aquifer type were downloaded via the "Aquifer Search" from "The B.C. Groundwater Wells and Aquifers". Following both datasets were 'cleaned' via Power BI, a business analytics software in Power Query and the aquifer data was merged with well ID data via aquifer ID.

OBS wells that were missing EMS ID and aquifer IDs were mapped and both databases were manually checked to identify any information on corresponding aquifers and wells in those locations. For OBS with unknown aquifers, descriptions of well lithology and nearby aquifers were utilized to determine the potential aquifer type. Table 8.2.1 in Section 8.2 (Appendix) shows the missing OBS well data, indicating how aquifer types were determined, and assumptions made. Furthermore, the linked dataset was downloaded from Power BI and merged into corresponding concentrations via OBS well number in Jupyter and posted in GitHub.

4.1.3 Addition of Data Indicating Temperature and Precipitation

Maximum daily temperature, minimum daily temperature and daily precipitation were downloaded from Pacific Climate Impacts Consortium's "B.C. Station Data" portal for date ranges between 01-02-1985 to 31-08-2022, since these data corresponded to well sampling dates along with a weather station metadata file (Pacific Climate Impacts Consortium, 2024).

I. Only stations that had corresponding climatology and observations were included in the assembly of temperature and precipitation. Soil temperature, soil liquid water contents, rainfall, rainfall 24-hour, rainfall 1 hour and 1 hour precipitation were excluded since there are very few data monitoring stations near the well stations. Furthermore, future research exploration might consider how metal concentration may be affected by 1 and 24-hour precipitation, as those conditions would be more representative of flooding (Mauclaire & Gibert, 1998).
II. Datasets from the B.C. Ministry of Forest were also excluded due to poor matching format. This data seemed to be designed for the purpose of fire monitoring, therefore stations were operational eight months out of a year and had slightly different parameters.
III. Snow-water equivalents and snowfall quantities were also excluded from the data set. This was due to the balance between flooding conditions, drought conditions and due to the difficulty in accounting for inconsistent measured data. Moreover, this acknowledged bias means that drought conditions may not be predicted as accurately as climate change reduces the water from spring runoffs and multiple classifications of droughts are based on said data (Ward et al., 2020). However future research studies could account for changes in snowfall to achieve better and more consistent results.

A second python script with Jupyter notebooks was created to link weather data to water quality measures in the well data.

I. The closest OBS well monitoring station was then matched with the closest weather station data that was operating during the sampling date via looping the station metadata with corresponding concentration station ID and OBS well data set.
II. Stations that have large gaps in operating time were removed from the original station metadata file and the loop was run again.

III. Afterwards, Linked station ID was extracted and merged again with a left join (one to many join) and extracted historic ID, operation network name, and other identifying data sets to form a third metadata file.

IV. The downloaded files containing the individual weather station data sheets with unmatched weather stations were deleted to increase computational speed. In addition, the datasets kept were from BC Hydro (BCH) and Environmental Canada (EC).

V. BCH data sheets had to be re-assessed using a power query and pivot table in excel as the timing of sampling switched from daily to multiple times per day throughout the data set. Therefore, collected results were merged to get "mean" daily temperatures and sum of daily precipitations. Following, the resultant data BCH data sheets were inputting into a Python dataframe containing the weather data.

VI. Both BCH and EC data were then being merged with their corresponding metadata. The data were furthermore concatenated into two dictionaries with the historic ID, station name, native ID, latitude and longitude from the third metadata file.

VII. The following data, namely one day rain, snow and ambient air temperature data were removed, and both dictionaries were concatenated together.

VIII. The monthly sum of one day precipitation, monthly mean of maximum temperature and the monthly mean of minimum temperature were established using Panda's date time. Then remerged with the third reference frame again.

Similarly, the corresponding climatology data set was downloaded from Pacific Climate Impacts Consortium's "BC Station Data" portal for date ranges and inputted to a Jupyter Pandas dataframe (Pacific Climate Impacts Consortium, 2024).

.

I. The resulting data frame was then merged with the precipitation climatology data set via the matching station and month, to create a working data set.

II. Missing values for precipitation, minimum temperature and maximum temperature were then extracted, removed from the first weather station metadata and the process was run again.

Figure 4.1.6 demonstrates the data model used.

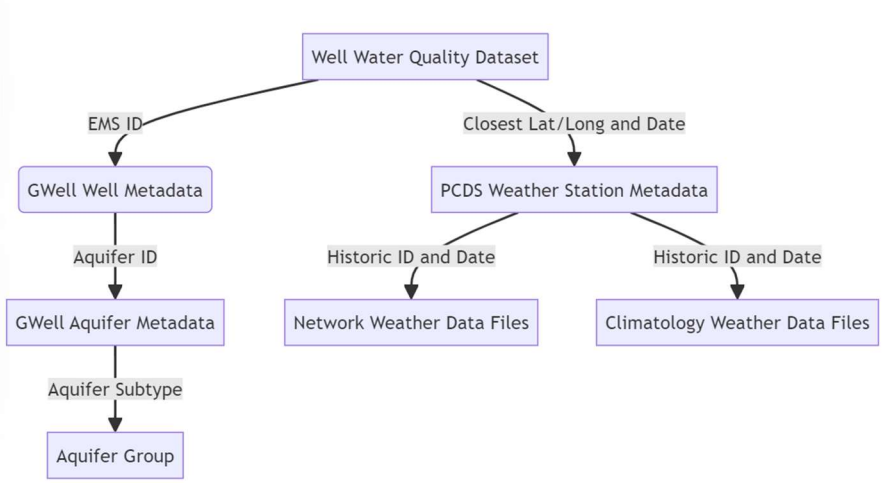

Figure 4.1.2: Snowflake data schema model.

4.2 Methodology for Preliminary Exploratory Data Analysis

4.2.1 Metals Preliminary Exploratory Data Analysis

Power BI was utilized for the initial exploratory data analyses due to its ability to rapidly explore data structures via 'filters' and 'slicers'.

I. Each metal of interest (Metals: As, Cd, Mn, Pb, and U) had their respective concentration magnitudes alongside the Guidelines for Canadian Drinking Water Quality limits plotted against "Other" corresponding factors that influence metal contamination. "Others" include Alkalinity, Fe, K, N, Ca, P, Sulfate, hardness and pH. This was to assess any influence of Others and was accomplished using scatter plots. Numbers from previous missing values from missing value step IV in 4.1.1 were removed via a filter.

II. In addition, each metal listed with the respective Guidelines for Canadian Drinking Water Quality limits were plotted against the seawater intrusion factors (SWI: Chloride, Residual Non Filterable 1 ug, Specific Conductance) and the corresponding cut off for seawater intrusion (Chloride ≥ 150 mg/L, Specific Conductance ≥ 1000 µS/cm, residual non filterable ≥ 700 mg/L) in scatter plots (British Columbia Ministry of Forest, 2016). This was to understand the influence of saltwater intrusion on said metals. Further discussion of this is in Appendix 8.2 and in Section 4.5.

III. Each unfiltered variable of Others, SWI and metals were then plotted against its own count to characterize the distribution of the data. The data was heavily skewed right in most variables.

IV. Scatter plots of each concentration of others, metals and SWI against time (in years) were made as well to understand variations throughout time. Further discussion of this is in Appendix 8.2 and in Section 4.5.

V. To further assess temporal variations, line graphs of metals and others, these were plotted against time in years with data summation set on “mean”. Further discussion of this is in Appendix 8.2 and in Section 4.5. SWI line graphs for time were created with data summation set on “max” as “mean” values do not account for wells with seawater intrusion. The average well does not have SWI and thus using mean instead of Max will not show anything.

VI. Duplicate line graphs for others and metals vs time and drilled down to “month” to observe any potential seasonality differences. Further discussion of this is in Appendix 8.2 and in Section 4.5.

Both scatter and line graphs were then filtered by “aquifer groups” to observe the differences between different aquifer types. Further discussion of this is in Appendix 8.2 and in Section 4.5.

Likewise, both scatter and line graph were filtered with the following (British Columbia Ministry of Forest, 2016):

I. Chloride ≥ 150 mg/L,

II. Specific Conductance ≥ 1000 µS/cm

III. residual non filterable ≥ 700 mg/L

IV. The metals of interest are ≥ the respective Guidelines for Canadian Drinking Water Quality limits(Canada, 2014).

The results of these were discarded as the exploratory data analysis had better methods to characterize patterns.

4.2.2 Second Preliminary Exploratory Data Analysis

The final data set was further processed in Power BI’s Power Query.

I. The time of sampling was split from the date of sampling, as linking done via sampling date was infrequent in the exact time.

II. The precipitation monthly climatology was subtracted from actual precipitation monthly values to account for flooding/droughts (‘FD’).

III. The minimum temperature climatology was subtracted from the mean monthly minimum temperature to obtain a representation of increased minimum temperature due to climate change ("MT"). The maximum temperature climatology was subtracted from mean monthly maximum temperature to obtain a representative with the potential rising maximum temperatures via climate change ("HW"). Both minimum and maximum temperature were used because minimum temperatures seem to be asymmetrically more affected by climate change and the decrease in diurnal temperature range is indicative of climate change impacts (T. R. Karl et al., 1993).

IV. Following a final star schema table was created by removing the dataset of most unused identification IDs for clarity.

The climatology values used to indicate climate change effects were simulated for the year 2000 despite global warming being far noticeable before then. This is due to PCBC's climatology modeling. In further studies, there may be reasons to consider better simulated values. Furthermore, the method to account for precipitation and temperature was chosen because it was determined as the best way to include geography. However, the effect of one- or two-week heat waves is minimized using this procedure(T. R. Karl et al., 1993). Future exploratory analyses should include more localized time series to better account for heat waves. In addition, future exploratory research may furthermore benefit by accounting for the more than month-long effects of droughts on wells and the groundwater system in general.

Power BI was utilized to further extend the data analyses due to its ability to rapidly explore data structures via "filters" and "slicers". Further discussion of the results is in Appendix 8.2 and in Section 4.5

I. Other factors were graphed against precipitation, mean minimum monthly temperature (min temp), mean maximum monthly temperature (max temp), FD, MT and HW using scatter plots.

II. Metals along with the corresponding Guidelines for Canadian Drinking Water Quality limits were graphed versus precipitation, mean minimum monthly temperature, mean maximum monthly temperature, FD, MT and HW, in scatter plots.

III. SWI factors along with corresponding seawater intrusion cut offs were graphed against precipitation, mean minimum monthly temperature, mean maximum monthly temperature, FD, MT and HW in scatter plots.

IV. Scatter plots summarized by mean values and line plots summarized by mean values were made for precipitation, FD, MT, and minimum temperatures plotted against time.

V. Scatter plots and line graphs with data summation set on 'max' were made for maximum temperature and HW, were then plotted against time to show the temperature effects of climate change over time.

VI. The line graphs time for precipitation, FD, HW, MT, max temperature and min temperature which were changed to "month" to identify the presence of any potential seasonality patterns.

VII. Precipitation, FD, HW, MT, and minimum temperature were subsequently plotted against their own data count to view the data distribution. The data in this case was reasonably distributed.

Both scatter and line graphs were then filtered by "aquifer groups" to observe the differences between different aquifer groups with climate change. Further discussion of this is in Appendix 8.2 and in Section 4.5.

Likewise, both scatter and line graph were filtered with the following (British Columbia Ministry of Forest, 2016),(Canada, 2014):

I. Chloride ≥ 150 mg/L,

II. Specific Conductance ≥ 1000 µS/cm

III. residual non filterable ≥ 700 mg/L

IV. The metals of interest are ≥ the respective Guidelines for Canadian Drinking Water Quality limit.

The results of these were discarded as the exploratory data analysis had better methods to characterize patterns.

4.3 Methodology for Exploratory Data Analysis

4.3.1 Data Processing

The remainder of the exploratory data analyses were completed using Jupyter notebook via python libraries. Python was chosen over R due to the ease of optimizing the processing speed

and due to the seaborne library. Furthermore, aquifer subtype was classified into three aquifer groups described in 3.1. No observation wells were identified as being on karstic limestone aquifers.

Summary statistics were calculated for the entire dataset. This meant, the mean, variance, standard deviation, maximum value, minimum value, skew, median and kurtosis, along with the 10%, 50% and 90% percentiles for each variable dimension using both numpy and Pandas libraries were saved as a CSV.

The summary statistics were then used in subsequent analyses to guide the scaling and data analysis techniques used. Following, percentiles of 10%, 50% and 90% elsewhere were chosen as previous Power BI analysis and forewarned of significant skewness, that in certain situations higher values were meaningful.

In addition, lower values may be highly sensitive to database normalization while higher values of metal concentration indicate contamination that could be past Canada's Drinking Water Guidelines. For example, uranium, due to the right skew, would have a large proportion of metal concentrations that are low. This is expected but influenced via detection limits and data gathering. Furthermore, to balance that issue while minimizing the effect of scale, extreme outliners needed to be replaced to maximum Canadian Drinking Water Guideline. In addition, the 90^{th} percentile served as a check to see if it was above Canadian Drinking Water Guidelines.

4.3.2 Outlier Removal

Outliers were removed next before scaling as some columns/data dimensions (such as maximum temperature) had impossible values (9999) that indicated equipment failure and therefore called for removal. However, other values such as factors of saltwater intrusion were expected to be higher, and the structure needed to be preserved.

Due to the data set being multidimensional and skewed with large differing scales, most outlier methods and removal methods including that of threshold multipliers and standard deviation were unsuitable. When used, threshold multipliers often remove large chunks of data in pH and similar columns due to the scale and skew of the full data set. Furthermore, the data set, reduced by threshold multipliers or standard deviation methods also indicated that there were no wells with saltwater intrusion. However, the previous Power BI analyses showed otherwise (Section 8.2, Appendix).

The removal method of outliers that gave an appropriate data set was replacing the outliers with interquartile thresholds (IQR) (Qingkai Kong et al., 2020). This method removed impossible outliers such as temperature extremes while maintaining outliers of metal concentrations above CDWG limits and SWI values over cutoff limits as indicated by the calculated summary statistics.

I. A function was created that calculated the 25th percentile and 75th percentile along with the IQR.
II. The upper and lower thresholds were 1.5 * IQR of both quantiles.
III. Anything above and below said thresholds was an outlier. Moreover, outliers were replaced with upper and lower thresholds instead of the means to preserve the data structure. This method covers 5% to 95% of the range and is far above the cutoffs for saltwater intrusion.
IV. If the upper threshold was still below a metal of interest's CDWG limit or SWI intrusion cutoff, it was not replaced.

Potential bias may have occurred as this considers each dimension as a single dimension and some metal concentrations such as uranium may have already been affected due to the right skew given that only four samples were above the Canadian Drinking Water Guidelines while the dataset contained multiple missing (thus replaced with half the concentration detection point) and samples with low concentrations.

4.3.3 Scaling and Normalization:

The severe right skew of some dimensions is contrary to the assumptions of regular normalization methods(Hastie et al., 2009). Other dimensions were not as skewed but had a severe difference in scale. Originally, both log and square root transformations were tried, and summary statistics were calculated. However, the skew values of some dimensions increased and were still far above unity.

In addition, monthly precipitation and minimum temperature had negative values. The scale needed to be similar to conserving computer processing time in most all data techniques. Therefore, the Yeo-Johnson Transformation was used for power transformation from Sklearn's Library (Hastie et al., 2009). This transformation inflates low variance data and deflates high variance data and creates some additional normalized uniform data set. However, this method

also decreases the significance of one dimension over others and makes summary graphs more difficult to read.

Summary statistics were further calculated and saved as CSV with said transformations producing the most appropriate skewness for each dimension/variable.

4.3.4 Correlations

The Pearson correlation coefficient matrix was calculated and saved as a CSV file to assess the linear relationship between variables. Likewise, the Kendall correlation matrix was calculated to identify the ranking of how each individual variable influences each other variable(Helsel et al., 2020). Last, the Spearman rank correlation matrices were calculated and saved as a CSV to assess nonlinear increases/decreases between each variable.

4.3.5 Mahalanobis Method for Multivariate Outliers

To assess multivariant outliers, the Manhalanobis method utilized SciPy (Hastie et al., 2009). Therefore, aquifer groups were encoded utilizing ‘one hot encoding’ method to account for non-ranking, categorical variables. Then the inverse of the covariance matrix and the data center was identified. Following, the data was regularized by adding a small constant to the day and the mean was identified.

An empty list was then created to store the Manhalanobis distances and the distance for each row was calculated utilizing the Manhalanobis row means, and inverse coefficient. Said distances were added to the data frame and the 99% cut-off for two-tailed chi-square test was found.

Outliers were then identified to be where the Manhalanobis distance was above said threshold. Without previous IQR outlier removal, this method removed over 50% of the data. With both previous transformation and previous outlier removal, 30 rows were removed which consisted of 3% of the data set. These data values were left in the data for future analyses to avoid over fitting.

Once the corresponding quantiles plot was plotted, with the Manhalanobis distances and then, calculated normal quantiles were given a normal distribution: Section 8.2 (Appendix) shows the resultant figure. This resulted in skewness and nonlinearity which could result in overfitting, therefore, was discarded.

4.3.6 Plot Generation

Plots that were too difficult to quickly create in Power BI were then generated via Seaborn (Appendix 8.2 and Section 4.6).

I. A graph was used to display the count of well samples per year and month for each aquifer group which was generated.
II. The graph and the amount of well aquifer samples per each OBS well with each aquifer group was generated.
III. A data frame called “metals total” which included As, Cd, Mn, Pb, U and aquifer group was created and a scatterplot (pairplot), histogram pairplot, and kernel density estimator (KDE) pairplots were generated.
IV. Another data frame for Precipitation factors [Precipitation, Min_Temp, Max_Temp, MT, HW, FD, Aquifer Group], then a scatterplot pairplot, histogram pairplot and kernel density estimator (KDE) pairplots were generated.
V. A data frame called OthersD was created with “Alkalinity Total 4.5”, “Ca-T”, chloride (“Chlorid:D"), “Fe-T”, “Mn-T”, “N.Kjel:T”, “P--T”, “Residue Filterable 1.0u”, “Specific Conductance”, “Sulfate:D", “pH”, “Hardness Total (T)”, “K--T”, and “Aquifer Group”. Then a scatterplot pairplot, histogram pairplot and kernel density estimator (KDE) pairplot were generated.
VI. Boxplots of each metal in each aquifer group were generated as well utilizing the scaled and transformed data.
VII. Scatter plots of each metal with the maximum limit for the Canadian Drinking Water Guideline over time was then generated from the unscaled data.
VIII. The count of the total amount of well samples for each above the standard was then determined.
IX. Sea water intrusion factors were graphed with the corresponding maximum for seawater intrusion throughout time in scatterplots from unscaled data.
X. The count of the total number of well samples for each, above the seawater intrusion, was then determined.
XI. Heatmaps of the maximum temperature per well over time in years, the minimum temperature per well over time in years, HW per well over time in years, MT per well

over time in years, nearby precipitation per well over time in years and FD per well over time in years were generated.

XII. In addition, heatmaps for seawater intrusion per well over time were generated utilizing specific conductance, chloride and Residue Filterable 1.0u'.

4.4 Methodology for Exploratory Data Analysis of Climate Change Factors

4.4.1 Potential Flood, Drought and Temperature Increases

Analyses of climate change factors were carried out in Python via the 4th Jupyter notebook.

For flooding, rows were taken in which FD > zero.

I. The number of wells above the Canadian Drinking Water Guideline limit were calculated for As, Mn, Pb and U (Section 4.2).
II. The total wells above seawater intrusion cut off limits were calculated for chloride, residue filterable 1.0u and specific conductance.
III. Outliers from the data set were removed as explained above and data was scaled via Yeo Johnson method using power transformer.
IV. Summary statistics, Pearson matrix, Kendall rank matrices, and Spearman correlation matrix were calculated and saved as CSV.
V. Furthermore, similar scatter, histogram, and KDE pairplots for “Other, metals and precipitation factors” as previously described were generated.
VI. Scatter Plots comparing each metal of interest with each variable/factor were generated via looping throughout the data set.

The resultant plots for flooding are shown in Appendix 8.2 and discussed in Section 4.6. Furthermore, Spearmen correlation matrices and additional summary statistics were deemed redundant and excluded.

A fifth Jupyter notebook which ran the same process was used where FD < 0 to analyze potential drought conditions. Alongside the effect of increasing temperature rise was analyzed by a sixth and seventh Jupyter notebook running the same process as above. The sixth notebook analyzed rows with HW > 0 to determine how the datetime temperature could influence potential contamination. The seventh notebook analyzed rows with MT > 0 to analyze any potential patterns between increasing nighttime temperature and other factors.

4.4.2 Exploratory Data Analysis for Sea Water Intrusion

The eighth Jupyter script took rows with Residue Filterable 1.0u' > 750 mg/L to analysis the effect of it on different factors and to figure out how accurate of a predictor it is for seawater intrusion.

I. The number of samples for As, Mn, Pb and U, that were above their respective Canadian Drinking Water Guidelines limit was calculated.
II. The amount of additional saltwater intrusion factors such as chloride and specific conductance above the respective cut off values for saltwater intrusion were additionally calculated.
III. Outliers were removed and the data set was transformed as previously described.
IV. Following summary statistics, Pearson correlation matrices, Spearman's correlation matrix, and Kendall rank matrices were calculated and saved as CSVs.
V. Scatter pairplots, histogram pairplots and KDE pairplots were calculated for metals [As, U, Pb, Mn, Cd, Aquifer Group],
VI. Scatter pairplots, histogram pairplots and KDE pairplots were calculated for OthersD [OthersD: “Alkalinity Total 4.5”, “Ca-T”, “Fe-T”, “N.Kjel:T”, “P--T”, “Sulfate:D", “pH”, “Hardness Total (T)”, “K--T”, “Aquifer Group”].
VII. Scatter pairplots, histogram pairplots and KDE pairplots were calculated for sea water intrusion factors (SWI: “Chlorid:D", “Residue Filterable 1.0u”, “Specific Conductance”, “Aquifer Group”).
VIII. Scatter pairplots, histogram pairplots and KDE pairplots were calculated for climate factors (Prep: “FD”, “HW”, “MT”, “Aquifer Group”, “PRECIPITATION”, “MAX_TEMP”, “MIN_TEMP”).
IX. Scatter plot graphs of As, Mn, Pb, U against each variable/dimension were created.
X. Then scatterplots of Cd, U, Pb, and Mn and respective drinking water standard limits were plotted against time for each aquifer group.
XI. Chloride and specific conductance were as well plotted against time for the aquifer group to understand any potential change in variables in wells that already were consistent with saltwater intrusion.
XII. The number of samples over the Canadian Drinking Water Guidelines limit for As, Mn, Pb and U and the number of samples of chloride and specific conductance that were

above the seawater intrusion cut off were calculated as a check to evaluate the effects of outlier removal.

XIII. Heatmaps of specific conductance and chloride throughout the years per well were then generated to further visualize the effects of seawater intrusion.

Additional Jupyter scripts ran similar analysis that focused on different combinations of sea water intrusion indicators:

I. The ninth Jupyter script took rows with ‘chloride'> 150 to analyze the effect of it on different factors and to figure out how accurate of a predictor it is for seawater intrusion. The number of samples for As, Mn, Pb and U that were above their respective Canadian Drinking Water Guidelines limit was calculated. Then the amount of additional saltwater intrusion factors such as chloride and specific conductance above the respective cut off values for saltwater intrusion were also calculated. Scatterplots of Cd, U, Pb, and Mn and respective drinking water standard limits were plotted against time for each aquifer group.

II. The same process as the 8th script was then repeated with Residue Filterable 1.0u replacing chloride in scatterplots and the heatmap.

III. The tenth Jupyter script took rows with specific conductance > 1000 µS/cm to analyze the effect of it on different factors and to figure out how accurate of a predictor it is for seawater intrusion. It replaced specific conductance with chloride in the scatterplots and heatmaps.

IV. Jupyter script eleven took rows with specific conductance > 1000 µS/cm or “chloride” > 150 mg/L to analyze whether both factors should be considered.

The key results are summarized in Section 4.7 and Appendix 8.2 focusing on IV. as other combinations were deemed to have an insufficient amount of data.

“Jupyter script 12” was used to further identify the underlying data structures of multiple seawater intrusion factors/identifiers.

I. Data rows in which all three seawater intrusion measures were above the respective seawater intrusion limit were filtered into a data frame (DataAll) and the number of samples with As, Mn, Pb or U over the respective limits were calculated.

II. A data frame with rows where both the chloride and residue filterable over their respective sea water intrusion cutoff was created and the number of samples with As, Mn, Pb or U over the respective limits were calculated.

III. Another data frame consisting of the rows in which both specific conductance and residue filterable were over their seawater intrusion cut offs, was created and the number of samples with As, Mn, Pb or U over their respective limits, along with chloride were calculated.

IV. Last, a data frame where both specific conductance and chloride were over their respective limits, (DataSCCl) was created and the number of samples with As, Mn, Pb or U over their respective drinking water limits along with residual filterable 1u were calculated.

V. Outliers were removed as previously described and Pearson correlation matrices, Kendall rank matrices, and spearman's correlation matrices were calculated for both DataAll and DataSCCl script.

VI. The script did not transform data due to the low amount of data set.

VII. Scatter, Histogram, and KDE pairplots/pairwise plots were run for metals, Prep (precipitation variables), SWI factors and others as previously described from DataAll.

VIII. Metals were then plotted in a scatter plot through time with the respective limit from the Canadian Drinking Water Guidelines for both DataAll and DataSCCl.

IX. The concentration of metals over said limit was then recalculated to check on the effects of outlier removal.

X. A heat map was then generated for concentration of manganese well throughout the year as it tended to exceed the drinking water standards limit more than the other metals.

The key results are summarized in Section 4.7 and Appendix 8.2. The heat maps and plots were deemed redundant due to having too few datapoints and hence omitted.

4.5 Initial Exploratory Data Analysis Using Power BI

The figures in Section 8.2, Appendix show the greatest degree for arsenic of its variable, filtered for Aquifer Group 1 (AG1). The wells that were above the Canadian Drinking Water Guidelines limit were turbid, more than those of sea water intrusion. However, the well samples did not have much chloride or specific conductance. Those samples all had high alkalinity (>150

mg/L)(Health Canada, 2015) but did not exhibit high levels of chloride, sulfate, or nitrogen. The graphs for Power BI show no specific pattern and incomplete data. Therefore, as a result the metal was discontinued for further analysis.

As a background, inorganic arsenic is in groundwater in two oxidation states: arsenite (As^{+3}) and arsenate (As^{+5}) with the geological environment favoriting one form over another (Shankar et al., 2014). Both forms exist at pH 6-9. While arsenate is favored thermodynamically in oxic water while arsenite is favored in anoxic, water with both states have been reported.

The release and mobility of arsenic in groundwater is related to both iron and aluminum oxides in sediments along with indigenous metal reducing bacteria in anoxic conditions (Shankar et al., 2014). This relationship was not seen due to the large spatial area of British Columbia. As leaches from iron minerals in oxic and high pH (Kanel et al., 2023). Low hydraulic gradients aquifers with higher residence time led to more dissolved arsenic (Kanel et al., 2023). The majority of geogenic arsenic comes from recently deposited alluvial sediments. Arsenic bearing sulfide minerals from geothermal deposits may also release arsenic into water via oxidation. A relatively diverse amount of micro-organisms have been discovered to utilize arsenic for energy generation via arsenite oxidation and arsenate reduction. These processes are reported to occur simultaneously with geochemical processes and observed to have an effect on arsenic speciation (Kanel et al., 2023; Liao et al., 2011). The primary microbial processes for arsenic transformation/mobilization are methylation, demethylation, oxidation, and reduction and are often tied to iron. Given the lack of iron patterns, this could indicate that geochemical controls may be more dominant than microbial ones.

Four possible ways of subsurface arsenic mobilization have been proposed by Oremland and Strolz: 1) As oxidation in pyrites, 2) iron oxide reduction leading to the release of As(V) via present allochthonous (indigenous) organic matter , 3) iron oxide reduction leading to the release of As(V) via present autochthonous (displaced) organic matter and 4) displacement of As(V) via phosphate (such as fertilizers) (Oremland & Stolz, 2003). Given the high turbidity with arsenic over CDWG limits and assuming it is geogenic in nature, it's likely that the sources were either 2) or 3) which could coincide with areas in B.C. with high groundwater arsenic such as the Lower Fraser Valley (Wilson et al., 2008). Otherwise, it could be due to previous mining runoffs.

B.C.'s alkalinity is predominantly a function of geology (Raudsepp et al., 2024). While Northeastern B.C. tends to have higher alkalinity over 200 mg/L due to carbonate rich bedrock such as limestone and dolostone while groundwater interacting with volcanic rocks in Southwestern B.C. is far lower (Earle, 2019b). Localised natural dissolution of carbonate minerals without other major ions that influence specific conductance could explain the gap between alkalinity and specific conductance (Arciszewski & Roberts, 2022).

Alkalinity represents the buffering capacity of alkalinity and buffers the water to the range which promotes arsenic dissolution (Shankar et al., 2014). The more feasibly the common aquifer geology contains carbonate rich aquifer mineralogy that is conductive to arsenic release under more alkaline reducing conditions (Health Canada, 2015; Mushtaq et al., 2018). Possible past flow paths might additionally have transported arsenic rich waters with alkalinity, which over time was isolated from other ionic sources (Q. Yang et al., 2015). Further research should view the relative ratios of chloride, sulfate and bromide to match that of seawater to analyse the effect of saltwater intrusion vs rock-water interactions (Saberimehr et al., 2017).

Manganese over the CDWG of 0.02 mg/L against other factors are shown in Section 8.2, Appendix (Health Canada, 2015). In Aquifer Group 1, manganese levels all had high iron levels, low phosphate levels and high levels of water hardness. Furthermore, these levels had low turbidity and moderate specific conductance that was not at the cut off for seawater intrusion.

The geochemistry of manganese and iron in groundwater is closely linked due to both existing in various redox states with groundwater chemistry and microbially mediation (Hamer et al., 2020). Low oxygen, reducing conditions indicate soluble Mn^{+2} and Fe^{+2} (ferrous), while Mn^{+4}/Fe^{+3} (ferric) form insoluble iron hydroxides in oxidizing conditions (Z. Zhang et al., 2020). Groundwater microbial interactions between the two are well studied and iron reducers tend to indirectly reduce manganese or vice versa (Gounot, 1994). Flow stratification matters as vertical and horizontal water paths in the aquifer form a series of reductions to carry out both geochemical and biogeochemical reduction process (Appelo & Postma, 2004). The observed linkage was expected, however as the coupling of iron and manganese is well known, however future research should consider aquifer and borehole properties as those may also affect the relationship (Hamer et al., 2020). Removal of iron and manganese is also common as both absorb to or coat sentiment soil grains during oxygenated recharge areas (Ahmad, 2012). Further

sedimentary aquifers and those with volcanic deposits show elevated manganese and iron. Granitic and metamorphic terrains yield lower due to less contact time with manganese/iron bearing minerals (Appelo & Postma, 2004). This is presumably the case for Aquifer Group 1. Manganese and iron also have been shown to absorb released phosphorus in similar types of aquifers (Huang et al., 2023).

In addition, lead above the Canadian Drinking Water Guidelines of 5 µg/L against all other factors from Aquifer Group 1 are shown in Section 8.2, Appendix and follow a similar pattern to manganese (Health Canada, 2015). Low specific conductance, low turbidity and very low chloride levels were apparent patterns along with higher lead concentrations leading to limited extent of hardness.

Higher lead concentrations in groundwater combined with low specific conductance, turbidity and chloride levels possibly indicate lead being mobilized from groundwater pipes and well fixtures instead of being leached from aquifer materials (Kampbell et al., 2003). However, corrosivity (calculated via the sulfate: chloride ratio) did not show any apparent patterns ((Nguyen et al., 2011). While localized contamination plumes from past industrial use of leaded petroleum and mining waste may possibly be an explanation for the raised lead, although not for other specific parameters (Earle, 2019b).

Meanwhile uranium had few levels above the Canadian Drinking Water Guidelines of 0.02 mg/L (Section 8.2, Appendix) (Health Canada, 2015). However, there was an apparent pattern when it came to, rising concentrations with rising specific conductance, hardness, calcium, dissolved sulfate, alkalinity, pH, and turbidity.

Likewise, the relationship between higher uranium and rising specific conductivity, total hardness, calcium, alkalinity, pH and turbidity indicate that ions released are coupled to increasing rock-water interactions that are influenced by evolving ion geochemistry (Appelo & Postma, 2004; Smedley & Kinniburgh, 2023). Uranium is soluble in water in its oxic state, uranium tetrafluoride (U(VI)) at neutral and alkaline pH (Alam & Cheng, 2014). Previous studies show calcium-carbonato-uranyl complexes promote uranium release (Skierszkan et al., 2020). In contrast to the scatterplot, sulfate reducing conditions are known to immobilize U as a precipitate or sorb it to mineral surfaces (Smedley & Kinniburgh, 2023). Spatial autocorrection may bring further understanding of the reason behind this observation.

Thermodynamic controls, mineral dissolution and uranium desorption control uranium mobility (Alam & Cheng, 2014). Uranium adsorption is often observed with Fe-Mn hydroxide minerals and influenced by natural organic matter, clay minerals and phosphate. The scatterplots may be indicative of de-absorption and weathering. The specific conductance, hardness and turbidity increase due to the dissolution of the native materials and as reactions consume carbonate buffering over time (Smedley & Kinniburgh, 2023). This might as well indicate that intrusion of saline waters created more oxidizing conditions (Sahu et al., 2020).

The line graphs of Aquifer Group 1 (Section 8.2, Appendix) show a downward trend of iron. Nonetheless it is difficult to tell if a yearly trend exists or if it is purely based on sampling frequency and distance. Future analysis would require de-seasonality and de-trending to verify any temporal patterns. Furthermore, lead goes down slightly as does arsenic, while there is a spike in uranium. The increase in uranium could be due to a growing interest in testing and lead decreasing due to a decrease in surface pollution. Moreover, seasonality is difficult to determine given that samples were taken in different places. However, specific conductance, turbidity and chloride show somewhat of a potential distinct seasonality pattern. In addition to the above analysis for saltwater intrusion, not enough data is available to make numerous or if any conclusions.

Increased changes in runoff and rainfall patterns might alter groundwater flow gradients and changed geochemical conditions to that of oxidizing conditions, removing iron from the water (Ghazavi et al., 2012). Specific conductance and chloride show seasonal patterns due to well pumping in aquifers that show saltwater intrusion (British Columbia Ministry of Forest, 2016). Likewise, turbidity would display a pattern due to seasonality, resulting soil and groundwater interactions (Sahu et al., 2020).

Section 8.2, Appendix shows the different metals along with their Canadian Drinking Water Guidelines limit against precipitation for AG1. The samples above Canadian Drinking Water Guidelines for Cd, Pb, U and As had low precipitation. Manganese above the drinking water guidelines was slightly related to low precipitation but said relationship was not as strong as the previous mentioned metals. Furthermore, higher specific conductance, turbidity and chloride above the saltwater intrusion cut off were related to low precipitation. Hardness had a slight

relation to low precipitation. Higher nitrogen, sulfate and alkalinity had lower precipitation levels. Meanwhile iron tended to slightly increase with higher precipitation.

Arsenic is already typically found to be high in inland basins in arid and semi-arid climates (Appelo & Postma, 2004). Pb, Mn and Cd above Canadian Drinking Water Guidelines could be due to the concentration effect via anthropogenic sources in more arid environments as well. Less precipitation provided it is not due to a severe drought could indicate that the water could be taken from deeper wells with longer flow paths, extended groundwater residence time, and less flushing for U (Alam & Cheng, 2014). Iron is known to be reduced with more water (Appelo & Postma, 2004). Drought effects reduces retention capacity for nitrogen on a wider scale and thus may be an explanation of the scatterplots (Winter et al., 2023).

The climatology monthly precipitation values were subtracted from precipitation to get the difference between the actual and predicted values ('FD'). Values > 0 were taken to be flooding conditions, while values <0 were taken to be drought conditions. For Aquifer Group 1, no pattern was observed for alkalinity, calcium, sulfate, Fe, PH, P and hardness. Considering most of the contaminates mentioned were associated with lower precipitation values, this might indicate that wells were an already dry area or a wet area for iron.

Further uranium over the Canadian Drinking Water Guidelines demonstrated a higher relationship with drought conditions. The higher amount of uranium in drought conditions is expected as results of the concentration effects. This also might be due to oxidation as drought conditions lead to a lowering of the groundwater table, exposing oxygen to uranium containing minerals in the unsaturated vadose zones (Z. Xu et al., 2022).

Flooding conditions were more associated with nitrogen, Cd over CDWG, Mn over CDWG, turbidity, and surprisingly chloride. Most of these are associated with overland contamination – nitrogen from fertilizer, cadmium from industrial activities, chloride from road salt and sea water, and turbidity from flooding sediment (Baborowski et al., 2004; Ciszewski & Grygar, 2016; Mullaney et al., 2009). Aquifer Group 1 are unconfined aquifers that consist of sand and gravel and often are influenced by overland water bodies and surface contaminates (Wei et al., 2016). This aquifer group has a high hydraulic connectivity thus the associations with those flooding and pollutants may be overland contamination brought in by floodwater (Ciszewski & Grygar, 2016). Mn over CDWG may be due to the increase in water and thus increase in

reducing conditions in a specific spatial area (Appelo & Postma, 2004). However, as B.C.'s ministry of environment is still mapping aquifers and groundwater levels are not consistently linked to the concentration database, further analysis is needed to make a definitive conclusion.

The time frames on the line graphs (Section 8.2, Appendix) indicates that there is a significant influence of geography as indicated by the variation of climatology, simulated values and seasonality in all temperature and precipitation factors.

Aquifer Group 2 (AG2) consisted of around 330 data samples. Line and seasonality graphs of the data variables indicated significant sampling errors with calcium, alkalinity, and hardness (Section 8.2, Appendix). Sulfate, specific conductance, and dissolved chloride indicated significant seasonality. However, the rest was difficult to identify between an actual seasonal pattern verse sampling and distant effects. Specific conductance indicated a slight decrease throughout time. Moreover, TDS and sulfate involved a noticeable increase.

Aquifer Group 2 is consistent of confined aquifers, thus not be as affected by seasonal effects. However multiple multi-aquifer wells can give induce seasonality effects in confined aquifers (Johnson et al., 2011). Seasonal pumping changes allow for leakages from the unconfined aquifers above into the confined aquifers and thus increase contamination. This could explain sulfate, specific conductance and chloride. Specific conductance, chloride and sulfate patterns could also be due to saltwater intrusion via seasonal pumping (Basack et al., 2022a). Likewise increase in sulfates and TDS might be due to overdrawing or contamination via pumping demands.

Uranium for Aquifer Group 2 (Section 8.2, Appendix) did not have any concentrations above the CDWG guidelines. However, a similar but smaller trend observed in Aquifer Group 1 was observed. Following lead concentrations above the CDWG guidelines for Aquifer Group 2 was partially related to alkalinity, while other factors contained no supporting patterns. Manganese samples that were over the CDWG guidelines had high alkalinity, low phosphate, high potassium, and high hardness. With arsenic above the CDWG guidelines, against all other variables had high turbidity and no other indication of patterns for Aquifer Group 2.

Lead is soluble in water as Pb^{+2} (Appelo & Postma, 2004). However, it is easily sorpted on clays, calcites, Mn-oxides and iron oxyhydroxides at and above neutral pH (Appelo & Postma, 2004). The alkalinity is likely related to geologic properties while lead could be related to

anthropogenic contamination from pipes or disturbances to confining layers that expose aquifers to surface lead sources (Jurgens et al., 2019)

High manganese levels with high iron, low turbidity, low phosphorus and high hardness potentially indicates aquifer materials that contain crystalline iron and manganese oxide/hydroxide minerals, under reducing conditions (Appelo & Postma, 2004). Potassium mineralogy weathering is a slower and more gradual process so the higher amounts coupled with lower turbidity may indicate a longer residence time (Appelo & Postma, 2004; Meyers et al., 2021). Furthermore, hardness is dominated by calcium/magnesium ions from carbonate mineral weathering rather than manganese/iron oxides (Appelo & Postma, 2004).

Precipitation for Aquifer Group 2 was graphed against all factors (Section 8.2, Appendix). Cd, Pb, As, and Mn along with CDWG limits and chloride, turbidity, and specific conductance above saltwater intrusion cut offs were associated with lower precipitation. Manganese above the CDWG limits was slightly associated with lower precipitation. Furthermore, the differences between actual monthly precipitation and simulated monthly precipitation was then compared to all other factors to simulate flood drought conditions. Drought like conditions were related to lead and arsenic above the CDWG guidelines. As well, flood like conditions were related to P and As below CDWG guidelines.

Drought like conditions for lead, cadmium and arsenic could relate to the draw down from above unconfined aquifers (Johnson et al., 2011). Confined aquifers in B.C. have high hydraulic diffusivity ranking, therefore drought stresses are able to propagate throughout the aquifers more rapidly (Gullacher et al., 2023). This effect would influence the water residence time and thus rock-water interactions (Bakari et al., 2012). This could indicate a shift in redox chemistry that may be difficult to reverse with time. Further studies would be required to understand said relationship between confined aquifers, geochemical drought shifts in confined aquifers and manganese. Specific conductance, chloride and turbidity could indicate saltwater intrusion from underlying previous saltwater aquifers or current seawater due to overpumping (Meyer et al., 2019).

For flooding conditions – arsenic and phosphate could be related to iron (Appelo & Postma, 2004). The effects of flooding on groundwater geochemistry in confined aquifers is relatively understudied. Yang and Tsai studied the relationship between shallow confined aquifers and

floods but focused mostly on anthropogenic contamination (S. Yang & Tsai, 2020). Both arsenic and phosphate are common anthropogenic pollutants and could likely be due to wellhead contamination from connecting wells (Basahi et al., 2018).

Chloride, uranium, and arsenic over Canadian Drinking Water Guidelines increased over time for Aquifer Group 2 with all factors indicating seasonality along with indications of the impact of geography. Further researcher into recharge areas would be needed for a definite explanation.

Aquifer Group 3 contained 300 samples. Arsenic above the Canadian Drinking Water Guidelines plotted against all other factors (Section 8.2, Appendix) had the low turbidity, low specific conductance and low chloride. Cadmium had no patterns again.

Fractured bedrock contains conduits which streamline flow and creates spaces for rock-water interactions. The main flow occurs around fissures while solute exchanges via diffusion occur with stagnant water in built rock (Appelo & Postma, 2004). Low permeability fractured flow with minimal rock-water interactions tend to produce clearer, lower ion concentrated groundwater. Furthermore, deep buried sediments in fractured sedimentary aquifers have undergone lithification, reducing fracture porosity and thus limiting rock-water interactions (Ofterdinger et al., 2019). Additionally phreatic zones are below the influences of most surface water processes (Wossenyeleh et al., 2020).

Manganese above the Canadian Drinking Water Guidelines (Section 8.2, Appendix) for Aquifer Group 3 showed high alkalinity, calcium, iron, potassium and hardness, following a similar concentration pattern to Aquifer Group 1. Additionally, it showed lower specific conductance and turbidity. Lead samples above the Canadian Drinking Water Guidelines for Aquifer Group 3 (Section 8.2, Appendix) were mostly alkaline while the specific conductivity followed a similar pattern to manganese. Furthermore, uranium did not have many values above the Canadian Drinking Water Guidelines. However, a smaller similar pattern for Aquifer Group 3 was observed in Aquifer Group 2.

Higher manganese, with higher alkalinity, calcium iron, potassium and hardness indicate an extended long rock-water interaction over long flow paths and stagnant water zones within the fracture network (Bakari et al., 2012). Upwelling of the formations after circulation could bring the ions to surface (Ofterdinger et al., 2019).

Line graphs indicate many sampling errors in Aquifer Group 2 (Section 8.2, Appendix). Furthermore, chloride and specific conductance had a noticeable increase along with variations that suggested potential seasonality.

Monthly precipitation was plotted against all other values for Aquifer Group 3 (Section 8.2, Appendix). Nitrogen, cadmium, and pH increased with increasing precipitation, while arsenic, uranium and iron increased with decreasing precipitation. Furthermore, the differences between simulated and actual monthly precipitation were also plotted against all other values. Flooding showed a similar pattern in Aquifer Group 2. Meanwhile, droughts showed an increase for Ca, specific conductance over the saltwater intrusion cut off, and Mn, As above the Canadian Drinking Water Guidelines limits.

The increased precipitation from higher recharge and rising water tables expands the saturation zone and increases the height storage capacity (Ciszewski & Grygar, 2016). This may dilute to a certain amount above the concentration of dissolved iron by flushing and mixing (Santos et al., 2011a).

Meanwhile, droughts shift aquifers to a closed system and change the geochemistry through continued rock-water exchange without replenishment (Wossenyeleh et al., 2020). The increased recharge allows more oxygen exchange in the vadose zone and changed redox conditions that may be impacting solubility of iron.

4.6 Descriptive and Summary Statistics

Given that most values are scaled to be centered around zero and with minimal sizing differences, the coefficients of variance are quite large (Section 8.2, Appendix). Variance and standard deviation were also sizeable, which indicated that there is a large spread of data. This is expected due to some wells being over the contamination standards, while others were not, due to groundwater chemistry in different geology and other factors.

The bar graph of aquifer samples (Section 8.2 Appendix) indicates that primarily well sampling was concentrated in Aquifer Group 1, with Aquifer Group 2 being secondary. Box plots (Section 8.2 Appendix) demonstrate that for Cd, Pb, U, and Mn there is a large variation in Aquifer Groups 2 and 3. A moderate amount of variation was showing for As in Aquifer Groups 1, 2, and 3 and for Mn in Aquifer Group 1. Uranium, lead and cadmium were usually low but had a lot of

extreme outliers indicating potential well contamination. This could be further explained via a spatial analysis.

Pearson, Kendall and Spearman correlations matrices were calculated for the entire dataset, drought dataset, flood dataset and seawater intrusion dataset. Pearson and Kendall correlations were focused on as the first represents linear correlations and the second is similar to Spearman's representing nonparametric correlations but considered to be more stringent (Hastie et al., 2009). The full Kendall correlation for the entire data set is shown in the appendix (Section 8.2, Appendix). Matrices did not take aquifer types into account and thus this may be an area for further study.

Table 4.1 displays both the Kendall rank correlation and Pearson correlation for the entire data set, flood data set and drought data set with a cut off P >= 0.5. Heavy metals of interest were chosen as variables and well as nitrogen as it has been extensively studied in these types of conditions (Winter et al., 2023). Both arsenic and nitrogen showed no significant correlation to any variables in all three data sets. This goes against previous studies in other areas which demonstrate both nitrogen and arsenic correlation (Appleyard et al., 2006; Winter et al., 2023). Said lack of correlation may also be due to lack of consistent sampling methods which is often demonstrated in large groundwater databases or spatial differences.

Manganese had a weak relationship to iron in the normal data set which remained somewhat consistent in the flooded data set but deteriorated in drought conditions. In general, iron and manganese are both abundant in the earth's crust and thus have a high co-occurrence (Hamer et al., 2020). Both elements are soluble in their reduced forms and occur in more anoxic waters. During flood and normal conditions, the water table is consistent and higher, with widespread uniformly distributed reducing conditions, thus leading to the continuation of the geochemical redox reactions discussed previously (Ciszewski & Grygar, 2016). Droughts led to a lowering of the water table and oxidizing condition thus in a stratified aquifer, only localized areas may have reducing conditions (Levy et al., 2021). This spatial uncoupling could lead to a deterioration shown by the correlations. These shifts in redox conditions often cause the divergence of each concentration (Appelo & Postma, 2004).

Lead had an extremely strong linear correlation with cadmium and a moderately nonparametric correlation with cadmium as well. Both these correlative relationships weakened in droughts. In

floods however, the linear correlation decreased but the parametric relationship remained somewhat consistent. This combination is usually anthropogenic and probably influenced linearly by geochemistry (Ciszewski & Grygar, 2016).

The Pearson coefficient for flood conditions is possibly due to sediment interactions and the difference in transport and deposition rates caused by said flooding (Santos et al., 2011a). Furthermore, sediment and depositional environments would indicate that there would be a varying and non-uniform contaminate that would delink the observed relationship in droughts.

Lead and cadmium have a strong Pearson correlation and a moderate Kendall correlation. This relationship has various natural sources and therefore the relationship is difficult to determine as B.C. has various natural sources of cadmium and lead, variable aquifer lithology, and has high areas of both mining, industrial activity and petroleum mining (D. Allen & Gleeson, 2023; Larry D. Jones, 1990; Wilson et al., 2008). A cadmium-lead relationship is typically observed in well water fixtures (Gavino-Lopez et al., 2022). Given that the observation well stations are governmentally run and undergo regular periods of maintenance, such a strong correlation is unlikely solely due to well water fixtures and more due to existing anthropogenic and natural contamination. The Kootenay region has historical lead contamination due to the joint emissions from decades of anthropogenic activity (Earle, 2019b). Likewise, the Trail, B.C. operation smelter in Southern B.C. admitted both lead and cadmium into the surrounding air, soil and water for over a hundred years (John et al., 1976). Therefore, spatial auto correction is needed to reveal more about this relationship. Moreover, the difference in Pearson is measured in linear correlations and is highly influenced by measurement errors while Kendall measures monotonic increase or decrease that could or possibly could not be linear (Helsel et al., 2020). This could account for the difference between the Kendall and Pearson relationship in cadmium and lead.

Uranium had a weak relationship with hardness and calcium that deteriorated in flood conditions and further deteriorated in drought conditions. These relationships were more likely linear due to the lower Kendall values.

There is a moderate linear relationship between uranium and calcium in the regular data. These relationships seem to be slightly weaker in the flooded data set and completely uncoupled in drought data sets. This weak relationship could be due to aquifer geology as uranium commonly occurs with calcium bearing minerals (Larry D. Jones, 1990). Rocks and minerals such as

limestone release uranium via weathering processes (Alam & Cheng, 2014). As well, BC has areas of carbonate bedrock (Larry D. Jones, 1990). Therefore, these two elements could be correlated due to geochemical reactions with longer groundwater residential times (Skierszkan et al., 2021).

Furthermore, flooding could slightly weaken the relationship via increased erosion and runoff that transport uranium in pathways independent of calcium in groundwater (Smedley & Kinniburgh, 2023). This again will slightly decouple their concentration lowering the Pearson correlation. However, the drought correlation may indicate that the mobility of uranium and calcium are governed by distinct geochemical factors such as redox conditions, mineral equilibria and microbial activity (Appelo & Postma, 2004). Lowering water table would de-couple them causing no statistical correlation to be observed.

Table 4.6.1: Pearson (cutoff $p \geq 0.5$) and kendall rank correlations for each element of interest (As, Mn, Pb, U) and N for the entire dataset, flood dataset and drought dataset.

Element of Interest	Related Element	Normal		Flood		Drought	
		Pearson	Kendall	Pearson	Kendall	Pearson	Kendall
As	-	-	-	-	-	-	-
Mn	Fe	0.5168	0.4111	0.5175	0.4092	-	-
N	-	-	-	-	-	-	-
Pb	Cd	0.9534	0.5630	0.7089	0.5768	0.6691	0.4870
U	Ca	0.5670	0.3620	0.4978	-	-	-
	Hardness	0.5610	0.3977	-	-	-	-

Kendall and Pearson correlation for normal and seawater intrusion data sets, As, Mn, N, Pb and U are shown in Table 4.2. Arsenic and nitrogen have no correlations. The correlation of lead with cadmium drops to a somewhat strong linear correlation, but the parametric correlation in the saltwater intrusion data set is similar to that of drought in the saltwater intrusion data set.

The relationship between iron and manganese is completely decoupled in saltwater intrusion. This could be due to different geochemical controls such as competing ions from seawater that interfere with the manganese/iron binding behaviors, weakening of the dissolution-precipitation of ferrihydrite or redox shifts from oxygenated seawater (Appelo & Postma, 2004; Zhu et al., 2022b). Kinetic factors as intrusion relatively to groundwater flow could affect the degree of geochemical distribution via the shifts in the equilibrium (Snyder et al., 2004).

The weaken interrelationship between lead and cadmium in saltwater intrusion could be due to multiple factors. Saltwater intrusion would disrupt the groundwater geochemical relationship and change the underlying redox interactions. In addition, the mixing of saltwater and freshwater would introduce different turbulence and flows into the aquifer (Meyer et al., 2019). Saltwater intrusion is known to corrode iron which in turn theoretically should dissolve lead (Basack et al., 2022a; Trueman et al., 2017). Likewise, legacy sources of lead may be mobilized via saltwater intrusion (Nai et al., 2019). Iron and lead contamination could also be brought in via intruding seawater. Further research on this coupling is needed to reach a definite conclusion.

Uranium in saltwater intrusion had weak linear and parametric correlations – positive potassium, hardness and alkalinity and negative chloride and lead. Firstly, these relationships could be due to location or sampling biases. Future research should utilize a larger dataset and spatial autocorrection. The relationship between uranium and potassium, chloride, and hardness seemed to be more linear based then nonparametric increase or decrease due to the lower-than-expected Kendall correlation. Due to lack of research and undetermined studies, the discussion of uranium geochemistry is based on few aquifer studies and general saltwater and marine sediments.

The positive correlation between uranium and calcium disappeared in saltwater intrusion. This previously seemed to be due to groundwater geochemistry. A common groundwater geochemical effect is the cation exchange of calcium with sodium (Appelo & Postma, 2004; Mora et al., 2020). Sodium has been utilized to displace uranium in uranium ore extraction and thus a smaller similar process may be occurring in the water (Seidel, 2007). The negative relationship between chloride and uranium contrast with other studies and what would be expected as uranium chloride is a water soluble solution (S. Singh et al., 2003). One possible explanation could be due to the rapid chromatographic transformation of the solute front commonly seen in saltwater intrusion (Appelo & Postma, 2004).

A weak negative relationship between lead and uranium was revealed in the saltwater intrusion data set. This could have had parametric or additional complexities due to the similarity in Kendall scores. This again could be partially due to the changing redox conditions by saline metals from previous legacy sources (Smedley & Kinniburgh, 2023). Normally lead and uranium coexist in rocks concurrently which forms the bases of lead isotope rock dating (L. Zhang et al.,

2022). Few studies have observed the geochemical behavior of uranium and lead with seawater intrusion. However, a possible explanation could be cation competition after both are re-suspended in the intruding saltwater. Additionally, under more stable freshwater conditions without geochemical/transport perturbation, subtle factors controlling uranium's association would be outweighed by intrinsic noise.

The relationship between uranium and calcium in the main dataset seem to be replaced by a similar relationship between uranium and potassium. Hardness remained nearly unchanged. Alkalinity showed weak correlation in the saltwater intrusion data set. In general, previous areas had positive correlations between uranium and potassium, hardness and alkalinity so this may be due to spatial influences (S. Singh et al., 2003). Potassium ratios are utilized in saltwater intrusion research and are common in seawater so this relationship could be due to environmental factors (Sudaryanto & Naily, 2018).

The hardness relationship heavily mimics that of flooding conditions. This could specify that the same issues of sediment disposal and redox conditions could remain despite the addition of different ions with magnesium from seawater replacing calcium (Sudaryanto & Naily, 2018). Future research could evaluate the influence of magnesium with uranium with intruding saltwater. Competition effects from magnesium/sodium does influence and displace calcium (Appelo & Postma, 2004).

Alkalinity is influenced by bicarbonate and carbonate ions which buffer pH changes. Sodium displaces calcium at a higher rate and slightly raises pH through ion exchange and carbonate mineral dissolution (Appelo & Postma, 2004). In turn this could push more release of bicarbonate and carbonate ions. The higher alkalinity and higher pH favor increased aqueous complexions of UO_2^{+2} (Smedley & Kinniburgh, 2023). Cation exchange is less sensitive to small variations in alkalinity and pH in regular water compared to sea water mixing (Appelo & Postma, 2004). In addition, sampling issues might be an influence due to the small amount of saltwater intrusion data.

Table 4.6.2: Pearson (cutoff p ≥ 0.5) and Kendall rank correlations for each element of interest (As, Mn, Pb, U) and N for the entire dataset, and with noticeable sea water intrusion.

Element of Interest	Related Element	Normal		Sea Water Intrusion	
		Pearson	Kendal	Pearson	Kendal
As	-	-	-	-	-
Mn	Fe	0.5168	0.4111	-	-
N	-	-	-	-	-
Pb	Cd	.9534	.5630	0.7810	0.4870
	Fe	-	-	0.5940	0.4338
	U	-	-	-0.5228	-0.4382
U	Ca	.5670	.3620	-	-
	Cl	-	-	-0.5538	-0.3452
	Pb	-	-	-0.5128	-0.4382
	K	-	-	0.5514	0.3521
	Hardness	0.5610	0.3977	0.5536	0.3399
	Alkalinity	-	-	0.6212	0.3873

Table 4.4 shows the amount of well samples with metals of interest that are above the limits set by the Canadian Drinking Water Guidelines in addition to saltwater intrusion factors above the respective cutoffs (British Columbia Ministry of Forest, 2016; Health Canada, 2022).

Uranium above cut-offs is scarce mainly as testing for it seems to be more recent and this might also be the reason why most of it is associated with droughts. Uranium above Canadian Drinking Water Guidelines had few values so it could not be determined if the there was an underlying general relationship or if it was due to spatial factors. Manganese above Canadian Drinking Water Guidelines was seen in both drought and flood likely due to underlying geology. The slight increase in manganese contamination for droughts may be due to draw down from more contaminated aquifers above or from older deeper aquifers (Levy et al., 2021; Ying et al., 2017).

Arsenic above Canadian Drinking Water Guidelines limits seem to have no clear pattern as it occurs in both flood and drought data sets. This might be due to anthropogenic means in combination with geochemical effects (Appelo & Postma, 2004). Lead above Canadian Drinking Water Guidelines limits was found in 289 samples and could be spatially influenced by anthropogenic sources due to inland mining and industrial activities (Ootes et al., 2017). Manganese had the most samples above recommended guidelines of 344. Most of those data points occurred in droughts. Potential lead and arsenic relationships with droughts are discussed in the previous section.

Turbidity, specific conductance and chloride over SWI cutoffs had a higher occurrence in drought conditions. This makes sense as those increase demand on vulnerable aquifers and thus lead to overpumping (Basack et al., 2022a).

Table 4.6.3: Metals of interest that are above the limits set by the Canadian Drinking Water Guidelines in addition to saltwater intrusion factors above their respective cutoffs for the full, drought, flood and saltwater intrusion datasets.

	As Above Limit	Pb Above Limit	Mn Above Limit	U Above Limit	Specific Conductance over cutoff	Residue Filterable 1.0u over cutoff	Chloride over cutoff	Total Data Points
Full Dataset	81	289	344	6	107	79	52	1147
Drought Dataset	37	138	162	4	69	49	29	530
Flood Dataset	31	124	135	1	32	22	18	455
Chloride or Specific Conductance	71	26	41	0	99	70	47	106

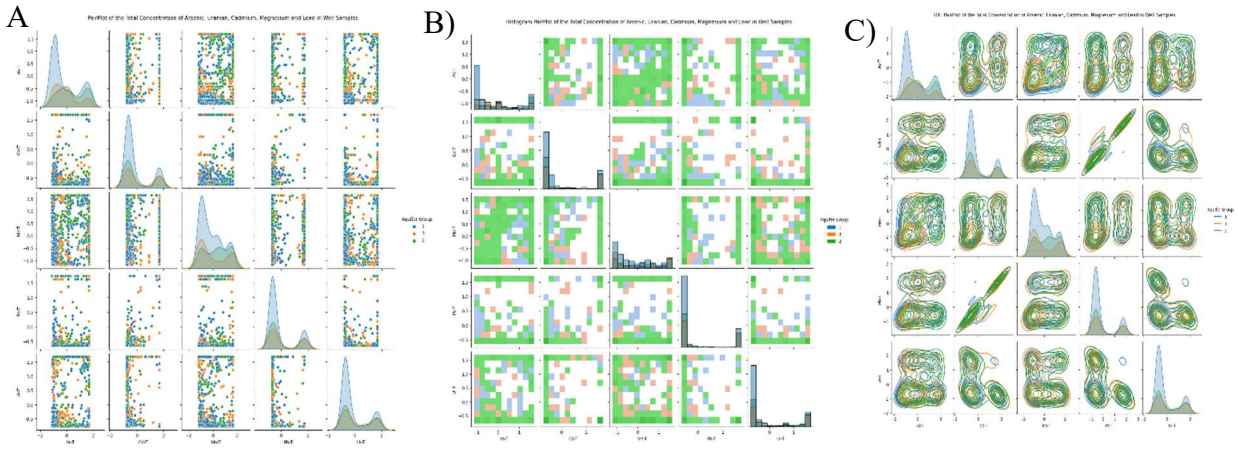

Figure 4.6.1: A) From left to right: A) pairplot, B) hisplot and C) KDE plots of the relationship between metals of interest for the full dataset.

Figure 4.7 shows the pair plot, histogram, and kernel density estimator (KDE)All the metals of Interest. Uranium's relationship with cadmium is seen on both the pair plot and KDE. Manganese and arsenic show no apparent pattern. A slight relationship between cadmium and lead is observed in the KDE plot and histogram plots along with manganese and cadmium.

Relationships of precipitation factors and other variables seem to display similar relationships to that showing with the correlation plots (Section 8.2, Appendix). There are no notable differences between the drought or flood in comparison to the entire data set. Lesser or greater variations of the same pattern are shown. Heat maps show somewhat decreasing precipitation/precipitation differences and increasing turbidity over the years per well location (Section 8.2 Appendix).

4.7 Saltwater Intrusion Exploratory Data Analysis

Section 8.2, Appendix shows various combinations of different saltwater intrusion cutoffs and the resultant data points, Metals of Interest and saltwater intrusion factors. From this, the best data set can be found by using the cutoff for chloride of 150 µg/L or a specific conductance of 1,000 S/cm (British Columbia Ministry of Forest, 2016). This gives a data set of 106 points that has no uranium over limits, few manganese over limit and few lead over limit. However, 71 of 81 samples of arsenic in the total data set also appeared in the saltwater intrusion dataset with these criteria.

Table 8.2.3 (Section 8.2, Appendix) shows the metals above Canadian Drinking Water Guidelines limits with saltwater intrusion. A high amount of arsenic above Canadian Drinking Water Guidelines occurs in the data set with chloride or specific conductance over saltwater intrusion limits, but not in the data set with both specific conductance over the saltwater intrusion cutoff. Arsenic is highly influenced by saltwater intrusion which causes competitive desorption and favors the biochemical reduction of arsenic (Yuan et al., 2023). The lack of Kendall or Pearson correlation previously may be due to the smaller dataset.

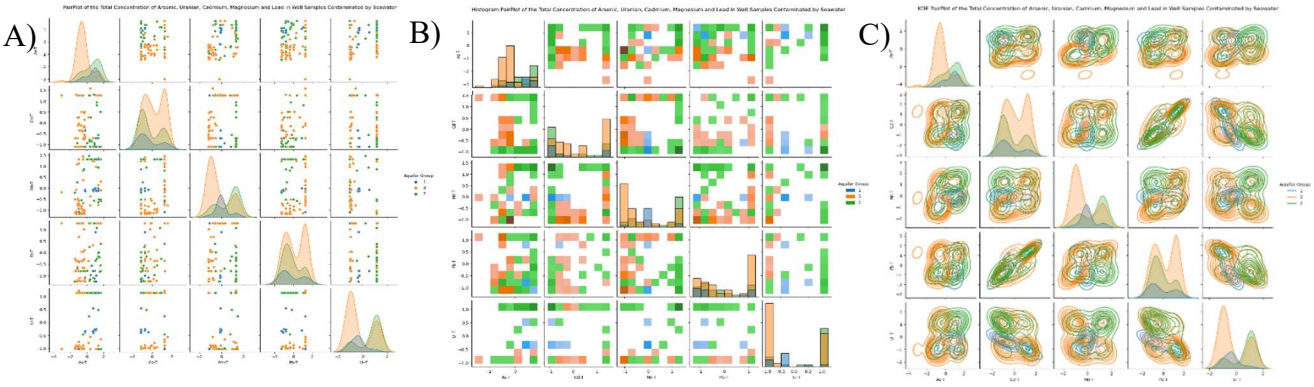

Figure 4.7.1: A) From Left to right: A) pairplot, B) hisplot and C) KDE plots of the relationship between metals of interest for SWI dataset where specfic conductance ≥ 1000 or chloride ≥ 150 µg/L.

Figure 4.8 shows the relationship between different metals with saltwater intrusion for each aquifer group. Some of the weak previous correlations are shown between uranium and lead. It also illustrates that a lot of the aquifer types with saltwater intrusion are Aquifer Group 2. This could be due to previous trapped seawater or other rock-water interactions (Saberimehr et al., 2017). Figures in the Appendix show expected or undetermined relationships for seawater

intrusion variables, temperature and precipitation variables and all other variables (Section 8.2, Appendix)

Chapter 5: Factor Analysis

5.1 Factor Analysis Methodology

5.1.1 Data Processing

The analyses were done via python on a Jupyter notebook. The libraries Factor Analyzer and Pingouin' were installed via pip. Data was then processed similar to that previously done in Power BI. In addition:

I. Climatology data was dropped from the dataset to avoid too many correlations.
II. Latitude and longitude were accounted for via equivalent distances calculated by the haversine formula (Rapp, 1991). A reference latitude and longitude were the means. Both latitude and longitude were converted into radians and the 'x' and 'y' distance in kilometers were calculated from the reference coordinates. Longitude and latitude were then dropped from the data frame.
III. Aquifer groups were converted into columns via one-hot encoding.
IV. Date was converted into numerical form ("Months_Since_First_Sample") by the months between each sample and the first sample taken.

Outliers were removed via IQR method and replaced threshold values (Hastie et al., 2009). Only lower outliers of uranium were removed to account for potential contamination above drinking water standards. Data was scaled via Yeo-Johnson method via Sklearn.

5.1.2 Initial Factor Analysis Setup

Multiple functions were created, the first function was called "analyze_continous_data" to check the suitability of the data for factor analysis and utilized "calculate_kmo and calculate_Bartlett_sphericity from factor_analyzer". This calculated the p and chi square and calculates the value which should be zero and tests if said the corresponding correlation matrix is an identity matrix with unique variables (Mulaik, 2009). Due to a larger dataset this outcome was expected but still run as a check. Then the Kaiser-Meyer-Olkin (KMO) values would be calculated for all variables. Furthermore, the overall KMO is printed as is the KMO for each sampling variables. The KMO is a measure of sampling adequacy and answers closer to one are ideal (Lorenzo-Seva & Ferrando, 2021).

The second function, "perform_factor_analysis" did the first step of factor analysis. It specifically fits factor analyzer to the data and calculates eigenvalues. Following, it then prints

the number of eigenvalues greater than one and the ratio of the sum of eigenvalues greater than 1 to the total sum of eigenvalues to represent how much of the data said factor will cover (Hair et al., 2019). Last, it prints a scree plot of the data. This function covered two main methods of finding the number of factors to use - the number of eigenvalues greater than 1 and the number of factors that corresponds to the greatest drop on the scree plot.

5.1.3 Preliminary Factor Analysis

For the first step of the primary factor analysis, the function "perform_factor_analysis_and_plot" was created.

I. This was essentially an intermediate factor analysis utilizing factor analyzer and "varimax" rotation (an orthogonal rotation used to maximize each variance between factor loadings, hence simplifying the analysis).
II. A heatmap was generated between the factors and the variables.
III. This function would then combine the calculated uniqueness and communality for each variable in a data frame, along with the proportional and cumulative variance for each factor/variable and would save as a CSV. This was designed as to allow for quicker factor elimination via excel column sorting.
IV. Last, a heatmap of each variable's uniqueness and communality was generated along with the total variance as a check (communality + uniqueness = 1) (Mulaik, 2009). Said figure was designed to allow for a visual representation to determine which variables could potentially be eliminated.

The function "analyze_continuous_data" was run on the primary dataset. A KMO result of .72 indicated that factor analysis was somewhat suitable for said dataset. "Perform_factor_analysis" with n_factors = 28 (data columns) showed 9 eigenvalues greater than 1 which composed of 75.5% of the total sum. The scree plot showed that anywhere between 7-9 was appropriate. Afterwards "perform_factor_analysis_and_plot" with 9 factors was run on the dataset.

FD and Hardness were eliminated regardless of the above results for the fact they have already been composed partially of other factors and led to the process being run with better fitting KMO scores and factors.

The CSV generated was opened. Any variable with < |.40| (above is strong correlation (Hair et al., 2019)) for no factor was considered a candidate for elimination. Further visual analysis was that two factors might potentially be eliminated due to none of them having a high enough correlation value. Last the difference between community and uniqueness was inspected. Variables with high uniqueness and low community could be elimination candidates based on factor scores alone, K, Fe, P, N, pH, y, and precipitation were eliminated. The results are discussed in Section 5 and Appendix 8.3.

5.1.4 Primary Factor Analysis

The "perform_factor_analysis_and_plotpro" function was made to perform second step of the primary factor analysis. This followed the same steps as "perform_factor_analysis_and_plot" except using the Promax method of rotation. Said rotation is oblique and allows for factors to be correlated and often better represents real world data(Mulaik, 2009). However, it does require previous orthogonal processing to be legible.

The variables in the data frame were not raised to any exponential power as doing so dropped the KMO value to an unsuitable score. The functions "analyze_continuous_data" and "perform_factor_analysis with n_factors = 16" were run again. Both the eigenvalue method and the scree plot indicated anywhere between 5 to 6 factors being appropriate. "Perform_factor_analysis_and_plotpro" was then run. The CSV generated was opened and variables >|.4| for each factor were put in a separate data frame.

A residue matrix was then calculated with the residues from the observed and predicted correlations from factor analysis with Promax rotation as a check.

The library pingouin furthermore, was utilized to calculate the Cronbach alpha for factors that only had positive correlations (F1 and F3). All results are discussed in Section 6 and Appendix 8.3.

5.1.5 Factor Analysis Focused on Metals of Interest

The function, "perform_factor_analysis_and_plotOBS" was created to directly analyze different conditions of wells. Said function is the same as the previous two except uses oblique rotational methods. An oblique rotation method that allows for correlation, but furthermore is used to maximize differences between factors (Mulaik, 2009). It is a balance between representing the realistic data structure and interpretability.

Additionally, four data frames for As, Mn, Pb and U were created to focus on which factors may potentially influence each metal. The variables FD and Hardness were dropped to avoid correlation along with the three metals not in focus. For each data frame, "analyze_continous_data" was performed and had a KMO value around ~.70 signaled that it was okay to proceed. Afterwards "perform_factor_analysis" was run for each, with n_factors specified as 21 (number of columns) to get the number of factors for use in the next step which was chosen as the number of eigenvalues greater than 1. Then "perform_factor_analysis_and_plotOBS" was run for each data frame. Resultant values are discussed in Section 6 and Appendix 8.3.

5.1.6 Factor Analysis Focused on Climate Change Variables

Two data frames were created to look at further analyzation in the effect of climate change factors on the entire dataset - one specifically was with the metals, nitrogen, aquifer groups, temperatures, distances, months and precipitation. While the second involved metals, nitrogen, saltwater intrusion factors, distances, months and aquifer groups. The function "analyze_continuous_data" was run on both, however the KMO score was too low to justify further analysis.

5.1.7 Factor Analysis Focused on Climate Change Events

Three additional data frames were created to analyze the effect of climate change effects on data sets with determined climate events.

- DatatSWI took any row where the chloride concentration was above 150 mg/L or where the specific conductance was above 1,000 uS/cm and was created to specifically analyses factors where wells had seawater intrusion.
- Then data drought took rows where FD < 0.
- data flood took rows with FD > 0 to analyse the effects of precipitation.

Furthermore, the functions "analyze_continuous_data, perform_factor_analysis" with n_factors=24, and "analyze_continuous_data" with the factors found from the previous function was then run on all 5 datasets. Figures and values obtained are discussed in Section 6 and Appendix 8.3.

As this is an exploratory factor analysis and not confirmatory, further calculation of Cronbach's alpha was deemed unnecessary.

5.2 Primary Factor Analysis

Exploratory factor analysis can identify important predictor variables, elucidate underlying processes and guide future predictive model structures (Briz-Kishore & Murali, 1992). It can also highlight sampling needs or where more data needs to be collected. This is a step above both Kendall and Pearson correlations because correlations generally measure the strength and direction of linear relationships between two variables while factor analysis looks at all the variables simultaneously (Mulaik, 2009). Moreover, Kendall is a pairwise relationship while measuring rank nonparametric statistics. As this data is non normal, it is better to follow with a deeper factor analysis to see the underlying multivariate structure (Hair et al., 2019). Factor loading represents the original correlation between the original variable and underlying factors while major correlation matrices only show the original correlations directly. Factor analysis looks at common underlying variables and multicollinearity.

Section 8.3, (Appendix) shows the original Bartlett and tests homoscedasticity. Due to the sample size, P values were expected to be 0 and the chi squared value to be extremely large (Mulaik, 2009). Hardness and climatology data were removed from the data set so to prevent further bias. The Kaiser-Meyer-Olkin (KMO) for the data set was 0.7526, which is average and acceptable for exploratory factor analysis but not as stringent for modeling (Hair et al., 2019). This indicates an average strength of partial correlations.

Sections in the appendix (Section 8.3, Appendix) show the results of the initial factor analysis with varimax rotation. Kaiser's rule was generally used to determine the number of factors. Variables that did not have any factor loading $\leq .4$ of a factor were removed (Mulaik, 2009). This eliminated precipitation and arsenic. Likewise, variables that were $.4 \leq$ and $\leq .7$ were then evaluated and those with high uniqueness/low community were removed (Hair et al., 2019). This eliminated both distance factors. The primary data set had 16 variables and a KMO = 0.7481. Five factors were identified (Section 8.3, Appendix). The secondary factor analysis performed via promax rotation had a cumulative variance of .70.

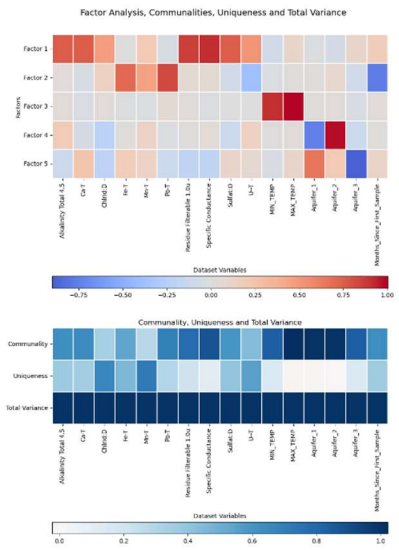

Figure 5.2.1: Final promax factor analysis on the complete dataset.

The first factor (F1) composed 24.4% of the proportional variance and seemed to be that of saltwater intrusion and rock geochemistry (Section 8.3, Appendix). The largest variables were specific conductance [loading = 0.9167], residue filterable [0 .8647], Ca [0.7572], alkalinity (alkalinity total 4.5) [0.75720], and sulfate [0.7530]. Uranium and chloride had a weaker makeup of said factor.

Specific conductance, residue filterable, calcium, alkalinity and sulfate could suggest a representation of saltwater intrusion or previously buried saltwater intrusion from different coastlines at different geological ages or rock-water geochemistry (Bethke & Marshak, 1990; Chen et al., 2018). Saltwater intrusion along with groundwater chemistry typically makes up the largest factor in previous groundwater factor analysis (Chen et al., 2018; Farnham et al., 2003; Kuppusamy & Giridhar, 2006). Specific conductance indicates potential groundwater chemistry. Potential other reasons for high levels of specific conductance would be geological factors including coastal sedimentary rocks like limestone, past seawater intrusion during periods of high sea level rises and buried residual salts along with saline fossil groundwater (Appelo & Postma, 2004). Even in the Northern British Columbia region a similar pattern with deeper wells is demonstrated due to past seawater intrusion and upward migration of older saline basal brines (VanGulck, 2016).

The specific parameters loading strongly suggest ion exchange, saline intrusion or diffusion as possible processes, but this content will need to be fully evaluated with more geological and

hydrological factors to further determine more underlying relationships (Appelo & Postma, 2004). Silica would need to be added to determine the difference between types of mineral weathering vs carbonate dissolution along with sulphide, and nitrite. To understand the underlying driving mechanisms, future research should correlate scores to pumping rates, distance to the coastline, recharge rates and overlay scores with aquifer properties and surface maps (Kuppusamy & Giridhar, 2006). Better accuracy might be obtained by separating hydraulic zones and geoclimatic zones as well as more geological factors such as carbonate and evaporate deposits (Belkhiri & Narany, 2015). Factor 1 may be influenced by evaporate deposits, carbonate rock, superficial geology, and structural geology as faults connects as conduits which bring up deeper saline fluids from subsurface evaporate deposits (Dalton & Upchurch, 1978). Future research should look at these specific lithological features as well as incorporate better spatial clustering.

Factor 2 (F2) consisted of Pb [0. 8249], Fe [0.7101] and a negative relationship to time (Months_Since_First_Sample) [-0.7700]. There was also a weak proponent of Mn.

Factors 2 is about 13.63% of the proportional variance. Time loads of very strongly negative correlation suggests some temporal changes in water quality over time in B.C. Metals such as Mn, Fe and Pb were positive loading and are often associated with redox reactions that can change with the biogeochemical conditions over time (Appelo & Postma, 2004). This might indicate a temporal component involving redox conditions. In general, groundwater geochemistry is known to evolve over time (Appelo & Postma, 2004). It is uncertain however if geochemical changes could endemically happen within the span of forty years or a shift could be due to climate change factors such as pumping or pollution. Previous changes in aquifer geochemistry have been documented with manganese in a large-scale study in the United States (Ayotte et al., 2015). Likewise, groundwater resident time would play a role in geochemical interactions – perhaps shorter time could indicate more interactions with manganese bearing rocks that are closer to the subsurface (Poeter et al., 2020).

Another possible explanation could be anthropogenic means, as lead and iron are common pollutants in well water fixtures and of mining pollution (Witkowski et al., 2020). Manganese has been known to be influenced via groundwater depth and well depths in shallow aquifers

(Hamer et al., 2020). Inclusion of these factors would be beneficial for future understanding. Spatial auto-corrections and comparison to other redox sensitive variables like nitrite and sulfide along with linking it underlying geology could help validate or understand said underlying suppose conditions (Appelo & Postma, 2004). Furthermore, bootstrap resampling methods would be able to generate competent intervals around trends to test stability (Biglari et al., 2018).

Factor 3 (F3) is 11.5 % of the proportional variance and has minimum and maximum average monthly temperature as the major proponents. This is the factor likely for climate change effects. Maximum temperature is >1.0 indicating that it is highly correlated with minimum temperature.

The Factor 3 loadings indicate a very large temperature effect. Lack of research indicates that F3 loadings cannot be directly confirmed and could indicate just the fluctuations of temperature alone (Riedel, 2019). Temperature effect on groundwater has been debated with some studies reporting a .1-.4 °C raise in groundwater temperature per decade for climate change, others saying it has slight effects on shallower aquifers while others stating reporting minuscule effects due to groundwater depth (Benz et al., 2017; R. Li, 2016; Neidhardt & Shao, 2023). Most research of climate changed induced temperature change for water is done on for geothermal and gas (Hemmerle & Bayer, 2020). Other research has been conducted in northern climates with permafrost playing a crucial role in dictating geotechnical properties and groundwater flow patterns (Gruber & Haeberli, 2007; JR Williams, 1970).

Due to Yeo-Johnson scaling, pure temperatures alone might be unlikely, and may indicate interannual variations in groundwater heat driven by surface temperature fluctuations due to seasonality (Noetzli & Gruber, 2009). Minimum and maximum temperatures are tightly paired and indicate the obvious common driver which may be climate change. Minimum (nighttime) and maximum temperature (daytime) do not increase at consistent rate (T. R. Karl et al., 1993). Climate change causes minimum temperature to rise at a greater rate than maximum temperature especially in the northern hemisphere. The fluctuation between the two-temperature difference basically indicates optimal seasonal conditions for redox reaction (Noetzli & Gruber, 2009; Sahu et al., 2020). Meteorologists often indicate that the difference between the two temperatures could better indicates the influence of climate change effects and perhaps should be analysed in future patterns (T. Karl et al., 1993). Few studies have included temperature effects in water

factor analysis. Future research should include well depth and perhaps the temperature differences between both expected and actual minimum and maximum temperature.

Factor 4 (F4) and Factor 5 (F5) relate to the aquifer groups and therefore represent a combination of hydraulic connection and geology or geography. These two factors compose about 20% of the proportional variance. The loadings represent three groups of groundwater hydraulic connections and flow rates.

For F4: Aquifer Group 1 encompasses unconfined aquifers often involving sand and gravel and that often have hydraulic connections to surface water (Wei et al., 2016). Unconfined aquifer types likely experience more oxygenated modern recharge from the and dilution effects thus pull a negative loading (Orecchia et al., 2022). Groundwater recharge and hydraulic connection has previously seen to have a similar effect on other studies (Ballukraya & Ravi, 1999; Briz-Kishore & Murali, 1992). Recharge times also play an important role. Meanwhile Aquifer Group 2 represents confined aquifers including some with glacial marine influence near the coast (Wei et al., 2016). Meanwhile confined aquifer types interact less with the surface and retain older alternative chemistry and result in positive loading (Skierszkan et al., 2021). A lot of deeper wells are confined and therefore assumably part of Aquifer Group 2 (Cabrera et al., 2017). Deeper wells often have longer groundwater residence times, greater hydrological age and thus more reducing conditions with different geochemistry (Bakari et al., 2012).

This factor differentiates between geochemical signatures of unconfined aquifers with a likely surface influences vs combined/deeper aquifer types with older set groundwater. In addition, this factor could appear to capture distinction between shallow and uncombined deeper aquifers based on divergent geochemical imprints. This is seen in further factor analysis studies as confined and unconfined aquifers have different properties (Chung et al., 2020).

For F5: Aquifer Group 3 loads extremely negatively and represent primarily fractured aquifers especially those in crystalline bedrock. Aquifer Group 1 loads positively and represents those with hydraulic connectivity and shallow sand and gravel.

This could be representative of two scenarios. One being the distinguishment between geochemical signatures of shallow alluvial aquifers versus deeper fractured crystalline bedrock aquifers.

The second representing the difference both diffusion and groundwater flow (Appelo & Postma, 2004). With Aquifer Group 1 in gravel and sand types, flow has a moderate surface area for groundwater interaction. Percolation through the vadose zone is relatively straightforward (Wossenyeleh et al., 2020). Fractured bedrock, however, has conduits where groundwater can quickly flow through (Appelo & Postma, 2004). As previously mentioned, the main flow occurs in faults or fissure while diffusion occurs in the stagnant bulk rock. This would mean less opportunities for rock-water interaction and an effect on contaminate transport.

There was inadequate sampling to look solely at both metals of interest and either the saltwater intrusion variables or the precipitation and temperature variables as KMO was < .7 (Mulaik, 2009). The dataset for saltwater intrusion also had inadequate sampling.

5.3 Factor Analysis for Each Individual Metal of Focus

To understand how each metal of interest is affected by the data set, other metals of interest were removed and an oblimin factor analysis was performed.

Figures and tables for the factor analysis focusing on arsenic can be found in Section 8.3 (Appendix). Figure 5.2 shows the final factor results with six factors ($F1_{As}$, $F2_{As}$, $F3_{As}$, $F4_{As}$, $F5_{As}$, $F6_{As}$) and a cumulative variance of 57%. Given the factor analysis focused on arsenic covered 0.5736 cumulative variance thus can be used for generalizations but any findings should be confirmed with more data (Mulaik, 2009). Arsenic was not a heavy underlying loading in any of the factors.

$F1_{As}$ represented about 20% of the cumulative variance and consisted of saltwater intrusion and groundwater chemistry variables. It was influenced strongly by Specific Conductance [0.9453], Residue Filterable [0.8944], Alkalinity [0.7637], Sulfate [0.7223] and Ca-T [0.7038] while having a weak influence of chloride and K. The cumulative variance and makeup of $F1_{As}$ remains somewhat consistent to Factor 1 in the main factor analysis but without uranium and with the addition of potassium. Potassium can be correlated with the overall mineralization but may indicate some unique influences beyond dissolved solids (Fulton et al., 2004). British Columbia is too diverse for potassium to be defined as a characteristic of a hydro chemical facies. Uranium and arsenic have been known to co-exist (Katsoyiannis et al., 2007; Skierszkan et al., 2020). These differences are likely due to spatial influence and geographical geology and

implies that arsenic contamination is likely spatially localised. Thus, future research should utilize spatial autocorrection.

$F2_{As}$, $F3_{As}$, and $F4_{As}$ are equivalent to F3, F5, and F4 of the main factor analysis with their proportional variances differing due to the removal of other metals of focus. $F2_{As}$ consisted of maximum temperature and minimum temperature. Temperature is discussed previously in the main factor analysis. Temperature effects have been shown to mobilize arsenic in geothermal groundwater studies, however it often required a larger temperature change and was overshadowed by desorption and weathering (Bonte et al., 2013; Xing et al., 2023).

$F3_{As}$, and $F4_{As}$ consisted of aquifer groups and were respectively equivalent to F5 and F4 of the main factor analysis. The variances indicated that fracture/flows were more important than hydraulic conductivity/confinement. This is in contrast to the assumption that anthropogenic arsenic would be more influenced by shallow unconfined aquifers (Khan et al., 2023). A possible explanation could be spatial location – perhaps mining activities and geogenic arsenic sources occur in places with more fractured bedrock (Earle, 2019b).

$F5_{As}$ had a strong relationship with iron [0.7581], and an inverse relationship with time. $F5_{As}$ of the factor was equivalent to that of F2 of the main factor analysis - with the removal of manganese and lead and perhaps indicates weathering (Appelo & Postma, 2004). Iron is still important but is also endemic in minerals especially minerals associated with arsenic (Fakhreddine et al., 2021). The proportional variance indicated that time was slightly less important as compared to the main factor analysis. Further research is needed to understand the reasons behind that.

While $F6_{As}$ had a weak inverse relationship with chloride. $F6_{As}$ is equivalent to $F6_{D}$ of the drought data without uranium or distance (latitude). This is likely still related to geographical location.

The factor analysis focused on manganese is shown in Figure 5.2 and Section 8.3 (Appendix). It had 6 factors ($F1_{Mn}$, $F2_{Mn}$, $F3_{Mn}$, $F4_{Mn}$, $F5_{Mn}$, $F6_{Mn}$). Again, said factor analysis only covered 0.5783 cumulative variance therefore can be used for generalizations, but any findings should be confirmed with more data (Mulaik, 2009). $F1_{Mn}$, $F2_{Mn}$, $F3_{Mn}$, and $F4_{Mn}$ had a similar trend to $F1_{As}$, $F2_{As}$, $F4_{As}$, and $F3_{As}$.

In $F1_{Mn}$, chloride was more important while alkalinity was less important. This runs counter to what was assumed, as manganese is well associated with mineral weathering (Appelo & Postma, 2004). The low proportional variance could be an explanation for this result.

$F3_{Mn}$ is similar to F3 of the main factor analysis while $F4_{Mn}$ is similar to F4 of the main factor analysis. This runs inverse to what is seen with arsenic. This could state that manganese relies more on longer residence times in confined slower moving aquifers as this combination of variable seem to maximize rock-water interactions (Appelo & Postma, 2004).

$F5_{Mn}$ had a weak inverse relationship with time and manganese in addition a strong relationship to iron [0.9201]. The relationship between Mn-Fe was already discussed in the exploratory data analysis. Meanwhile the inverse relationship with time is similar to that in the main factor analysis.

$F6_{Mn}$ showed a weak inverse relationship to chloride, a weak relationship to pH and X. Those variable loadings suggested both a localised anthropogenic effect. The influence of pH along with chloride in this case would work for both anthropogenic as mining/industrial activities (Bradl, 2005). The centroid of which the X equivalent of latitude is calculated for would land no more eastward than Kamloops. The West Coast of B.C. has a history of industrial activities and is highly populated (Earle, 2019b).

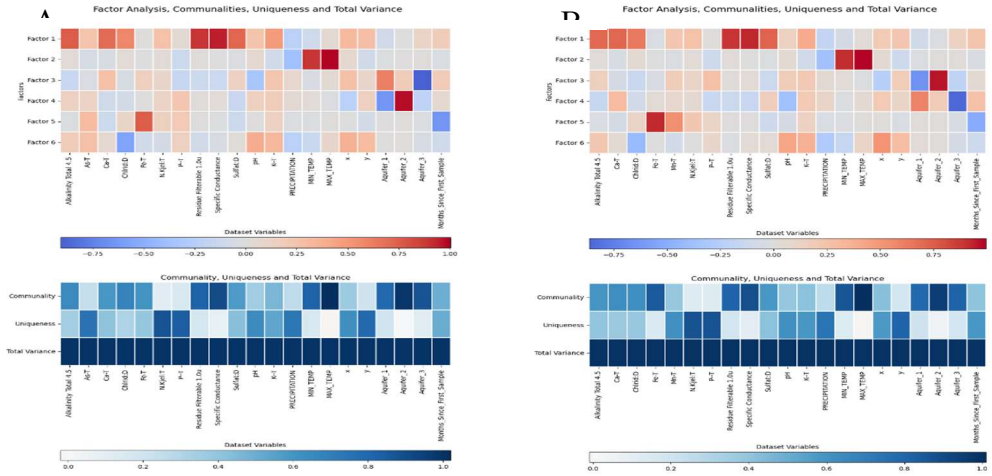

Figure 5.3.1: A) Factor analysis with oblimin rotation on a dataset with only As as the metal of interest. Community, Uniqueness and Total Variance are also graphed.
B) Factor analysis with oblimin rotation on a dataset with only Mn as the metal of interest. Community, Uniqueness and Total Variance are also graphed.

Figure 5.3 and Section 8.3 (Appendix) shows the factor analysis performed focused on lead data consisting of six factors ($F1_{Pb}$, $F2_{Pb}$, $F3_{Pb}$, $F4_{Pb}$, $F5_{Pb}$, $F6_{Pb}$) and made up 61% of cumulative variances. Thus, it has an acceptable variance to demonstrate some underlying structural patterns (Mulaik, 2009).

$F1_{Pb}$, $F3_{Pb}$, $F4_{Pb}$, and $F5_{Pb}$ are similar to $F1_{Mn}$, $F2_{Mn}$, $F3_{Mn}$ and $F4_{Mn}$. $F1_{Pb}$ followed a similar pattern to the previous metals and indicated saltwater intrusion/groundwater chemistry variables that were strongly influenced by specific conductance, residue filterable, alkalinity and sulfate while being weakly influenced by potassium, chloride and calcium. $F1_{Pb}$ places a lesser loading on calcium and greater loading on alkalinity then $F1_{Mn}$. This might be due to the buffering capacity of bicarbonate ions (Arciszewski & Roberts, 2022).

$F2_{Pb}$ presented 10% of the proportional variance and was strongly influenced by Pb [0.9200], strongly inversely influenced by time and weekly influenced by iron. The position of the proportional variance is similar to that of F2 in main factor analysis and indicates that groundwater geochemical conditions play an important role in lead speciation and transport. Iron and lead are commonly found together and inverse relationship to time indicates that lead could possibly be anthropogenic (Jurgens et al., 2019). Previous factor analyses in groundwater have found similar relationships of lead and iron (Love et al., 2004).

$F3_{Pb}$, $F4_{Pb}$, and $F5_{Pb}$ followed a similar relationship to the $F2_{Mn}$ $F3_{Mn}$, $F4_{Mn}$ profiles stating the importance of groundwater age and confinement. $F6_{Pb}$ showed a weak inverse relationship to Chloride and a weak relationship to X. This is similar to $F6_{Mn}$ but without pH. Lead can be highly corrosive, but it was unlikely a sample reached the pH level that would be required to leach lead (Appelo & Postma, 2004). Most pH samples hovered around 7, thus it could be an unnecessary consideration.

The underlying factor analysis focusing on uranium is shown in Figure 5.3 and Section 8.3 (Appendix). This factor analysis produced six factors ($F1_U$, $F2_U$, $F3_U$, $F4_U$, $F5_U$, $F6_U$) and only covered 0.5783 cumulative variance. Therefore, it can be used for generalizations, but any findings also should be confirmed with more data (Mulaik, 2009).

$F1_U$, $F2_U$, $F3_U$, and $F4_U$ are similar to $F1_{Mn}$, $F2_{Mn}$, $F3_{Mn}$, and $F4_{Mn}$. This could indicate that the underlying dominates variables affect the concentration of both metals in a similar manner. $F1_U$ represented saltwater intrusion factors and rock geochemistry with about 19% of the cumulative

variance. Compared to $F1_{Mn}$, $F1_U$ was influenced more by chloride then sulfate and influenced by calcium instead of potassium. This could represent different groundwater geochemistry from uranium bearing minerals (Larry D. Jones, 1990). Weak positive correlations have been found between uranium and chloride in groundwater studies (Selvi et al., 2016). Calcium also would be due to how uranium is found in rock and the formation of uranyl−calcium−carbonato complexes that dominate aqueous speciation (Skierszkan et al., 2021; Stewart et al., 2010). Uranium also had a weak influence in F1 of main factor analysis but did not appear in $F1_U$ perhaps likely due to lack of sampling data. Through the fundamental rock-water interactions govern major ion geochemistry, uranium seems to be more sensitive to saltwater intrusion factors given that all three saltwater intrusion factors have significant loadings. This again is in contrast to other studies which have not determined the sensitivity of uranium to saltwater intrusion (Smedley & Kinniburgh, 2023).

$F2_U$, $F3_U$ and $F4_U$ were similar to $F2_{Mn}$, $F3_{Mn}$ and $F4_{Mn}$ evidencing that the underlying variables and effects could be similar to both metal contaminates.

$F5_U$ mimics that of $F6_D$ (Drought) - weakly inversely related to chloride and weakly related to X and U. Chloride and uranium are both anthropogenic contaminates (Bradl, 2005). It is also indicated this factor is highly based on geography as the centroid of X is also near a more industrialized and populated area of B.C. The placement of this factor also may indicate that anthropogenic sources of uranium are slightly more common than geogenic sources.

$F6_U$ had a strong relationship to time (0.7409), a weak relationship to uranium and an inverse weak relationship to Fe. With these combinations, $F6_U$ may represent geogenic weathering/redox reactions for uranium along with the temporal relationships representing groundwater chemistry. (Appelo & Postma, 2004; Skierszkan et al., 2021).

$F6_u$ was similar to F2 of the main factor analysis or $F5_{Mn}$ but without Pb and/or Mn. However, unlike both the previous factor analysis, $F6_U$ has a moderate negative relationship/loading to iron while time takes a strong positive relationship. In permafrost areas, geogenic uranium mobilization is driven by sorption–desorption of rock and oxidation is often driven via weathering of calcium carbonate mineral weathering (Alam & Cheng, 2014; Skierszkan et al., 2021). Uranyl–calcium–carbonate complexes provide resilience to reduction for U(IV) even below that of Fe(III) reduction. Longer residence time means more increased reactions and thus

more desorption (Appelo & Postma, 2004). In addition, iron can reduce uranium and cause it to precipitate (Smedley & Kinniburgh, 2023).

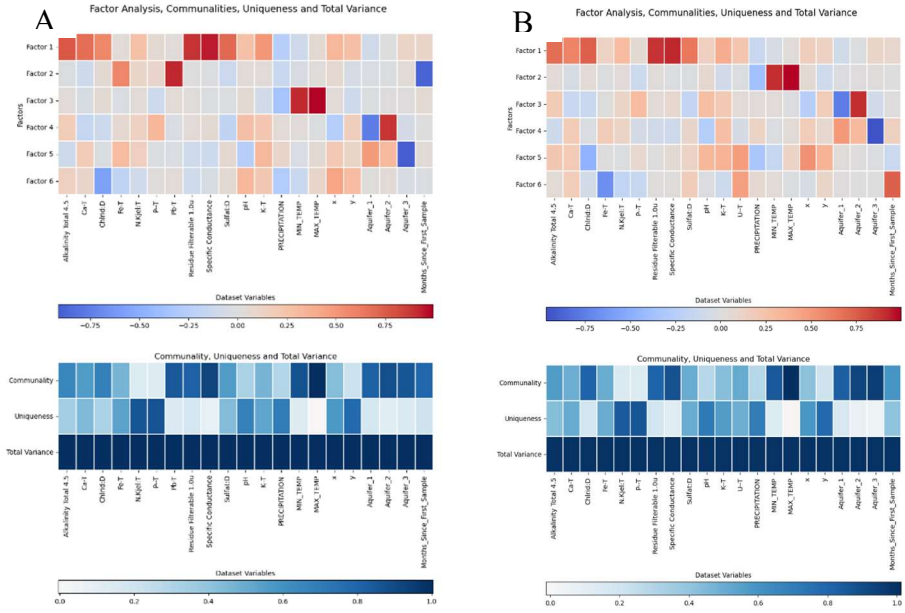

Figure 5.3.2: A) Factor analysis with oblimin rotation on a dataset with only Pb as the metal of interest. Community, Uniqueness and Total Variance are also graphed.
B) Factor analysis with oblimin rotation on a dataset with only U as the metal of interest. Community, Uniqueness and Total Variance are also graphed.

5.4 Factor Analysis with Climate Change Conditions

Datasets to represent drought and flood were created as in a similar way to the exploratory data analysis. Oblique rotation was used to balance an understanding of a correlated data set with analysis (Mulaik, 2009).

The supplementary data for the drought dataset is in Section 8.3 (Appendix). The factor analysis for drought resulted in six factors ($F1_D$, $F2_D$, $F3_D$, $F4_D$, $F5_D$, $F6_D$) that made up 57% of the total proportional variance. This is below the acceptable cut off of 0.60, the observations provide useful information of the underlying structure of the relationship, but still need more data to be a guiding influence for future protective models (Mulaik, 2009). British Columbia has complex geology and hydrogeology patterns across different regions and thus a cumulative variance of 58% might be moderate but could indicate some reasonable interconnectivity between variation and some dominant underlying insights (Earle, 2019b). In addition, different factor methods or spatial influences could account for the difference between the main factor analysis and drought.

$F1_D$ to $F3_D$ capture the dominate natural influence of geology/hydrogeology, temporal water quality changes and climate/meteorology.

$F1_D$ again was indicative of saltwater intrusion and rock geochemistry. It made up for 19% of the entire cumulative variance. $F1_D$ consisted of specific conductance (0.9592), residue filterable 1.0u (0.8999), alkalinity (0.7639), sulfate (0.7152) with a weak relationship of chloride and calcium. This is indicative of both saltwater intrusion and groundwater geochemistry (Appelo & Postma, 2004; British Columbia Ministry of Forest, 2016). This is further indicted as total dissolved solids/conductivities are primary natural factors influencing groundwater composition.

$F1_D$ shows similar variables to that of the main data except with stronger loadings. Geochemical droughts reduce recharge and intensify geochemical reactions via additional oxidation, concentration effects and localised groundwater retention time (Kampbell et al., 2003; Meyers et al., 2021). Unlike F1 in the main factor analysis, uranium was not a variable in $F1_D$, while Ca was weaker, and chloride was stronger. Uranium has been previously linked to drought (Nolan & Weber, 2015). A possible explanation of this is that evapotranspiration may transport uranium to the soil surface where it precipitates as evaporite (Noel, 2022). In addition, uranium often utilizes nitrate for oxidation and droughts decrease the catchment's nitrogen retention (Nolan & Weber, 2015; Winter et al., 2023).

Saltwater intrusion increases with increased pumping during drought which might explain the stronger effect of chloride (British Columbia Ministry of Forest, 2016). Calcium is also replaced by Na (Appelo & Postma, 2004). This type of relationship has been similarly observed in previous factor analysis in the Chitravati river basin during a drought (Briz-Kishore & Murali, 1992). Potassium is missing in $F1_D$ despite it being part of the first factor in most of the metal analysis. This may indicate a potential groundwater geochemical shift.

$F2_D$ had a strong negative correlation for time (-0.8908), a positive relation for lead (0.9083) and a weak relation for iron. It consisted of a 9% proportional loading. $F2_D$ is indicative of temporal influence of water quality and water geochemical processes.

$F2_D$ is similar to F2 in the main factor analysis but with a weaker factor loading of iron and without manganese. Manganese for this factor is also part of the metals factor analysis. Manganese had a weak relationship in F2 of the main factor analysis and regularly was linked to Fe (Hu et al., 2022). From the exploratory data analysis, drought breaks that correlation. The Mn-Fe relationship deteriorated with drought as other unmeasured factors started to influence geochemistry (Hamer et al., 2020). Timewise, the negative variable suggests a shorter residual time with less mobilization of contamination (Meyers et al., 2021). This makes sense given the geochemical capacity reduction that comes with aquifers undergoing droughts (Winter et al., 2023; Wossenyeleh et al., 2020).

$F3_D$ was about 9% of the proportional loading and indicated climate change variables. It was strongly composed of min_temp (0.9420), max_temp (0.9793) and weakly inversely related to precipitation. Negative loading of precipitation implies a greater influence of meteorological conditions during drier climatic periods with less water recharge. The rapid addition of rain and recovery of the aquifer will change the dominate geochemical processes. Longstanding droughts often influence soil and aquifer capacity and have a time lag of up to fifteen years in shallow aquifers to recovery (Schreiner-McGraw & Ajami, 2021).

$F4_D$ represented aquifer types – particularly aquifer confinement and hydraulic connectivity. $F4_D$ has a stronger inverse loading for Aquifer Group 1 and a weaker positive loading for Aquifer Group 2 in comparison to F4 of the main factor analysis and the relevant factors of the analyses focused on specific metals. Aquifer Group 1 consists of unconfined aquifers especially unconfined aquifers with a strong hydraulic connection. A drought and lowering of the water

table would dry out the pores, affect geochemistry and compromise the vadose zone effects, thus leading to a stronger negative loading (Riches et al., 2007; Wossenyeleh et al., 2020). Confined aquifers are not prone to evaporation effects and often have to worry about pumping (Gullacher et al., 2023).

Meanwhile $F5_D$ consisted of 7% of the proportional variant. It had weaker loading of Aquifer Group 2, Mn and K with a moderate inverse loading for Aquifer Group 3. $F5_D$ is similar to F5 in the main factor analysis and $F4_U$, $F5_{Pb}$, $F4_{Mn}$, or $F3_{As}$ in the factor analyses focusing on individual metals. However, in $F5_D$, Mn and K are variables, the effect of Aquifer Group 3 is weaker and Aquifer Group 1 is replaced by Aquifer Group 2. During droughts, streamflow is affected in fractured bedrock due to the lowering of the groundwater table and water pumping (Nicholas et al., 1996). Aquifer Group 1 would have a similar effect. However, in confined aquifers, groundwater is often isolated from the effects other than pumping, allow for diffusion and thus would have a positive loading (Orecchia et al., 2022). Manganese and Potassium could be due to the geochemical properties of the confined aquifers.

$F6_D$ made up 5% the proportional variance and was composed of weak relationships to X, U and inversely chloride. X is the distance equivalent calculation for latitude. The main factor analysis utilized an extremely stringent variable selection and thus it is not shown due to methodological differences (Mulaik, 2009). These variables are similar to the summation of the equivalent factors in the factor analyses on the metals of focus. This could indicate anthropogenic or land uses on the groundwater composition, as road salts and agriculture fertilizers (P. Li et al., 2021).

Supporting factor analysis for flooded data are shown in Section 8.3 (Appendix) and consistent of 60% of the cumulative variance and seven factors ($F1_F$, $F2_F$, $F3_F$, $F4_F$, $F5_F$, $F6_F$, $F7_F$).

$F1_F$ again seemed to indicate groundwater chemistry and saltwater intrusion variables. In comparison to F1 of the main factor analysis and the metals factor analyses, $F1_F$ has a greater influence of chloride, and less of an influence of alkalinity, sulfate and calcium. This is likely due to the dilution effect and floods often bring in chloride from the surface (Basahi et al., 2018; Ghazavi et al., 2012). $F1_F$ also had a greater influence of chloride in comparison to $F1_D$. Flooding effects can overwhelm most geogenic processes (Crawford et al., 2022).

$F2_F$ demonstrated a similar relationship with $F2_D$ of drought with a stronger relation for Pb (0.9527) but a slightly less inverse relationship to time. Manganese had no significant influence while iron only had weaker influences. Again, flooding would overwhelm most geogenic processes and prevent geochemical interactions with high flow rates (Masoud et al., 2018). Lead can be transported via flood waters (Ciszewski & Grygar, 2016).

$F3_F$ is like that of $F4_D$ and F4 of the main factor analysis. It is strongly inversely influenced by Aquifer Group 1 and strongly influenced by Aquifer Group 2. Similar to the main factor analysis and the factor analysis for the metals of focus and in contrast to $F4_D$, both aquifer groups have strong loadings. Aquifer Group 1 is unconfined and often hydraulically connected with the surface. This allows for a quicker dilution response and flow especially in flood like scenarios (Wei et al., 2016). Confined aquifers are not as affected by overland flood and thus can maintain constant geochemical conditions (Chung et al., 2020). As temperature isn't as relevant to floods compared to aquifer confinement of flows, $F3_F$ has a greater proportional variance then temperature/direct climate change factors (Geris et al., 2022).

$F4_F$ is similar to that of $F3_D$ and F3 of the main factor analysis. This was previously explained above.

$F5_F$ and $F6_F$ consisted of weaker loadings and would likely have been eliminated for a more conservative factor analysis (Mulaik, 2009). $F5_F$ consisted of weak relationships with X (distance version of latitude), y (distance version of longitude), U and was inversely related to precipitation. This is the equivalent to $F6_D$ or $F6_{As}$, $F6_{Mn}$, $F6_{Pb}$, or $F6_U$ in the analysis focused on metals. Hence, it is likely to be anthropogenic. Chloride was not a variable perhaps due to overland flooding diluting it. Precipitation had a negative loading as it can dilute anthropogenic pollution (Hervai et al., 2020). Due to the locations of the wells, both the Y and X center is still down more in Southwestern B.C. where there is a history of mining and pollution (Earle, 2019b). Overland anthropogenic pollution would also cause more variability in a flood (Ghazavi et al., 2012).

$F6_F$ had weak relationships of manganese and iron along with an inverse weak relationship to Aquifer Group 3. It made up 0.0588 of the proportional variances and is the equivalent of $F5_D$, Factor 5 in the main factor analyses and $F3_{As}$, $F4_{Mn}$, $F5_{Pb}$, or $F4_U$ in the analyses focused on metals. Unlike the other analyses, the loading of Aquifer Group 3 was far weaker while K,

Aquifer Group 2 and Aquifer Group 1 were not variables. Saturated soil/sand and confined aquifers may not have an effect on groundwater in a flood (Orecchia et al., 2022; Wossenyeleh et al., 2020). In addition, saturated soil loses the vadose effects. Iron and manganese often co-linked and thus it is plausible to them both to be variables (Santos et al., 2011a).

Factor 7 ($F7_F$), which made up 5% of proportional variance had a strong relationship to arsenic (.8069) and a weak relationship to phosphorus. $F7_F$ is unique to flooded data and has the moderate variable loadings for phosphorus and strong loadings for arsenic. Both these can be natural or anthropogenic contamination sources as they are both used in land and industrial use (P. Li et al., 2021; Peel et al., 2022). However, this paring only appearing during flooding indicates anthropogenic perhaps via flooding sediments over natural contamination as there would be some apparent relationship in the main factor analysis or metals factor analysis if the sources were geogenic. Arsenic and phosphorus have previously been found to be driving anthropogenic variables in other factor analyses of groundwater (Ayotte et al., 2015; Kuppusamy & Giridhar, 2006).

Chapter 6: Conclusion

This thesis took the initial steps to help create a knowledge foundation on which to build future predictive models and policies for protecting human health and the environment from groundwater metal contamination in the face of climate change. This is one of the few specific sources that compile research/trends for groundwater contamination and analyses, widespread data for the relationship between groundwater metal contamination and climate change influences. However, these analyses did have restrictions – lack of data especially that of geology, aquifer, groundwater residence time, water table depth, well depth, and inclusion of snowmelt limited the definite conclusions that could be made. It is indicative that future research needs to focus on spatial auto correction to further determine whether the influences of metals are in part due to different geoclimatic zones or localized anthropogenic influences. The Power BI indicated some potential seasonality when it came to specific contaminants. Detrending and de-seasonalizing would be indicative for future research to determine how vulnerable groundwater to metal contamination caused by secondary climate change effects and to understand more of risks and resiliencies. Moreover, incorporating GIS would account for temperature and climactic zones while utilizing time space cubes would differentiate spatial-temporal changes. Future research could utilize this to account for topography and better link aquifer lithology.

Initial exploratory data analysis indicated that groundwater contamination was influenced by aquifer and groundwater chemistry, adsorption, and redox reactions, given influence of alkalinity influences on most metal, lower turbidity, and the correlations between manganese and iron. Incorporating groundwater levels would be a necessity for future models due to the significance of understanding the differences in oxidation states. Confined aquifers and fractured aquifers were influenced differently than unconfined aquifers that often had a hydraulic connection to overland water bodies – especially when it came to seasonality and time effects. Lead geochemistry did not have much of a relationship with corrosivity. Furthermore, low precipitation seems to demonstrate a concentration effect or perhaps a change in redox chemistry. In addition, flooding often resulted in a dilution effect in a lot of metal contamination. “Drought” conditions had a stronger relationship with uranium, but the concentrations remained below the Canadian Drinking Water Guidelines. As expected, arsenic was very influenced by less precipitation and oxidating conditions and Fe-Mn was highly related to reducing conditions.

However surprisingly, soluble uranium seemed to persist in reducing conditions. This might be due to the complex's uranium forms with calcium. The effect of older water seemed to be more significant than previously predicted.

Furthermore, rising specific conductance and chloride indicates that there is a likely link to saltwater intrusion and elevated metals especially with uranium, manganese and arsenic in groundwater. This study is more exploratory, definite conclusions will require more validation with a larger data.

The description and summary statistical analysis the Kendall and Pearson correlations between different metals in different climate change scenarios. In the regular dataset, the relationship between Mn-Fe and U-Ca was likely due to groundwater geochemistry as those are common geochemical relationships. The correlation between Pb-Cd was more likely anthropogenic due to B.C.'s history of pollution.

The correlations between the contaminates lessened or remained consistent in flooding conditions, which could be due to flooding keeping the same spread of plumes and groundwater geochemistry consistent. Flooding would raise the water table and keep a reducing environment that most contaminates remain soluble in. An increase in iron was indicative in the scatterplots was also observed during flooding conditions. Future studies might want to look at the influx of sediment and remobilization of contaminates and account for different aquifer types in the correlations.

Meanwhile, drought led to a decoupling of a lot of correlations between contaminates. This includes that of uranium and Mn-Fe. This could be due to the lowering of the water table due to drought that causes more oxidation, and only spatial localised areas for geochemical reactions. Pb-Cd still had a relationship due to potential anthropogenic sources. Surprisingly, arsenic or nitrogen did not have any correlations despite previous studies showing otherwise. This might be due to the spatial location of arsenic or nitrogen. More research is needed to tell if there is a definite deterioration or concentration effect. Ideally these observations should be verified against the hydraulic and low flow zones of B.C. preferably with kriging, and Queens and Moran autocorrection.

Saltwater intrusion was best characterized by using the sample cut off above 1,000 µS/cm for specific conductance or above 150 mg/L for chloride. The saltwater intrusion dataset showed a

high number of samples with arsenic above Canadian Drinking Water Guidelines which potentially indicate changing geochemistry but will require more research to verify. Moreover, saltwater intrusion changed the correlations between metals. The Fe-Mn correlation was completely decoupled. Lead had a somewhat lower correlation with cadmium in addition to a weak correlation to iron and negative weak correlation to uranium. This might be due turbulent mixing, corrosion byproducts and changing redox conditions with previous legacy sources.

As expected with saltwater intrusion, the correlation between calcium and uranium deteriorated, as calcium is commonly replaced by sodium in the process. The additional correlations between uranium and chloride, potassium and hardness were unexpected as uranium geochemistry in saltwater intrusion is not well understood. However, potassium and chloride can be potentially explained by their effects from saltwater intrusion. Hardness remained consistent indicating that calcium must also be replaced by magnesium.

Exploratory factor analysis was performed to identify potential predictor variables and elucidate underlying processes. The primary factor analysis had an acceptable KMO of 0.753 for exploratory analysis. More data along with other variables should be included in any confirmatory factor analyses. The first factor was had the largest proportional variance and indicative of groundwater geochemistry, especially weathering and saltwater intrusion. This was due to the variable loadings of specific conductance, residual filterable, calcium, alkalinity, sulfate, chloride and uranium. This was similar to previous studies. As it was composed of saltwater intrusion variables, it indicates that sea water intrusion does have an impact on the overall data set and on metal contamination. Further studies especially with a confirmatory factor analysis is needed to verify this and also to determine how this influences risk of uranium contamination. The second factor involved redox factors perhaps with groundwater residence time while the third factor involved direct climatology such as temperatures. The fourth factor was composed of aquifer groups and likely represented aquifer confinement and recharge/hydraulic connectivity. The fifth factor may represent fractures, flow and diffusion. The first, fourth and fifth factors were expected. Unexpectedly, what may be residence time was a variable while direct arsenic was not. Hydraulic connectivity and other aquifer characteristics had a stronger influence than pure precipitation which did not show up as a variable for any of the factors and thus any secondary effects might need a more specific analysis such as non-

negative factorization to determine further vulnerability and distinguish pure climate change effects. Future models should incorporate more in-depth spatial factor analyses methods.

In addition, factor analyses were conducted focusing on arsenic, manganese, lead and uranium. These factor analyses were largely affected by lack of data and smaller sampling sizes. There was a large indication that other variables should be included. However, the core factors remained somewhat consistent, thought the proportional variances of each changed and key variable loadings could differ. This indicated that there each metal was affected by some different underlying geochemical processes. In addition, there was often a sixth factor representing anthropogenic contamination.

Future research should incorporate larger data sets especially when it comes to analyzing the data sets for climate change effects. A factor analysis for saltwater intrusion should be done as future research as the current data set did not have enough samples. With droughts, there is indication that the groundwater chemistry slightly shifts with longer resident times for localized rock-water interactions. Variable loadings of groundwater geochemistry were stronger with a weaker relationship of calcium but stronger relationship for chloride. This is consistent with drought geochemistry. The relationship with uranium disappeared for this. The factor representing groundwater resident time and redox had weaker relationships as compared to the main factor analysis and manganese was not a variable. This makes sense as droughts result in more pumping, decreased aquifer capacity and the lowering of water tables. The climatology factor also included a weak inverse relationship to direct precipitation.

Meanwhile, the factor for confinement and direct recharge had a stronger relationship to unconfined aquifers and weaker to confined aquifers. Again, confined aquifers would be affected only by pumping and not overland water loss. This may indicate a higher vulnerability to groundwater contamination. Further research is still required to understand the differences of hydraulic connections and generalized groundwater. The fifth factor representing diffusions and flow for drought had a weaker relationship of confined aquifers, stronger inverse relationship to fractured aquifers and a weak relationship to potassium and manganese. In the drought dataset, confined aquifers replace unconfined aquifers as a variable likely since confined still maintain more capacity to carry out diffusion reactions.

Drought also seems to be more influenced by anthropogenic activity affecting groundwater contamination. A sixth factor, likely representing anthropogenic contamination with latitudinal distance, uranium and chloride was identified. Further spatial analyses are needed to determine if these lead to a concentration effect in well water.

The factor for saltwater intrusion and groundwater geochemistry for the flooding factor analysis was composed of slightly different variable proportions indicating flooding does have some influence on groundwater geochemistry. Chloride had a stronger influence while alkalinity, sulfate and calcium had less of one. This may indicate a dilution effect accompanied by the influx of surface contamination. Future studies should overlay these results with the different hydrological zones, low flow zones or any indication of peak flows to fully assess the generalized vulnerability of groundwater with flooding.

For the second factor, groundwater residence time had a weaker inverse relationship, lead had a stronger and iron had a weak influence. Again, flooding would overwhelm most geogenic processes – bringing in sediments and preventing geochemical interactions due to the influx of additional water. The factor representing aquifer confinement and potential recharge was the third factor and unlike drought or the main factor analysis, had more of an effect on floods then climatology. The variable relationships were like the main factor analysis. Overland flow from unconfined and often hydraulically connected aquifers would lead to a dilution effect. Meanwhile the fourth factor representing climatology was similar to the climatology factor of the main factor analysis.

The fifth factor of flooding was the anthropogenic one similar to that of drought. It consisted of latitudinal distance, longitudinal distance, and uranium without chloride. It also had an inverse relationship to precipitation. This is indicative of anthropogenic influences and the proportional variance indicates that groundwater contamination may be more of a risk for floods then droughts. The sixth factor of flooding represented flow/diffusion and weakly composed of fractured aquifers. Both K, confined and unconfined variables were not variables. This is likely due to confined aquifers would not have much influence from overland flooding and saturated soil/sand in unconfined aquifers lose vadose effects.

Last, the flood factor analysis had a unique seventh factor which may represent additional anthropogenic contamination. It consisted of strong relationship with arsenic and weak

relationship with phosphorus. Future studies should consider how flooded sediments may affect metal contamination in groundwater.

References

Abbaspour, N., Hurrell, R., & Kelishadi, R. (2014). Review on iron and its importance for human health. *Journal of Research in Medical Sciences : The Official Journal of Isfahan University of Medical Sciences*, *19*(2), 164–174.

Agency for Toxic Substances and Disease Registry. (2004). *INTERACTION PROFILE FOR: ARSENIC, CADMIUM, CHROMIUM, AND LEAD*. U.S. Department of Health and Human Services. https://www.atsdr.cdc.gov/interactionprofiles/IP-metals1/ip04.pdf

Ahmad, M. (2012). *Iron and manganese removal from groundwater: Geochemical modeling of the Vyredox method* [Master thesis]. https://www.duo.uio.no/handle/10852/12540

Alam, Md. S., & Cheng, T. (2014). Uranium release from sediment to groundwater: Influence of water chemistry and insights into release mechanisms. *Journal of Contaminant Hydrology*, *164*, 72–87. https://doi.org/10.1016/j.jconhyd.2014.06.001

Allen, D., & Gleeson, T. (2023). Groundwater Resource Allocation in British Columbia: Challenges and Ways Forward. *Confluence: Journal of Watershed Science and Management*, *6*(1), Article 1. https://doi.org/10.22230/jwsm.2023v6n1a49

Allen, D. M., Stahl, K., Whitfield, P. H., & Moore, R. D. (2014). Trends in groundwater levels in British Columbia. *Canadian Water Resources Journal / Revue Canadienne Des Ressources Hydriques*, *39*(1), 15–31. https://doi.org/10.1080/07011784.2014.885677

Alvarez, C. C., Bravo Gómez, M. E., & Hernández Zavala, A. (2021). Hexavalent chromium: Regulation and health effects. *Journal of Trace Elements in Medicine and Biology*, *65*, 126729. https://doi.org/10.1016/j.jtemb.2021.126729

Amanambu, A. C., Obarein, O. A., Mossa, J., Li, L., Ayeni, S. S., Balogun, O., Oyebamiji, A., & Ochege, F. U. (2020). Groundwater system and climate change: Present status and future

considerations. *Journal of Hydrology*, *589*, 125163. https://doi.org/10.1016/j.jhydrol.2020.125163

Andrade, L., O'Dwyer, J., O'Neill, E., & Hynds, P. (2018). Surface water flooding, groundwater contamination, and enteric disease in developed countries: A scoping review of connections and consequences. *Environmental Pollution*, *236*, 540–549. https://doi.org/10.1016/j.envpol.2018.01.104

Appelo, C. A. J., & Postma, D. (2004). *Geochemistry, Groundwater and Pollution*. CRC Press.

Appleyard, S. J., Angeloni, J., & Watkins, R. (2006). Arsenic-rich groundwater in an urban area experiencing drought and increasing population density, Perth, Australia. *Applied Geochemistry*, *21*(1), 83–97. https://doi.org/10.1016/j.apgeochem.2005.09.008

Arciszewski, T. J., & Roberts, D. R. (2022). Analyzing Relationships of Conductivity and Alkalinity Using Historical Datasets from Streams in Northern Alberta, Canada. *Water*, *14*(16), Article 16. https://doi.org/10.3390/w14162503

Argos, M., Ahsan, H., & Graziano, J. H. (2012). ARSENIC AND HUMAN HEALTH: EPIDEMIOLOGIC PROGRESS AND PUBLIC HEALTH IMPLICATIONS. *Reviews on Environmental Health*, *27*(4), 191–195. https://doi.org/10.1515/reveh-2012-0021

Ayotte, J. D., Belaval, M., Olson, S. A., Burow, K. R., Flanagan, S. M., Hinkle, S. R., & Lindsey, B. D. (2015). Factors affecting temporal variability of arsenic in groundwater used for drinking water supply in the United States. *Science of The Total Environment*, *505*, 1370–1379. https://doi.org/10.1016/j.scitotenv.2014.02.057

Baborowski, M., von Tümpling, & Friese, K. (2004). Behaviour of suspended particulate matter (SPM) and selected trace metals during the 2002 summer flood in the River Elbe

(Germany) at Magdeburg monitoring station. *Hydrology and Earth System Sciences*, *8*(2), 135–150. https://doi.org/10.5194/hess-8-135-2004

Bae, D.-S., Gennings, C., Carter, W. H., Jr., Yang, R. S. H., & Campain, J. A. (2001). Toxicological Interactions among Arsenic, Cadmium, Chromium, and Lead in Human Keratinocytes. *Toxicological Sciences*, *63*(1), 132–142. https://doi.org/10.1093/toxsci/63.1.132

Bakari, S. S., Aagaard, P., Vogt, R. D., Ruden, F., Brennwald, M. S., Johansen, I., & Gulliksen, S. (2012). Groundwater residence time and paleorecharge conditions in the deep confined aquifers of the coastal watershed, South-East Tanzania. *Journal of Hydrology*, *466–467*, 127–140. https://doi.org/10.1016/j.jhydrol.2012.08.016

Ballukraya, P. N., & Ravi, R. (1999). Characterization of Groundwater in the Unconfined Aquifers of Chennai City, India, Part 2—Factor Analysis. *Geological Society of India*, *54*(1), Article 1.

Barbieri, M., Barberio, M. D., Banzato, F., Billi, A., Boschetti, T., Franchini, S., Gori, F., & Petitta, M. (2023). Climate change and its effect on groundwater quality. *Environmental Geochemistry and Health*, *45*(4), 1133–1144. https://doi.org/10.1007/s10653-021-01140-5

Barringer, J. L., Szabo, Z., Reilly, P. A., Barringer, J. L., Szabo, Z., & Reilly, P. A. (2013). Occurrence and Mobility of Mercury in Groundwater. In *Current Perspectives in Contaminant Hydrology and Water Resources Sustainability*. IntechOpen. https://doi.org/10.5772/55487

Basack, S., Loganathan, M. K., Goswami, G., & Khabbaz, H. (2022a). Saltwater Intrusion into Coastal Aquifers and Associated Risk Management: Critical Review and Research Directives. *Journal of Coastal Research*, *38*(3), 654–672.

Basack, S., Loganathan, M. K., Goswami, G., & Khabbaz, H. (2022b). Saltwater Intrusion into Coastal Aquifers and Associated Risk Management: Critical Review and Research Directives. *Journal of Coastal Research*, *38*(3), 654–672. https://doi.org/10.2112/JCOASTRES-D-21-00116.1

Basahi, J. M., Masoud, M. H. Z., & Rajmohan, N. (2018). Effect of flash flood on trace metal pollution in the groundwater—Wadi Baysh Basin, western Saudi Arabia. *Journal of African Earth Sciences*, *147*, 338–351. https://doi.org/10.1016/j.jafrearsci.2018.06.032

B.C. Ministry of Environment and Climate Change Strategy. (2023, February 28). *British Columbia Regional Streamflow Inventory Reports* [Govermental]. Province of British Columbia. https://www2.gov.bc.ca/gov/content/environment/air-land-water/water/water-science-data/water-data-tools/provincial-hydrology-program/resources/streamflow-inventory#reports

bcgov. (2024). *DataBC Data Publication Standard Practices, Guidelines and Processes for the BC Data Catalogue (BCDC)* [Computer software]. https://bcgov.github.io/data-publication/pages/dsg_bcdc.html

Beckers, F., & Rinklebe, J. (2017). Cycling of mercury in the environment: Sources, fate, and human health implications: A review. *Critical Reviews in Environmental Science and Technology*, *47*(9), 693–794. https://doi.org/10.1080/10643389.2017.1326277

Belkhiri, L., & Narany, T. S. (2015). Using Multivariate Statistical Analysis, Geostatistical Techniques and Structural Equation Modeling to Identify Spatial Variability of

Groundwater Quality. *Water Resources Management*, *29*(6), 2073–2089. https://doi.org/10.1007/s11269-015-0929-7

Benz, S. A., Bayer, P., & Blum, P. (2017). Global patterns of shallow groundwater temperatures. *Environmental Research Letters*, *12*(3), 034005. https://doi.org/10.1088/1748-9326/aa5fb0

Bethke, C. M., & Marshak, S. (1990). Brine Migrations Across North America—The Plate Tectonics of Groundwater. *Annual Review of Earth and Planetary Sciences*, *18*(1), 287–315. https://doi.org/10.1146/annurev.ea.18.050190.001443

Biglari, H., Saeidi, M., Karimyan, K., Narooie, M. R., & Sharafi, H. (2018). Data for factor analysis of hydro-geochemical characteristics of groundwater resources in Iranshahr. *Data in Brief*, *19*, 548–563. https://doi.org/10.1016/j.dib.2018.05.039

Bjørklund, G., Semenova, Y., Pivina, L., Dadar, M., Rahman, Md. M., Aaseth, J., & Chirumbolo, S. (2020). Uranium in drinking water: A public health threat. *Archives of Toxicology*, *94*(5), 1551–1560. https://doi.org/10.1007/s00204-020-02676-8

Blake, W. H., Walsh, R. P. D., Barnsley, M. J., Palmer, G., Dyrynda, P., & James, J. G. (2003). Heavy metal concentrations during storm events in a rehabilitated industrialized catchment. *Hydrological Processes*, *17*(10), 1923–1939. https://doi.org/10.1002/hyp.1218

Bonte, M., van Breukelen, B. M., & Stuyfzand, P. J. (2013). Temperature-induced impacts on groundwater quality and arsenic mobility in anoxic aquifer sediments used for both drinking water and shallow geothermal energy production. *Water Research*, *47*(14), 5088–5100. https://doi.org/10.1016/j.watres.2013.05.049

Bost, M., Houdart, S., Oberli, M., Kalonji, E., Huneau, J.-F., & Margaritis, I. (2016). Dietary copper and human health: Current evidence and unresolved issues. *Journal of Trace*

Elements in Medicine and Biology, *35*, 107–115. https://doi.org/10.1016/j.jtemb.2016.02.006

Bradl, H. B. (2005). Chapter 1 Sources and origins of heavy metals. In H. B. Bradl (Ed.), *Interface Science and Technology* (Vol. 6, pp. 1–27). Elsevier. https://doi.org/10.1016/S1573-4285(05)80020-1

Brender, J. D., Suarez, L., Felkner, M., Gilani, Z., Stinchcomb, D., Moody, K., Henry, J., & Hendricks, K. (2006). Maternal exposure to arsenic, cadmium, lead, and mercury and neural tube defects in offspring. *Environmental Research*, *101*(1), 132–139. https://doi.org/10.1016/j.envres.2005.08.003

British Columbia Ministry of Forest. (2016). *Best Practices for Prevention of Saltwater Intrusion*. British Columbia. https://www2.gov.bc.ca/assets/gov/environment/air-land-water/water/water-wells/saltwaterintrusion_factsheet_flnro_web.pdf

Briz-Kishore, B. H., & Murali, G. (1992). Factor analysis for revealing hydrochemical characteristics of a watershed. *Environmental Geology and Water Sciences*, *19*(1), 3–9. https://doi.org/10.1007/BF01740571

Butterman, W. C., & Reston, J. P. (2004). *MINERAL COMMODITY PROFILES CADMIUM* (U.S. GEOLOGICAL SURVEY 02–238; Open-File Report). U.S. DEPARTMENT OF THE INTERIOR. https://pubs.usgs.gov/of/2002/of02-238/of02-238.pdf

Cabrera, A., Blarasin, M., & Maldonado, L. (2017). Groundwater age and hydrothermalism of confined aquifers in the Argentine Pampean plain. *Geothermal Energy*, *5*(1), 6. https://doi.org/10.1186/s40517-017-0064-1

Canada, H. (2014, October 22). *Guidelines for Canadian Drinking Water Quality—Summary Tables* [Guidance]. https://www.canada.ca/en/health-canada/services/environmental-

workplace-health/reports-publications/water-quality/guidelines-canadian-drinking-water-quality-summary-table.html

Carmichael, V., Kenny, S., Gellein, C., Wei, M., & Allen, D. (2008). *Re-evaluating the aquifer hydraulic properties within the Okanagan Valley, British Columbia, Canada*. GeoEdmonton'08. https://members.cgs.ca/documents/conference2008/GEO2008/pdfs/193.pdf

Cedergreen, N. (2014). Quantifying Synergy: A Systematic Review of Mixture Toxicity Studies within Environmental Toxicology. *PLOS ONE*, *9*(5), e96580. https://doi.org/10.1371/journal.pone.0096580

Chen, T., Zhang, H., Sun, C., Li, H., & Gao, Y. (2018). Multivariate statistical approaches to identify the major factors governing groundwater quality. *Applied Water Science*, *8*(7), 215. https://doi.org/10.1007/s13201-018-0837-0

Chouaib, W., & Caissie, D. (2021). Regional disparities in water availability and low flow conditions in rivers across Canada. *Journal of Hydrology*, *598*, 126195. https://doi.org/10.1016/j.jhydrol.2021.126195

Chung, S. Y., Rajendran, R., Senapathi, V., Sekar, S., Ranganathan, P. C., Oh, Y. Y., & Elzain, H. E. (2020). Processes and characteristics of hydrogeochemical variations between unconfined and confined aquifer systems: A case study of the Nakdong River Basin in Busan City, Korea. *Environmental Science and Pollution Research*, *27*(9), 10087–10102. https://doi.org/10.1007/s11356-019-07451-6

Ciszewski, D., & Grygar, T. M. (2016). A Review of Flood-Related Storage and Remobilization of Heavy Metal Pollutants in River Systems. *Water, Air, & Soil Pollution*, *227*(7), 239. https://doi.org/10.1007/s11270-016-2934-8

Corlin, L., Rock, T., Cordova, J., Woodin, M., Durant, J. L., Gute, D. M., Ingram, J., & Brugge, D. (2016). Health Effects and Environmental Justice Concerns of Exposure to Uranium in Drinking Water. *Current Environmental Health Reports*, *3*(4), 434–442. https://doi.org/10.1007/s40572-016-0114-z

Coulson, C. H., & Obedkoff, Q. (1998). *British Columbia Streamflow Inventory* (2227; Ecological Reports Catalogue). British Columbia Ministry of Environment. https://a100.gov.bc.ca/pub/acat/public/viewReport.do?reportId=2227

Crawford, S. E., Brinkmann, M., Ouellet, J. D., Lehmkuhl, F., Reicherter, K., Schwarzbauer, J., Bellanova, P., Letmathe, P., Blank, L. M., Weber, R., Brack, W., van Dongen, J. T., Menzel, L., Hecker, M., Schüttrumpf, H., & Hollert, H. (2022). Remobilization of pollutants during extreme flood events poses severe risks to human and environmental health. *Journal of Hazardous Materials*, *421*, 126691. https://doi.org/10.1016/j.jhazmat.2021.126691

Dalton, M. G., & Upchurch, S. B. (1978). Interpretation of Hydrochemical Facies by Factor Analysis. *Groundwater*, *16*(4), 228–233. https://doi.org/10.1111/j.1745-6584.1978.tb03229.x

Data Catalogue. (n.d.). Retrieved December 5, 2023, from https://catalogue.data.gov.bc.ca/

Daughney, C. J. (2003). Iron and manganese in New Zealand's groundwater. *Journal of Hydrology (New Zealand)*, *42*(1), 11–26.

DeSimone, L., McMahon, P., & Rosen, M. (2014). *The quality of our Nation's waters—Water quality in Principal Aquifers of the United States 1991-2010* (ISSN 2330–5703; U.S. Geological Survey Circular 1360). U.S. Geological Survey. https://pubs.usgs.gov/circ/1360/

Earle, S. (2019a). *6.2 Chemical Sedimentary Rocks*. https://opentextbc.ca/physicalgeology2ed/chapter/6-2-chemical-sedimentary-rocks/

Earle, S. (2019b). *Physical Geology—2nd Edition*. BCcampus. https://opentextbc.ca/physicalgeology2ed/

Edwards, E. C., Nelson, C., Harter, T., Bowles, C., Li, X., Lock, B., Fogg, G. E., & Washburn, B. S. (2022). Potential effects on groundwater quality associated with infiltrating stormwater through dry wells for aquifer recharge. *Journal of Contaminant Hydrology*, *246*, 103964. https://doi.org/10.1016/j.jconhyd.2022.103964

Fakhreddine, S., Prommer, H., Scanlon, B. R., Ying, S. C., & Nicot, J.-P. (2021). Mobilization of Arsenic and Other Naturally Occurring Contaminants during Managed Aquifer Recharge: A Critical Review. *Environmental Science & Technology*, *55*(4), 2208–2223. https://doi.org/10.1021/acs.est.0c07492

Fallahati, A., Soleimani, H., Alimohammadi, M., Dehghanifard, E., Askari, M., Eslami, F., & Karami, L. (2019). Impacts of drought phenomenon on the chemical quality of groundwater resources in the central part of Iran-application of GIS technique. *Environmental Monitoring and Assessment*, *192*(1), 64. https://doi.org/10.1007/s10661-019-8037-4

Farnham, I. M., Johannesson, K. H., Singh, A. K., Hodge, V. F., & Stetzenbach, K. J. (2003). Factor analytical approaches for evaluating groundwater trace element chemistry data. *Analytica Chimica Acta*, *490*(1), 123–138. https://doi.org/10.1016/S0003-2670(03)00350-7

Federal-Provincial-Territorial Committee on Drinking Water. (2016). *Manganese in Drinking Water* [Consultations]. Health Canada. https://www.canada.ca/en/health-

canada/programs/consultation-manganese-drinking-water/manganese-drinking-water.html

Fulton, R. J. (1989). *Quaternary Geology of Canada and Greenland*. Geological Society of America. https://doi.org/10.1130/DNAG-GNA-K1

Fulton, R. J., Ryder, J. M., & Tsang, S. (2004). The Quaternary glacial record of British Columbia, Canada. In J. Ehlers & P. L. Gibbard (Eds.), *Developments in Quaternary Sciences* (Vol. 2, pp. 39–50). Elsevier. https://doi.org/10.1016/S1571-0866(04)80184-2

G W Kennedy. (2021). *A Manganese in Well Water Risk Map for Nova Scotia* (Open File Report ME 2021-002). Nova Scotia Energy and Mines Geological Survey. https://novascotia.ca/natr/meb/data/ofr/ofr_me_2021-002.pdf

Ganoulis, J. (2009). *Risk Analysis of Water Pollution*. John Wiley & Sons.

Gavino-Lopez, N., Eaves, L. A., Enggasser, A. E., & Fry, R. C. (2022). Developing Toxic Metal Environmental Justice Indices (TM-EJIs) for Arsenic, Cadmium, Lead, and Manganese Contamination in Private Drinking Wells in North Carolina. *Water*, *14*(13), Article 13. https://doi.org/10.3390/w14132088

Gerhardsson, L. (2022). Chapter 28—Diagnosis and treatment of metal poisoning general aspects∗∗This chapter is based on the chapter "Diagnosis and Treatment of Metal Poisoning General Aspects" by Lars Gerhardsson and George Kazaantzis in the fourth edition of this handbook. In G. F. Nordberg & M. Costa (Eds.), *Handbook on the Toxicology of Metals (Fifth Edition)* (pp. 663–684). Academic Press. https://doi.org/10.1016/B978-0-12-823292-7.00017-6

Geris, J., Comte, J.-C., Franchi, F., Petros, A. K., Tirivarombo, S., Selepeng, A. T., & Villholth, K. G. (2022). Surface water-groundwater interactions and local land use control water

quality impacts of extreme rainfall and flooding in a vulnerable semi-arid region of Sub-Saharan Africa. *Journal of Hydrology*, *609*, 127834. https://doi.org/10.1016/j.jhydrol.2022.127834

Ghazavi, R., Vali, A. B., & Eslamian, S. (2012). Impact of Flood Spreading on Groundwater Level Variation and Groundwater Quality in an Arid Environment. *Water Resources Management*, *26*(6), 1651–1663. https://doi.org/10.1007/s11269-012-9977-4

Gounot, A. M. (1994). Microbial oxidation and reduction of manganese: Consequences in groundwater and applications. *FEMS Microbiology Reviews*, *14*(4), 339–349. https://doi.org/10.1111/j.1574-6976.1994.tb00108.x

Griffith, D. (1992). What is spatial autocorrelation? Reflections on the past 25 years of spatial statistics. *L'Espace Géographique*, *21*(3), 265–280. https://doi.org/10.3406/spgeo.1992.3091

Gruber, S., & Haeberli, W. (2007). Permafrost in steep bedrock slopes and its temperature-related destabilization following climate change. *Journal of Geophysical Research: Earth Surface*, *112*(F2). https://doi.org/10.1029/2006JF000547

Gullacher, A., Allen, D. M., & Goetz, J. D. (2023). *Indicators of Groundwater Drought in British Columbia* (WSS2023-01; Water Science Series). British Columbia Ministry of Environment. https://a100.gov.bc.ca/pub/acat/documents/r60200/GW_Drought_Indicators_1673396362732_BDD4B484D0.pdf

Hair, J. F., Black, W. C., Babin, B. J., & Anderson, R. E. (2019). *Multivariate Data Analysis*. Cengage.

Hamer, K., Gudenschwager, I., & Pichler, T. (2020). Manganese (Mn) Concentrations and the Mn-Fe Relationship in Shallow Groundwater: Implications for Groundwater Monitoring. *Soil Systems*, *4*(3), Article 3. https://doi.org/10.3390/soilsystems4030049

Hanna-Attisha, M., LaChance, J., Sadler, R. C., & Champney Schnepp, A. (2016). Elevated Blood Lead Levels in Children Associated With the Flint Drinking Water Crisis: A Spatial Analysis of Risk and Public Health Response. *American Journal of Public Health*, *106*(2), 283–290. https://doi.org/10.2105/AJPH.2015.303003

Hartmann, A., Jasechko, S., Gleeson, T., Wada, Y., Andreo, B., Barberá, J. A., Brielmann, H., Bouchaou, L., Charlier, J.-B., Darling, W. G., Filippini, M., Garvelmann, J., Goldscheider, N., Kralik, M., Kunstmann, H., Ladouche, B., Lange, J., Lucianetti, G., Martín, J. F., … Wagener, T. (2021). Risk of groundwater contamination widely underestimated because of fast flow into aquifers. *Proceedings of the National Academy of Sciences*, *118*(20), e2024492118. https://doi.org/10.1073/pnas.2024492118

Hasana, S., & Fitrianah, D. (2023). A Study on Enhanced Spatial Clustering Using Ensemble DBscan and UMAP to Map Fire Zone in Greater Jakarta, Indonesia. *Jurnal Riset Informatika*, *5*(3), 409–418. https://doi.org/10.34288/jri.v5i3.557

Hastie, T., Tibshirani, R., & Friedman, J. (2009). *The Elements of Statistical Learning: Data Mining, Inference, and Prediction, Second Edition*. Springer Science & Business Media.

Health Canada. (2015). *Guidelines for Canadian Drinking Water Quality: Guideline Technical Document – pH* [Research;guidance]. https://www.canada.ca/en/health-canada/services/publications/healthy-living/guidelines-canadian-drinking-water-quality-guideline-technical-document-ph.html

Health Canada. (2022). *Guidelines for Canadian Drinking Water Quality—Summary Tables*. Water and Air Quality Bureau, Healthy Environments and Consumer Safety Branch, Health Canada. https://www.canada.ca/content/dam/hc-sc/migration/hc-sc/ewh-semt/alt_formats/pdf/pubs/water-eau/sum_guide-res_recom/summary-tables-sept-2022-eng.pdf

Helsel, D. R., Hirsch, R. M., Ryberg, K. R., Archfield, S. A., & Gilroy, E. J. (2020). Statistical methods in water resources. In *Techniques and Methods* (4-A3). U.S. Geological Survey. https://doi.org/10.3133/tm4A3

Hemmerle, H., & Bayer, P. (2020). Climate Change Yields Groundwater Warming in Bavaria, Germany. *Frontiers in Earth Science*, *8*. https://doi.org/10.3389/feart.2020.575894

Herdianita, N. R., & Priadi, B. (2008). Arsenic and Mercury Concentrations at Several Geothermal Systems in West Java, Indonesia. *Journal of Mathematical and Fundamental Sciences*, *40*(1), Article 1. https://doi.org/10.5614/itbj.sci.2008.40.1.1

Hervai, A., Farics, É., Sisák, I., Farkas, G., Kovács, J., & Lóczy, D. (2020). Influence of Flood Waves, Production Wells, and Precipitation on Shallow Groundwater Using a Linear Regression Model Approach Based on a Case Study of Mohács Island, Hungary. *Water*, *12*(5), Article 5. https://doi.org/10.3390/w12051359

Hopenhayn, C. (2006). Arsenic in Drinking Water: Impact on Human Health. *Elements*, *2*(2), 103–107. https://doi.org/10.2113/gselements.2.2.103

Hu, M., Zhou, P., & Chen, C. (2022). Spatial and temporal distribution and affecting factors of iron and manganese in the groundwater in the middle area of the Yangtze River Basin, China. *Environmental Science and Pollution Research*, *29*(40), 61204–61221. https://doi.org/10.1007/s11356-022-20253-7

Huang, S., Chen, L., Li, J., Xu, J., Xie, W., & Zhang, C. (2023). The effects of colloidal Fe and Mn on P distribution in groundwater system of Jianghan Plain, China. *Science of The Total Environment*, *854*, 158739. https://doi.org/10.1016/j.scitotenv.2022.158739

Hussain, M. S., Abd-Elhamid, H. F., Javadi, A. A., & Sherif, M. M. (2019). Management of Seawater Intrusion in Coastal Aquifers: A Review. *Water*, *11*(12), Article 12. https://doi.org/10.3390/w11122467

iMapBC. (n.d.). Retrieved December 1, 2023, from https://maps.gov.bc.ca/ess/hm/imap4m/

Jia, K. (2015). *Iron and manganese reduction driven by organic matter and mixing of fresh and saline groundwater in the Fraser River delta aquifer, Vancouver, Canada* [University of British Columbia]. https://doi.org/10.14288/1.0167190

John, M. K., Van Laerhoven, C. J., & Bjerring, J. H. (1976). Effect of a smelter complex on the regional distribution of cadmium, lead and zinc in litters and soil horizons. *Archives of Environmental Contamination and Toxicology*, *4*(1), 456–468. https://doi.org/10.1007/BF02221042

Johnson, R. L., Clark, B. R., Landon, M. K., Kauffman, L. J., & Eberts, S. M. (2011). Modeling the potential impact of seasonal and inactive multi-aquifer wells on contaminant movement to public water-supply wells. *Journal of the American Water Resources Association*, *47*(3), 588–596. https://doi.org/10.1111/j.1752-1688.2011.00526.x

Jones Jr., J. B. (1987). Nitrogen. *Journal of Plant Nutrition*, *10*(9–16), 1675–1682. https://doi.org/10.1080/01904168709363706

JR Williams. (1970). *Ground Water in the Permafrost Regions of Alaska* (United States Geological Survey 696; Geological Survey Professional Paper, p. 90). United States Department of the INterior. https://pubs.usgs.gov/pp/0696/report.pdf

Jurgens, B. C., Parkhurst, D. L., & Belitz, K. (2019). Assessing the Lead Solubility Potential of Untreated Groundwater of the United States. *Environmental Science & Technology*, *53*(6), 3095–3103. https://doi.org/10.1021/acs.est.8b04475

Kampbell, D. H., An, Y.-J., Jewell, K. P., & Masoner, J. R. (2003). Groundwater quality surrounding Lake Texoma during short-term drought conditions. *Environmental Pollution*, *125*(2), 183–191. https://doi.org/10.1016/S0269-7491(03)00072-1

Kanel, S. R., Das, T. K., Varma, R. S., Kurwadkar, S., Chakraborty, S., Joshi, T. P., Bezbaruah, A. N., & Nadagouda, M. N. (2023). Arsenic Contamination in Groundwater: Geochemical Basis of Treatment Technologies. *ACS Environmental Au*, *3*(3), 135–152. https://doi.org/10.1021/acsenvironau.2c00053

KAPAJ, S., PETERSON, H., LIBER, K., & BHATTACHARYA, P. (2006). Human Health Effects From Chronic Arsenic Poisoning–A Review. *Journal of Environmental Science and Health, Part A*, *41*(10), 2399–2428. https://doi.org/10.1080/10934520600873571

Karl, T., Jones, P., Knight, R., Kukla, G., Plummer, N., Razuvayev, V., Gallo, K., Lindseay, J., Charlson, R., & Peterson, T. (1993). Asymmetric Trends of Daily Maximum and Minimum Temperature. *School of Natural Resources: Faculty Publications*. https://digitalcommons.unl.edu/natrespapers/185

Karl, T. R., Jones, P. D., Knight, R. W., Kukla, G., Plummer, N., Razuvayev, V., Gallo, K. P., Lindseay, J., Charlson, R. J., & Peterson, T. C. (1993). A New Perspective on Recent Global Warming: Asymmetric Trends of Daily Maximum and Minimum Temperature. *Bulletin of the American Meteorological Society*, *74*(6), 1007–1024. https://doi.org/10.1175/1520-0477(1993)074<1007:ANPORG>2.0.CO;2

Katsoyiannis, I. A., Hug, S. J., Ammann, A., Zikoudi, A., & Hatziliontos, C. (2007). Arsenic speciation and uranium concentrations in drinking water supply wells in Northern Greece: Correlations with redox indicative parameters and implications for groundwater treatment. *Science of The Total Environment*, *383*(1), 128–140. https://doi.org/10.1016/j.scitotenv.2007.04.035

Kennedy, G., & Drage, J. (2017). *An Arsenic in Well Water Risk Map for Nova Scotia based on Observed Patterns of Well Water Concentrations of Arsenic in Bedrock Aquifers* (Open File Report ME 2017-003). NS Department of Natural Resources.

Kennedy, G., & Drage, J. (2018). *A Review and Summary of Activities Related to Uranium in Nova Scotia Well Water* (Open File Report ME 2018-006). Nova Scotia Energy and Mines Geological Survey.

Kennedy, G. W., & Drage, J. (2020). *A review of private well contaminants, testing, and mitigation behaviours in Nova Scotia* (Open File Report ME 2020-004). Nova Scotia Energy and Mines Geological Survey. https://novascotia.ca/natr/meb/data/pubs/20ofr04/ofr_me_2020-004.pdf

Khan, J., Shrivastava, R., Gupta, G., & Singh, N. K. (2023). Heavy Metal Contamination in Groundwater: Environmental Concerns and Mitigation Measures. In R. P. Singh, P. Singh, & A. Srivastava (Eds.), *Heavy Metal Toxicity: Environmental Concerns, Remediation and Opportunities* (pp. 139–165). Springer Nature. https://doi.org/10.1007/978-981-99-0397-9_7

Klein, T., Nilsson, M., Persson, A., & Håkansson, B. (2017). From Open Data to Open Analyses—New Opportunities for Environmental Applications? *Environments*, *4*(2), Article 2. https://doi.org/10.3390/environments4020032

Koller, L. D. (1980). Immunotoxicology of heavy metals. *International Journal of Immunopharmacology*, *2*(4), 269–279. https://doi.org/10.1016/0192-0561(80)90027-2

Kumar, C. P. (2012). Climate Change and Its Impact on Groundwater Resources. *International Journal of Engineering and Science*, *1*(5). https://d1wqtxts1xzle7.cloudfront.net/70632823/CC_GW_Inventy-libre.pdf?1632973558=&response-content-disposition=inline%3B+filename%3DClimate_Change_and_Its_Impact_on_Groundw.pdf&Expires=1704925698&Signature=LMhFw3sKuxHB6DfL3VfbXUkCgcZSy0h4JCBsQezG2fykFgoa~9cbgBwzR1LG5FyleNJFZIG7jBe4tXMeJrY2LJoqalMHXwo7YjR-d2ZGmTAYDdGqoN-BO63YbyNQvc0UoqtEmys4T5WjDedpRiLdQjrQyaWoj1d5UzYe7uwnYBO9oS2~MYabuVxQ0vLpArmjSmJ7D~cG60KKOsVhTUaq2dyNlEYbu9ODT9dZBc7zh4DCUd5KxjUvulQ6fGbrHm6dTVEBljbzGNH-xwU3yhb0vKHJWfbnvNpSPL3~hPZZ3AY3~x45SKbgaR~mB3gtbI~63jaef~5B42Ro9kjH4vJ1yg__&Key-Pair-Id=APKAJLOHF5GGSLRBV4ZA

Kuppusamy, M. R., & Giridhar, V. V. (2006). Factor analysis of water quality characteristics including trace metal speciation in the coastal environmental system of Chennai Ennore. *Environment International*, *32*(2), 174–179. https://doi.org/10.1016/j.envint.2005.08.008

Kurttio, P., Komulainen, H., Leino, A., Salonen, L., Auvinen, A., & Saha, H. (2005). Bone as a Possible Target of Chemical Toxicity of Natural Uranium in Drinking Water. *Environmental Health Perspectives*, *113*(1), 68–72. https://doi.org/10.1289/ehp.7475

Larry D. Jones. (1990). *URANIUM AND THORIUM OCCURRENCES IN BRITISH COLUMBIA* (OPEN FILE 1990–32). Minisby of Energy, Mines and Petroleum Resources.

https://cmscontent.nrs.gov.bc.ca/geoscience/publicationcatalogue/OpenFile/BCGS_OF1990-32.pdf

Lavkulich, L. (2021). *Soils of British Columbia and Yukon: The Western Cordillera*. https://openpress.usask.ca/soilscience/chapter/the-soils-of-british-columbia-and-yukon/

Levallois, P., Barn, P., Valcke, M., Gauvin, D., & Kosatsky, T. (2018). Public Health Consequences of Lead in Drinking Water. *Current Environmental Health Reports*, *5*(2), 255–262. https://doi.org/10.1007/s40572-018-0193-0

Levy, Z. F., Jurgens, B., Burow, K., Voss, S., Faulkner, K., Arroyo-Lopez, J., & Fram, M. (2021). Critical Aquifer Overdraft Accelerates Degradation of Groundwater Quality in California's Central Valley During Drought. *Geophysical Research Letters*, *48*. https://doi.org/10.1029/2021GL094398

Lewandowski, J., Meinikmann, K., & Krause, S. (2020). Groundwater–Surface Water Interactions: Recent Advances and Interdisciplinary Challenges. *Water*, *12*(1), Article 1. https://doi.org/10.3390/w12010296

Leyden, E., Cook, F., Hamilton, B., Zammit, B., Barnett, L., Lush, A. M., Stone, D., & Mosley, L. (2016). Near shore groundwater acidification during and after a hydrological drought in the Lower Lakes, South Australia. *Journal of Contaminant Hydrology*, *189*, 44–57. https://doi.org/10.1016/j.jconhyd.2016.03.008

Li, P., Karunanidhi, D., Subramani, T., & Srinivasamoorthy, K. (2021). Sources and Consequences of Groundwater Contamination. *Archives of Environmental Contamination and Toxicology*, *80*(1), 1–10. https://doi.org/10.1007/s00244-020-00805-z

Li, R. (2016). Assessing Groundwater Pollution Risk in Response to Climate Change and Variability. In A. Fares (Ed.), *Emerging Issues in Groundwater Resources* (pp. 31–50). Springer International Publishing. https://doi.org/10.1007/978-3-319-32008-3_2

Liao, V. H.-C., Chu, Y.-J., Su, Y.-C., Hsiao, S.-Y., Wei, C.-C., Liu, C.-W., Liao, C.-M., Shen, W.-C., & Chang, F.-J. (2011). Arsenite-oxidizing and arsenate-reducing bacteria associated with arsenic-rich groundwater in Taiwan. *Journal of Contaminant Hydrology*, *123*(1–2), 20–29. https://doi.org/10.1016/j.jconhyd.2010.12.003

Liu, P., Xia, Y., & Shang, M. (2020). A bench-scale assessment of the effect of soil temperature on bare soil evaporation in winter. *Hydrology Research*, *51*(6), 1349–1357. https://doi.org/10.2166/nh.2020.044

Lorenzo-Seva, U., & Ferrando, P. J. (2021). MSA: The Forgotten Index for Identifying Inappropriate Items Before Computing Exploratory Item Factor Analysis. *Methodology*, *17*(4), Article 4. https://doi.org/10.5964/meth.7185

Love, D., Hallbauer, D., Amos, A., & Hranova, R. (2004). Factor analysis as a tool in groundwater quality management: Two southern African case studies. *Physics and Chemistry of the Earth, Parts A/B/C*, *29*(15), 1135–1143. https://doi.org/10.1016/j.pce.2004.09.027

Lucchini, R. G., Guazzetti, S., Zoni, S., Benedetti, C., Fedrighi, C., Peli, M., Donna, F., Bontempi, E., Borgese, L., Micheletti, S., Ferri, R., Marchetti, S., & Smith, D. R. (2014). Neurofunctional dopaminergic impairment in elderly after lifetime exposure to manganese. *NeuroToxicology*, *45*, 309–317. https://doi.org/10.1016/j.neuro.2014.05.006

Ma, M., Wang, R., Xu, L., Xu, M., & Liu, S. (2020). Emerging health risks and underlying toxicological mechanisms of uranium contamination: Lessons from the past two decades. *Environment International*, *145*, 106107. https://doi.org/10.1016/j.envint.2020.106107

Ma, T., Deng, X., Chen, L., & Xiang, W. (2020). The soil properties and their effects on plant diversity in different degrees of rocky desertification. *Science of The Total Environment*, *736*, 139667. https://doi.org/10.1016/j.scitotenv.2020.139667

Maqsoom, A., Aslam, B., Khalil, U., Ghorbanzadeh, O., Ashraf, H., Faisal Tufail, R., Farooq, D., & Blaschke, T. (2020). A GIS-based DRASTIC Model and an Adjusted DRASTIC Model (DRASTICA) for Groundwater Susceptibility Assessment along the China–Pakistan Economic Corridor (CPEC) Route. *ISPRS International Journal of Geo-Information*, *9*(5), Article 5. https://doi.org/10.3390/ijgi9050332

Martinez, V. D., Vucic, E. A., Becker-Santos, D. D., Gil, L., & Lam, W. L. (2011). Arsenic Exposure and the Induction of Human Cancers. *Journal of Toxicology*, *2011*, 431287. https://doi.org/10.1155/2011/431287

Masoud, M. H. Z., Basahi, J. M., & Rajmohan, N. (2018). Impact of flash flood recharge on groundwater quality and its suitability in the Wadi Baysh Basin, Western Saudi Arabia: An integrated approach. *Environmental Earth Sciences*, *77*(10), 395. https://doi.org/10.1007/s12665-018-7578-0

Masuda, H. (2018). Arsenic cycling in the Earth's crust and hydrosphere: Interaction between naturally occurring arsenic and human activities. *Progress in Earth and Planetary Science*, *5*(1), 68. https://doi.org/10.1186/s40645-018-0224-3

Matsunaga, T., Karametaxas, G., von Gunten, H. R., & Lichtner, P. C. (1993). Redox chemistry of iron and manganese minerals in river-recharged aquifers: A model interpretation of a

column experiment. *Geochimica et Cosmochimica Acta*, *57*(8), 1691–1704. https://doi.org/10.1016/0016-7037(93)90107-8

Mauclaire, L., & Gibert, J. (1998). Effects of pumping and floods on groundwater quality: A case study of the Grand Gravier well field (Rhône, France). *Hydrobiologia*, *389*(1), 141–151. https://doi.org/10.1023/A:1003566101271

McMahon, P. B., Belitz, K., Reddy, J. E., & Johnson, T. D. (2019). Elevated Manganese Concentrations in United States Groundwater, Role of Land Surface–Soil–Aquifer Connections. *Environmental Science & Technology*, *53*(1), 29–38. https://doi.org/10.1021/acs.est.8b04055

Meyer, R., Engesgaard, P., & Sonnenborg, T. O. (2019). Origin and Dynamics of Saltwater Intrusion in a Regional Aquifer: Combining 3-D Saltwater Modeling With Geophysical and Geochemical Data. *Water Resources Research*, *55*(3), 1792–1813. https://doi.org/10.1029/2018WR023624

Meyers, Z. P., Frisbee, M. D., Rademacher, L. K., & Stewart-Maddox, N. S. (2021). Old groundwater buffers the effects of a major drought in groundwater-dependent ecosystems of the eastern Sierra Nevada (CA). *Environmental Research Letters*, *16*(4), 044044. https://doi.org/10.1088/1748-9326/abde5f

Miao, Z., Brusseau, M. L., Carroll, K. C., Carreón-Diazconti, C., & Johnson, B. (2012). SULFATE REDUCTION IN GROUNDWATER: CHARACTERIZATION AND APPLICATIONS FOR REMEDIATION. *Environmental Geochemistry and Health*, *34*(4), 539–550. https://doi.org/10.1007/s10653-011-9423-1

Mike Wei, Diana Allen, Alan Kohut, Steve Grasby, Kevin Ronneseth, & Bob Turner. (2009). Understanding the Types of Aquifers in the Canadian Cordillera Hydrogeologic Region to

Better Manage and Protect Groundwater. *Streamline Watershed Management Bulletin*, *13*(1). https://www.academia.edu/10219261/Understanding_the_Types_of_Aquifers_in_the_Canadian_Cordillera_Hydrogeologic_Region_to_Better_Manage_and_Protect_Groundwater

Ministry of Environment and Climate Change Strategy. (n.d.). *Aquifer Subtype Code Description—Province of British Columbia*. Province of British Columbia. Retrieved December 5, 2023, from https://www2.gov.bc.ca/gov/content/environment/air-land-water/water/groundwater-wells-aquifers/understanding-aquifers/aquifer-subtype-code-description

Ministry of Environment and Climate Change Strategy. (2023, September 13). *Environmental Monitoring System—Province of British Columbia*. Province of British Columbia. https://www2.gov.bc.ca/gov/content/environment/research-monitoring-reporting/monitoring/environmental-monitoring-system

Ministry of Natural Gas Development. (2016). *Petroleum Geology—Province of British Columbia*. Province of British Columbia. https://www2.gov.bc.ca/gov/content/industry/natural-gas-oil/petroleum-geoscience/petroleum-geology

Mohan, C., Gleeson, T., Forstner, T., Famiglietti, J. S., & de Graaf, I. (2023). Quantifying Groundwater's Contribution to Regional Environmental-Flows in Diverse Hydrologic Landscapes. *Water Resources Research*, *59*(6), e2022WR033153. https://doi.org/10.1029/2022WR033153

Mohod, C., & Dhote, J. (2013). Review of heavy metals in drinking water and their effect on human health. *International Journal of Innovative Research in Science, Engineering and Technology*, *2*, 2992–2996.

Mora, A., Mahlknecht, J., Ledesma-Ruiz, R., Sanford, W. E., & Lesser, L. E. (2020). Dynamics of major and trace elements during seawater intrusion in a coastal sedimentary aquifer impacted by anthropogenic activities. *Journal of Contaminant Hydrology*, *232*, 103653. https://doi.org/10.1016/j.jconhyd.2020.103653

Mosley, L. M., Fitzpatrick, R. W., Palmer, D., Leyden, E., & Shand, P. (2014). Changes in acidity and metal geochemistry in soils, groundwater, drain and river water in the Lower Murray River after a severe drought. *Science of The Total Environment*, *485–486*, 281–291. https://doi.org/10.1016/j.scitotenv.2014.03.063

Mossop, G. D., & Shetsen, I. (1994). *Geological atlas of the Western Canada Sedimentary Basin*. Canadian Society of Petroleum Geologists and Alberta Research Council. https://ags.aer.ca/reports/atlas-western-canada-sedimentary-basin

Mukherjee, A. B., & Bhattacharya, P. (2001). Arsenic in groundwater in the Bengal Delta Plain: Slow poisoning in Bangladesh. *Environmental Reviews*, *9*(3), 189–220. https://doi.org/10.1139/a01-007

Mulaik, S. A. (2009). *Foundations of Factor Analysis*. CRC Press.

Mullaney, J. R., Arntson, A. D., & Lorenz, D. L. (2009). *Chloride in Groundwater and Surface Water in Areas Underlain by the Glacial Aquifer System, Northern United States* (Scientific Investigations Report Scientific Investigations Report 2009–5086; National Water-Quality Assessment Program). U.S. Geological Survey. https://pubs.usgs.gov/sir/2009/5086/pdf/sir2009-5086.pdf

Mushtaq, N., Younas, A., Mashiatullah, A., Javed, T., Ahmad, A., & Farooqi, A. (2018). Hydrogeochemical and isotopic evaluation of groundwater with elevated arsenic in alkaline aquifers in Eastern Punjab, Pakistan. *Chemosphere*, *200*, 576–586. https://doi.org/10.1016/j.chemosphere.2018.02.154

Nai, C., Sun, X., Wang, Z., Xu, Y., Liu, Y., Liu, J., Dong, L., Huang, Q., & Wang, Y. (2019). Complex resistivity characteristics of saltwater-intruded sand contaminated by heavy metal. *Scientific Reports*, *9*(1), Article 1. https://doi.org/10.1038/s41598-019-47167-8

Nayak, S. K., & Nandimandalam, J. R. (2023). Impacts of climate change and coastal salinization on the environmental risk of heavy metal contamination along the odisha coast, India. *Environmental Research*, *238*, 117175. https://doi.org/10.1016/j.envres.2023.117175

Neidhardt, H., & Shao, W. (2023). Impact of climate change-induced warming on groundwater temperatures and quality. *Applied Water Science*, *13*(12), 235. https://doi.org/10.1007/s13201-023-02039-5

Nguyen, C. K., Stone, K. R., & Edwards, M. A. (2011). Chloride-to-sulfate mass ratio: Practical studies in galvanic corrosion of lead solder. *Journal AWWA*, *103*(1), 81–92. https://doi.org/10.1002/j.1551-8833.2011.tb11384.x

Nicholas, J. R., Rowe, G. L., & Brannen, J. R. (1996). Hydrology, water quality, and effects of drought in Monroe County, Michigan. In *Water-Resources Investigations Report* (94–4161). U.S. Geological Survey. https://doi.org/10.3133/wri944161

Noel, V. (2022, October 9). *URANIUM (IM)MOBILIZATION DRIVEN BY EVAPORITE WET-DRY CYCLING: IMPACT ON GROUNDWATER QUALITY*. GSA Connects 2022 meeting

in Denver, Colorado. https://gsa.confex.com/gsa/2022AM/webprogram/Paper377168.html

Noetzli, J., & Gruber, S. (2009). Transient thermal effects in Alpine permafrost. *The Cryosphere*, *3*(1), 85–99. https://doi.org/10.5194/tc-3-85-2009

Nolan, J., & Weber, K. A. (2015). Natural Uranium Contamination in Major U.S. Aquifers Linked to Nitrate. *Environmental Science & Technology Letters*, *2*(8), 215–220. https://doi.org/10.1021/acs.estlett.5b00174

Ofterdinger, U., MacDonald, A. M., Comte, J.-C., & Young, M. E. (2019). *Groundwater in Fractured Bedrock Environments: Managing Catchment and Subsurface Resources*. Geological Society of London. https://doi.org/10.1144/SP479

O'Neal, S. L., & Zheng, W. (2015). Manganese Toxicity Upon Overexposure: A Decade in Review. *Current Environmental Health Reports*, *2*(3), 315–328. https://doi.org/10.1007/s40572-015-0056-x

Ootes, L., Elliott, J., & Rowins, S. (2017). *Testing the relationship between the Llewellyn fault, gold mineralization, and Eocene volcanism in northwest British Columbia: A preliminary report*.

Orecchia, C., Giambastiani, B. M. S., Greggio, N., Campo, B., & Dinelli, E. (2022). Geochemical Characterization of Groundwater in the Confined and Unconfined Aquifers of the Northern Italy. *Applied Sciences*, *12*(15), Article 15. https://doi.org/10.3390/app12157944

Oremland, R. S., & Stolz, J. F. (2003). The ecology of arsenic. *Science (New York, N.Y.)*, *300*(5621), 939–944. https://doi.org/10.1126/science.1081903

Oulhote, Y., Mergler, D., & Bouchard, M. F. (2014). Sex- and age-differences in blood manganese levels in the U.S. general population: National health and nutrition examination survey 2011–2012. *Environmental Health*, *13*, 87. https://doi.org/10.1186/1476-069X-13-87

Oyem, H. H., Oyem, I. M., & Usese, A. I. (2015). Iron, manganese, cadmium, chromium, zinc and arsenic groundwater contents of Agbor and Owa communities of Nigeria. *SpringerPlus*, *4*, 104. https://doi.org/10.1186/s40064-015-0867-0

P. Erdmer & Y. Cui. (2009). *Geological Map of British Columbia* [British Columbia Geological Survey]. British Columbia Geological Survey. https://www2.gov.bc.ca/gov/content/industry/mineral-exploration-mining/british-columbia-geological-survey/publications/geosciencemaps

Pacific Climate Impacts Consortium. (2024). *BC Station Data*. https://www.pacificclimate.org/data/bc-station-data

Parmalee, N. L., & Aschner, M. (2016). Manganese and aging. *NeuroToxicology*, *56*, 262–268. https://doi.org/10.1016/j.neuro.2016.06.006

Patel, P., Mehta, D., & Sharma, N. (2022). A review on the application of the DRASTIC method in the assessment of groundwater vulnerability. *Water Supply*, *22*(5), 5190–5205. https://doi.org/10.2166/ws.2022.126

Peel, H. R., Balogun, F. O., Bowers, C. A., Miller, C. T., Obeidy, C. S., Polizzotto, M. L., Tashnia, S. U., Vinson, D. S., & Duckworth, O. W. (2022). Towards Understanding Factors Affecting Arsenic, Chromium, and Vanadium Mobility in the Subsurface. *Water*, *14*(22), Article 22. https://doi.org/10.3390/w14223687

Pieper, K. J., Nystrom, V. E., Parks, J., Jennings, K., Faircloth, H., Morgan, J. B., Bruckner, J., & Edwards, M. A. (2018). Elevated Lead in Water of Private Wells Poses Health Risks: Case Study in Macon County, North Carolina. *Environmental Science & Technology*, *52*(7), 4350–4357. https://doi.org/10.1021/acs.est.7b05812

Plumlee, G. S., Montour, M., Taylor, C. D., Wallace, A. R., & Klein, D. P. (2004). *Preliminary compilation of descriptive geoenvironmental mineral deposit models* (Open-File Report 95–831). U.S. DEPARTMENT OF THE INTERIOR U.S. GEOLOGICAL SURVEY. https://pubs.usgs.gov/of/1995/ofr-95-0831/

Poeter, E., Fan, Y., Cherry, J., Wood, W., & Mackay, D. (2020). *Groundwater in Our Water Cycle*. The Groundwater Project. https://doi.org/10.21083/978-1-7770541-1-3

Porowski, A., Porowska, D., & Halas, S. (2019). Identification of Sulfate Sources and Biogeochemical Processes in an Aquifer Affected by Peatland: Insights from Monitoring the Isotopic Composition of Groundwater Sulfate in Kampinos National Park, Poland. *Water*, *11*(7), Article 7. https://doi.org/10.3390/w11071388

Province of British Columbia. (2023). *Groundwater Wells and Aquifers*. https://apps.nrs.gov.bc.ca/gwells/

Qingkai Kong, Timmy Siauw, & Alexandre Bayen. (2020). *Python Programming And Numerical Methods: A Guide For Engineers And Scientists* (1st ed.). Academic Press. https://pythonnumericalmethods.berkeley.edu/notebooks/Index.html

Rapp, R. H. (1991, April). *Geometric Geodesy Part I* [Lecture Notes]. http://hdl.handle.net/1811/24333

Raudsepp, M. J., Wilson, S., Zeyen, N., Arizaleta, M. L., & Power, I. M. (2024). Magnesite everywhere: Formation of carbonates in the alkaline lakes and playas of the Cariboo

Plateau, British Columbia, Canada. *Chemical Geology*, *648*, 121951. https://doi.org/10.1016/j.chemgeo.2024.121951

Rehman, K., Fatima, F., Waheed, I., & Akash, M. S. H. (2018). Prevalence of exposure of heavy metals and their impact on health consequences. *Journal of Cellular Biochemistry*, *119*(1), 157–184. https://doi.org/10.1002/jcb.26234

Riches, J., Batey, J., Jones, M., Butcher, A. S., Newell, A. J., & Gale, I. N. (2007). *Hydrogeochemistry of aquifer storage and recovery in the Lower Greensand (London, UK) for seasonal and drought public supply* (P. Fox, Ed.; pp. 198–208). Acacia Publishing Incorporated. http://acaciapublishing.com/

Riedel, T. (2019). Temperature-associated changes in groundwater quality. *Journal of Hydrology*, *572*, 206–212. https://doi.org/10.1016/j.jhydrol.2019.02.059

Rodrigues, E. G., Kile, M., Dobson, C., Amarasiriwardena, C., Quamruzzaman, Q., Rahman, M., Golam, M., & Christiani, D. C. (2015). Maternal–infant biomarkers of prenatal exposure to arsenic and manganese. *Journal of Exposure Science & Environmental Epidemiology*, *25*(6), Article 6. https://doi.org/10.1038/jes.2015.45

Rusydi, A. F., Onodera, S.-I., Saito, M., Ioka, S., Maria, R., Ridwansyah, I., & Delinom, R. M. (2021). Vulnerability of groundwater to iron and manganese contamination in the coastal alluvial plain of a developing Indonesian city. *SN Applied Sciences*, *3*(4), 399. https://doi.org/10.1007/s42452-021-04385-y

Saberimehr, S., Asgharimoghaddam, A., & Field, M. S. (2017). Hydrogeological and Geochemical Evidence for the Origin of Brackish Groundwater in the Shabestar Plain Aquifer, Northwest Iran. *Sustainable Water Resources Management*, *5*, 1381–1404. https://doi.org/10.1007/s40899-017-0192-6

Saeed, T. U., & Attaullah, H. (2014). Impact of extreme floods on groundwater quality (in Pakistan). *British Journal of Environment and Climate Change*, *4*(1), 133–151.

Sahu, M., Sar, S. K., Baghel, T., & Dewangan, R. (2020). Seasonal and geochemical variation of uranium and major ions in groundwater at Kanker district of Chhattisgarh, central India. *Groundwater for Sustainable Development*, *10*, 100330. https://doi.org/10.1016/j.gsd.2020.100330

Santos, I. R., de Weys, J., & Eyre, B. D. (2011a). Groundwater or floodwater? Assessing the pathways of metal exports from a coastal acid sulfate soil catchment. *Environmental Science & Technology*, *45*(22), 9641–9648. https://doi.org/10.1021/es202581h

Santos, I. R., de Weys, J., & Eyre, B. D. (2011b). Groundwater or Floodwater? Assessing the Pathways of Metal Exports from a Coastal Acid Sulfate Soil Catchment. *Environmental Science & Technology*, *45*(22), 9641–9648. https://doi.org/10.1021/es202581h

Sato, T., Murakami, T., Yanase, N., Isobe, H., Payne, T. E., & Airey, P. L. (1997). Iron Nodules Scavenging Uranium from Groundwater. *Environmental Science & Technology*, *31*(10), 2854–2858. https://doi.org/10.1021/es970058m

Schilling, J., Hertig, E., Tramblay, Y., & Scheffran, J. (2020). Climate change vulnerability, water resources and social implications in North Africa. *Regional Environmental Change*, *20*(1), 15. https://doi.org/10.1007/s10113-020-01597-7

Schnorbus, M., Werner, A., & Bennett, K. (2010). *Quantifying the water resource impacts of mountain pine beetle and associated salvage harvest operations across a range of watershed scales: Hydrologic modelling of the Fraser River Basin*. Natural Resources Canada, Canadian Forest Service, Pacific Forestry Centre.

Schreiner-McGraw, A. P., & Ajami, H. (2021). Delayed response of groundwater to multi-year meteorological droughts in the absence of anthropogenic management. *Journal of Hydrology*, *603*, 126917. https://doi.org/10.1016/j.jhydrol.2021.126917

Science, C. S. of S. (2021). *Digging into Canadian Soils*. Canadian Society of Soil Science. https://openpress.usask.ca/soilscience/

Seidel, D. C. (2007). Extracting uranium from its ores. *IAEA BULLETIN*, *23*. https://www.iaea.org/sites/default/files/publications/magazines/bulletin/bull23-2/23204882428.pdf

Selvi, B. S., Vijayakumar, B., Rana, B. K., & Ravi, P. M. (2016). Distribution of natural uranium in groundwater around Kudankulam. *Radiation Protection & Environment*, *39*(1), 25–29. https://doi.org/10.4103/0972-0464.185164

Shankar, S., Shanker, U., & Shikha. (2014). Arsenic Contamination of Groundwater: A Review of Sources, Prevalence, Health Risks, and Strategies for Mitigation. *The Scientific World Journal*, *2014*, 304524. https://doi.org/10.1155/2014/304524

Singh, A., Sharma, A., Verma, R. K., Chopade, R. L., Pandit, P. P., Nagar, V., Aseri, V., Choudhary, S. K., Awasthi, G., Awasthi, K. K., Sankhla, M. S., Singh, A., Sharma, A., Verma, R. K., Chopade, R. L., Pandit, P. P., Nagar, V., Aseri, V., Choudhary, S. K., … Sankhla, M. S. (2022). Heavy Metal Contamination of Water and Their Toxic Effect on Living Organisms. In *The Toxicity of Environmental Pollutants*. IntechOpen. https://doi.org/10.5772/intechopen.105075

Singh, N., Gupta, V. K., Kumar, A., & Sharma, B. (2017). Synergistic Effects of Heavy Metals and Pesticides in Living Systems. *Frontiers in Chemistry*, *5*, 70. https://doi.org/10.3389/fchem.2017.00070

Singh, S., Rani, A., Mahajan, R. K., & Walia, T. P. S. (2003). Analysis of uranium and its correlation with some physico-chemical properties of drinking water samples from Amritsar, Punjab. *Journal of Environmental Monitoring*, *5*(6), 917–921. https://doi.org/10.1039/B309493F

Skierszkan, E. K., Dockrey, J. W., Helsen, J., Findlater, L.-L., Bataille, C. P., de Laplante, G., McBeth, J. M., Mayer, K. U., & Beckie, R. D. (2021). Persistence of Uranium in Old and Cold Subpermafrost Groundwater Indicated by Linking 234U-235U-238U, Groundwater Ages, and Hydrogeochemistry. *ACS Earth and Space Chemistry*, *5*(12), 3474–3487. https://doi.org/10.1021/acsearthspacechem.1c00307

Skierszkan, E. K., Dockrey, J. W., Mayer, K. U., & Beckie, R. D. (2020). Release of geogenic uranium and arsenic results in water-quality impacts in a subarctic permafrost region of granitic and metamorphic geology. *Journal of Geochemical Exploration*, *217*, 106607. https://doi.org/10.1016/j.gexplo.2020.106607

Smedley, P. L., & Kinniburgh, D. G. (2023). Uranium in natural waters and the environment: Distribution, speciation and impact. *Applied Geochemistry*, *148*, 105534. https://doi.org/10.1016/j.apgeochem.2022.105534

Snow, B. D. (2012). *Living with lead: An environmental history of Idaho's Coeur d'Alenes, 1885–2011* [Ph.D., Montana State University]. https://www.proquest.com/docview/1030143964/abstract/B3C7725642B04E90PQ/1?sourcetype=Dissertations%20&%20Theses

Snyder, M., Taillefert, M., & Ruppel, C. (2004). Redox zonation at the saline-influenced boundaries of a permeable surficial aquifer: Effects of physical forcing on the

biogeochemical cycling of iron and manganese. *Journal of Hydrology*, *296*(1), 164–178. https://doi.org/10.1016/j.jhydrol.2004.03.019

Soil Classification Working Group. (1998). *The Canadian System of Soil Classification, 3rd edition* (ISBN 0-660-17404-9; 1646, p. 187). Agriculture and Agri-Food Canada. https://sis.agr.gc.ca/cansis/taxa/cssc3/index.html

Staben, N., Nahrstedt, A., & Merkel, W. (2015). Securing safe drinking water supply under climate change conditions. *Water Supply*, *15*(6), 1334–1342. https://doi.org/10.2166/ws.2015.099

Stewart, B. D., Mayes, M. A., & Fendorf, S. (2010). Impact of Uranyl−Calcium−Carbonato Complexes on Uranium(VI) Adsorption to Synthetic and Natural Sediments. *Environmental Science & Technology*, *44*(3), 928–934. https://doi.org/10.1021/es902194x

Subramanian, K. S., Sastri, V. S., Elboujdaini, M., Connor, J. W., & Davey, A. B. C. (1995). Water contamination: Impact of tin-lead solder. *Water Research*, *29*(8), 1827–1836. https://doi.org/10.1016/0043-1354(95)00005-6

Sudaryanto, & Naily, W. (2018). Ratio of Major Ions in Groundwater to Determine Saltwater Intrusion in Coastal Areas. *IOP Conference Series: Earth and Environmental Science*, *118*(1), 012021. https://doi.org/10.1088/1755-1315/118/1/012021

Sujith, P. P., Mourya, B. S., Krishnamurthi, S., Meena, R. M., & Loka Bharathi, P. A. (2014). Mobilization of manganese by basalt associated Mn(II)-oxidizing bacteria from the Indian Ridge System. *Chemosphere*, *95*, 486–495. https://doi.org/10.1016/j.chemosphere.2013.09.103

Sýs, V., Fošumpaur, P., & Kašpar, T. (2021). The Impact of Climate Change on the Reliability of Water Resources. *Climate*, *9*(11), Article 11. https://doi.org/10.3390/cli9110153

Tansel, B., & Zhang, K. (2022). Effects of saltwater intrusion and sea level rise on aging and corrosion rates of iron pipes in water distribution and wastewater collection systems in coastal areas. *Journal of Environmental Management*, *315*, 115153. https://doi.org/10.1016/j.jenvman.2022.115153

Tapia, J., Murray, J., Ormachea, M., Tirado, N., & Nordstrom, D. K. (2019). Origin, distribution, and geochemistry of arsenic in the Altiplano-Puna plateau of Argentina, Bolivia, Chile, and Perú. *Science of The Total Environment*, *678*, 309–325. https://doi.org/10.1016/j.scitotenv.2019.04.084

Trueman, B. F., Sweet, G. A., Harding, M. D., Estabrook, H., Bishop, D. P., & Gagnon, G. A. (2017). Galvanic Corrosion of Lead by Iron (Oxyhydr)Oxides: Potential Impacts on Drinking Water Quality. *Environmental Science & Technology*, *51*(12), 6812–6820. https://doi.org/10.1021/acs.est.7b01671

Ulmer-Scholle, D. S., Scholle, P. A., Schieber, J., & Raine, R. J. (Eds.). (2015). Diagenesis: Replacement & Recrystallization. In *A Color Guide to the Petrography of Sandstones, Siltstones, Shales and Associated Rocks* (Vol. 109, p. 0). American Association of Petroleum Geologists. https://doi.org/10.1306/13521923M1093637

US EPA, O. (2020, December 21). *Revised Lead and Copper Rule* [Overviews and Factsheets]. https://www.epa.gov/ground-water-and-drinking-water/revised-lead-and-copper-rule

U.S. EPA Office of Water. (2021). *2021 Multi-Sector General Permit (MSGP)—Appendix J*. U.S. EPA. https://www.epa.gov/sites/default/files/2021-01/documents/2021_msgp_-_appendix_j_-_calculating_hardness.pdf

van Genuchten, C. M., Behrends, T., Stipp, S. L. S., & Dideriksen, K. (2020). Achieving arsenic concentrations of <1 μg/L by Fe(0) electrolysis: The exceptional performance of magnetite. *Water Research*, *168*, 115170. https://doi.org/10.1016/j.watres.2019.115170

VanGulck, J. (2016). *Preliminary State of Groundwater Knowledge in the Transboundary Region of the Mackenzie River Basin, Northwest Territories*. ARKTIS Solutions Inc. https://www.gov.nt.ca/ecc/sites/ecc/files/preliminary_state_of_groundwater_knowledge_in_the_transboundary_region_of_the_mackenzie_river_basin_nwt_march_2016.pdf

Vogels, M. F. A. (2014). *Effects of past and present mining on fine sediment geochemistry of floodplain soils, Horsefly River, BC, Canada* [Master Thesis]. https://studenttheses.uu.nl/handle/20.500.12932/16199

Voutchkova, D. D., Ernstsen, V., Schullehner, J., Hinsby, K., Thorling, L., & Hansen, B. (2021). Roadmap for Determining Natural Background Levels of Trace Metals in Groundwater. *Water*, *13*(9), Article 9. https://doi.org/10.3390/w13091267

Wallace, D. R., & Buha Djordjevic, A. (2020). Heavy metal and pesticide exposure: A mixture of potential toxicity and carcinogenicity. *Current Opinion in Toxicology*, *19*, 72–79. https://doi.org/10.1016/j.cotox.2020.01.001

Wang, S., Ran, Y., Lu, B., Li, J., Kuang, H., Gong, L., & Hao, Y. (2020). A Review of Uranium-Induced Reproductive Toxicity. *Biological Trace Element Research*, *196*(1), 204–213. https://doi.org/10.1007/s12011-019-01920-2

Ward, P. J., de Ruiter, M. C., Mård, J., Schröter, K., Van Loon, A., Veldkamp, T., von Uexkull, N., Wanders, N., AghaKouchak, A., Arnbjerg-Nielsen, K., Capewell, L., Carmen Llasat, M., Day, R., Dewals, B., Di Baldassarre, G., Huning, L. S., Kreibich, H., Mazzoleni, M., Savelli, E., … Wens, M. (2020). The need to integrate flood and drought disaster risk

reduction strategies. *Water Security*, *11*, 100070. https://doi.org/10.1016/j.wasec.2020.100070

Water Protection & Sustainability Branch. (2024). *Ministry of Environment—Water Stewardship Division—Aquifers* [Govermental]. Water Protection & Sustainability Branch. https://www.env.gov.bc.ca/wsd/plan_protect_sustain/groundwater/aquifers/

Wei, M., Klaus Rathfelder, & Jennifer Turner. (2016). *Determining the Likelihood of Hydraulic Connection – Guidance for the Purpose of Apportioning Demand from Diversion of Groundwater on Streams* (Technical WSS2016-01; Water Science Series). Water Protection and Sustainability Branch, Ministry of Environment of British Columbia. https://a100.gov.bc.ca/pub/acat/documents/r50832/HydraulicConnectMW3_1474311684426_4310694949.pdf

Weiss, P. T., LeFevre, G., & Gulliver, J. S. (2008). *Contamination of Soil and Groundwater Due to Stormwater Infiltration Practices, A Literature Review* [Report]. St. Anthony Falls Laboratory. http://conservancy.umn.edu/handle/11299/115341

Werner, A. D., Bakker, M., Post, V. E. A., Vandenbohede, A., Lu, C., Ataie-Ashtiani, B., Simmons, C. T., & Barry, D. A. (2013). Seawater intrusion processes, investigation and management: Recent advances and future challenges. *Advances in Water Resources*, *51*, 3–26. https://doi.org/10.1016/j.advwatres.2012.03.004

Wilson, J. E., Brown, S., Schreier, H., Scovill, D., & Zubel, M. (2008). Arsenic in Groundwater Wells in Quaternary Deposits in the Lower Fraser Valley of British Columbia. *Canadian Water Resources Journal / Revue Canadienne Des Ressources Hydriques*, *33*(4), 397–412. https://doi.org/10.4296/cwrj3304397

Winter, C., Nguyen, T. V., Musolff, A., Lutz, S. R., Rode, M., Kumar, R., & Fleckenstein, J. H. (2023). Droughts can reduce the nitrogen retention capacity of catchments. *Hydrology and Earth System Sciences*, *27*(1), 303–318. https://doi.org/10.5194/hess-27-303-2023

Witkowski, A. J., Jakóbczyk-Karpierz, S., Czekaj, J., & Grabala, D. (2020). *Groundwater Vulnerability and Pollution Risk Assessment*. CRC Press.

Wossenyeleh, B. K., Verbeiren, B., Diels, J., & Huysmans, M. (2020). Vadose Zone Lag Time Effect on Groundwater Drought in a Temperate Climate. *Water*, *12*(8), 2123. https://doi.org/10.3390/w12082123

Xing, S., Guo, H., Sun, X., Zhang, L., & Su, A. (2023). Temperature-induced arsenic accumulation in groundwater from Pliocene aquifers of a semiarid continental basin. *Geochimica et Cosmochimica Acta*, *343*, 98–114. https://doi.org/10.1016/j.gca.2022.12.029

Xu, D., Zhang, Q., Ding, Y., & Zhang, D. (2021). Spatiotemporal Pattern Mining of Drought in the Last 40 Years in China Based on the SPEI and Space–Time Cube. *Journal of Applied Meteorology and Climatology*, *60*(9), 1219–1230. https://doi.org/10.1175/JAMC-D-21-0049.1

Xu, Z., Serata, R., Wainwright, H., Denham, M., Molins, S., Gonzalez-Raymat, H., Lipnikov, K., Moulton, J. D., & Eddy-Dilek, C. (2022). Reactive transport modeling for supporting climate resilience at groundwater contamination sites. *Hydrology and Earth System Sciences*, *26*(3), 755–773. https://doi.org/10.5194/hess-26-755-2022

Yang, Q., Culbertson, C. W., Nielsen, M. G., Schalk, C. W., Johnson, C. D., Marvinney, R. G., Stute, M., & Zheng, Y. (2015). Flow and sorption controls of groundwater arsenic in

individual boreholes from bedrock aquifers in central Maine, USA. *The Science of the Total Environment*, *505*, 1291–1307. https://doi.org/10.1016/j.scitotenv.2014.04.089

Yang, S., & Tsai, F. T.-C. (2020). Understanding impacts of groundwater dynamics on flooding and levees in Greater New Orleans. *Journal of Hydrology: Regional Studies*, *32*, 100740. https://doi.org/10.1016/j.ejrh.2020.100740

Yang, Y., Deng, Y., Xu, Y., Yan, J., Du, Y., Xie, X., & Wang, Y. (2023). Manganese mobilization from sediment to groundwater in alluvial-lacustrine aquifer system along the lower reaches of Han River. *Journal of Hydrology*, *627*, 130400. https://doi.org/10.1016/j.jhydrol.2023.130400

Ying, S. C., Schaefer, M. V., Cock-Esteb, A., Li, J., & Fendorf, S. (2017). Depth Stratification Leads to Distinct Zones of Manganese and Arsenic Contaminated Groundwater. *Environmental Science & Technology*, *51*(16), 8926–8932. https://doi.org/10.1021/acs.est.7b01121

Yuan, C., Wei, Y., Xu, X., & Cao, X. (2023). Transport and transformation of arsenic in coastal aquifer at the scenario of seawater intrusion followed by managed aquifer recharge. *Water Research*, *229*, 119440. https://doi.org/10.1016/j.watres.2022.119440

Zhang, L., Wang, F., Zhou, T., & Chen, Z. (2022). Contrasting U-Pb geochronology and geochemistry of uraninite from the Xianshi and Xiwang uranium deposits, South China: Implications for ore genesis. *Ore Geology Reviews*, *149*, 105120. https://doi.org/10.1016/j.oregeorev.2022.105120

Zhang, Z., Xiao, C., Adeyeye, O., Yang, W., & Liang, X. (2020). Source and Mobilization Mechanism of Iron, Manganese and Arsenic in Groundwater of Shuangliao City, Northeast China. *Water*, *12*(2), Article 2. https://doi.org/10.3390/w12020534

Zhu, L., Zhang, X., Zhang, J., Liu, T., & Qiu, Y. (2022a). Saltwater intrusion weakens Fe-(oxyhydr)oxide-mediated (im)mobilization of Ni and Zn in redox-fluctuating soil–groundwater system. *Water Research*, *221*, 118799. https://doi.org/10.1016/j.watres.2022.118799

Zhu, L., Zhang, X., Zhang, J., Liu, T., & Qiu, Y. (2022b). Saltwater intrusion weakens Fe-(oxyhydr)oxide-mediated (im)mobilization of Ni and Zn in redox-fluctuating soil–groundwater system. *Water Research*, *221*, 118799. https://doi.org/10.1016/j.watres.2022.118799

Appendix

8.1 Description of British Columbia

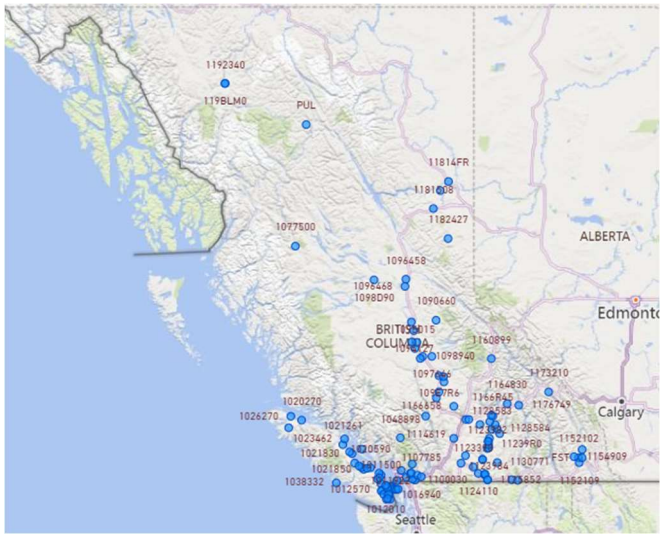

Figure 8.1.1: Power BI map of the corresponding linked weather station labelled with Native ID.

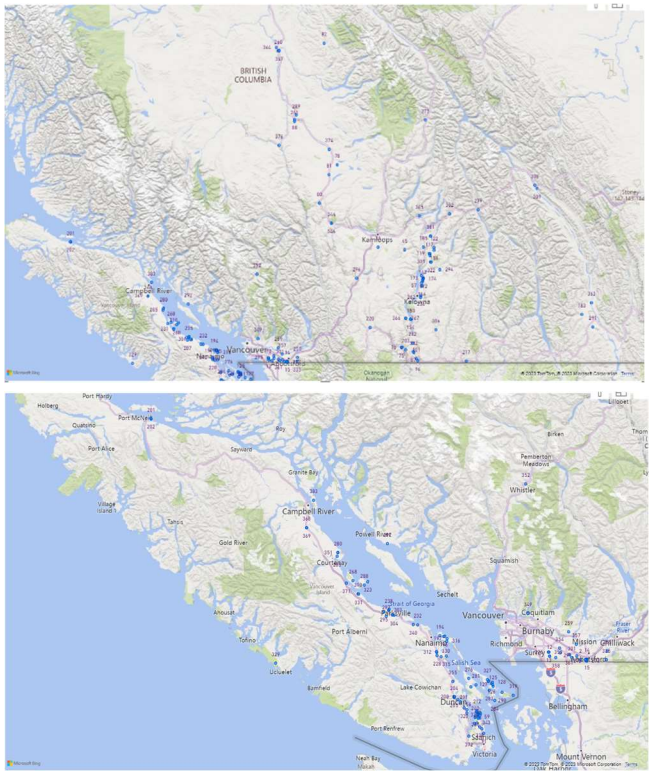

Figure 8.1.2: Zoomed Power BI map of OBS well stations.

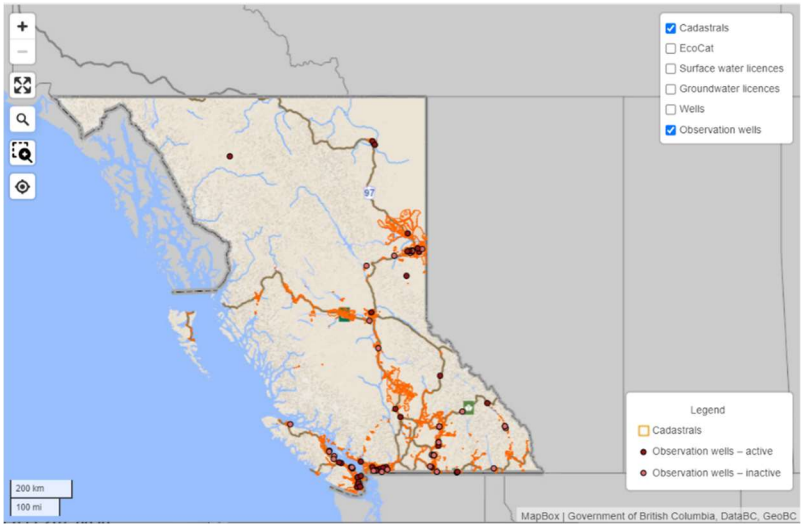

Figure 8.1.3: Observation wells of British Columbia with mapped aquifer regions (iMapBC, n.d.).

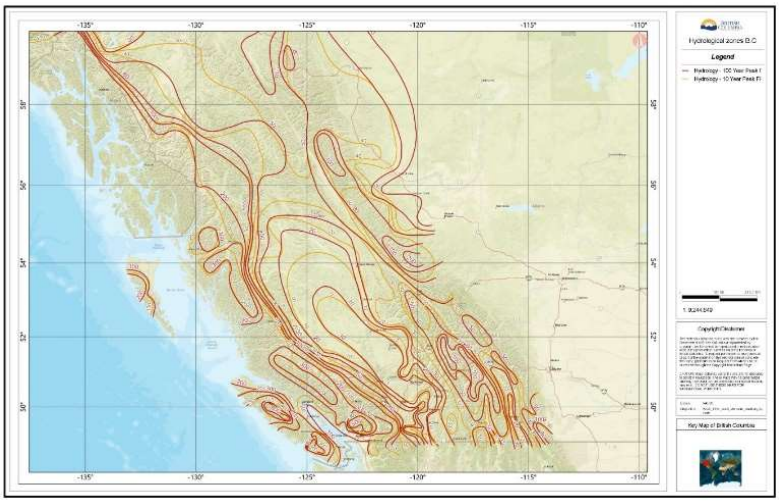

*Figure 8.1.4: Hydrological 10 and 100 year peak flow lines for British Columbia (*iMapBC*, n.d.).*

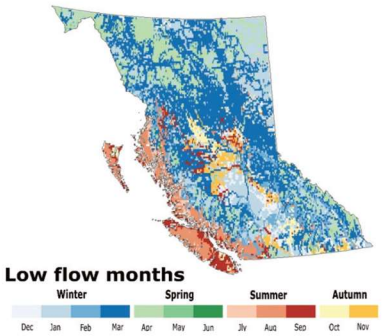

Figure 8.1.5: Hydroclimatic variability across British Columbia for the months with low flow (D. Allen & Gleeson, 2023)

Table 8.1.1: Maximum monthly precipitation of each well.

OBSWELL	Max of PRECIPITATION	LOCATION
2	340	ABBOTSFORD (AIRPORT; HUNTINGDON RD W OF CLEARBROOK RD)
8	340	ABBOTSFORD (VYE RD E OF MCCALLUM RD)
12	150.7	LANGLEY (2145 200 ST)
13	150.7	LANGLEY (19659 36TH AVE)
14	256.4	ABBOTSFORD (FRASER VALLEY TROUT HATCHERY; VYE RD)
15	340	ABBOTSFORD (FRASER VALLEY TROUT HATCHERY; VYE RD)
35	68.8	STUMP LAKE (HWY 5A & OLD KAMLOOPS ROAD)
45	118.8	WESTWOLD (STATION ROAD)
54	58.8	CARRS LANDING (JERSEY ROAD)
57	40.2	WINFIELD
58	119.4	NORTH SAANICH (MAINWARING RD.)
59	29.2	NORTH SAANICH
60	29.2	NORTH SAANICH (LITTLEWOOD RD.)
61	119.4	SOUTH SAANICH (GLIDDON ROAD)
62	24.4	NORTH SAANICH (WAIN ROAD)
63	19.2	NORTH SAANICH
64	74.4	NORTH SAANICH
65	149	SIDNEY (VICTORIA INTERNATIONAL AIRPORT)
66	110.4	NORTH SAANICH (WAIN ROAD)
67	4.4	NORTH SAANICH
69	22.4	NORTH SAANICH
70	5.2	NORTH SAANICH
71	170.8	SAANICH (CORDOVA BAY ROAD)
75	43.8	KEREMEOS (6TH AVE & 5TH ST.)
76	55.2	KEREMEOS (9TH AVE & 3RD ST.)
77	0	KEREMEOS (MORRISON RD.)
78	60.6	LONE BUTTE NEAR RAIL STATION
80	52	CLINTON (RODEO GROUNDS CARIBOO HWY 97N)
81	98.6	83 MILE (CARIBOO HWY 97N)
82	139.7	BARKERVILLE (LOWER)
87	6.8	OLIVER
88	72.6	WILLIAMS LAKE - SCOUT ISLAND
89	132.4	SMITHERS CORNER POWELL & LUND
96	64.6	OSOYOOS (WREN PLACE)
101	28.2	OSOYOOS (160TH AVE & HWY 97)
117	17.8	ARMSTRONG (OTTER LAKE CROSS RD.)
118	70.5	ARMSTRONG
119	60.5	ARMSTRONG (PLEASANT VALLEY RD.)
122	150.5	ENDERBY (HWY 97A)
124	48	CHARLIE LAKE
125	81.2	MAYNE ISLAND (HORTON BAY RD.)
126	32	MAYNE ISLAND (GEORGINA POINT RD.)
127	75.4	MAYNE ISLAND
128	141.3	MAYNE ISLAND (SKANA GATE ROAD)
153	36.2	SUMMERLAND
154	0	SUMMERLAND (HWY 97 & THORNNBER ST.)
162	54.6	OYAMA (TREWHITT ROAD)
172	58.8	OYAMA (SAWMILL RD.)
173	54.6	OYAMA (SAWMILL RD.)
174	54.6	OYAMA (OYAMA RD.)
175	54.6	KALAWOODS
176	10.4	OYAMA (BROADWATER RD.)
177	11.4	KALAWOODS SOUTH OF WOOD LAKE
180	65.6	ARMSTRONG (SPALLUMCHEEN WAY & CROZIER RD.)
183	25.6	MARYSVILLE
185	109	SALMON RIVER (SALMON RIVER ROAD; SALMON ARM)
194	85	GABRIOLA ISLAND (HWYS YARD; NORTH RD.)
196	103.5	GABRIOLA ISLAND (BUTTERCUP RD.)
197	141.7	GABRIOLA ISLAND - (NORTH ROAD)

199	61.6	VANDERHOOF
200	74.6	DEASE LAKE
201	281.4	ALERT BAY (FIR ST.)
202	98.8	ALERT BAY AIRPORT
203	47.1	CAWSTON (BARCELO RD.)
204	290.2	DUNCAN (DUNCAN RV PARK NORTH; BOYS RD.)
205	18	DUNCAN (DUNCAN RV PARK SOUTH; BOYS RD.)
208	0.6	DUNCAN
211	18	DUNCAN (MARINE HARVEST CANADA (BOYS RD.)
212	116.9	NORTH SAANICH (MAPLE RD.)
217	89.6	GRAND FORKS (RICHMOND AVE.)
220	73.8	PRINCETON
228	130.9	CASSIDY (TIMBERLANDS RD.)
232	70.8	LANTZVILLE (HARBY RD.)
233	517.4	COWICHAN BAY (VEE ROAD)
235	57.6	QUALICUM
236	54.9	RUTLAND (TIMRICK COURT)
240	116.9	NORTH SAANICH (CARNOUSITE CR.)
255	315.3	CHILLIWACK (4035 ECKERT ST; YARROW)
256	27.6	MILL BAY
258	49	GALIANO ISLAND (SHOPLAND RD.)
259	472.6	MAPLE RIDGE (272 ST & 110 AVE; WHONNOCK)
260	58.3	QUESNEL RED BLUFF (MAPLE DRIVE & BORREGARD ROAD)
261	101.6	WILLIAMS LAKE (DOG CREEK ROAD)
262	54.9	KELOWNA (MCCLULLOCH RD. & KLO RD.)
265	119.5	NORTH SAANICH (GLENEG ROAD)
268	463.8	DENMAN ISLAND (DENMAN ROAD)
272	340	ABBOTSFORD (34288 FARMER RD)
273	331	ABBOTSFORD (FARMER RD)
274	75.1	ABBOTSFORD (VYE RD)
275	214.9	SURREY (36TH AVE NEAR 194TH ST)
276	18.7	SALTSPRING ISLAND
279	61.2	REVELSTOKE (SIMPSON ST.)
280	34.8	COMOX
281	120.4	SALTSPRING ISLAND (LONG HARBOUR RD.)
282	45.6	WILLOWBROOK/MEYERS FLATS (MEYERS RD.)
283	94.2	PENDER ISLAND (PAISLEY ROAD)
284	94.2	PENDER ISLAND (PIRATES ROAD)
285	17.1	COMOX
286	48.5	TUMBLER RIDGE
287	185.8	COOMBS (BURGOYNE ROAD)
288	144.5	HORNBY ISLAND (CENTRAL RD. AT SANDPIPER RD.)
289	124.7	WILLIAMS LAKE (PINE VALLEY SUBDIVIDSION)
290	41.2	SATURNA ISLAND (EAST POINT RD. AT GAINES RD.)
291	37.2	CRANBROOK (GOLD CREEK RD. & 42ND AVE.)
292	238.8	POWELL RIVER (VICTORY RD)
293	71	FERGUSON LAKE N. KELLY RD.
294	150.5	LUMBY (WHITEVALE RD. & HORNER RD.)
295	151	QUALICUM BEACH (BERWICK ROAD)
296	62.8	MERRITT (GARCIA ROAD; AT LIBRARY)
297	131.2	COWICHAN BAY
299	300.4	ABBOTSFORD (MT LEHMAN RD N OF MARSHALL RD EXTENSION)
301	310	ABBOTSFORD (KING RD W OF BRADNER RD)
302	110.8	MALAKWA (LOFTUS ROAD)
303	151	QUALICUM BEACH (YAMBURY RD.)
304	99	PARKSVILLE (DESPARD RD. AT SPRINGWOOD PARK)
306	39.2	BEAVERDELL (HWY 33 & 42ND AVE.)
308	43.2	GOLDEN (RIVER ST.)
309	116	GOLDEN (HIGHWAY 95 & ALMBERG RD.)
310	463.8	BOWSER (DEEP BAY NORTH AT GAINSBURG RD.)
311	74.5	VERNON (KEDDLESTON RD.) BX CREEK
312	208.8	CASSIDY (HASLAM CREEK ON T-BRIDGE RD.)
314	151	PARKSVILLE (SPRINGHILL RD.)
315	36	LADYSMITH (YELLOWPOINT ROAD)

316	29.8	GABRIOLA ISLAND (OYSTER WAY)
317	34.3	GABRIOLA ISLAND (WILD CHERRY TERRACE)
318	166.4	DUNCAN FISH HATCHERY (WHARNCLIFFE RD.)
319	116.6	SATURNA ISLAND (TUMBO CHANNEL RD.)
320	118.2	COBBLE HILL (BRAITHWAITE ESTATES)
321	405.6	QUALICUM (LEEWARD WAY)
322	54	VERNON (FALCON RD.) SILVER STAR MTN
323	24.8	HORNBY ISLAND (WHALING STATION BAY)
326	97.9	GALIANO ISLAND (STURDIES BAY RD.)
327	97.9	GALIANO ISLAND (COMMUNITY SCHOOL)
329	498.6	UCLUELET (HWYS YARD)
330	112.6	CASSIDY (NANAIMO RIVER AT HARMAC)
331	38.8	BOWSER (DEEP BAY SOUTH)
332	12.6	OLIVER (87TH ST.)
333	156.2	CENTRAL SAANICH
335	315.3	COLUMBIA VALLEY (800 COLUMBIA VALLEY RD)
337	267.8	LADYSMITH (WOODLEY RANGE)
338	157.4	CENTRAL SAANICH (SEABROOK RD.)
340	80	LANTZVILLE (VALMAR ROAD)
342	105.9	PRINCE GEORGE FISH TRAP ISLAND
343	61.7	CENTRAL SAANICH (MT NEWTON X ROAD)
344	42.5	CACHE CREEK (JACKSON PARK; VALLEYVIEW DRIVE)
345	44	COBBLE HILL (ARBUTUS RIDGE)
346	42.5	CACHE CREEK (JACKSON PARK; VALLEYVIEW DRIVE)
347	79.9	QUESNEL (RED BLUFF 638 FIR ST.)
349	288.8	BELCARRA (3400-BLOCK MAIN AVE)
351	148	COMOX (GREENWOOD RD.)
352	210.6	WHISTLER (LAKESHORE DR)
353	214.6	LANGLEY (19638 36 AVE)
354	310	LANGLEY (238 ST NEAR 50 AVE)
355	170.6	CHEMAINUS (MT SICKER RD.)
356	39.4	WINFIELD (JIM BAILEY RD.)
357	312	ABBOTSFORD (30244 TAYLOR RD)
358	124.9	LANGLEY (22317 16TH AVE)
359	246.3	LANGLEY (3364 240 ST)
360	180.8	LANGLEY (2145 200 ST)
361	340	LANGLEY (26B AVE; ALDERGROVE)
363	102.8	WASA (HWY 93)
364	73.8	QUESNEL - 2 MILE FLATS (PINECREST ROAD)
365	87.6	SHUSWAP LAKE PARK DEEP (SQUILAX - ANGLEMONT ROAD)
365	51.6	SHUSWAP LAKE PARK SHALLOW (SQUILAX - ANGLEMONT ROAD)
366	31.6	SUMMERLAND (BATHVILLE RD.)
367	38.6	SUMMERLAND (BATHVILLE RD. PR-15274; WW-1; E229670)
368	267.1	BLACK CREEK GRAVEL PIT - OYSTER R. BEDROCK
369	267.1	BLACK CREEK GRAVEL PIT - OYSTER R. UNCONSOLIDATED
371	523.2	T`SABLE RIVER (HWY 19A)
372	95	DISTRICT OF HIGHLANDS - GOWLLAND TOD PARK
373	185.6	SALT SPRING ISLAND (MT BELCHER HEIGHTS)
374	35.5	108 MILE SUBDIVISION
375	134.6	BLUE RIVER (MURTLE LAKE ROAD)
376	37.2	JUNCTION SHEEP RANGE PARK
378	54.1	PRINCE GEORGE AT 5TH AND OSPIKA
381	93.8	CANOE CREEK SHALLOW (SALMON ARM - GRINDROD HWY 97B)
383	104.2	QUADRA ISLAND (HERIOT BAY RD.)
464	93.8	CANOE CREEK DEEP (SALMON ARM - GRINDROD HWY 97B)

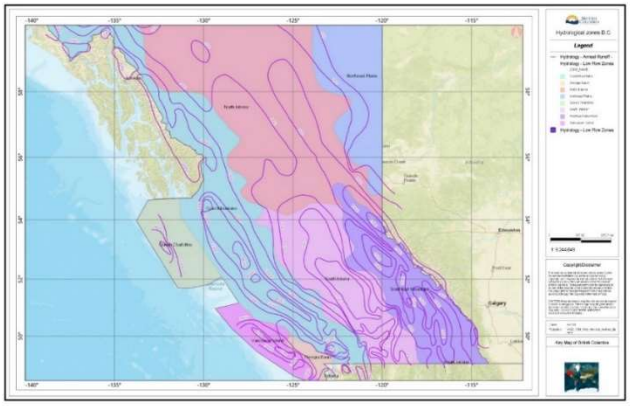

*Figure 8.1.6: Low flow zones and annual average runoff for British Columbia (*iMapBC*, n.d.).*

Figure 8.1.7: Example of water boundary/streamflow mapping that can be done on iMAP B.C. (Schnorbus et al., 2010)

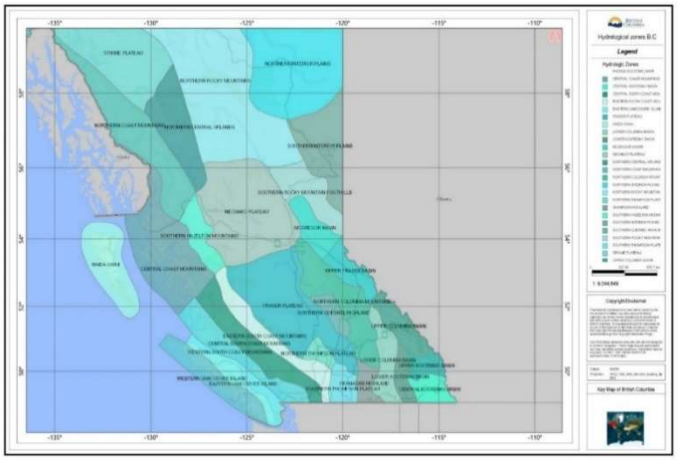

*Figure 8.1.8: Updated hydrologic zones (*iMapBC*, n.d.).*

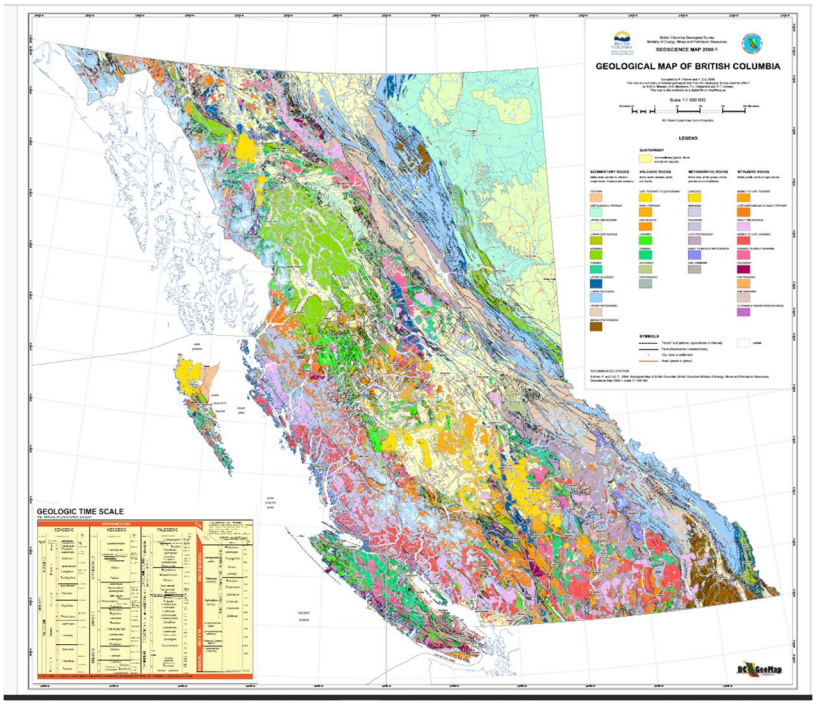

Figure 8.1.9: Geological map of British Columbia. (P. Erdmer & Y. Cui, 2009)

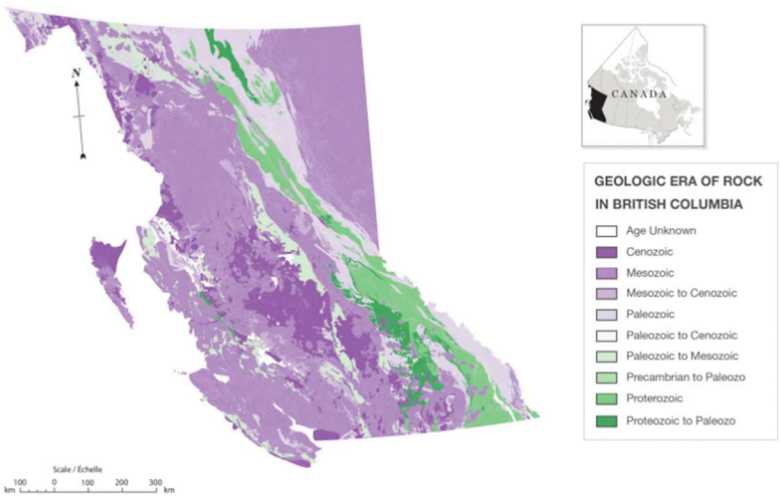

Figure 8.1.10: Geologic era of rock in British Columbia. (Fulton et al., 2004).

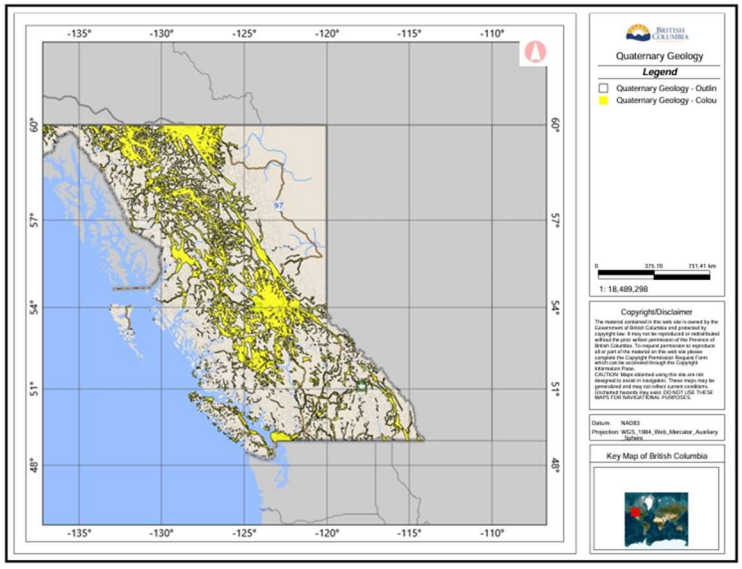

*Figure 8.1.11: Quaternary geology of rock in British Columbia (*iMapBC*, n.d.).*

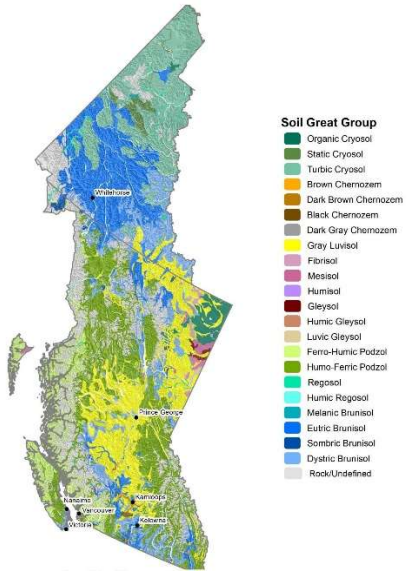

Figure 8.1.12: Soil great groups in British Columbia. (Science, 2021).

8.2 Exploratory Data Analysis

8.2.1 Methodology

Table 8.2.1: Aquifer type determination for unlinked wells.

OBS	Well Tag	EMS ID	Aquifer #	Notes and Link
082	20904	1401079	NA	Link: https://apps.nrs.gov.bc.ca/gwells/well/85742 Closest aquifer is 4b. Most lithology missing. Assuming Aquifer type 4b due to glaciation
276			1143	Most nearby are 6a bedrock
286	52975	E264141	635	Under different EMS ID Link: https://apps.nrs.gov.bc.ca/gwells/well/52975
369	83157	E262078	NA	Oyster river surficial well; approximately 20 feet south east Link: https://apps.nrs.gov.bc.ca/gwells/well/83157 Lithology: Mostly gravel and sand. Assuming Aquifer type 2
367	85742	E229670	NA	Bedrock 6b. Map overlay
358	17459	1401023	50	Known as 004: Not in records so used location. Only well at said location Link: https://apps.nrs.gov.bc.ca/gwells/well/17459 6a bedrock

Table 8.2.2: Element, lowest detected limit in dataset and maximum concentration limits from Guidelines for Canadian Drinking Water Quality (Health Canada, 2022).

Element	Lowest Detected Limit in Dataset [mg/L]	Half Value of Lower Limit [mg/L]	Canadian Drinking Water Guideline Maximum [µg/L]
As	0.00002	0.00001	0.010
Ca	0.05	0.025	
Cd	0.000005	0.0000025	0.007
Chloride	0.5	0.25	
Fe	0.001	0.0005	
Mg	0.005	0.0025	
Mn	0.000008	0.000004	0.12
P	0.002	0.001	
Pb	0.000005	0.0000025	0.005
K	0.05	0.025	
U	0.000002	0.000001	0.02
Na	0.05	0.025	

N:Kjel	0.01	0.005	
Residue Filterable 1.0u	10	5	
Specific conductance	1	0.5	
Sulfat:D	0.3	0.15	
Alkalinity 4.5	0.5	0.25	
Hardness	.5	.25	

Table 8.2.3: B.C. Aquifer Subtype Code(Ministry of Environment and Climate Change Strategy, n.d.)

Aquifer Subtype Code	Description
1a	Predominantly unconfined fluvial or glacio-fluvial sand and gravel Aquifers found along major rivers of higher stream order with the potential to be hydraulically influenced by the river.
1b	Predominantly unconfined fluvial or glacio-fluvial sand and gravel Aquifers found along rivers of moderate stream order with the potential to be hydraulically influenced by the river.
1c	Predominantly unconfined fluvial or glacio-fluvial sand and gravel Aquifers found along lower order (< 3-4) streams in confined valleys with relatively undeveloped floodplains, where aquifer thickness and lateral extent are more limited.
2	Predominantly unconfined deltaic sand and gravel aquifers are commonly found in deltas where a stream or smaller river flows into a standing body of water.
3	Alluvial or colluvial fan sand and gravel aquifers typically occur at or near the base of mountain slopes, either along the side of valley bottoms, or if formed during the last period of glaciation, raised above the valley bottoms.
4a	Unconfined glacio-fluvial outwash or ice contact sand and gravel aquifers generally formed near or at the end of the last period of glaciation.
4b	*Confined Glacio-fluvial sand and gravel aquifers underneath till, in between till layers, or underlying glacio-lacustrine deposits.*
4c	*Confined sand and gravel aquifer associated with glacio-marine environments near the coast.*
5a	**Fractured sedimentary rock aquifers primarily found in association with old sedimentary basins.**
5b	Karstic limestone aquifers
6a	**Crystalline bedrock aquifers associated with flat-lying to gently-dipping volcanic flows.**
6b	**Fractured crystalline (igneous intrusive or metamorphic, meta-sedimentary, meta-volcanic, volcanic) rock aquifers**
UNK	Unknown

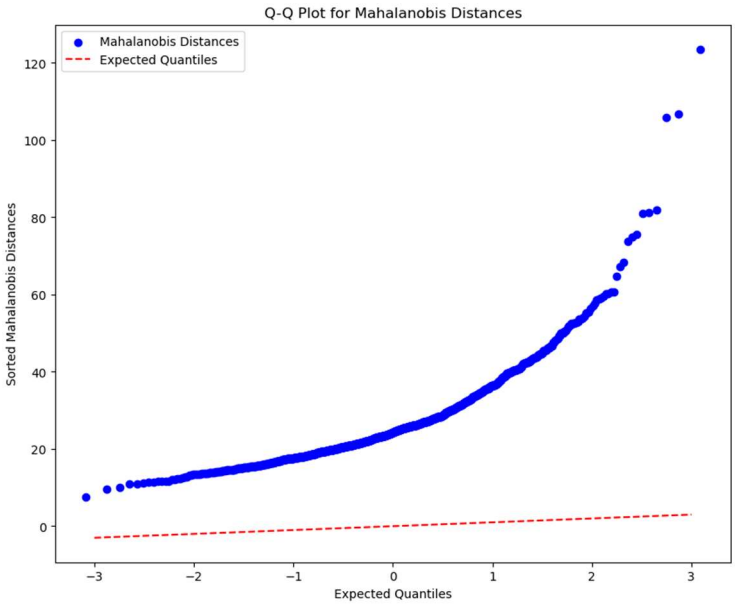

Figure 8.2.1: Quantile-Quantile plot of Mahalanobis distances. Plotting against scaled F-distribution would have been more accurate instead of linear quantiles due to the left data skew.

8.2.2 Exploratory Data Analysis Graphs

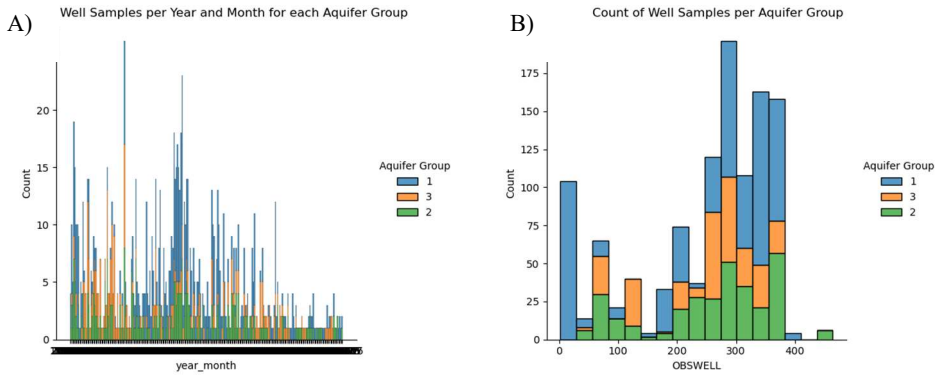

Figure 8.2.2: A) Well sampling per aquifer group throughout time.
B) Well sampling per aquifer group for related observation well station number (OBSWELL).

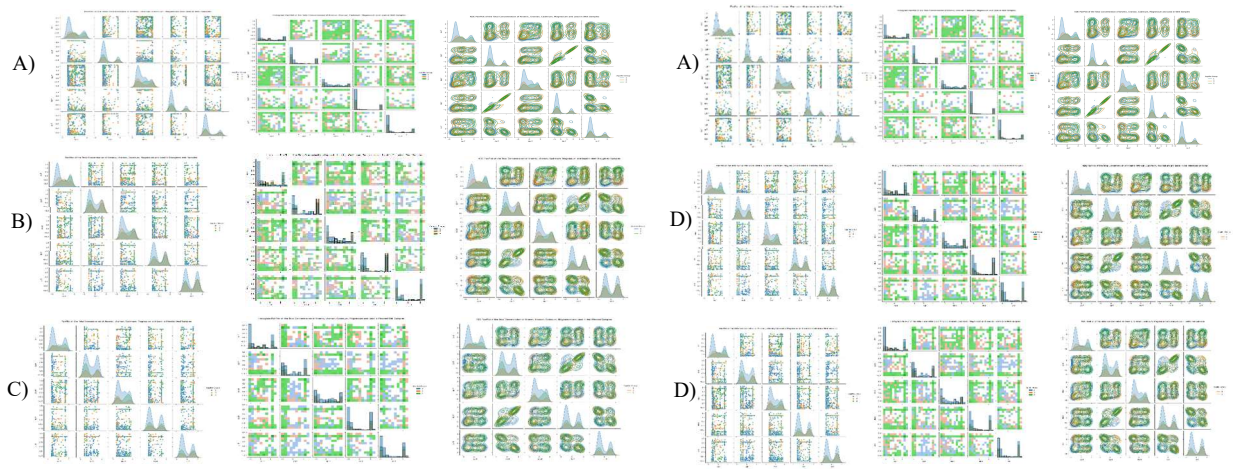

Figure 8.2.3: A) From left to right: pairplot, hisplot and KDE plots of the relationship between metals of interest for full dataset.
B) From left to right: pairplot, hisplot and KDE plots of the relationship between metals of interest for drought dataset.
C) From left to right: pairplot, hisplot and KDE plots of the relationship between metals of interest for Flood dataset.
D) From left to right: pairplot, hisplot and KDE plots of the relationship between metals of interest for dataset with rising minimum temperatures.
E) From left to right: pairplot, hisplot and KDE plots of the relationship between metals of interest for dataset with rising maximum temperatures.

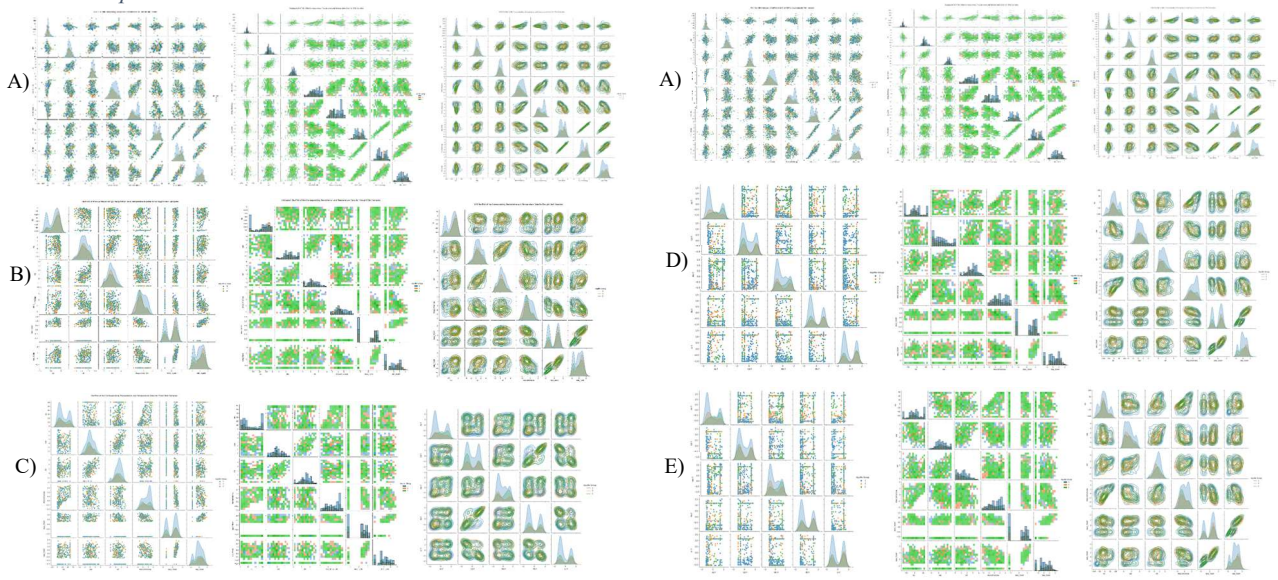

Figure 8.2.4: A) From left to right: pairplot, hisplot and KDE plots of the relationship between precepitation /temperature for full dataset.
B) From left to right: pairplot, hisplot and KDE plots of the relationship between precepitation /temperature for drought dataset.
C) From left to right: pairplot, hisplot and KDE plots of the relationship between precepitation/temperature for flood dataset.
D) From left to right: pairplot, hisplot and KDE plots of the relationship between precepitation /temperature for dataset with rising minimum temperatures.
E) From left to right: pairplot, hisplot and KDE plots of the relationship between precepitation /temperature for dataset with rising maximum temperatures.

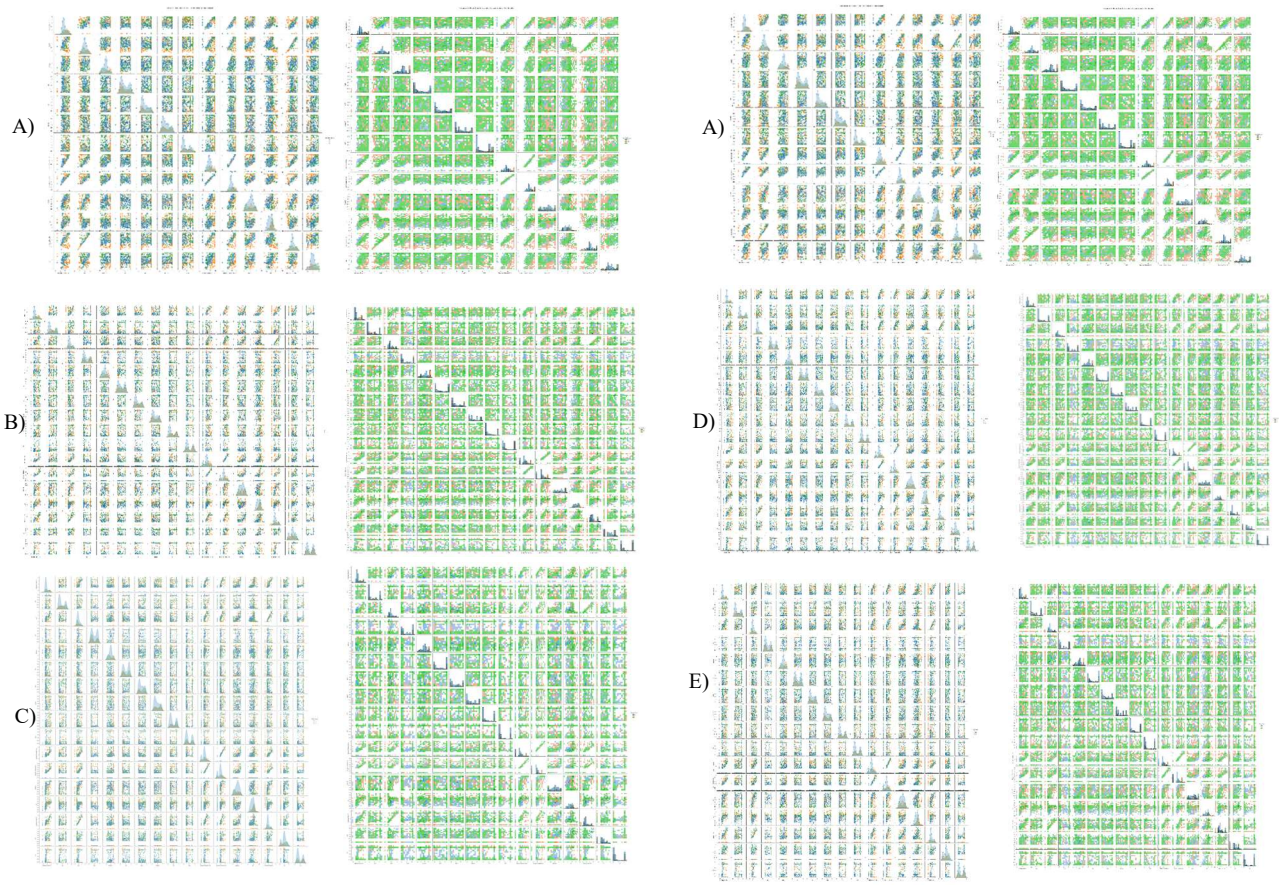

Figure 8.2.5: A) From left to right: pairplot and hisplot plots of the relationship between other variables for full dataset. B) From left to right: pairplot and hisplot plots of the relationship between other variables for drought dataset. C) From left to right: pairplot and hisplot plots of the relationship between other variables for flood dataset. D) From left to right: pairplot and hisplot plots of the relationship between other variables for dataset with rising minimum temperatures. E) From left to right: pairplot and hisplot plots of the relationship between other variables for dataset with rising maximum temperatures.

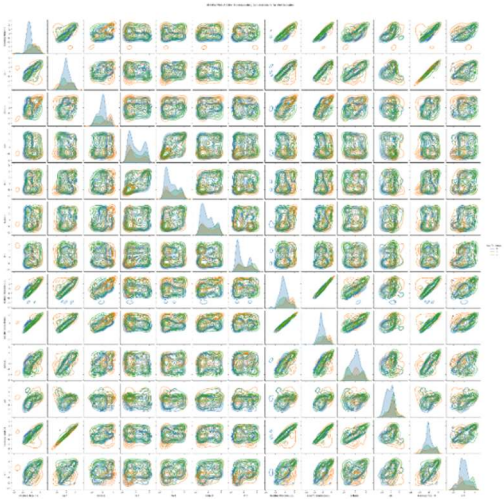

Figure 8.2.6: KDE plots of the relationship between other variables for full dataset

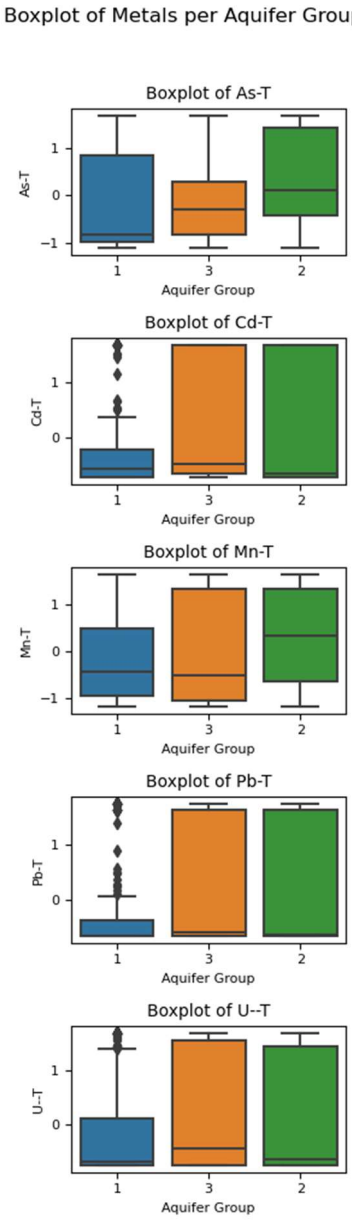

Figure 8.2.7: Box plots of the metals of interest per aquifer group for the scaled data.

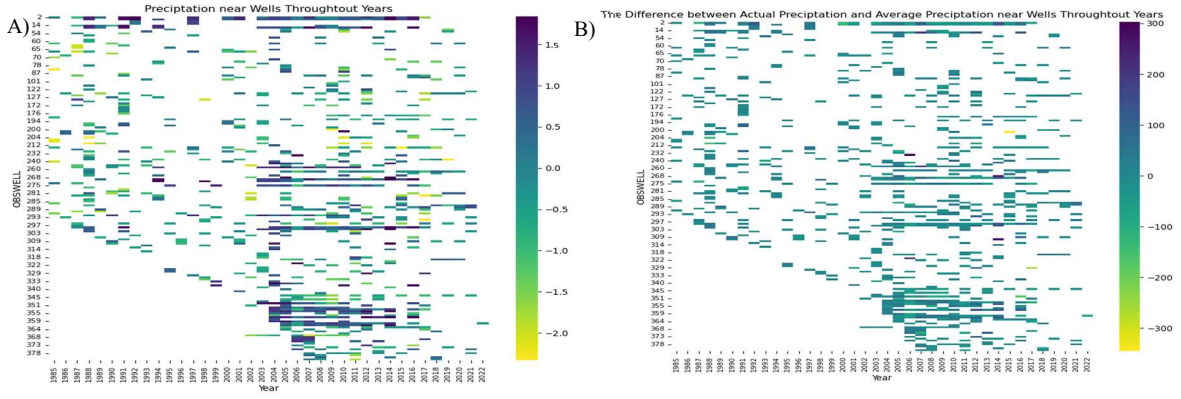

Figure 8.2.8: A) Heatmap of monthly preciptation nearby wells (OBSWELL) through the years. B) Heatmap of the difference between measured monthly preciptation and sitmulated monthly monthly preciptation nearby wells (OBSWELL) through the years.

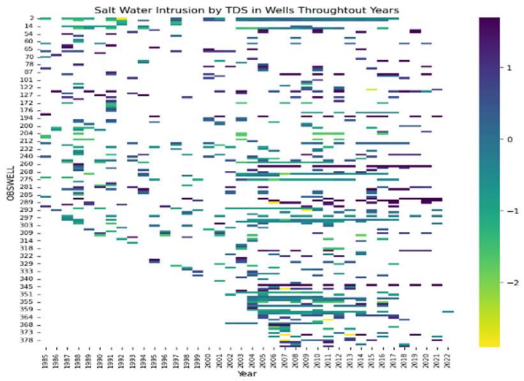

Figure 8.2.9: Heatmap of Residue Filterable 1.0u (a sea water intrusion indicator) in wells (OBSWELL) through the years.

8.2.3 Saltwater Intrusion Exploratory Analysis

Table 8.2.4: Summary of the datapoints resultant from combinations of different sea water intrusion factors (British Columbia Ministry of Forest, 2016)

Dataset Based on SWI over Limit	As Above Limit	Pb Above Limit	Mn Above Limit	U Above Limit	Specific Conductance over cutoff	Residue Filterable 1.0u over cutoff	Chloride over cutoff	Total data points
Normal	81	289	344	6	107	79	52	1147
Residue Filterable 1.0u	5	17	26	0	70	-	32	71
Chloride	2	13	13	0	38	31	-	45
Specific Conductance	7	22	38	0	-	70	32	98
Chloride + Specific Conductance	2	9	10	0	-	24	-	37

Residue Filterable 1.0u + Specific Conductance	5	17	26	0	-	-	24	70
Chloride + Residue Filterable 1.0u	2	9	10	0	24	-	-	31
Chloride or Specific Conductance	71	26	41	0	99	70	47	106
All	2	9	10	0	-	-	-	24

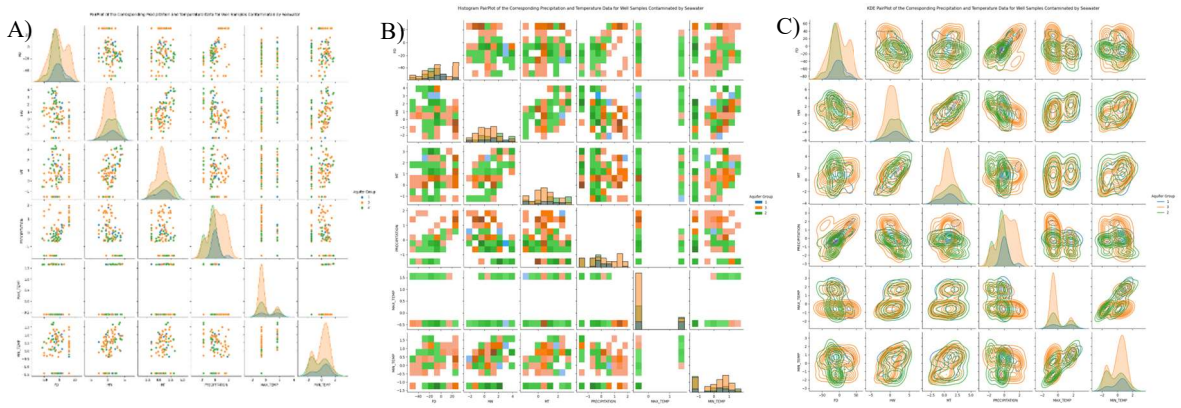

Figure 8.2.10: A) Pairplot, B) Hisplot and C) KDE plots of the relationship between temperature/precepitation variables for SWI dataset where specfic conductance ≥ 1000 or chloride ≥ 150 µg/L

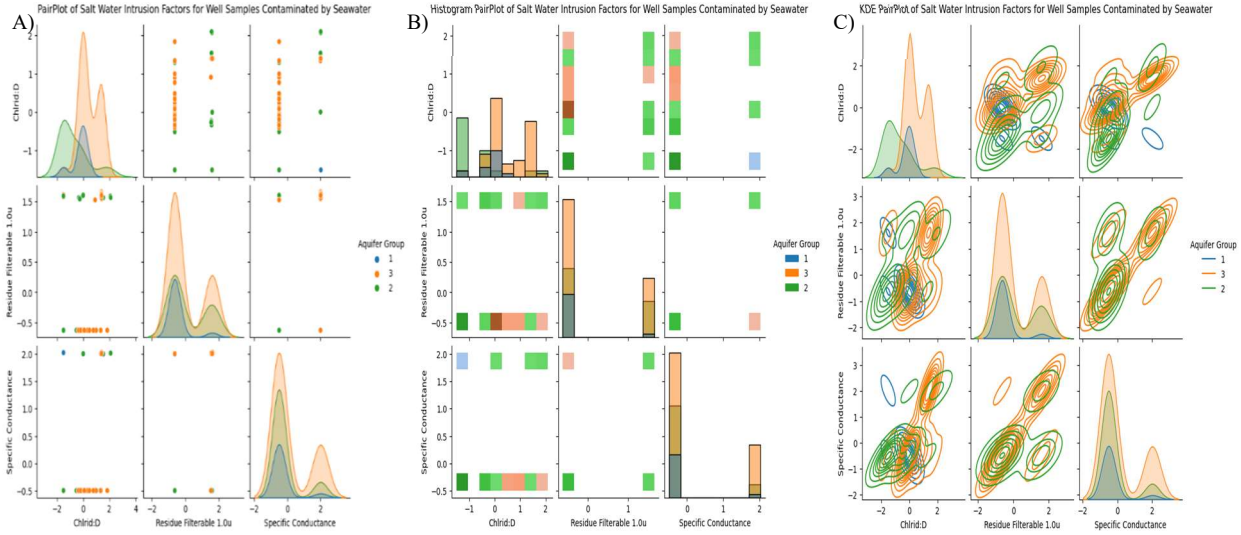

Figure 8.2.11: A) Pairplot, B) Hisplot and C) KDE plots of the relationship between seawater intrusion variables for SWI dataset where specfic conductance ≥ 1000 or chloride ≥ 150 µg/L.

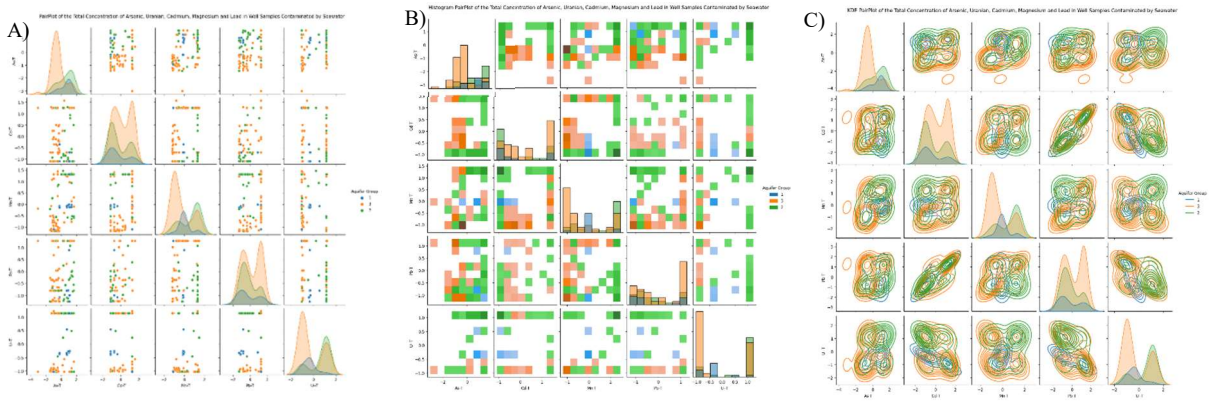

Figure 8.2.12: A) Pairplot, B) Hisplot and C) KDE plots of the relationship between metals of interest for SWI dataset where specfic conductance ≥ 1000 or chloride ≥ 150 µg/L.

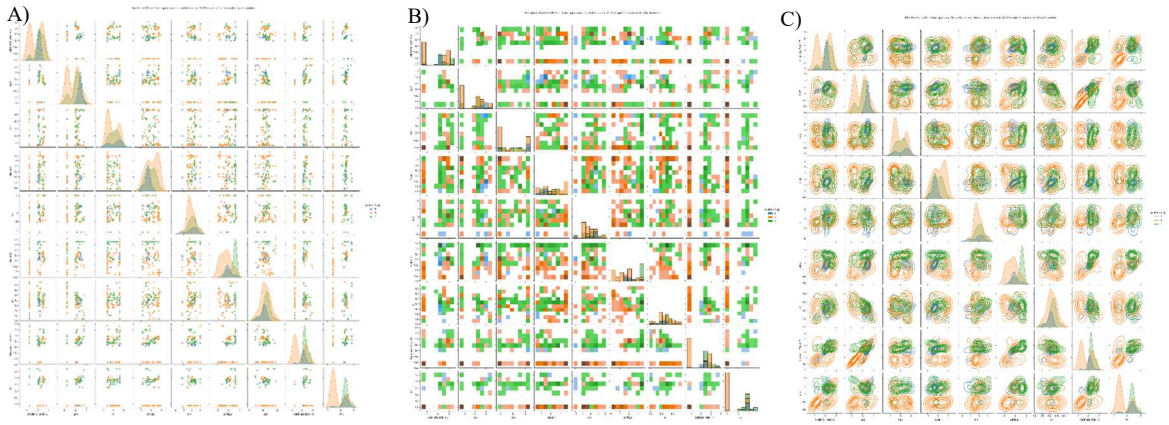

Figure 8.2.13: A) Pairplot, B) Hisplot and C) KDE plots of the relationship between other variables for SWI dataset where specfic conductance ≥ 1000 or chloride ≥ 150 µg/L.

8.2.4 Power BI Analysis

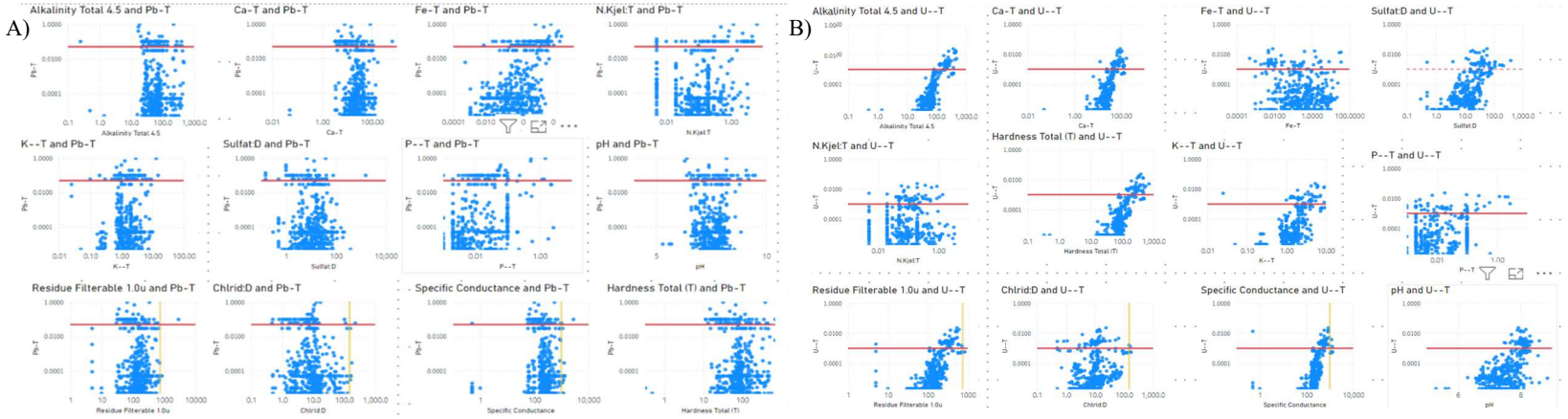

Figure 8.2.14: A) Scatterplot of well samples with Lead and the Canadian Water Drinking Standards maximum limit (red line) against other factors including sea water intrusion factors and cutoffs (yellow line) for Aquifer Group 1.
B) Scatterplot of well samples with Uranium against other factors including sea water intrusion factors and cutoffs (yellow line).

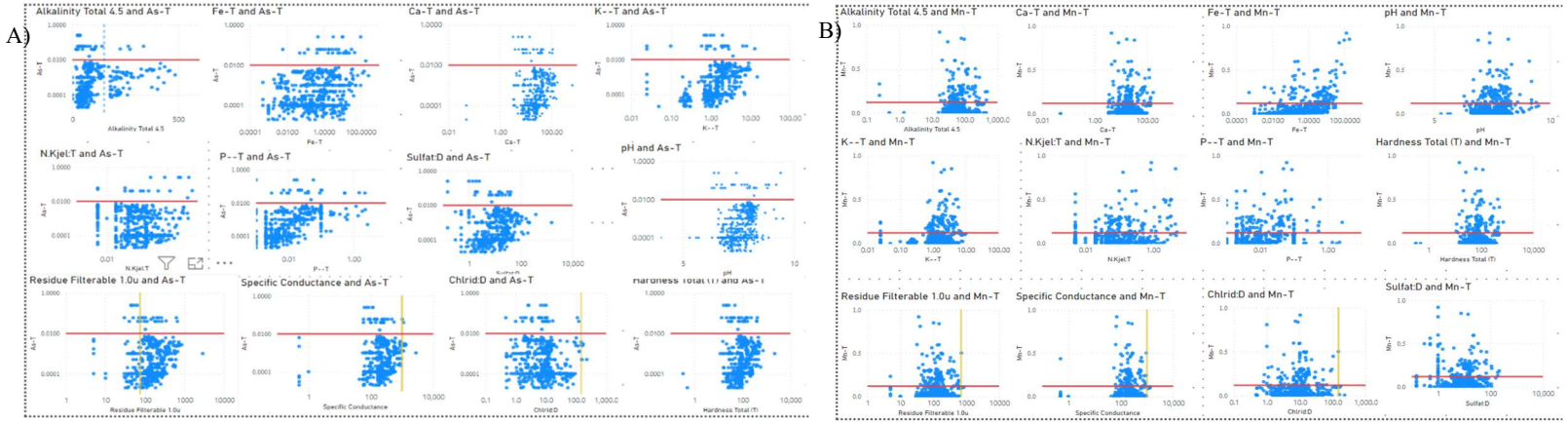

Figure 8.2.15: A) Scatterplot of well samples with Arsenic and the Guidelines for Canadian Drinking Water Quality maximum limit (red line) against other factors including sea water intrusion factors and cutoffs (yellow line) for Aquifer Group 1.
B) Scatterplot of well samples with Manganese against other factors including sea water intrusion factors and cutoffs (yellow line).

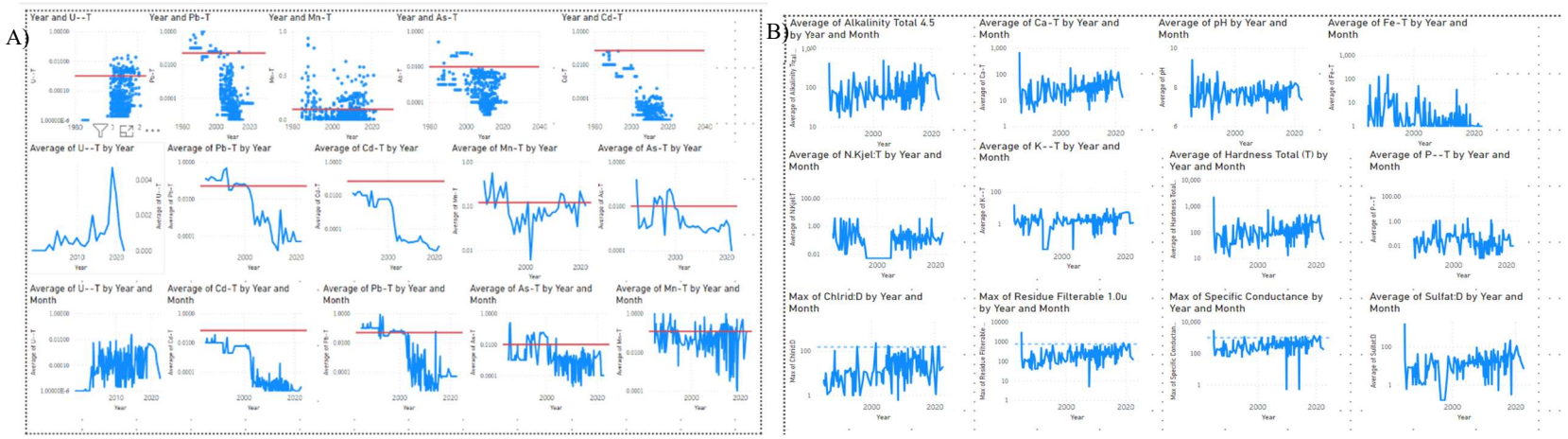

Figure 8.2.16: A) Scatterplots per year, line graphs of mean concentration per year, and line graphs of mean concentration per year, line graphs of mean concentration per year and month to indicate seasonality of various metals for Aquifer Group 1 and any corresponding Guidelines for Canadian Drinking Water Quality maximum limits (red line) per year in Power BI.
B) Mean concentration line graphs per month and year to indicate seasonality of different corresponding compounds in Aquifer Group 1

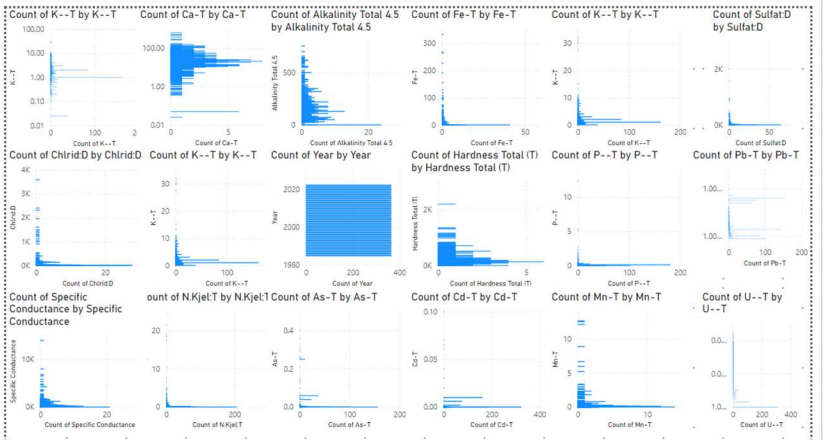

Figure 8.2.17: Histograms of all metals in Power BI (count by concentration) in all aquifer groups.

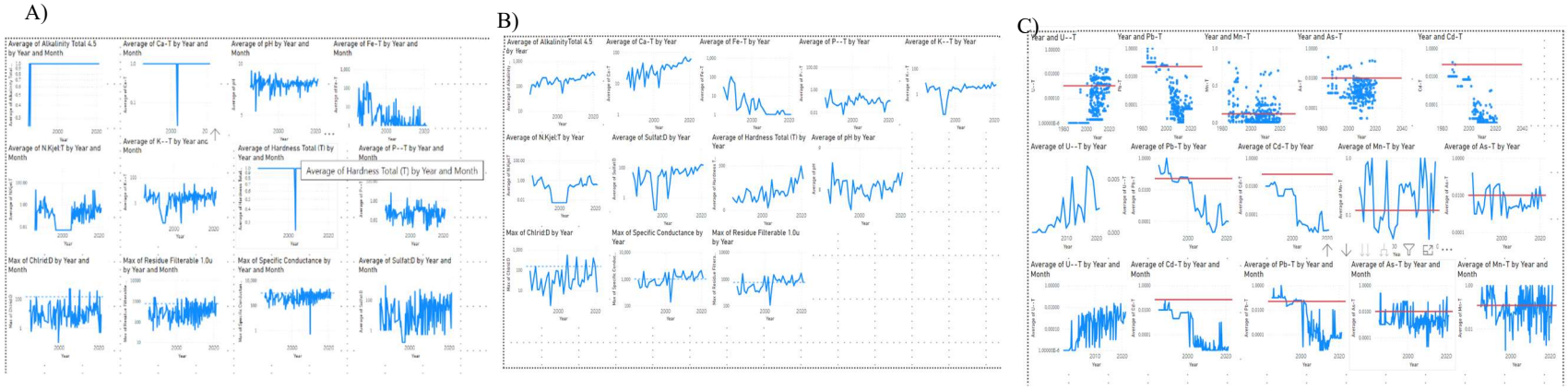

Figure 8.2.18: A) Line graphs of mean concentration per year and month to indicate seasonality of different corresponding compounds in Aquifer Group 2. B) line graphs of mean concentration per year of different corresponding compounds in Aquifer Group 2. C) Scatter plots of concentration per year, line graphs of mean concentration per year, line graphs of mean concentration per year and month to indicate seasonality of various metals for Aquifer Group 2 and any corresponding Guidelines for Canadian Drinking Water Quality maximum limits (red line) per year in Power BI.

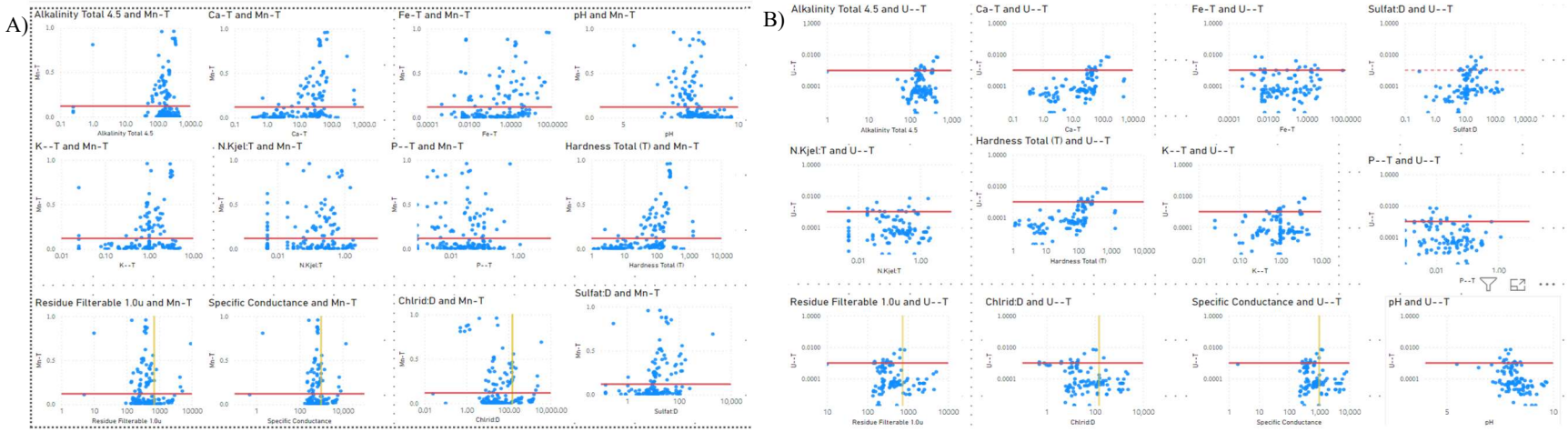

Figure 8.2.19: A) Scatterplots of well samples with Manganese and the Guidelines for Canadian Drinking Water Quality maximum limit (red line) against other factors including sea water intrusion factors and cutoffs (yellow line) for Aquifer Group 3 in Power BI. B) Scatterplot of well samples with Uranium in Aquifer Group 3 against other factors including sea water intrusion factors and cutoffs (yellow line).

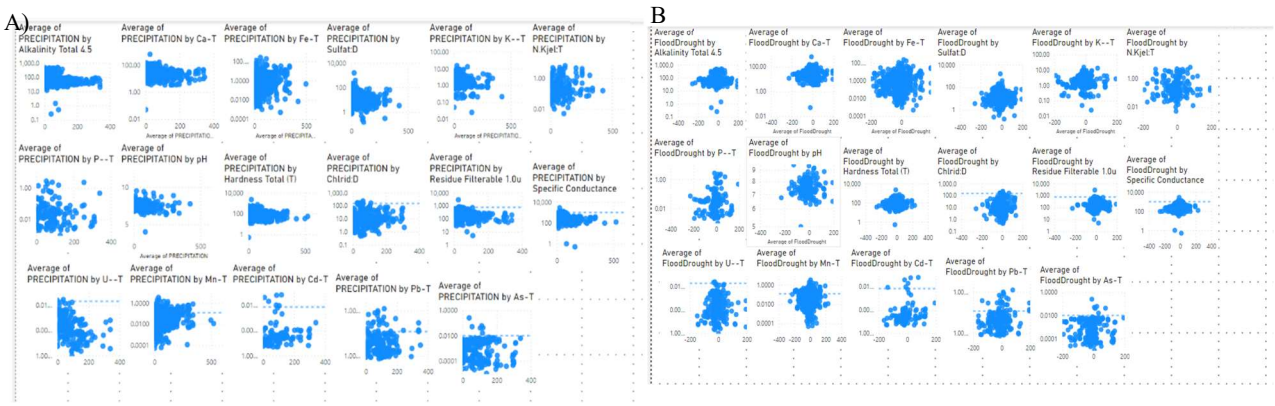

Figure 8.2.20: A) Power BI Scatterplots of nearby precipitation values against the average of all variables - the Guidelines for Canadian Drinking Water Quality maximum limit (blue dashed line) is shown for metals and cutoffs for sea water intrusion factors (blue dashed line) for Aquifer Group 1.
B) 'FloodDrought' is the expected simulated monthly precipitation subtracted from the actual precipitation. Power BI scatterplots of it against the average of all variables - the Guidelines for Canadian Drinking Water Quality maximum limit (blue dashed line) is shown for metals and cutoffs for sea water intrusion factors (blue dashed line) for Aquifer Group 1.

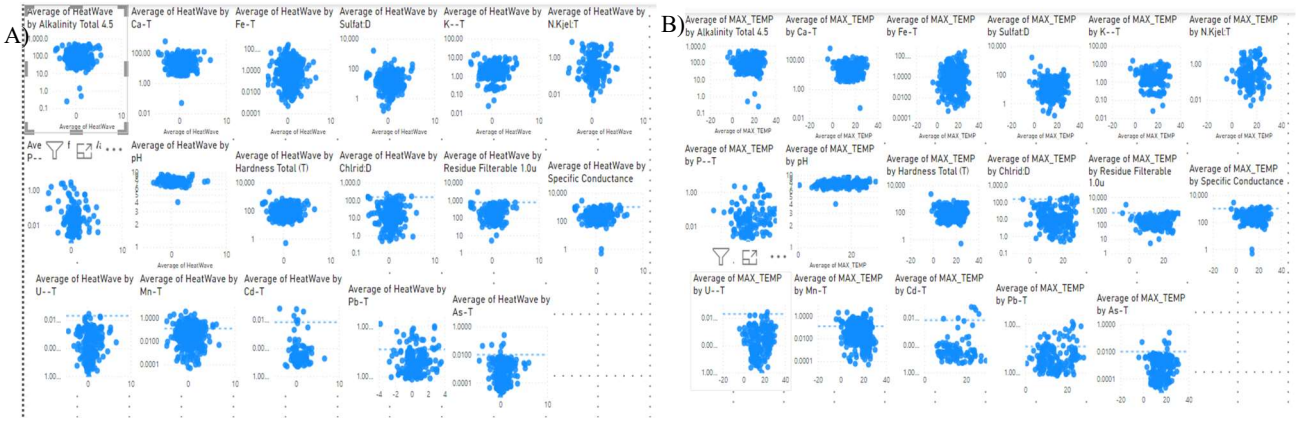

Figure 8.2.21: A) Power BI Scatterplots of nearby mean monthly maximum temperature values against the average of all variables - the Guidelines for Canadian Drinking Water Quality maximum limit (blue dashed line) is shown for metals and cutoffs for sea water intrusion factors (blue dashed line) for Aquifer Group 1.
B) 'Heat wave' is the expected simulated mean monthly maximum temperature from the actual mean monthly maximum temperature. Power BI scatterplots of it against the average of all variables - the Guidelines for Canadian Drinking Water Quality maximum limit (blue dashed line) is shown for metals and cutoffs for sea water intrusion factors (blue dashed line) for Aquifer Group 1.

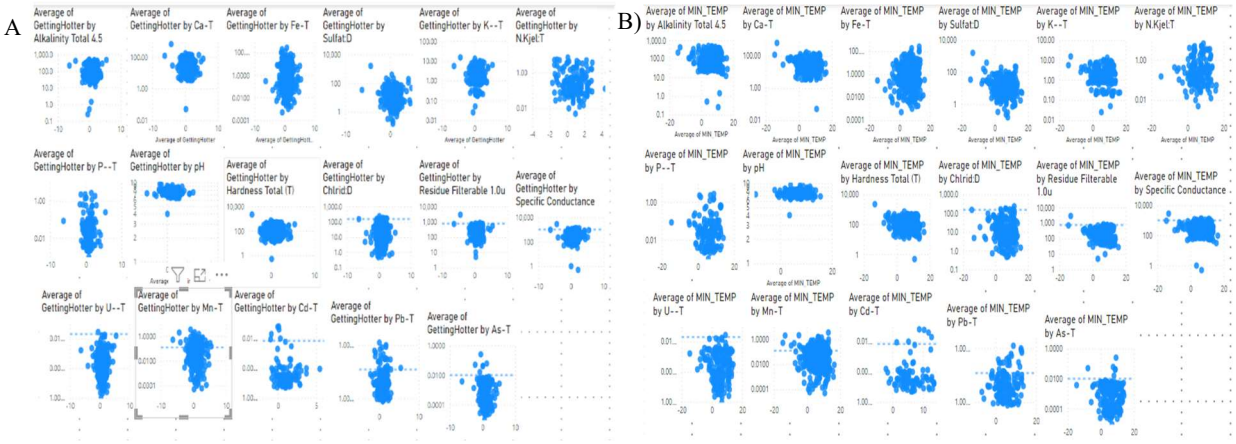

Figure 8.2.22: A) 'GettingHotter' is the expected simulated mean monthly minimum temperature from the actual mean monthly minimum temperature. Power BI scatterplots of it against the average of all variables - the Guidelines for Canadian Drinking Water Quality maximum limit (blue dashed line) is shown for metals and cutoffs for sea water intrusion factors (blue dashed line) for Aquifer Group 1.
B) Power BI Scatterplots of nearby mean monthly minimum temperature values against the average of all variables - the Guidelines for Canadian Drinking Water Quality maximum limit (blue dashed line) is shown for metals and cutoffs for sea water intrusion factors (blue dashed line) for Aquifer Group 1.

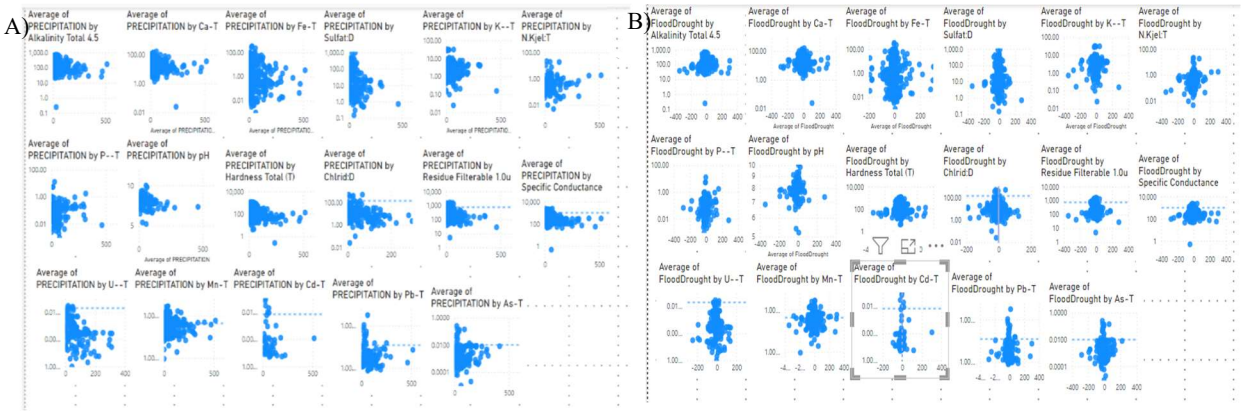

Figure 8.2.23: A) Power BI Scatterplots of nearby precipitation values against the average of all variables - the Guidelines for Canadian Drinking Water Quality maximum limit (blue dashed line) is shown for metals and cutoffs for sea water intrusion factors (blue dashed line) for Aquifer Group 2.
B) 'FloodDrought' is the expected simulated monthly precipitation subtracted from the actual precipitation. Power BI scatterplots of it against the average of all variables – the Guidelines for Canadian Drinking Water Quality maximum limit (blue dashed line) is shown for metals and cutoffs for sea water intrusion factors (blue dashed line) for Aquifer Group 2.

Figure 8.2.24: A) 'GettingHotter' is the expected simulated mean monthly minimum temperature from the actual mean monthly minimum temperature. Power BI scatterplots of it against the average of all variables - the Guidelines for Canadian Drinking Water Quality maximum limit (blue dashed line) is shown for metals and cutoffs for sea water intrusion factors (blue dashed line) for Aquifer Group 2.
B) 'Heat wave is the expected simulated mean monthly maximum temperature from the actual mean monthly maximum temperature. Power BI scatterplots of it against the average of all variables - the Guidelines for Canadian Drinking Water Quality maximum limit (blue dashed line) is shown for metals and cutoffs for sea water intrusion factors (blue dashed line) for Aquifer Group 2.
C) Power BI Scatterplots of nearby mean monthly minimum temperature values against the average of all variables - the Guidelines for Canadian Drinking Water Quality maximum limit (blue dashed line) is shown for metals and cutoffs for sea water intrusion factors (blue dashed line) for Aquifer Group 2.

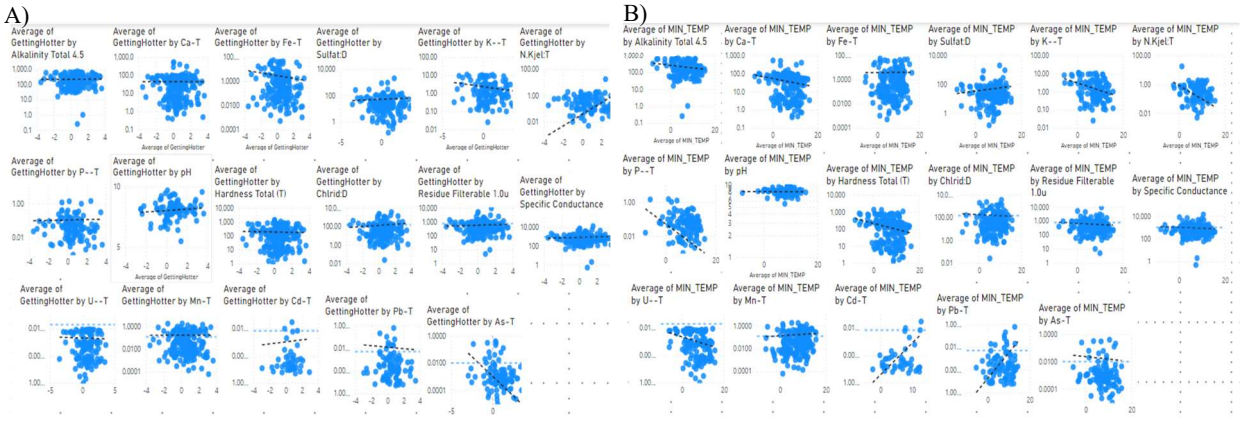

Figure 8.2.25: A) 'GettingHotter' is the expected simulated mean monthly minimum temperature from the actual mean monthly minimum temperature. Power BI scatterplots of it against the average of all variables - the Guidelines for Canadian Drinking Water Quality maximum limit (blue dashed line) is shown for metals and cutoffs for sea water intrusion factors (blue dashed line) for Aquifer Group 3.
B) Power BI Scatterplots of nearby mean monthly minimum temperature values against the average of all variables - the Canadian Water Drinking Standards maximum limit (blue dashed line) is shown for metals and cutoffs for sea water intrusion factors (blue dashed line) for Aquifer Group 3.

8.2.5 Exploratory Data Analysis Tables

Table 8.2.5: Unscaled, log scaled and yeo Johnson scaled skew for each variable per aquifer group.

Aquifer group	Scale	Alkalinity Total 4.5	As-T	Ca-T	Cd-T	Chlrid: D	Fe-T	Mn-T	N.Kjel: T	P--T	Pb-T	Residue Filterable 1.0u	Specific Conductance	Sulfat: D	pH	Hardness Total (T)	K--T	U--T	PRECIPITATION	MIN_TEMP	MAX_TEMP	Precip_Climatology	Tn_Climatology	Tx_Climatology	FD	HW	MT
1	No Scaling	-0.272	8.723	0.076	7.247	0.612	1.645	4.282	3.085	6.606	9.200	-0.769	-2.474	0.068	-1.023	-0.042	0.695	7.492	1.283	-0.468	0.042	0.822	-0.135	0.140	-0.167	0.165	-0.294
1	Log	-0.272	8.723	0.076	7.247	0.612	1.645	4.282	3.085	6.606	9.200	-0.769	-2.474	0.068	-1.023	-0.042	0.695	7.492	1.283	-0.468	0.042	0.822	-0.135	0.140	-0.167	0.165	-0.294
1	Yeo-Johnson	0.552	0.779	0.443	1.718	-0.160	0.135	0.348	0.327	0.672	1.505	-0.753	-1.031	-0.217	-0.084	0.339	-0.179	1.202	1.283	-0.468	0.042	0.822	-0.135	0.140	-0.167	0.165	-0.294
2	No Scaling	-1.476	6.041	-0.146	7.996	1.009	1.501	3.575	4.004	6.524	14.445	-0.147	-1.613	0.591	-1.169	-0.092	0.470	4.687	2.146	-0.731	-0.253	1.405	-0.607	-0.336	-0.058	-0.010	-0.349
2	Log	1.456	5.425	1.426	7.968	6.910	6.854	7.517	7.565	10.929	16.119	2.042	1.783	3.834	-0.776	1.939	4.140	4.330	2.070	-0.759	-0.220	1.448	-0.604	-0.315	1.028	0.053	-0.330
2	Yeo-Johnson	-0.407	0.102	0.084	0.970	0.195	-0.058	-0.258	-0.164	-0.286	0.890	-0.138	-0.474	0.419	-0.303	0.227	-0.422	0.500	2.146	-0.731	-0.253	1.405	-0.607	-0.336	-0.058	-0.010	-0.349
3	No Scaling	-2.177	4.788	-0.196	2.108	0.196	1.937	2.278	3.815	4.310	4.053	-0.244	-1.829	0.134	-0.607	-0.295	1.113	2.240	2.060	-0.706	-0.424	1.455	-0.671	-0.498	-0.138	-0.169	-0.229
3	Log	1.222	6.733	4.725	2.169	5.731	3.773	3.130	12.728	5.346	5.392	6.496	5.690	9.684	-0.222	2.216	2.289	2.056	1.964	-0.739	-0.431	1.645	-0.743	-0.603	1.312	-0.163	-0.214
3	Yeo-Johnson	-1.224	0.691	0.068	0.678	-0.689	0.664	0.405	0.207	0.060	0.630	-0.226	-0.409	-0.219	0.006	-0.055	0.473	0.582	2.060	-0.706	-0.424	1.455	-0.671	-0.498	-0.138	-0.169	-0.229

Table 8.2.6: Final summary statistics for each variable per aquifer group in the entire dataset

Aquifer Group		Alkalinity Total 4.5	As-T	Ca-T	Cd-T	Chlrid: D	Fe-T	Mn-T	N.Kjel: T	P--T	Pb-T	Residue Filterable 1.0u	Specific Conductance	Sulfat:D	pH	Hardness Total (T)	K--T	U--T	PRECIPITATION	MIN_TEMP	MAX_TEMP	Precip_Climatology	Tn_Climatology	Tx_Climatology	FD	HW	MT
1	mean	-0.368	-0.166	0.037	-0.136	-0.073	0.029	-0.143	-0.120	-0.278	-0.131	-0.316	-0.341	0.000	-0.382	-0.043	-0.085	-0.153	0.158	-0.078	-0.048	0.216	-0.104	-0.051	-1.403	0.493	0.804
1	var	0.623	1.048	0.651	0.818	0.678	0.994	0.837	0.864	0.841	0.851	0.716	0.664	0.734	0.788	0.592	0.712	0.851	1.020	0.920	0.989	0.990	0.920	0.991	3288.998	2.638	1.833
1	std	0.789	1.024	0.807	0.905	0.823	0.997	0.915	0.930	0.917	0.923	0.846	0.815	0.857	0.888	0.769	0.844	0.922	1.010	0.959	0.995	0.995	0.959	0.996	57.350	1.624	1.354
1	min	-3.157	-1.116	-2.527	-0.735	-1.825	-1.135	-1.194	-1.199	-1.132	-0.644	-2.903	-4.371	-1.738	-2.783	-2.702	-2.103	-0.766	-2.333	-2.489	-2.748	-2.035	-2.481	-2.179	-255.883	-4.491	-6.314
1	max	1.818	1.677	1.782	1.678	1.517	1.525	1.639	1.622	1.750	1.729	1.693	1.714	1.545	2.774	1.675	1.681	1.684	1.838	2.308	2.142	1.988	2.179	2.047	230.800	6.630	5.464
1	skew	0.889	0.786	0.228	1.396	0.063	0.321	0.624	0.579	0.768	1.445	-0.027	-0.036	-0.140	0.161	0.353	0.015	1.243	-0.324	-0.004	0.056	-0.354	0.099	0.093	0.271	0.217	-0.377
1	median	-0.520	-0.827	-0.024	-0.581	-0.010	-0.198	-0.435	-0.379	-0.786	-0.635	-0.360	-0.426	0.115	-0.315	-0.147	-0.101	-0.698	0.309	-0.154	-0.219	0.299	-0.176	-0.125	1.000	0.308	0.918
1	kurt	0.663	-1.027	-0.165	0.143	-0.242	-1.479	-0.936	-0.924	-0.958	0.183	0.805	2.013	-0.753	0.147	0.080	0.128	-0.227	-0.604	-0.731	-1.005	-1.134	-0.787	-1.120	1.942	0.664	2.023
1	10.0% percentile	-1.196	-1.052	-0.988	-0.735	-1.208	-1.114	-1.128	-1.199	-1.095	-0.644	-1.392	-1.335	-1.283	-1.624	-1.044	-0.916	-0.766	-1.189	-1.319	-1.254	-1.184	-1.196	-1.212	-77.804	-1.552	-0.875
1	50.0% percentile	-0.520	-0.827	-0.024	-0.581	-0.010	-0.198	-0.435	-0.379	-0.786	-0.635	-0.360	-0.426	0.115	-0.315	-0.147	-0.101	-0.698	0.309	-0.154	-0.219	0.299	-0.176	-0.125	1.000	0.308	0.918
1	90.0% percentile	0.908	1.612	1.167	1.678	1.272	1.525	1.374	1.544	0.970	1.729	0.670	0.708	1.126	0.631	1.093	1.173	1.684	1.379	1.168	1.292	1.321	1.294	1.240	60.071	2.527	2.331
1	cv	-2.145	-6.159	21.655	-6.674	-11.233	34.812	-6.402	-7.756	-3.300	-7.050	-2.676	-2.393	3756.487	-2.326	-17.957	-9.884	-6.024	6.406	-12.229	-20.694	4.609	-9.256	-19.450	-40.863	3.291	1.684
2	mean	0.318	0.362	-0.013	0.043	-0.345	0.169	0.308	0.217	0.419	0.071	0.045	0.092	-0.146	0.357	0.193	0.486	0.147	-0.050	-0.081	-0.028	-0.121	-0.076	-0.025	3.969	0.457	0.654
2	var	0.931	0.897	1.019	1.120	0.944	0.971	0.965	1.110	1.054	1.079	1.138	1.109	1.528	0.859	1.088	1.107	1.105	0.871	1.146	1.215	0.879	1.164	1.239	3495.618	2.365	2.070
2	std	0.965	0.947	1.009	1.058	0.971	0.985	0.982	1.054	1.027	1.039	1.067	1.053	1.236	0.927	1.043	1.052	1.051	0.933	1.071	1.102	0.937	1.079	1.113	59.124	1.538	1.439

2	min	-3.239	-1.116	-2.539	-0.735	-2.139	-1.133	-1.194	-1.199	-1.132	-0.644	-2.903	-2.013	-1.738	-2.783	-2.765	-2.103	-0.766	-2.333	-2.489	-2.944	-1.780	-2.481	-2.832	-345.500	-4.491	-6.314
2	max	1.818	1.677	1.782	1.678	1.517	1.525	1.639	1.622	1.750	1.729	1.693	1.714	1.545	2.774	1.675	1.681	1.684	1.838	2.565	2.413	1.988	1.934	2.062	302.800	4.300	4.533
2	skew	-0.099	0.112	0.179	0.844	0.418	0.191	-0.093	-0.023	-0.094	0.910	0.012	0.096	0.230	-0.510	0.047	-0.568	0.521	0.241	-0.161	-0.199	0.276	-0.207	-0.289	1.028	0.053	-0.330
2	median	0.295	0.110	-0.244	-0.666	-0.374	-0.022	0.313	0.260	0.541	-0.620	-0.056	0.007	-0.382	0.514	0.004	0.627	-0.643	-0.182	-0.055	-0.058	-0.400	-0.041	-0.066	-2.800	0.219	0.624
2	kurt	-0.609	-1.361	-0.913	-1.214	-0.765	-1.484	-1.361	-1.519	-1.556	-1.124	-0.536	-1.064	-1.592	0.948	-0.995	-0.542	-1.536	-0.577	-0.686	-0.744	-1.088	-0.732	-0.763	10.817	0.005	1.861
2	10.0% percentile	-0.820	-0.915	-1.266	-0.735	-1.505	-1.092	-1.082	-1.199	-0.953	-0.643	-1.226	-1.201	-1.569	-0.972	-1.013	-0.993	-0.766	-1.073	-1.395	-1.404	-1.303	-1.363	-1.560	-47.162	-1.295	-1.040
2	50.0% percentile	0.295	0.110	-0.244	-0.666	-0.374	-0.022	0.313	0.260	0.541	-0.620	-0.056	0.007	-0.382	0.514	0.004	0.627	-0.643	-0.182	-0.055	-0.058	-0.400	-0.041	-0.066	-2.800	0.219	0.624
2	90.0% percentile	1.626	1.677	1.481	1.678	1.313	1.525	1.639	1.622	1.750	1.729	1.693	1.714	1.545	1.183	1.675	1.681	1.684	1.322	1.240	1.292	1.263	1.364	1.240	59.100	2.499	2.441
2	cv	3.031	2.618	-76.618	24.470	-2.813	5.844	3.190	4.847	2.453	14.607	23.956	11.474	-8.490	2.599	5.418	2.163	7.173	-18.787	-13.162	-38.758	-7.754	-14.115	-45.159	14.898	3.364	2.201
3	mean	0.440	-0.052	-0.066	0.247	0.558	-0.257	-0.041	0.013	0.127	0.205	0.641	0.640	0.167	0.426	-0.128	-0.372	0.167	-0.288	0.265	0.138	-0.334	0.315	0.140	-3.085	0.508	0.497
3	var	1.312	0.811	1.750	1.171	1.323	0.959	1.256	1.098	0.912	1.163	0.844	0.948	0.938	0.991	1.745	1.094	1.115	0.977	0.928	0.764	0.945	0.870	0.730	1830.333	2.165	1.572
3	std	1.145	0.901	1.323	1.082	1.150	0.979	1.121	1.048	0.955	1.079	0.919	0.974	0.968	0.996	1.321	1.046	1.056	0.989	0.963	0.874	0.972	0.933	0.855	42.782	1.472	1.254
3	min	-3.239	-1.116	-2.382	-0.735	-2.139	-1.135	-1.194	-1.199	-1.132	-0.644	-2.552	-3.999	-1.738	-2.783	-2.559	-2.103	-0.766	-2.333	-2.386	-2.036	-2.070	-2.105	-2.124	-176.100	-6.025	-3.538
3	max	1.818	1.677	1.782	1.678	1.517	1.525	1.639	1.622	1.750	1.729	1.693	1.714	1.545	2.774	1.675	1.681	1.684	1.838	2.118	1.937	1.975	2.179	1.836	281.500	4.668	3.631
3	skew	-1.366	0.788	-0.201	0.464	-0.994	0.796	0.508	0.337	0.251	0.632	-0.678	-0.978	-0.280	-0.129	-0.214	0.458	0.531	0.111	-0.461	-0.418	0.579	-0.481	-0.587	1.312	-0.163	-0.214
3	median	0.610	-0.308	0.191	-0.497	0.927	-0.775	-0.534	-0.291	-0.028	-0.585	0.702	0.708	0.190	0.414	0.025	-0.561	-0.443	-0.367	0.506	0.365	-0.615	0.601	0.437	-8.700	0.465	0.416
3	kurt	2.393	-0.566	-1.422	-1.685	-0.319	-0.982	-1.456	-1.414	-1.311	-1.568	-0.135	1.402	-0.736	0.833	-1.333	-0.553	-1.571	-0.555	-0.475	-0.565	-0.771	-0.413	-0.525	9.770	1.905	0.646
3	10.0% percentile	-0.858	-0.975	-1.889	-0.735	-1.463	-1.122	-1.151	-1.199	-1.032	-0.643	-0.930	-0.920	-1.363	-0.809	-1.986	-1.719	-0.766	-1.663	-1.013	-1.072	-1.301	-0.900	-1.015	-39.324	-1.151	-0.979
3	50.0% percentile	0.610	-0.308	0.191	-0.497	0.927	-0.775	-0.534	-0.291	-0.028	-0.585	0.702	0.708	0.190	0.414	0.025	-0.561	-0.443	-0.367	0.506	0.365	-0.615	0.601	0.437	-8.700	0.465	0.416
3	90.0% percentile	1.818	1.677	1.638	1.678	1.517	1.525	1.639	1.622	1.667	1.729	1.693	1.714	1.545	1.688	1.675	1.296	1.684	0.991	1.390	1.151	1.182	1.397	1.006	37.867	2.249	2.203
3	cv	2.606	-17.259	-19.908	4.379	2.063	-3.818	-27.247	83.783	7.525	5.269	1.433	1.521	5.802	2.339	-10.356	-2.808	6.334	-3.432	3.630	6.339	-2.915	2.963	6.086	-13.868	2.895	2.524

Table 8.2.7: Kendall rank correlation for each variable per aquifer group in the entire dataset.

	Alkalinit Total 4.5	As-T	Ca-T	Cd-T	Chlrid:I	Fe-T	Mn-T	N.Kjel:	P--T	Pb-T	Residue Filterabl 1.0u	Specific Conductanc	Sulfat:	pH	Hardnes Total (T	K--T	U--T	PRECIPITATIO N	MIN_TEM	MAX_TEM	Precip_Climatolo y	Tn_Climatolo	Tx_Climatolo	FD	HW	MT
Alkalinity Total 4	1.0000	0.2859	0.4113	-0.1002	0.2360	-0.0782	0.0787	0.0983	0.1310	0.0275	0.6316	0.6830	0.3806	0.4533	0.5083	0.3038	0.3283	-0.2204	-0.0050	0.0872	-0.2678	0.0018	0.0848	-0.0151	0.0328	-0.0024
As-T	0.2859	1.0000	0.1762	0.0651	-0.0077	0.1267	0.2156	0.0058	0.2742	0.1863	0.2001	0.2036	0.1552	0.2348	0.2146	0.2540	0.0414	-0.0796	-0.0200	0.0326	-0.0862	-0.0065	0.0365	-0.0099	-0.0066	-0.0459
Ca-T	0.4113	0.1762	1.0000	-0.0720	0.1786	-0.1058	0.0762	0.0600	0.0271	-0.0502	0.5269	0.5360	0.4687	0.0908	0.8359	0.2383	0.3977	-0.1543	-0.0779	0.0215	-0.1801	-0.0795	0.0203	-0.0281	0.0168	0.0214
Cd-T	-0.1002	0.0651	-0.0720	1.0000	0.0946	0.3724	0.1678	0.0077	0.1010	0.5632	0.0032	-0.0114	-0.0911	-0.0960	-0.0462	-0.0636	-0.4427	-0.0419	0.0160	0.0134	-0.0400	0.0370	0.0188	0.0010	-0.0395	-0.0991
Chlrid:D	0.2360	-0.0077	0.1786	0.0946	1.0000	0.0420	0.0657	0.1126	-0.0368	0.0406	0.3940	0.4019	0.2121	0.0107	0.1836	0.0204	0.0417	-0.0578	0.0623	0.0417	-0.0799	0.0546	0.0307	-0.0116	0.0378	0.0468
Fe-T	-0.0782	0.1267	-0.1058	0.3724	0.0420	1.0000	0.4111	0.0734	0.0970	0.3749	-0.0667	-0.0737	-0.0973	-0.1104	-0.0560	0.0619	-0.2901	0.0257	-0.0053	-0.0028	0.0260	-0.0074	-0.0003	0.0128	-0.0135	-0.0149
Mn-T	0.0787	0.2156	0.0762	0.1678	0.0657	0.4111	1.0000	0.1564	0.1005	0.1604	0.0503	0.0648	0.0272	-0.0060	0.1156	0.1414	-0.1260	-0.0086	-0.0046	-0.0059	-0.0166	-0.0024	-0.0128	0.0187	0.0046	-0.0381
N.Kjel:T	0.0983	0.0058	0.0600	0.0077	0.1126	0.0734	0.1564	1.0000	-0.0165	-0.0092	0.1519	0.1665	0.0853	0.0518	0.0883	0.1691	0.0284	-0.0613	0.0076	0.0393	-0.0685	0.0181	0.0443	0.0127	-0.0134	-0.0492

P--T	0.1310	0.2742	0.0271	0.1010	-0.0368	0.0970	0.1005	-0.0165	1.0000	0.1419	0.0998	0.0925	-0.0061	0.1514	0.0392	0.2030	0.0040	0.0283	-0.0471	-0.0245	0.0125	-0.0411	-0.0285	0.0362	0.0133	-0.0011
Pb-T	0.0275	0.1863	-0.0502	0.5632	0.0406	0.3749	0.1604	-0.0092	0.1419	1.0000	0.0515	0.0397	-0.0774	0.0665	-0.0200	-0.0103	-0.3152	-0.1433	0.0368	0.0623	-0.1481	0.0588	0.0594	-0.0353	0.0171	-0.0769
Residue Filterabl 1.0u	0.6316	0.2001	0.5269	0.0032	0.3940	-0.0667	0.0503	0.1519	0.0998	0.0515	1.0000	0.8749	0.4913	0.2861	0.5943	0.2463	0.2919	-0.1908	0.0066	0.0764	-0.2296	0.0052	0.0694	-0.0223	0.0409	0.0245
Specific Conductance	0.6830	0.2036	0.5360	-0.0114	0.4019	-0.0737	0.0648	0.1665	0.0925	0.0397	0.8749	1.0000	0.4943	0.3262	0.6196	0.2795	0.3165	-0.2126	-0.0095	0.0672	-0.2518	-0.0096	0.0614	-0.0270	0.0421	0.0137
Sulfat:D	0.3806	0.1552	0.4687	-0.0911	0.2121	-0.0973	0.0272	0.0853	-0.0061	-0.0774	0.4913	0.4943	1.0000	0.1340	0.4697	0.2278	0.3450	-0.1230	-0.0358	0.0189	-0.1263	-0.0434	0.0125	-0.0409	0.0252	0.0271
pH	0.4533	0.2348	0.0908	-0.0960	0.0107	-0.1104	-0.0060	0.0518	0.1514	0.0665	0.2861	0.3262	0.1340	1.0000	0.1723	0.2818	0.1832	-0.1614	0.0252	0.0917	-0.1907	0.0406	0.0919	-0.0082	0.0343	-0.0324
Hardness Total (T	0.5083	0.2146	0.8359	-0.0462	0.1836	-0.0560	0.1156	0.0883	0.0392	-0.0200	0.5943	0.6196	0.4697	0.1723	1.0000	0.3187	0.3624	-0.1877	-0.0696	0.0497	-0.2157	-0.0734	0.0477	-0.0306	0.0198	0.0232
K--T	0.3038	0.2540	0.2383	-0.0636	0.0204	0.0619	0.1414	0.1691	0.2030	-0.0103	0.2463	0.2795	0.2278	0.2818	0.3187	1.0000	0.2347	-0.0911	-0.1096	-0.0077	-0.1069	-0.1202	-0.0104	-0.0016	0.0163	0.0297
U--T	0.3283	0.0414	0.3977	-0.4427	0.0417	-0.2901	-0.1260	0.0284	0.0040	-0.3152	0.2919	0.3165	0.3450	0.1832	0.3624	0.2347	1.0000	-0.0741	-0.1004	-0.0429	-0.0757	-0.1225	-0.0543	-0.0309	0.0612	0.1054
PRECIPITATION	-0.2204	-0.0796	-0.1543	-0.0419	-0.0578	0.0257	-0.0086	-0.0613	0.0283	-0.1433	-0.1908	-0.2126	-0.1230	-0.1614	-0.1877	-0.0911	-0.0741	1.0000	-0.1994	-0.3195	0.5823	-0.2340	-0.2882	0.4212	-0.1841	0.0868
MIN_TEMP	-0.0050	-0.0200	-0.0779	0.0160	0.0623	-0.0053	-0.0046	0.0076	-0.0471	0.0368	0.0066	-0.0095	-0.0358	0.0252	-0.0696	-0.1096	-0.1004	-0.1994	1.0000	0.7097	-0.2887	0.8332	0.6806	0.0474	0.1553	0.1241
MAX_TEMP	0.0872	0.0326	0.0215	0.0134	0.0417	-0.0028	-0.0059	0.0393	-0.0245	0.0623	0.0764	0.0672	0.0189	0.0917	0.0497	-0.0077	-0.0429	-0.3195	0.7097	1.0000	-0.3805	0.7025	0.8587	-0.0255	0.1964	0.0419
Precip_Climatolo y	-0.2678	-0.0862	-0.1801	-0.0400	-0.0799	0.0260	-0.0166	-0.0685	0.0125	-0.1481	-0.2296	-0.2518	-0.1263	-0.1907	-0.2157	-0.1069	-0.0757	0.5823	-0.2887	-0.3805	1.0000	-0.3084	-0.3899	0.0015	-0.0713	-0.0023
Tn_Climatology	0.0018	-0.0065	-0.0795	0.0370	0.0546	-0.0074	-0.0024	0.0181	-0.0411	0.0588	0.0052	-0.0096	-0.0434	0.0406	-0.0734	-0.1202	-0.1225	-0.2340	0.8332	0.7025	-0.3084	1.0000	0.7221	0.0131	0.0684	-0.0473
Tx_Climatology	0.0848	0.0365	0.0203	0.0188	0.0307	-0.0003	-0.0128	0.0443	-0.0285	0.0594	0.0694	0.0614	0.0125	0.0919	0.0477	-0.0104	-0.0543	-0.2882	0.6806	0.8587	-0.3899	0.7221	1.0000	0.0138	0.0518	-0.0326
FD	-0.0151	-0.0099	-0.0281	0.0010	-0.0116	0.0128	0.0187	0.0127	0.0362	-0.0353	-0.0223	-0.0270	-0.0409	-0.0082	-0.0306	-0.0016	-0.0309	0.4212	0.0474	-0.0255	0.0015	0.0131	0.0138	1.0000	-0.1707	0.1376
HW	0.0328	-0.0066	0.0168	-0.0395	0.0378	-0.0135	0.0046	-0.0134	0.0133	0.0171	0.0409	0.0421	0.0252	0.0343	0.0198	0.0163	0.0612	-0.1841	0.1553	0.1964	-0.0713	0.0684	0.0518	-0.1707	1.0000	0.3690
MT	-0.00243	-0.04588	0.02138	-0.09900	0.04677	-0.0149	-0.0381	-0.0491	-0.0010	-0.07688	0.02449	0.013654	0.02706	-0.03240	0.02324	0.02974	0.10537	0.086835	0.124069	0.041896	-0.00227	-0.0473	-0.03263	0.13761	0.36897	1

8.3 Factor Analysis

8.3.1 Initial Factor Analysis Data

Table 8.3.1: Barlett's sphericity and Kaiser's test results.

Dataset	Bartlett's		KMO	Data Points
	Chi-square value	P-value	Overall MSA	
DataHotTP	4474.7157	0	0.5434	
DataHotSWI	4758.4707	0	0.6489	
DatatSWIHot	1545.1009	7.5840e-202	0.5901	106
DatatDroughtHot	6841.2284	0	0.7574	530
DatatFloodHot	5553.4703	0	0.7340	433
DatatHWHot	7255.0378	0	0.7662	611
DatatMTHot	8790.9545	0.0	0.7560	
DatatHotAs	9243.17432	0	0.7383	985
DatatHotMn	9352.7581	0	0.7289	985
DatatHotPb	10171.7002	0	0.7296	985
DatatHotU	9727.2657	0	0.7601	985
DatatHotNoBias	12030.6319	0	0.7526	985
DatatHotNoBiasP2	8758.1577	0	0.7481	985

Table 8.3.2: Information regarding Kaiser's test to determine number of factors necessary.

Dataset	Eigenvalues> 1	∑ Eigenvalues> 1	∑Eigenvalues> 1/ ∑Eigenvalues
DatatDroughtHot	6	16.3616	0.6817
DatatFloodHot	7	17.5539	0.7314
DatatHWHot	7	17.3239	0.7218
DatatMTHot	7	17.3162	0.7215
DatatHotAs	7-6	15.3774	0.7323
DatatHotMn	6	14.4536	0.6883
DatatHotPb	6	14.7770	0.7037
DatatHotU	6	14.6479	0.6975
DatatHotNoBias	7	17.2115	0.7171
DatatHotNoBiasP2	5	12.3570	0.7724

Table 8.3.3: Mean squared amount of each metal of focus in the factor analysis for metals.

Element Alone	MSA
As-T	0.7156
Mn-T	0.5670
Pb-T	0.5881
U--T	0.8479

8.3.2 Main Factor Analysis

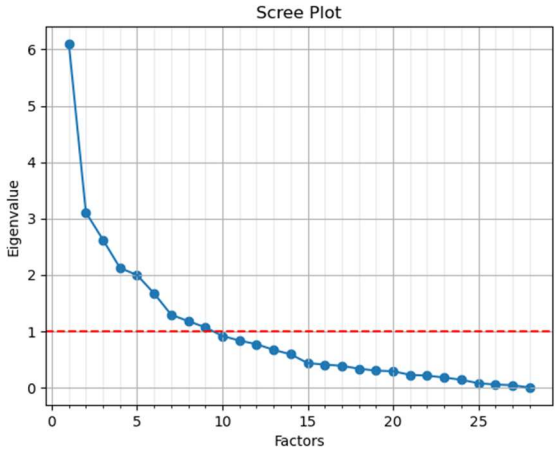

Figure 8.3.1: Scree plot of resultant eigenvalues and factors of the total dataset before factor analysis with varimax rotation.

Figure 8.3.2: Factor analysis with varimax rotation on the full dataset against each variable. Community, Uniqueness and Total Variance are also graphed below.

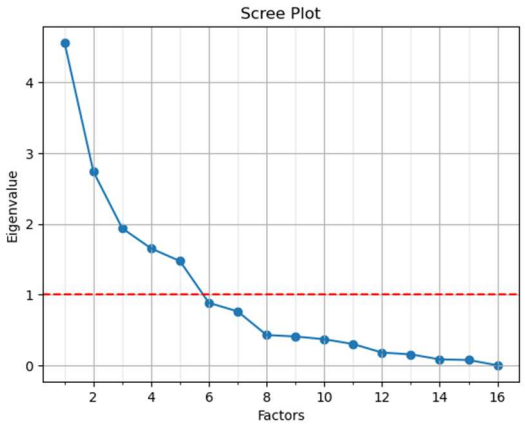

Figure 8.3.3: Scree plot of resultant eigenvalues and factors of the total dataset, after removal of previous variables and before factor analysis with promax rotation.

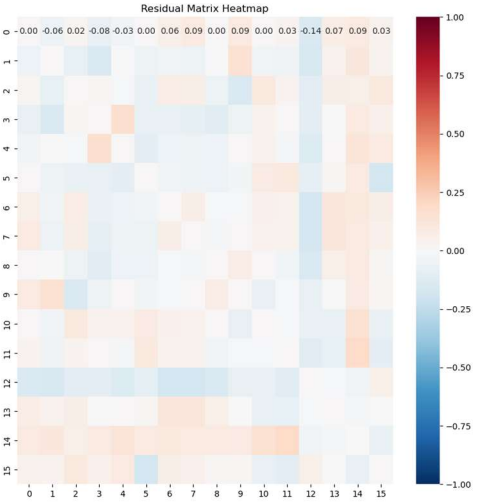

Figure 8.3.4: Residual matrix heatmap of each variable of the full dataset after factor analysis.

Table 8.3.4: Factor analysis of the total dataset after promax rotation. Cutoff p >0.40 (Hair et al., 2019).

Factor 1		**Factor 2**		**Factor 3**	
Chlrid:D	0.4804	Months_Since_First_Sample	-0.7700	MIN_TEMP	0.9116
U--T	0.5178	Mn-T	0.4511	MAX_TEMP	1.0015
Sulfat:D	0.7530	Fe-T	0.7101		
Alkalinity Total 4.5	0.7572	Pb-T	0.8249		
Ca-T	0.7577				
Residue Filterable 1.0u	0.8647				
Specific Conductance	0.9167				

Factor 4		**Factor 5**			
Aquifer_1	-0.7567	Aquifer_3	-0.9000		
Aquifer_2	0.9726	Aquifer_1	0.6588		

Table 8.3.5: Communality and Uniqueness for important variables (p>40) using factor analysis of the total dataset after promax rotation.

	Communality	Uniqueness
Aquifer_3	0.8404	0.1596
Chlrid:D	0.3416	0.6584
Specific Conductance	0.8827	0.1173
Residue Filterable 1.0u	0.7888	0.2112
Pb-T	0.6985	0.3015
Alkalinity Total 4.5	0.6245	0.3755
MIN_TEMP	0.8387	0.1613
U--T	0.4443	0.5557
MAX_TEMP	1.0222	-0.0222
Sulfat:D	0.5980	0.4020
Months_Since_First_Sample	0.6375	0.3625
Mn-T	0.2810	0.7190
Fe-T	0.5378	0.4622
Aquifer_2	1.0021	-0.0021
Ca-T	0.6411	0.3589
Aquifer_1	1.0074	-0.0074

Table 8.3.6: Factor loadings, proportional variance and cumulative variance for each factor using factor analysis of the total dataset after promax rotation.

	SS Loadings	Proportional Variance	Cumulative Variance
Factor 1	3.9052	0.2441	0.2441
Factor 2	2.1807	0.1363	0.3804
Factor 3	1.8433	0.1152	0.4956
Factor 4	1.6742	0.1046	0.6002
Factor 5	1.5834	0.0990	0.6992

8.3.3 As Factor Analysis

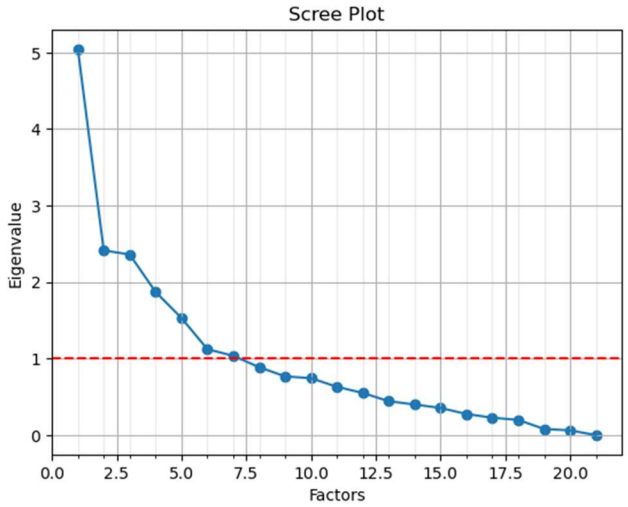

Figure 8.3.5: Scree plot of resultant eigenvalues and factors of the total dataset with As as the only metal of focus.

Table 8.3.7: Factor analysis of the total dataset with As as the only metal of focus with Oblimin rotation. Cutoff p >0.40 (Hair et al., 2019).

Factor 1		**Factor 2**		**Factor 3**		**Factor 4**	
K--T	0.4937	MIN_TEMP	0.8921	Aquifer_3	-0.9074	Aquifer_1	-0.6451
Chlrid:D	0.5813	MAX_TEMP	1.0033	Aquifer_1	0.6110	Aquifer_2	0.9753
Ca-T	0.7038						
Sulfat:D	0.7223						
Alkalinity Total 4.5	0.7637						
Residue Filterable 1.0u	0.8944						
Specific Conductance	0.9453						
Factor 5		**Factor 6**					
Months_Since_First_Sample	-0.6442	Chlrid:D	-0.5683				
Fe-T	0.7581						

Table 8.3.8: Communality and Uniqueness for important variables (p>40) with factor analysis using Oblimin rotation of the total dataset with As as the only metal of focus.

	Communality	Uniqueness
Chlrid:D	0.6814	0.3186
MIN_TEMP	0.8262	0.1738
Months_Since_First_Sample	0.4974	0.5026
Residue Filterable 1.0u	0.8218	0.1782

Fe-T	0.6082	0.3918
Aquifer_3	0.8813	0.1187
Specific Conductance	0.9134	0.0866
Aquifer_1	0.7974	0.2026
Aquifer_2	0.9886	0.0114
Sulfat:D	0.5770	0.4230
Ca-T	0.5926	0.4074
MAX_TEMP	1.0200	-0.0200
Alkalinity Total 4.5	0.6538	0.3462
K--T	0.4649	0.5351

Table 8.3.9: Factor loadings, proportional variance and cumulative variance for each factor in a factor analysis with Oblimin rotation of the total dataset with As as the only metal of focus.

	SS Loadings	Proportional Variance	Cumulative Variance
Factor 1	4.3658	0.2079	0.2079
Factor 2	1.9960	0.0950	0.3029
Factor 3	1.7243	0.0821	0.3851
Factor 4	1.6937	0.0807	0.4657
Factor 5	1.2098	0.0576	0.5233
Factor 6	1.0558	0.0503	0.5736

8.3.4 Mn Factor Analysis Data

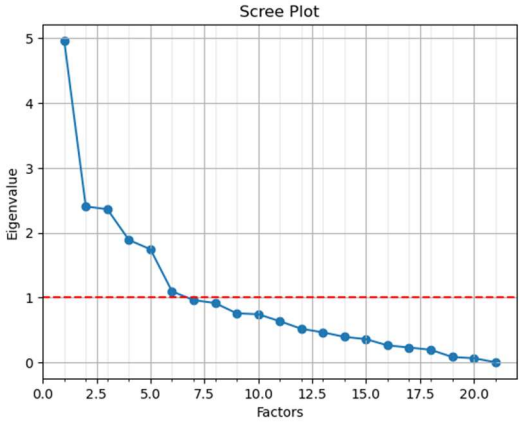

Figure 8.3.6: Scree plot of resultant eigenvalues and factors of the total dataset with Mn as the only metal of focus.

Table 8.3.10: Factor analysis of the total dataset with Mn as the only metal of focus with Oblimin rotation. Cutoff p >0.40 (Hair et al., 2019).

Factor 1		**Factor 2**		**Factor 3**		**Factor 4**	
K--T	0.4003	MIN_TEMP	0.9118	Aquifer_1	-0.6557	Aquifer_3	-0.8653
Chlrid:D	0.6305	MAX_TEMP	0.9967	Aquifer_2	0.9566	Aquifer_1	0.5945
Alkalinity Total 4.5	0.7084						
Ca-T	0.7183						
Sulfat:D	0.7283						
Residue Filterable 1.0u	0.8901						
Specific Conductance	0.9300						
Factor 5		**Factor 6**					
Months_Since_First_Sample	-0.5116	Chlrid:D	-0.4255				
Mn-T	0.5394	pH	0.4438				
Fe-T	0.9201	x	0.5253				

Table 8.3.11: Communality and Uniqueness for important variables (p>40) with factor analysis using Oblimin rotation of the total dataset with Mn as the only metal of focus.

	Communality	Uniqueness
Chlrid:D	0.6192	0.3808
MIN_TEMP	0.8598	0.1402
Months_Since_First_Sample	0.4089	0.5911
Mn-T	*0.3875*	*0.6125*
Aquifer_3	0.8146	0.1854
Residue Filterable 1.0u	0.8085	0.1915
Fe-T	0.8500	0.1500
Aquifer_2	0.9527	0.0473
Aquifer_1	0.7932	0.2068

Sulfat:D	0.5866	0.4134
Specific Conductance	0.8880	0.1120
Ca-T	0.6244	0.3756
MAX_TEMP	1.0095	-0.0095
Alkalinity Total 4.5	0.5989	0.4011
K--T	0.4136	0.5864
pH	*0.3917*	*0.6083*
x	0.4217	0.5783

Table 8.3.12: Factor loadings, proportional variance and cumulative variance for each factor in a factor analysis with Oblimin rotation of the total dataset with Mn as the only metal of focus.

	SS Loadings	Proportional Variance	Cumulative Variance
Factor 1	4.112	0.1958	0.1958
Factor 2	2.002	0.0953	0.2911
Factor 3	1.743	0.0830	0.3741
Factor 4	1.681	0.0800	0.4542
Factor 5	1.522	0.0725	0.5267
Factor 6	1.084	0.0516	0.5783

8.3.5 Pb Factor Analysis Data

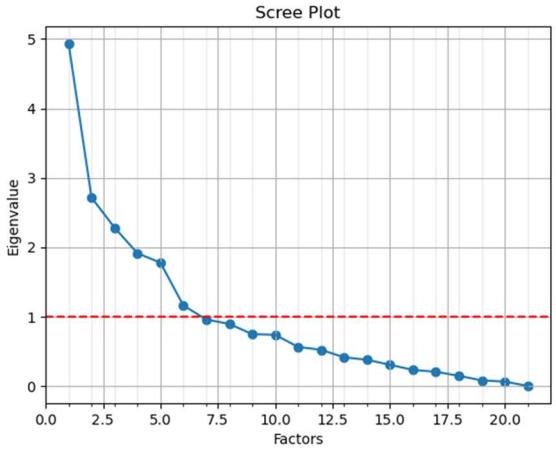

Figure 8.3.7: Scree plot of resultant eigenvalues and factors of the total dataset with Pb as the only metal of focus.

Table 8.3.13: Factor analysis of the total dataset with Pb as the only metal of focus with Oblimin rotation. Cutoff p >0.40 (Hair et al., 2019).

Factor 1		**Factor 2**		**Factor 3**	
K--T	0.5030	Months_Since_First_Sample	-0.8820	MIN_TEMP	0.9175
Chlrid:D	0.5760	Fe-T	0.5728	MAX_TEMP	0.9941
Ca-T	0.6876	Pb-T	0.9200		
Sulfat:D	0.7070				
Alkalinity Total 4.5	0.7685				
Residue Filterable 1.0u	0.8951				
Specific Conductance	0.9490				
Factor 4		**Factor 5**		**Factor 6**	
Aquifer_1	-0.7596	Aquifer_3	-0.9129	Chlrid:D	-0.5748
Aquifer_2	0.8864	Aquifer_1	0.4833	x	0.4404

Table 8.3.14: Communality and Uniqueness for important variables (p>40) with factor analysis using Oblimin rotation of the total dataset with Pb as the only metal of focus.

	Communality	Uniqueness
Chlrid:D	0.6810	0.3190
Fe-T	0.4658	0.5342
MIN_TEMP	0.8740	0.1260
Residue Filterable 1.0u	0.8220	0.1780
Specific Conductance	0.9189	0.0811

Aquifer_3	0.8557	0.1443
Months_Since_First_Sample	0.7932	0.2068
Aquifer_1	0.8202	0.1798
Aquifer_2	0.8856	0.1144
Pb-T	0.8527	0.1473
Sulfat:D	0.5592	0.4408
MAX_TEMP	1.0043	-0.0043
Ca-T	0.5588	0.4412
Alkalinity Total 4.5	0.6562	0.3438
K--T	0.4706	0.5294
x	*0.4253*	*0.5747*

Table 8.3.15: Factor loadings, proportional variance and cumulative variance for each factor in a factor analysis with Oblimin rotation of the total dataset with Pb as the only metal of focus.

	SS Loadings	Proportional Variance	Cumulative Variance
Factor 1	4.3040	0.2050	0.2050
Factor 2	2.0352	0.0969	0.3019
Factor 3	2.0015	0.0953	0.3972
Factor 4	1.8317	0.0872	0.4844
Factor 5	1.6009	0.0762	0.5606
Factor 6	0.9745	0.0464	0.6070

8.3.6 U Factor Analysis Data

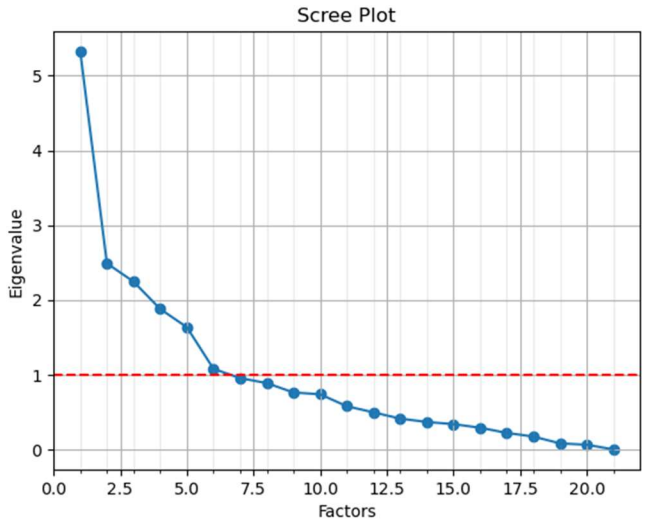

Figure 8.3.8: Scree plot of resultant eigenvalues and factors of the total dataset with U as the only metal of focus.

Table 8.3.16: Factor analysis of the total dataset with U as the only metal of focus with Oblimin rotation. Cutoff p >0.40 (Hair et al., 2019).

Factor 1		**Factor 2**		**Factor 3**	
Ca-T	0.5968	MIN_TEMP	0.9095	Aquifer_1	-0.7605
Sulfat:D	0.6445	MAX_TEMP	0.9973	Aquifer_2	0.9100
Alkalinity Total 4.5	0.6839				
Chlrid:D	0.7431				
Residue Filterable 1.0u	0.8917				
Specific Conductance	0.9274				
Factor 4		**Factor 5**		**Factor 6**	
Aquifer_3	-0.9658	Chlrid:D	-0.4759	Fe-T	-0.6709
Aquifer_1	0.4926	U--T	0.4832	U--T	0.4635
		x	0.5339	Months_Since_First_Sample	0.7409

Table 8.3.17: Communality and Uniqueness for important variables (p>40) with factor analysis using Oblimin rotation of the total dataset with U as the only metal of focus.

	Communality	Uniqueness
Fe-T	0.5023	0.4977
Chlrid:D	0.8046	0.1954
x	0.4128	0.5872
MAX_TEMP	1.0115	-0.0115
Aquifer_2	0.9259	0.0741
Aquifer_3	0.9507	0.0493
Aquifer_1	0.8292	0.1708
Specific Conductance	0.8779	0.1221
Residue Filterable 1.0u	0.8056	0.1944
MIN_TEMP	0.8569	0.1431
Alkalinity Total 4.5	0.5662	0.4338
Sulfat:D	0.4979	0.5021
Ca-T	0.4936	0.5064
U--T	0.5095	0.4905
Months_Since_First_Sample	0.5951	0.4049

Table 8.3.18: Factor loadings, proportional variance and cumulative variance for each factor in a factor analysis with Oblimin rotation of the total dataset with U as the only metal of focus.

	SS Loadings	Proportional Variance	Cumulative Variance
Factor 1	3.8896	0.1852	0.1852
Factor 2	2.0008	0.0953	0.2805
Factor 3	1.8523	0.0882	0.3687
Factor 4	1.6231	0.0773	0.4460
Factor 5	1.4023	0.0668	0.5128
Factor 6	1.3737	0.0654	0.5782

8.3.7 Drought Dataset Factor Analysis

Table 8.3.19: Factor analysis for drought dataset with Oblimin rotation. Cutoff >0.40 (Hair et al., 2019)

Factor 1		**Factor 2**		**Factor 3**	
Chlrid:D	0.6574	Months_Since_First_Sample	-0.8908	PRECIPITATION	-0.4580
Ca-T	0.6622	Fe-T	0.5335	MIN_TEMP	0.9420
Sulfat:D	0.7152	Pb-T	0.9083	MAX_TEMP	0.9420
Alkalinity Total 4.5	0.7639				
Residue Filterable 1.0u	0.8999				
Specific Conductance	0.9592				
Factor 4		**Factor 5**		**Factor 6**	
Aquifer_1	-0.9078	Aquifer_3	-0.6996	Chlrid:D	-0.5008
Aquifer_2	0.5639	Mn-T	0.4201	U--T	0.4459
		K--T	0.4673	x	0.4965
		Aquifer_2	0.5668		

Table 8.3.20: Factor loadings, proportional variance and cumulative variance for each factor in a factor analysis with Oblimin rotation with drought dataset

	SS Loadings	Proportional Variance	Cumulative Variance
Factor 1	4.6660	0.1944	0.1944
Factor 2	2.2683	0.0945	0.2889
Factor 3	2.1034	0.0876	0.3766
Factor 4	1.9089	0.0795	0.4561
Factor 5	1.7085	0.07120	0.5273
Factor 6	1.2118	0.05049	0.5778

Table 8.3.21: Communality and Uniqueness for important variables (p>40) with factor analysis using Oblimin rotation for drought dataset.

	Communality	Uniqueness
‘Chlrid:D	0.7202	0.2798
‘Mn-T	*0.3972*	*0.6028*
‘PRECIPITATION	*0.3845*	*0.6155*
‘Fe-T	0.5154	0.4847
‘MIN_TEMP	0.9148	0.08517
‘Aquifer_3	0.6810	0.3190
‘Residue Filterable 1.0u	0.8227	0.1773
‘Months_Since_First_Sample	0.8134	0.1866
Specific Conductance	0.9333	0.06666
Aquifer_1	0.8456	0.1544
Aquifer_2	0.6529	0.3471
Pb-T	0.8336	0.1664
MAX_TEMP	0.9729	0.02708
Sulfat:D	0.5616	0.4384
Alkalinity Total 4.5	0.6429	0.3571
Ca-T	0.5323	0.4677
K--T	0.5084	0.4916
U--T	0.4939	0.5061
x	0.4706	0.5294

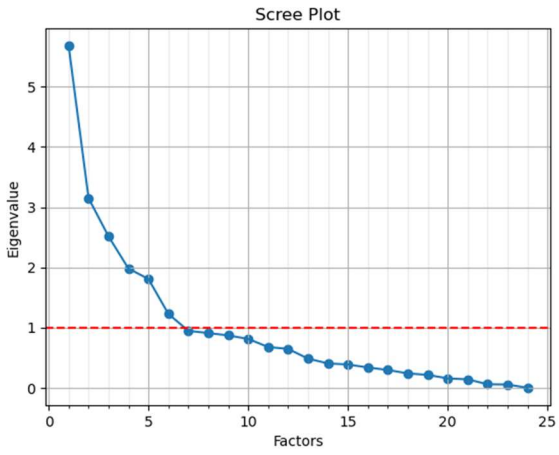

Figure 8.3.9: Scree plot of resultant eigenvalues and factors using drought (FD<0) dataset.

8.3.8 Flood Dataset Factor Analysis

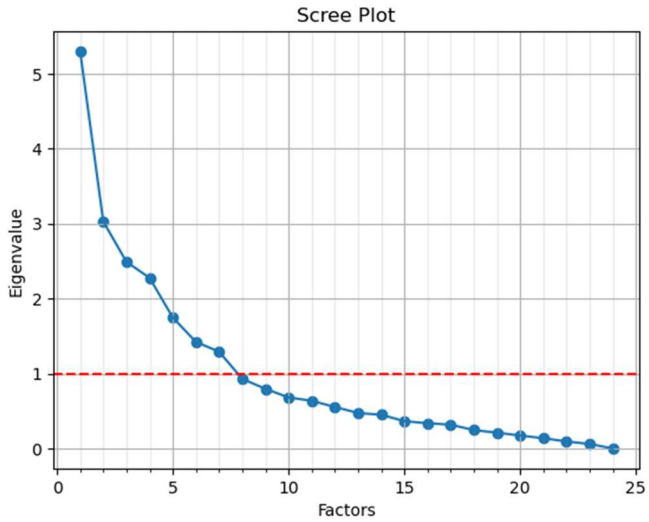

Figure 8.3.10: Scree plot of resultant eigenvalues and factors using Flood (FD>0) dataset.

Table 8.3.22: Factor analysis for flood dataset with Oblimin rotation. Cutoff >0.40 (Hair et al., 2019).

Factor 1		**Factor 2**		**Factor 3**		**Factor 4**	
Ca-T	0.5321	Months_Since_First_Sample	-0.8346	Aquifer_1	-0.9084	MAX_TEMP	0.9337
Sulfat:D	0.5668	Fe-T	0.5478	pH	0.3791	MIN_TEMP	0.9854
Alkalinity Total 4.5	0.5695	Pb-T	0.9527	Aquifer_2	0.7827		
Chlrid:D	0.7402						
Residue Filterable 1.0u	0.8536						
Specific Conductance	0.8665						
Factor 5		**Factor 6**		**Factor 7**			
PRECIPITATION	-0.6322	Aquifer_3	-0.6475	As-T	0.8069		
U--T	0.4571	Mn-T	0.4574	P--T	0.4451		
y	0.4865	Fe-T	0.5002				
x	0.6484						

Table 8.3.23: Communality and Uniqueness for important variables (p>40) with factor analysis using Oblimin rotation for flood dataset.

	Communality	Uniqueness
As-T	0.6967	0.3033
Sulfat:D	0.5106	0.4894
Ca-T	0.5237	0.4763
Alkalinity Total 4.5	0.5028	0.4972
U--T	0.4417	0.5583
pH	*0.3171*	*0.6829*
Mn-T	0.4446	0.5554
PRECIPITATION	0.5353	0.4647
Residue Filterable 1.0u	0.7478	0.2522
Aquifer_2	0.7976	0.2024
Specific Conductance	0.7849	0.2151
Pb-T	0.9204	0.07958
MIN_TEMP	0.9915	0.008498
MAX_TEMP	0.9064	0.09357
Aquifer_1	0.8966	0.1034
Fe-T	0.5943	0.4057
y	*0.3757*	*0.6243*
x	0.4950	0.5050
Aquifer_3	0.6230	0.3770
Months_Since_First_Sample	0.7388	0.2612
Chlrid:D	0.7026	0.2974

Table 8.3.24: Factor loadings, proportional variance and cumulative variance for each factor in a factor analysis with Oblimin rotation with flood dataset

	SS Loadings	Proportional Variance	Cumulative Variance
Factor 1	3.5170	0.1465	0.1465
Factor 2	2.3533	0.0981	0.2446
Factor 3	2.0974	0.0874	0.3320
Factor 4	1.9757	0.0823	0.4143
Factor 5	1.8906	0.0788	0.4931
Factor 6	1.4109	0.0588	0.5519
Factor 7	1.2473	0.0520	0.6038